Dynamic Constitutional Protein-Carbohydrate and Polyoxometalate Systems –towards Biomimetic Sensors and Membranes

Eugene Mahon

UNIVERSITE MONTPELLIER II

SCIENCES ET TECHNIQUES DU LANGUEDOC

T H E S E

pour obtenir le grade de

DOCTEUR DE L'UNIVERSITE MONTPELLIER II

Discipline :Chimie et Physicochimie des Materiaux.

Ecole Doctorale : Sciences Chimiques

présentée et soutenue publiquement

par

Eugene Mahon

le 3 Juillet 2009

Systèmes Protéine-Saccharides et Polyoxométallates Dynamiques Constitutionnels pour Capteurs et Membranes Biomimétiques

Dynamic Constitutional Protein-Carbohydrate and Polyoxometalate Systems –towards Biomimetic Sensors and Membranes

---

JURY

Pr. MONTERO Jean-Louis	Président
Pr. HASENKNOPF Bernold	Rapporteur
Pr. VINCENT Stéphane	Rapporteur
Dr. AASTRUP Teodor	Examinateur
Dr. BARBOIU Mihail	Directeur de Thèse

Acknowledgements

The research reported in this thesis was performed as part of the Adaptive Supramolecular Nanosystems group (NSA) at the European Institute of Membranes under the direction of Dr. Mihai Barboiu. It was financed by the Marie Curie Grant as part of the Marie Curie Research Training Network "Dynamic Interactive Chemical Biology and Biomedicine- DYNAMIC" (MRTN-CT-2005-019561).

Collaboration played an integral part in this work and I would like to express my appreciation for the work and support delivered by Remi Caraballo and Dr. Olof Rämstrom at the KTH Royal Institute of Technology in Stockholm and equally so to the Dr. Teodor Aastrup and Dr. Henrik Anderson at the Attana AB sensor technologies company where I spent a month long training stay to become well acquainted with the Quartz Crystal Microbalance instrument.

Other external contributions have also been made such as the input of Pr. Achim Müller in discussions and interpretations of the work on polyoxomolybdate nanoarchitectures.
I would like to extend gratitude to the NSA team around me at IEMM, particularly Mihai for his guidance as well as the group members for their project collaborations and general contributions such as Yann and Laurence in the Fluorescence measurements, Yves-Marie for general discussion in the office as well as Simona, Gihane and Adinela.
I would especially like to thank Laurence for her time spent on translating of documents.

On a personal note I would like to thank Vincent, Geraldine, Karen, Emily and Conor Mahon, who, for their everlasting support deserve great gratitude. Thanks to Dr. Mary Connolly for her support and promptings and finally to all my friends and colleagues who partook in the "balancing" of life.

Introduction

The aim of this work was to explore the interaction between biomimetic supramolecular and dynamic constitutional systems (nanoparticles, nanocapsules, membranes) and simple biological motifs (proteins, ion-channels, etc.).

The methodology of this process involved three steps. Firstly preparation at the molecular level of precursors using synthetic chemistry, secondly controlled assembly of the precursors to the biologically relevant scale of nanomaterials and lastly study of properties and specific biointeractions of these materials using highly sensitive techniques such as nanogravimetry, fluorimetry and nuclear magnetic resonance spectroscopy.

Research was performed in the following areas of interest: carbohydrate-protein interaction, vesicles, bilayers, ion channels and membrane transport constituting three projects.

The carbohydrate-protein interaction is seen as a vital recognition step in many biological processes. The exploration of interaction was performed by combining the quartz crystal microbalance technique with signal amplifying biomimetic nanoparticle platforms with the results showing highly evident specificity of recognition and multivalency affinity enhancement.

A novel type of synthetic ion-channel formed by polyoxomolybdate nanoarchitectures has been advanced in recent times by theoretical study. Allied to the theoretical evidence for spontaneous insertion they have been shown to possess specific cation complexing properties as well as tuneable pore size and complexing functionality. In this work bilayer insertion as well as cationic transport properties are investigated using supported phospholipid bilayer platforms and phospholipid vesicles.

Transport properties for a simple combinatorial library of disaccharides across a lectin occluding nanoemulsion were assessed with a view towards library amplification by selective transport. Supported liquid membranes were used to contain the hydrocarbon lectin-nanoemulsion phase with the transport properties interpreted by ^{1}HNMR studies.

This work was performed as part of the Marie Curie Research Training Network “Dynamic Interactive Chemical Biology and Biomedicine” (MRTN-CT-2005-019561). Collaborations with Remi Caraballo and Pr. Olof Ramström at KTH in Stockholm and Dr. Teodor Aastrup and Dr. Henrik Anderson at Attana Biosensor Technologies also in Stockholm contributed greatly.

1 General Considerations

1.1 Cell Membrane Function

All cells in the prokaryote and eukaryote world possess a cell membrane. It provides structure while creating a selectively permeable barrier between the extracellular environment and the highly functional and environmentally sensitive intracellular one. This barrier thus regulates what enters and exits the cell having evolved in unison with the complex biological processes which it envelops as they adapted to a constantly changing environment.

Many vital processes in the biological world are consequently mediated through the cell membrane. In the structured and specialised ensemble of cells that is the human body cell-cell communication is an absolutely vital process. Cells can respond to electromagnetic signals such as light and to mechanical signals such as touch but most cell to cell signalling is chemical in nature. These chemical signalling events, occurring across the complicated matrix of extracellular fluid show specificity and affinity which can be described based on the principles of molecular recognition.

Molecular recognition in biological systems occurs mostly at interfacial environments such as at membrane surfaces, enzyme reaction sites, or at the interior of the DNA double helix. At the cell membrane surface supramolecular recognition principles of complementarity apply to a range of specific non-covalent interactions including immune response [1], cell adhesion [2], cell-cell interaction, cell-cell communication, cell proliferation and cell death based on carbohydrate-protein recognition. Protein-protein recognition meanwhile can account for signalling processes [3] cell-cell recognition, cell adhesion [2] and ion channel structure [4] [5-7].

Supramolecular chemistry lies at the interface of biological and molecular systems [8]. As “chemistry beyond the molecule” it is underpinned by the labile, reversible yet highly specific interactions which exist throughout nature defining structures, mediating information transfer etc. As an area of research it has been developed over the past 20 years incorporating interactions observed in nature such as hydrophobic interaction, hydrogen bonding, metal ion coordination, electrostatic interactions and π-stacking. Complementary to the novel science based around supramolecular interactions, synthetic bioinspired supramolecular designs can in turn provide a greater depth of understanding of biological mechanisms. Through the principles of self-assembly, self organisation and molecular recognition allied to synthetic

chemistry we can access a range of materials which can interact with biology on a biological scale and in a biological manner with the possibility to incorporate built-in information transmitters from the nano to the macroscale.

This growing multidisciplinary field of nanobiotechnology could have important contributions to make to the future of medicine [9,10], as part of which, the consideration of molecular recognition events at the cell membrane surface as supramolecular information transfer could have important implications when applied to pharmaceutical development and nanopharmaceuticals. [11]

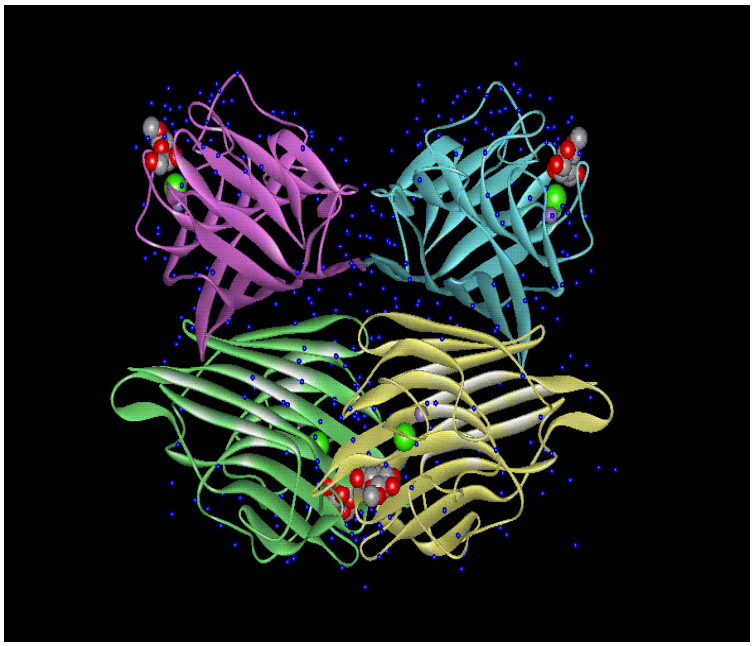

Figure 1 Crystal structure of Peanut Lectin complexed with 1-Me-β-D-galactopyranoside [12].

1.2 Carbohydrates in biological systems

It is known that glycosides play a fundamental role in molecular recognition processes throughout the natural world. The role is such that it can lead to the introduction of the concept of a "*glycocode*", in other words biological information transfer by sugars [13]. This type of spatial coding offers huge numbers of structural permutations for oligosaccharides through variation of glycosidic linkage position as well as orientation. There exists also another level to this information in overall glycan shape. Compared to oligopeptides the range of movement in glycosidic chains is highly restricted and so to the accessible conformational space.

In biology cell surfaces present dense areas of carbohydrate known as “glycocalyx”. In these situations they normally appear conjugated to lipids or proteins (glycolipids and glycoproteins) [14,15]. There appears to be two forms of recognition processes through which carbohydrates can facilitate information transfer namely carbohydrate–protein [16-18] and carbohydrate–carbohydrate [19,20] interactions.

The “decoding devices” for these sugar ensembles are specifically recognising proteins. These proteins can be separated into three distinct groups, enzymes which can degrade, assemble and modify the glycan, immunoglobulins acting as antigens and finally lectins. The lectins encompass all carbohydrate binding proteins which are neither antibodies nor enzymes.

1.3 Lectins

Present throughout nature lectins have shown important function in viruses and bacteria as well as plants and animals. They have been found to be involved in a range of biological processes [21] including clearance of glycoproteins from the circulatory system [22] [23], adhesion of infectious agents to host cells [24], recruitment of leucocytes to inflammatory sites [25], cell interactions in the immune system, in malignancy and metastasis [26].

They are defined as carbohydrate binding proteins and so they interact with carbohydrates in a supramolecular manner i.e. mainly through hydrogen bonding and the hydrophobic interaction. These interactions have shown very high specificity.

Most lectins belong to three classes simple, mosaic and macromolecular. The simple class comprises practically all known plant lectins and most of the galectin family and consist of a small number of subunits with each monomeric unit containing a carbohydrate binding site [27]. Commonly lectins possess two or more binding sites hence showing agglutination activity for carbohydrate presenting entities with these processes being inhibited by the carbohydrate for which the lectin is specific.
Amongst this simple lectin class lies the legume lectins which are abundant in plant seeds and show a wide range of saccharide specificities.

1.3.1 Legume Lectins as models

The legume lectins represent the largest and most well studied family of lectins. Concanavalin A is the prototype member of this family. They normally consist of two or four identical or near-identical subunits of 25-30 kDa each which are commonly single polypeptide chains of about 250 amino acids presenting one or two N-linked oligosaccharides. Each monomer contains one carbohydrate binding site as well as a tightly bound Ca^{2+} and transition metal (usually $Mn^{2+)}$ binding site.

On the primary, secondary and tertiary level legume lectin monomers are very similar although they exhibit considerable variation in their quaternary structure due to small differences in their amino acid sequences at the monomer-monomer interfaces.

This quaternary structure is also in most cases pH dependent and can reversibly dissociate as for example in the case of Concanavalin A where it exists as a dimer below pH6 and as a tetramer at physiological pH, or Peanut Lectin PNA which dissociates to a dimer at pH below 5.1 while again being tetrameric at physiological pH.

Typically these lectins have been used as model lectins to study the carbohydrate-protein interaction due mainly to their abundance and availability. Of these Concanavalin A the first lectin isolated pure [28,29], sequenced [30,31], and to have it's structure determined by X-ray crystallography [32,33], is the most commonly used due to high relative abundance in jack bean and it ease of preparation as a result of which it became the first lectin commercially available.

1.3.2 Lectin-Carbohydrate interaction

The binding of carbohydrates by legume lectins occurs in shallow pockets on the protein surface. These recognising pockets appear to be preformed as little conformational change occurs on binding [34]. The interaction itself is mediated mainly through hydrogen bonding and hydrophobic effects with Van der Waals interactions also playing a considerable role in the binding energy situation [35]

Taking the highly appropriate case of Concanavalin A recognition the selectivity principles may be demonstrated. The interactions in the binding site are typical for all legume lectin-carbohydrate complexes elucidated by X-ray crystallography. In this case the Concanavalin A was crystallised with methyl α-D-mannopyranoside which binds in the so called

monosaccharide binding pocket. Each binding pocket is formed by a Tyr12, Asn14, Leu99, Tyr100, Asp208 and Arg228 series of amino acids. From the binding scheme proposed by Naismith et al. [36] (Figure 2) one can see the important hydrogen bonds formed by the O3,O4,O5 and O6 of the mannose moiety. O4 and O6 form a bidentate hydrogen bond with the carboxylate of Asp208 and O5 and O6 form a bidentate hydrogen bond with backbone amide N atoms of Leu99 and Tyr100. The calcium ion is attached to three of the four loops which bind the saccharide. They proposed that in the absence of calcium it is likely that one or more of these loops moves out of position thus abolishing saccharide binding.

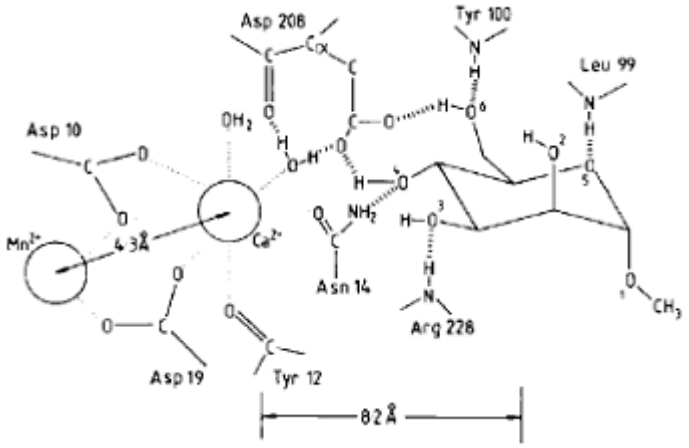

Figure 2 Methyl α-D-mannopyranoside complexed with Con A monosaccharide binding site [36].

There are also present essential Van der Waals interactions between aromatic residue Tyr12 and the sugar ring. The steric disposition of the hydroxyl groups on sugar moieties creates hydrophobic patches [37] that can interact with hydrophobic regions of the protein [38]. There is also now evidence of CH–π interactions between the sugar and the aromatic residues, something like a H-bond, although there is also a hydrophobic aspect to this observed interaction [39]. Spatial organization of aromatic entities thus plays an important role in selectivity such as differentiating between mannopyranose and glucopyranose structures in the Concanavalin A monosaccharide binding pocket.

The highest affinity ligand for Concanavalin A is the trimannosyl core Manα1-3-[Manα1-6]-Manα1-3 found in *N*-glycans [40]. The apparent affinity is realised through an extended binding site with specific interaction with all three sugar residues by way of hydrogen bonds. Water molecules play mediating roles in lectin–carbohydrate interactions with tightly bound water molecules playing structuring roles and imparting selectivity [41]. For example in the

above (Figure 2) there are water bridges between the bound Ca^{2+} and the Asp208 and Asn14 residues. Water molecules also act as direct hydrogen bonding bridges between ligand and protein [42].

Based on the energetics of theses interactions the resultant affinities between lectins and carbohydrates have been shown to be typically of the order of $10^3 M^{-1}$ for monosaccharides and up to $10^7 M^{-1}$, or even higher, for complex carbohydrates. In the case of Concanavalin A specifically, the methyl α-D-mannopyranoside ligand shows an affinity constant of $8.2x10^3$ M^{-1} with the trimannoside showing a 6-fold increase at 49 $x10^3$ M^{-1}. It shows a reduced affinity for α-D-glucopyranoside at $2.7x10^3 M^{-1}$ and no galactopyranose affinity [43,44].

These interactions are in any case relatively weak due to the solvent exposed nature of the binding site and few direct contacts with the ligands [45]. The question then arises as to how the affinities exhibited in nature for carbohydrate protein interactions are effected. Lectins show both high affinity and rare selectivity in the natural recognition processes with oligosaccharide structures of glycoproteins and glycolipids. Evidence has suggested that these recognition proceses are governed by multiple interactions or “multivalency”.

1.3.2.1 Multivalency

Multiple simultaneous interactions appear to have evolved in many biological processes as a means of maximising specificity without having too great a cost on overall affinity [46]. These polyvalent interactions have been shown to be much stronger than their corresponding monovalent ones. The multivalency phenomenon may impart on the entity recognition properties qualitatively different from those displayed by its constituents. Examples of multivalent biological interactions range from viral adhesion to the cell, bacterial adhesion, cell-cell and cell-antibody binding. [46] All these processes involve multivalent carbohydrate –protein recognition. Commonly bacteria [47] and viruses [48] adhere through lectin-like recognition of glycolipid clusters and glycoproteins. Also the immune response is largely realized by multivalent recognition. Antibodies which are a key protein in this response have multiple equivalent receptor sites which recognise in a multivalent manner “undesirable” structures. Through this recognition they may inhibit infection and/or promote clearance. The characteristic repeating epitopes of invading pathogens can facilitate high affinity binding through multivalent recognition.

Thermodynamics of Multivalency

In the search for a greater understanding of the power of multivalency the concept of cooperativity was introduced designated by "α". This factor is defined by:

$$\Delta G_{avg}^{poly} = \alpha \Delta G^{mono}$$

Eq 1

where:

$\Delta G_{avg}^{poly} =$ the average free energy change per monovalent interaction.

$\Delta G^{mono} =$ the free energy change of the equivalent monovalent interaction.

We can thus assign these interactions as cooperative (α>1), non-cooperative ((α=1) or negatively cooperative (α<1).

But as Mamman et al. pointed out even though multivalent interactions may be negatively cooperative (α<1) the measured affinity may still be much higher and not many if any multivalent systems have demonstrated positive cooperativity. Cooperativity is notoriously difficult to access [49] and tighter binding does not require positive cooperativity. Non-cooperative associations have generally been assumed for Con A meaning a value of 1 for α [50,51].

For many polyvalent systems *N* the number of ligand-receptor interactions is unknown and without which no interpretation regarding cooperativity is possible. Another constant was thus introduced being a ratio of multivalent avidity to monovalent affinity constant and known as the "enhancement factor"

$$\beta = \frac{K_a^{multi}}{K_a^{mono}}$$

Eq 2

$$\ln \beta = -\frac{\Delta G^{multi} - \Delta G^{mono}}{RT}$$

Eq 3

The concept of enhancement by decreased conformational entropy cost was introduced in earlier works. It described how when the free energies of association are compared between two ideal systems we can come to appreciate this "enhancement factor as entropic in origin.

Consider ”multi” as a system with one multivalent ligand containing *n* ligands binding a receptor with *n* receptor sites while ”mono” refers to *n* free ligands binding *n* free receptors.

$$\Delta S^{multi} = \Delta S^{multi}_{trans} + \Delta S^{multi}_{rot} + \Delta S^{multi}_{conf} + \Delta S^{multi}_{H_2O}$$

Eq 4

The total entropy can be considered in terms of contributions from changes in translational, rotational and conformational entropies on association. In cases where the mass difference between multivalent and monovalent ligand is not so great (<100 times) so as to greatly affect the translational entropy difference then we can assume that the translational and rotational contributions are equal leaving the configurational one as the only difference based on the linking of the monovalent ligands. Linking of the ligand therefore lowers the entropic cost of binding as described in following equations.

$$n\Delta G^{mono} = n\Delta H^{mono} - nT\Delta S^{mono}$$

Eq 5

$$\Delta G^{multi} = \Delta H^{multi} - T\Delta S^{multi} \approx n\Delta H^{mono} - nT\Delta S^{mono} - T\Delta S^{multi(n)}(conformational)$$

Eq 6

(*assuming ΔH equal and translational and rotational entopy contributions equal)*

$$\Delta G^{multi} - n\Delta G^{mono} = (n-1)T\Delta S^{mono} - T\Delta S^{multi(n)}$$

Eq 7

The free energy difference (Eq 7) equation shows that enhancement will be exhibited based to a large degree on entropy of monovalent binding with the greater the number of, and the more the negative the monovalent entropy of binding the greater the enhancement. The enhancement factor thus generally becomes greater in systems that show a higher valency number, and rigid linkers (a lower degree of conformational entropy loss).

In further work towards a thermodynamic model for multivalency Kitov and Bundle [52] utilize the additivity of free energies as suggested by Jenks before them [53] in analysing a system which considers a multivalent ligand interacting with multivalent receptor.

$$\Delta G^{O}_{multi} = i\Delta G^{O}_{mono} + \Delta G^{O}_{\text{int}eraction}$$

Eq 8

Here ΔG^{O}_{mono} is the binding energy of the corresponding monovalent interaction and *i* represents the valency of the complex. $\Delta G^{O}_{\text{int}\,eraction}$ is a balance between the favourable and unfavourable effects of tethering. They go further in considering the avidity binding energy to be made of three components.

-Intrinsic free binding energy of initial bimolecular interaction similar to the free energy of the intrinsic monovalent interaction ΔG^{O}_{mono} .

-Intrinsic free binding energy for intramolecular binding of ligand branches to remaining binding sites on the receptor surface

-A combinatorial factor representing the degeneracy of bound states hence highly dependant on valency.

These last two contributions constitute facets of multivalency effects: additional specific interactions and the statistical factor.

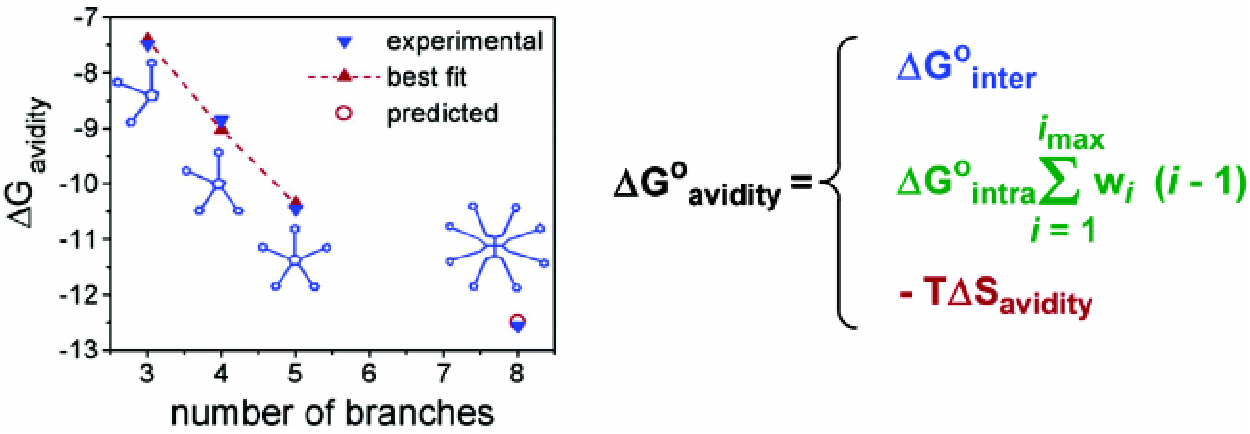

Figure 3 Avidity Free Energy Concept [52]

$$\Delta G^{O}_{avidity} = \Delta G^{O}_{\text{int}\,er} + \Delta G^{O}_{\text{int}\,ra}\sum_{i=1}^{i_{\max}} w_i (i-1) + RT\sum_{i=1}^{i_{mxx}} w_i \ln(w_i / \Omega_i)$$

Eq 9

The last term corresponds to avidity entropy $\Delta S^{O}_{avidity}$ and is a measure of the number of microscopically distinct complexes possible and therefore grows with ligand valency. Multivalency effects, when demonstrated by carbohydrates, give rise to what is known as the "cluster glycoside effect".

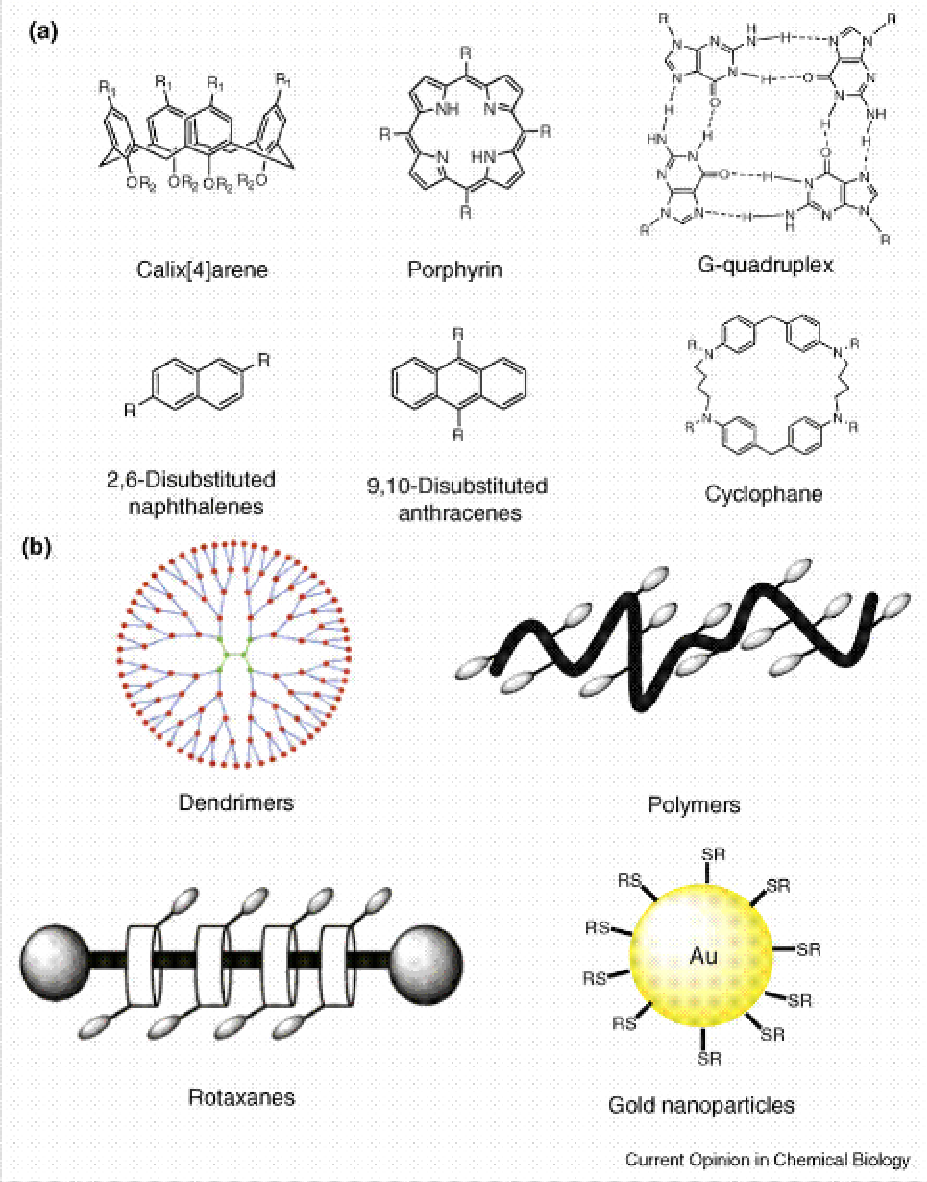

Equation 1 Examples of multivalent scaffolds [54]

1.3.2.2 The Cluster Glycoside Effect

"The enhancement in the activity of a multivalent ligand beyond what would be expected due to the increase in sugar local concentration alone" is the definition of an effect known as the "cluster glycoside effect".

As previously alluded to, exhibited carbohydrate–protein affinities in nature are realised through multivalency. Based on this understanding many multivalent carbohydrate presenting ligands have been prepared with most showing an enhancement in activity compared to the corresponding monovalent ligand on per mole of saccharide or valence corrected basis [55,56].

These polyvalent glycoligands generally fall into the categories of dendrimeric, polymeric and liposomes or other amphiphilically driven assemblies. In Lundquist and Toone's extensive review of this effect up to 2002 [55] they analyse reported affinity enhancements to search for trends. They noticed overall that:

-All multivalent ligands showed some enhancement

-There exists tremendous variation in the magnitude of the effect

-there appears to be a trend of increasing enhancement with increasing valency

-there appears to be an assay measurement technique dependency.

- For instances where more than one method was used to investigate binding considerable discrepancies were observed.

In terms of a molecular understanding of the "cluster glycoside effect" the authors go on to describe at least two models that can be proposed, a chelate effect (intramolecular binding) and aggregation/precipitation (intermolecular binding).

Toone and co-workers propose that in the vast majority of cases where dendrititic ligands are used to demonstrate the multivalency effect the distance presented between lectin binding sites is too large too be spanned (65 Å apart in ConA [57]) and so the chelate effect is ruled out as a mechanism of affinity enhancement [55]. They thus propose an aggregative model as by far the most reasonable. Lectin aggregation can be designated as the driving force for the observed affinity enhancement in many cases. Citing earlier work with Concanavalin A as lectin model, evidence for this aggregative theory is forthcoming. Naismith and Toone report structural and energetic studies of Con A binding to dendritic ligands [58] and they concluded that multivalent ligands bound to multivalent lectins can form several species and are capable of forming cross-links. The observations of high affinity of multivalent glycoconjugates reflect the propensity of such ligands to form aggregates rather than on any enhancement on the actual protein-carbohydrate affinity. These conclusions are based on observation of cloudiness in solution as well as diminished enthalpies of binding for higher valence dendrimer consistent with an aggregation mechanism.

More recent work by Wolfenden and Cloninger [50] with glycodendrimers bearing up to 170 sugar residues of mannose/glucose/galactose combinations fits the earlier model of Whitesides [46] mentioned earlier:

$$K_N^{Multi} = (K^{mono})^{\alpha N}$$

Eq 10

K_{mono} = monovalent association constant

K_N^{Multi} = multivalent association constant

N = number of receptor-ligand interactions

α = cooperativity factor

By setting α=1 and N=2 (maximum multivalent interaction possible due to shape considerations of lectin and spherical dendrimer) for the larger dendrimers (generation G4, G5 and G6) which can span two binding sites on Con A. In the optimised binding scenario replacing all the mannose residues with glucose should cause a 16 (= 4^2) fold increase in binding (as methyl α-D-mannopyranoside has an affinity constant four times that of methyl α-D-glucopyranoside) which is close to what they observed. Monovalent binding differences, in this case between mannose and glucose residues, appeared to be amplified by multivalency in line with the equation described by Whitesides and co-workers [46]. The activity of these glycodendrimers was measured by hemagglutination inhibition assays and the number of Con A lectins recruited by each dendrimer was also measured using precipitation assays. The results presented indicate that these numbers are size dependant and don't change much with functionality. Effectively it claims that the number of lectins that can be bound to each dendrimer is not affected when the relative activity is altered by an order of magnitude as measured at precipitation.

To summarize it appears that the cluster glycoside effect is something which definitely exists based on observation; however there appears to be ambiguities in the reporting of causes and understanding of the effect. The measurement technique is important as is the multivalent scaffold as based on its form different effects can come into play such as cross-linking and chelate effects. The thermodynamics behind this effect have been described as being based on a lowering of the configurational entropy cost on binding and also as occurring through a combination of chelating effects with a statistical increase in the number of bound configurations with valency and therefore entropically favourable.

1.4 Nanoscience exploration of biological function

1.4.1 2-D NanoPlatforms

Self-assembled and hybrid monolayers, where host or guest are arranged in two dimensional arrays with high directionality are prone to multivalent binding. On the other hand combinations of small relatively rigid three dimensional entities such as particles and dendrimers are prone to intermolecular binding as was previously described (see section 1.3.2.2).

2-D assemblies offer a number of advantages over solution systems in the study of multivalent interactions. The structure, density and environment of the immobilized functionalities are easily varied through employment of the routine gold and silica surface chemistries [59].

Effective concentration at surfaces has been shown to play an important role in binding affinities and multivalent interactions at surfaces have been studied for a range of cases such as cyclodextrin host-guest complexes [60-62], vancomycin dimer with self assembled monolayers (SAMs) presenting D-Ala-D-Ala functionalities [63] while not forgetting the protein-carbohydrate interaction with SAM's [64-67] as well as supported bilayer types [68,69].

1.4.2 Surface based Biosensors

A biosensor can be defined as a device incorporating a biological sensing element connected to or integrated within a transducer.
It usually consists of 3 parts:

-*sensitive biological element* (biological material (e.g. tissue, microorganisms, organelles, cell receptors, enzymes, antibodies, nucleic acids, etc) or biomimetic such as carbohydrate array or MIP.
-*transducer* that transforms the signal resulting from the interaction of the analyte with the biological element into another signal that can be more easily measured and quantified.
-*processors* that are primarily responsible for the display of the results in a user-friendly way.

Surface based systems for biosensing in terms of real-time label-free measurement of biological interactions have been developed which exploit the electro-optical properties of metals (Surface Plasmon Resonance), piezoelectric properties (Quartz Crystal Microbalance) and electrochemical transduction.

SPR is an optical reflectance procedure which is sensitive to changes in the optical properties of medium close to a metal surface. The sensitivity of SPR can be very high, nanomolar concentrations of proteins larger than 10^4 Da can be detected [70]. The sensitivity is determined by the polarizability and mass density of adsorbed materials and so for those materials of similar polarizabilites the response can be calibrated to mass.

For coloured or turbid samples one can turn to electrochemical detection and QCM detection as optical detection may become impracticable in these conditions. The electrochemical biosensors can be categorised into amperometric, potentiometric and conductometric biosensors. Potentiometric biosensors can measure a change in potential at electrodes due to chemical changes at an electrode surface proving highly efficient sensors.

This present work will however concentrate on quartz crystal microbalance (QCM) detection, also known as nanogravimetry.
The normal QCM setup as later described consists of a quartz crystal sandwiched between two gold electrodes which generate bulk waves perpendicular to the sensor surface. The resonant frequency of this piezoelectric material is highly sensitive to adsorbed mass and so combined with microfluidic setups forms a way in which kinetics and thermodynamics of surface interactions can be deduced. Again like SPR the sensitivity is mass limited as the signal is also proportional to the mass of the analyte.

Biosensor functional surfaces provide ideal platforms for the immobilization of the desired biomolecules which can be achieved by physical adsorption, including electrostatic and hydrophobic interaction, covalent bonding, and specific interactions such as biotin-avidin, antibody-antigen interaction and DNA hybridization. The immobilization of biomolecules by molecular recognition and specific interactions on the surfaces as part of the biosensor fabrication process can yield good orientation and stability of the immobilized biomolecules thus leading to high-functionality.

1.4.2.1 . Surface functionalization

In order that biosensors be efficient measuring devices problems such as non-specific adsorption, and biological activity of immobilised species should be controlled. Surface engineering through development of surface chemistry methodologies and biochemistry have led to the design of more efficient and highly selective surfaces.

Organic monolayers

Self assembled monolayers are spontaneously formed due to the formation of covalent bonds between a surface and the molecule of choice resulting in a thin film typically 1-3 nm thick of controlled functionality [71]. They provide a powerful means by which to fabricate molecularly defined highly selective surfaces for biosensors [59]. The most highly investigated surfaces amenable to this technique are gold and silica. Gold–thiol chemistry provides the basis for gold surface functionalisation and is a well developed area of research [72,73]. On the other hand hydroxyl groups of metal oxide surfaces like silicon dioxide can react with alkyltrichlorosilane or alkyltriethoxysilane and form covalent siloxane bonds at the surface [74,75]. For both established surface chemistries a range of surface functions can be introduced, many from commercially available monomers [76].

Supported Bilayers

Supported bilayers can represent biomimetic platforms with which to study biointeractions. This group can be separated into the so called SLBs (supported lipid bilayer) and HBMs (hybrid bilayer membranes).

The SLB is conventionally formed on silica surfaces and stabilized by interactions between the hydrophilic hydroxyl surface and the phospholipids headgroups [77,78]. It is a purely phospholipid bilayer stabilised only by electrostatics and the hydrophobic effect, which, through incorporation of bioactive structures such as membrane proteins, glycolipids and glycoproteins can give a real biomimetic response with interacting species in solution.

The HBM consists of two differing leaves normally generated on a gold or silica surface. The lower leaf is a long chain alkyl self assembled monolayer while the upper leaf is phospholipid monolayer [79,80]. This type of bilayer may show increased stability due to the covalent

nature of the lower leaf fixation however it would present a system further from the biological condition given this fixed nature and more limited fluidity [81].

Biomacromolecule layers

For immobilisation of biomacromolecules such as lectins or enzymes the most important feature is the retention of biological activity normally related to native structure [82]. Direct immobilisation can be accomplished by different routes including electrostatic interaction [83], [84], hydrophobic interaction [85,86], covalent bonding and specific interaction [87]. There are advantages and disadvantages to each approach, for example, electrostatic and hydrophobic are both simpler to achieve, fast and direct but can result in random molecular orientation and possible denaturation. Covalent binding gives good stability and long-term use but is slow, normally irreversible and requires the use of linker molecules. Specific interaction has the benefits of improved orientation, reversibility and high functionality but requires a biocompatible linker.

Polymers

Polymer films have been used for the functionalisation of surfaces as applied in electrochemical, QCM [88-92] and SPR based sensing [93-95]. Bioactive surfaces may be prepared by polymer adsorption, either physical or covalent, giving highly specific surfaces which may incorporate anti-non-specific binding properties by tuning of the main chain functionality.

1.4.2.2 Nanomaterials as biosensors

The study of the interaction of nanomaterials and biological structures has undergone much growth in recent times. This interface has encompassed such topics as drug delivery, anti-pathogenic adhesion, targeting, etc. Their particular suitability to this purpose lies in their scale as between 1 and 100nm lies the scale on which many biological entities such as antibodies, viruses etc., interact. The interactions are normally governed at the molecular level and so by exploitation of the experience of nanochemistry in the preparation and functionalization of nanomaterials we can produce biomimetic entities possessing special intrinsic properties to facilitate biointeraction studies.

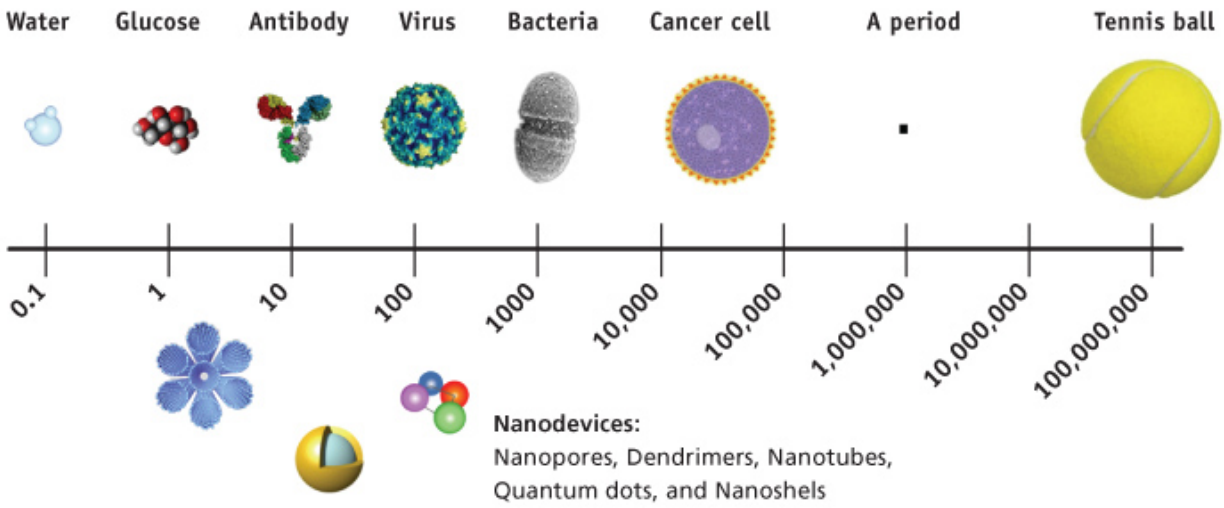

Figure 4.The Scale of things (nm) [96].

In terms of biosensors nanomaterials such as gold nanoparticles, carbon nanotubes, magnetic nanoparticles and quantum dots have been actively investigated.

Functional materials at the nanoscale may possess novel properties not present in the bulk material. For example gold nanoparticles show an SPR absorption band in the visible region giving the characteristic coloured solutions [97]. Based on this absorption biosensing assays can be prepared as this adsorption profile is influenced by interparticle distance[98-101].
There also exists many examples of nanoparticles being deposited on electrode surfaces, with this nanostructured surface providing a biocompatible adsorption matrix for biological objects such as enzymes [102,103]. These modifications greatly increase the amount of immobilised biomolecules at the surface thus improving sensitivity [104]. Nanoparticles have been used in biosensing by SPR and QCM which will be discussed in more detail in the next chapter (see 2.1.4.5).

Carbon nanotubes since their discovery in 1991 by Iijima have shown great potential in applications such as nanoelectronics, biomedical engineering and biosensing [105]. The CNT has a high surface to volume ratio, is biocompatible and shows fast electron transfer mediation for a wide range of electroactive species. Polymer CNT composites offering the possibility of ultra-sensitive electrochemical biosensors [106] and CNT framework modified

electrodes for enzyme immobilisation covalently or non-covalently are amongst CNT application to electrochemical sensors [107].

In terms of surface based optical and acoustic there have also been examples of CNT exploitation. Biotinylated tween adsorbed on CNT's have been used as surface area augmenters for streptavidin detection by QCM [108] but their application in bionsensors is mainly centred around their electrical properties.

1.4.2.3 Multivalency and Supramolecular Scaffolds

Multivalent ligands represent multiple copies of a recognition element connected in some way to a central scaffold. Resultant affinity can be highly dependant on the nature of the scaffold as multivalent interactions have been shown to be influenced by such factors as shape, valency, orientation and flexibility. Supramolecular scaffolds can exhibit a large range of valencies. Lower valency categories are supramolecules such as calixarenes and porphyrins with higher valency scaffolds include dendrimeric structures and nanoparticles.

1.4.2.4 Outlook

The appliance of nanotechnology in medicine at present includes areas from sunscreen and cosmetics to targeted drug delivery and targeted imaging techniques. The possibility of designing and engineering devices which can interact as biological entities is at the forefront of medically oriented research .This work is an investigation using supramolecular chemistry combined with characterisation techniques QCM, NMR and Fluorescence Spectroscopy of the dynamic interplay between supramolecular assemblies and biointeractions which occur at the cell membrane namely protein-carbohydrate and ion channel-cation interactions.

2 Multivalent binding studied by QCM

2.1 Introduction

2.1.1 Gold Nanoparticles

Gold nanoparticles have become a huge area of interest in the last 15 years with the growth of nanoscience, the desire for controlled assembly at the nanoscale and a greater understanding of supramolecular processes in biological systems. Their size and shape endows them with optical and electronic properties intrinsic to the nanoscale including an intense absorption at their surface plasmon resonance frequency (around 510-530 nm for gold nanoparticles) while also rendering them highly applicable for the study of interactions on the biological scale.

History

Colloidal gold is known since antiquity when it was used to make ruby glass and to colour ceramics. Later ”Soluble gold“ was used up to the middle ages as a form of miracle cure for various diseases and as a dye in different mixed forms. In 1857 Faraday reported the formation of deep red solutions of colloidal gold upon reduction of an aqueous solution of tetrachloaurate using CS_2. Turkevich in 1951 introduced the citrate reduction of chloroauric acid ($H[AuCl_4]$), later refined by Frens it remains to this day a most simple and effective method to produce spherical gold nanoparticles with a degree of size tenability [109-111]. The next major breakthrough in gold nanoparticle synthesis arrived with the two-phase Brust method [112] opening the way for a range of new ligand shell functionalised nanoparticles. Proceeding work then looked for ways in which to control size and shape homogeneity in such systems as well as producing functional nanoparticles in order to exploit their extraordinary properties. The use of gold nanoparticles for biological applications is known since the 1970s with the immunogold staining procedures [113].

2.1.1.1 Gold Nanoparticle Synthesis

2.1.1.1.1 Turkevich Method of Gold Nanoparticle Preparation

As mentioned an early form of controlled nanoparticle synthesis was the Turkevich citrate reduction method [109,110]. Gold nanoparticles are formed by reduction of gold salts back to the element usually in the presence of a capping agent i.e. something to prevent precipitation of the metallic gold due to Van de Waals attraction. According to DLVO (Derjaguin, Landau, Verwey and Overbeek) theory which combines the effects of Van der Waals interaction and electrostatic repulsion [114]:

$$W(D) = W(D)_A + W(D)_R$$

$W(D)_R$ = repulsive interaction energy due two electric repulsion

$W(D)_A$ = attractive interaction energy due to van der Waals interaction.

The long range Van der Waals interaction is overcome in this case by a surface layer of negatively charged citrate ions around which lies another layer of positive sodium counterions ions. Under the right conditions the particles will remain in colloidal solution indefinitely.
This method results in a relatively narrow size distribution for particles between 10 and 20nm and this size can be controlled by adjusting the ratio of citrate to $AuCl^{4-}$ ions [111,115]. The mechanism of particle growth for this preparation has recently been revisited by Pong et al [116] where they describe, in contrast to an earlier widely accepted mechanism known as the LaMer nucleation-growth model [117], how the initially formed 5nm nanospheres self assemble into nanowire structures before fragmenting into segments and forming the final 13nm citrate stabilised particles. This process can be witnessed as a colour change from yellow to dark blue, dark purple, purple and finally ruby red.

2.1.1.1.1.1 Properties of Citrate Passivated Gold Nanoparticles

The nanoparticle size range that results from this thermal preparation goes from 9 up to 120nm by variation of the citrate: gold salt ratio with the drawback being that the quality decreases as you increase the size, with elongated particles forming for the large sizes (>85nm). Best size dispersion (13-16%) can be achieved for particles below 40 nm [115]. The particle concentration is quite limited, below 2 mM in gold salt for stable particles and below 1mM to avoid a concentration dependence for the final size.

2.1.1.1.2 Brust Method of Nanaoparticle Synthesis

An organic solution based synthesis was later developed known as the Brust method [112,118]. This is a two-phase synthesis where a phase transfer catalyst, tetraoctylammonium bromide, is used to transfer Gold (III) chloride hydrate into the organic phase where it is then reduced by $NaBH_4$ to elemental gold in the presence of a stabilising thiol. This preparation results in air stable nanoparticles which handle like an organic compound. Using this method a range of functionalised nanoparticles soluble in organic solvents have been prepared.

Other related one-step procedures in organic media have also been developed. A single phase method was realised in THF thereby allowing the incorporation of a large range of ligands. This method however involves the use of a very strong reducing agent, Superhydride (lithium triethylborohydride) which reduces esters, amides and other functional groups which would otherwise have survived the brust method [119]. A milder single phase method has also been reported which uses $LiBH_4$ as reducing agent again in THF and allows the use of a broader range of ligand functionalities [120]. The Brust method was also adapted to preparing water soluble particles, the gold salt is reduced by $NaBH_4$ in the presence of the passivating ligand with a water-methanol (1:9) mixture as solvent. This procedure was originally demonstrated for 4-mercaptophenol [118] and was later extended to the preparation of AuNPs(gold nanoparticles) with a variety of water soluble ligands [121].

2.1.1.1.2.1. Properties

With the development of the Brust method a whole new range of ligands in the form of organic thiols could be incorporated for monolayer protected gold clusters. The size range of the clusters is controllable through ligand:gold ratio like in the Turkevich case although tighter size dispersions are thought possible using this method. Another advantage is that far higher concentrations in solution may be prepared due to far higher stability against agglomeration and the particles can be stored as stable powders. The stability is somewhat dependant on the thiol structure, with long alkyl chain ligands leading to the most stable particles. Dark brown solutions of moderately polydisperse particles in the size range of 1–5 nm can be obtained, depending on the reaction conditions. The typical ruby red-colour of colloidal gold emerges with particle sizes above ca. 5 nm, the distinctive surface plasmon absorption is absent for smaller particles.

2.1.1.1.3 Surface Bound Ligand exchange to Introduce Functionality

Prepared nanoparticle solutions may have their composition modified through ligand exchange reactions. These exchange reactions are driven by the overall solution thermodynamics whereby an increasing excess of exterior ligand can be used to drive up the percentage replacement although there are a multitude of other factors. The most commonly used method is one that was first introduced by Murray et al. [122,123]. In this approach the initial particle ligands are replaced with functionalised ligands through simple surface-solution ligand exchange to convey particle function.

Citrate replacement has also proven a viable route to optically active functionalised particles [124]. Gold nanoparticles exhibiting both excellent optical sensitivity and stability can be obtained by the synthesis of nanoparticles of homogenous size dispersion with an optimised citrate reduction, followed by surface modification through chemisorption of a thiol derivative. Diameters in the range of 10-15nm provide the best balance between stability, homogeneity and optical activity. When the gold nanoparticles are exposed to a solution of thiols, the interaction of these molecules with the gold surface takes place. To chemisorb, the thiols must displace the stabilising citrate anions that act as protecting agents for the gold colloid. A drawback to this approach is that desorption of this charged species may effect the electrostatic stability and sometimes causes irreversible aggregation [125,126]. Aggregation can be easily observed by a colour change from ruby red to violet to blue. TEM images of these systems reveal the fusion of gold cores [127] leading to the assumption that during electrostatic ligand displacement the electrostatic stability is lost.

There are however cases where this strategy has proven highly efficient such as the work by Field and Russell [99,128,129] amongst others.

2.1.1.1.4 Seeded Growth Approach to Nanoparticle Synthesis

In the pursuit of nanoparticles featuring interesting optical properties, thus larger than 5nm, particles can be grown from smaller seed particles through epithaxial addition of metal atoms. Studies have shown that particles of quite narrow dispersion in the size range of 5-40 nm can be prepared by this method with size control achieved through variation of the seed to metal salt ratio [130-132].

2.1.1.2 Dynamic Properties of Monolayer on Protected Gold Clusters

While dependant on preparation procedure monolayer protected clusters (MPC) or nanoparticles possess some very interesting intrinsic properties when it comes to applications for biorecognition:

Dynamic surface

Thiol mobility has been studied by Rotello and co-workers and has been shown to be limited by intramonolayer hydrogen bonding [133-135]. They noticed a surface adaptation towards increased binding affinity over time for their system based on a mixed monolayer protected cluster interacting with Flavin. This shows that these functional nanospheres possess an adaptive quality which could be vital in the recognition of biomacromolecules. The ligands

can reorganise on the particle surface during interactions to the most energetically favourable configuration. This may in a sense impart on these particles an even higher multivalent affinity through adaptation.

Another example of this dynamic behaviour was demonstrated by X-ray diffraction and reflectivity on particles immobilised at the air-water interface by Nørgaard and co-workers [136]. These mixed monolayer protected particles (hydrophobic/hydrophilic) were deemed environmentally responsive to the hydrophobic effect as their ligand groups were shown to reorganise to give a more stable equilibrium interface.

2.1.1.3 . Gold Nanoparticle Characterisation as applied to Biosensing

2.1.1.3.1 Optical Spectroscopy

The most common and accessible means of nanoparticle characterisation is optical spectroscopy. As mentioned earlier the size and shape of the gold clusters results in an intense surface plasmon absorbance normally from 510-530 nm not present in the bulk metal.

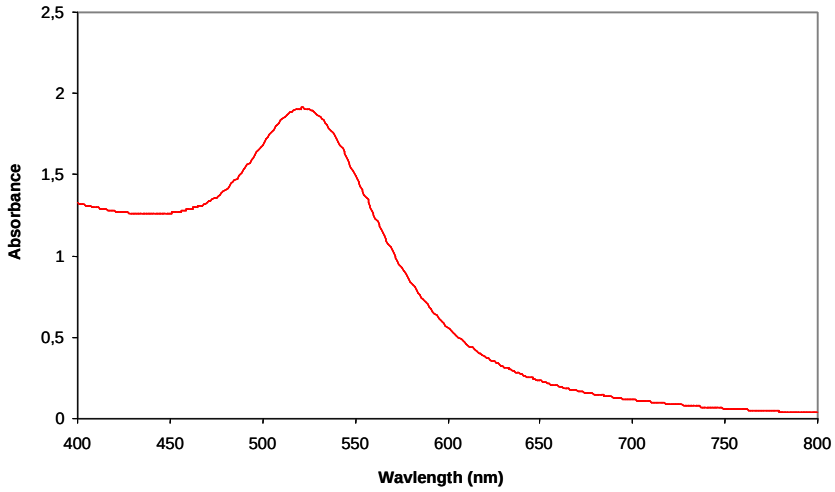

Figure 5 Typical optical absorption spectrum for citrate stabilised gold nanoparticle solution.

This intense absorption is due to the excitation of a surface plasmon resonance. Surface plasmons are surface electromagnetic waves that propagate in a direction parallel to the metal/dielectric interface. Since the wave is on the boundary of the metal and the external medium, these oscillations are very sensitive to any change of this boundary, such as the adsorption of molecules to the metal surface. Information on the states of such colloidal systems can be easily gleaned from optical spectra. The extinction maximum is dependant on particle size, interparticle distance and is also sensitive to surface modification [97,137].

The nature of the surface plasmon absorbance band was rationalised by Mie in 1908 [138]. The resonances denoted as surface plasmons were described quantitatively by solving Maxwell's equations for spherical particles with appropriate boundary conditions. This theory attributes the plasmon band of the spherical particles to the dipole oscillations of the free electrons in the conduction band occupying the energy states immediately above the Fermi energy level [139]. The theory behind the optical properties of nanoparticle solutions has since been developed to incorporate variation in shape, dielectric environment and particle composition [140-142]

The factors affecting the optical absorption include particle size (Figure 6) and shape, metal composition and surrounding medium (Figure 7). Functionalisation of particles also has a significant impact on plasmon absorbance. The commonly used thiolate ligands for example are responsible for a strong ligand field interacting with the surface electron cloud which shows up usually as a red shift in absorbance on comparison to naked theoretical particles or electrostatically stabilised particles of equal size.

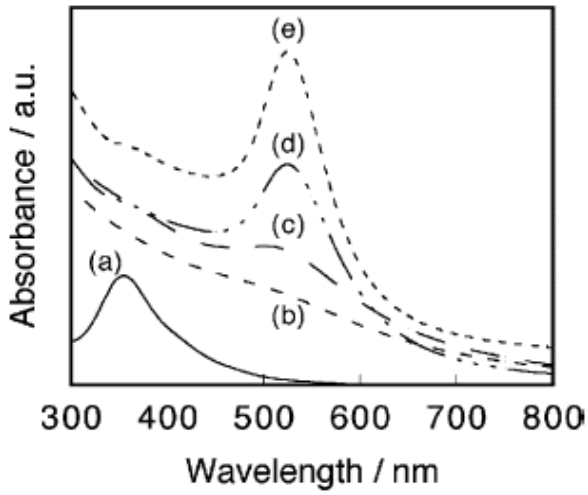

Figure 6. UV-vis absorption spectra of gold nanoparticles corresponding to (a) 1.5 nm, (b) 3.4 nm, (c) 5.4 nm, (d) 6.8 nm, and (e) 8.7 nm. Absorptions due to interactions with surface plasmons feature extinction coefficients that increase with particle size, making particles with average diameters >8 nm appropriate for optical applications [143].

Of particular interest in biological applications is the sensing capability of nanoparticles based on the sensitivity of the surface plasmon band to the surrounding environment (Figure 8). The absorption shows an interparticle distance dependency which is very useful in terms of selective particle aggregation studies using biofunctionalised particles [144].

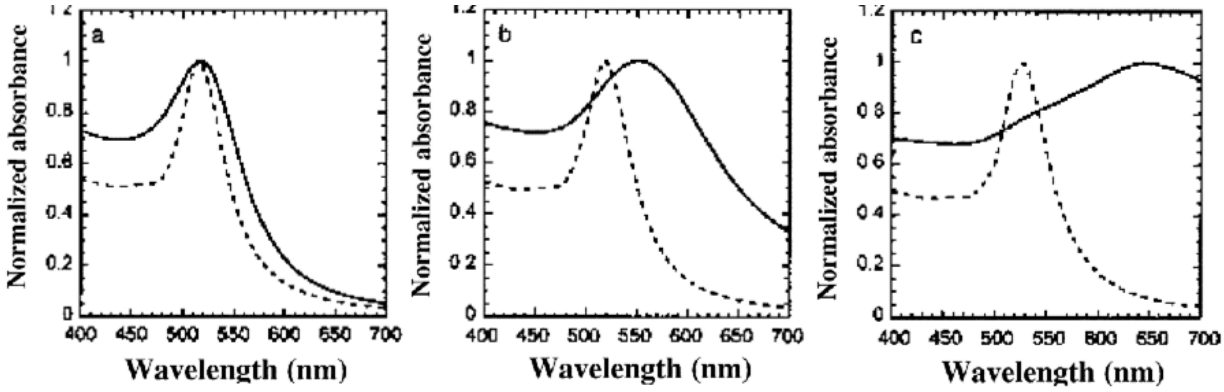

Figure 7 Optical absorption spectra of AuNP's of 8.3nmin diameter dispersed in (a) water, (b)ethanol and (c) chloroform. Dashed lines represent values calculated from Mie theory [145].

When AuNP's aggregate their surface plasmons combine and the aggregate assembly acts as one large particle in its optical behaviour. It has been observed in theoretical and experimental studies that when the individual spherical gold particles come into close proximity to one another, electromagnetic coupling of clusters becomes effective for cluster-cluster distances smaller than five times the cluster radius (d <5R, where, d is the centre-to-centre distance and R is the radius of the particles) and may lead to complicated extinction (extinction = absorbance + scattering) spectra depending on the size and shape of the formed cluster aggregate. This effect is negligible if d > 5R but becomes increasingly important at smaller distances [146]. Aggregation causes a coupling of the gold nanoparticle's plasma modes, which results in a red shift and broadening of the longitudinal plasma resonance in the optical spectrum [147]. The wavelength at which absorption due to dipole-dipole interactions occurs may be varied from 520 nm (effectively isolated particles) through 750 nm (particles that are separated by only 0.5 nm), and the resulting spectra are a composite of the conventional plasmon resonance due to single spherical particles and the new peaks resulting from particle-particle interactions [148]. This interparticle plasmon coupling during biointeraction induced aggregation has been exploited for DNA and antibody detection and colorimetric detection of lectin-carbohydrate interactions using functionalised particles [128,149,150] among others. Non-specific adsorption of biomacromolecules can be minimised by using ethylene glycol based linkers to protect the gold core [151].

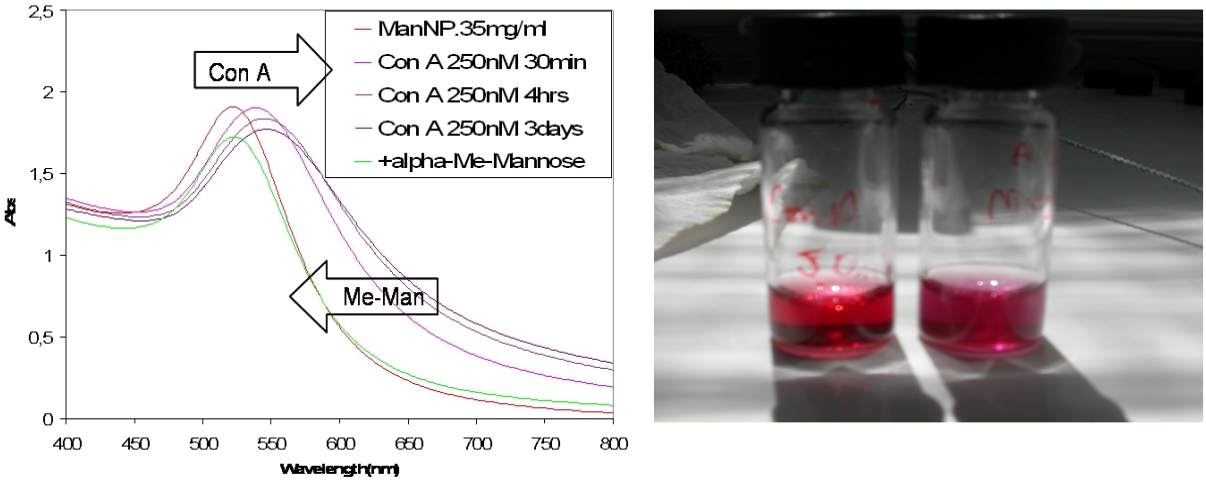

Figure 8 Red Shift due to specific recognition of Con A by mannose functionalised nanoparticles used in present work reversible with excess of high affinity ligand .

2.1.1.3.2 Transmission Electron Microscopy

TEM is a very powerful technique in nanoparticle characterisation as it produces a real image of the gold cores [112,118,152]. Hence it can be used to examine particle size distribution and nanoarray organisation directly (Figure 9). HRTEM can be used to examine individual nanocrystal atomic structure [153] with the highest resolution presently attainable being 0.08 nm. Morphologies of larger particles have traditionally been studied using SEM but for particles smaller than 10nm the resolution limit is approached for this technique.

The mean diameter of the cores taken form TE.M. pictures can be use to determine the mean number of gold atoms, $N_{Au,}$ (Eq 11) [154].

$$N_{Au} = \frac{4\pi(\frac{d}{2})^3}{v_{Au}}$$

Eq 11

Using this data along with elemental analysis which give the Au:S ratio the average number of ligands per nanoparticle can be calculated. This number may also be accessed by XPS (X-Ray Photoelectron Spectroscopy) or TGA (Thermogravimetric Analysis) [155].

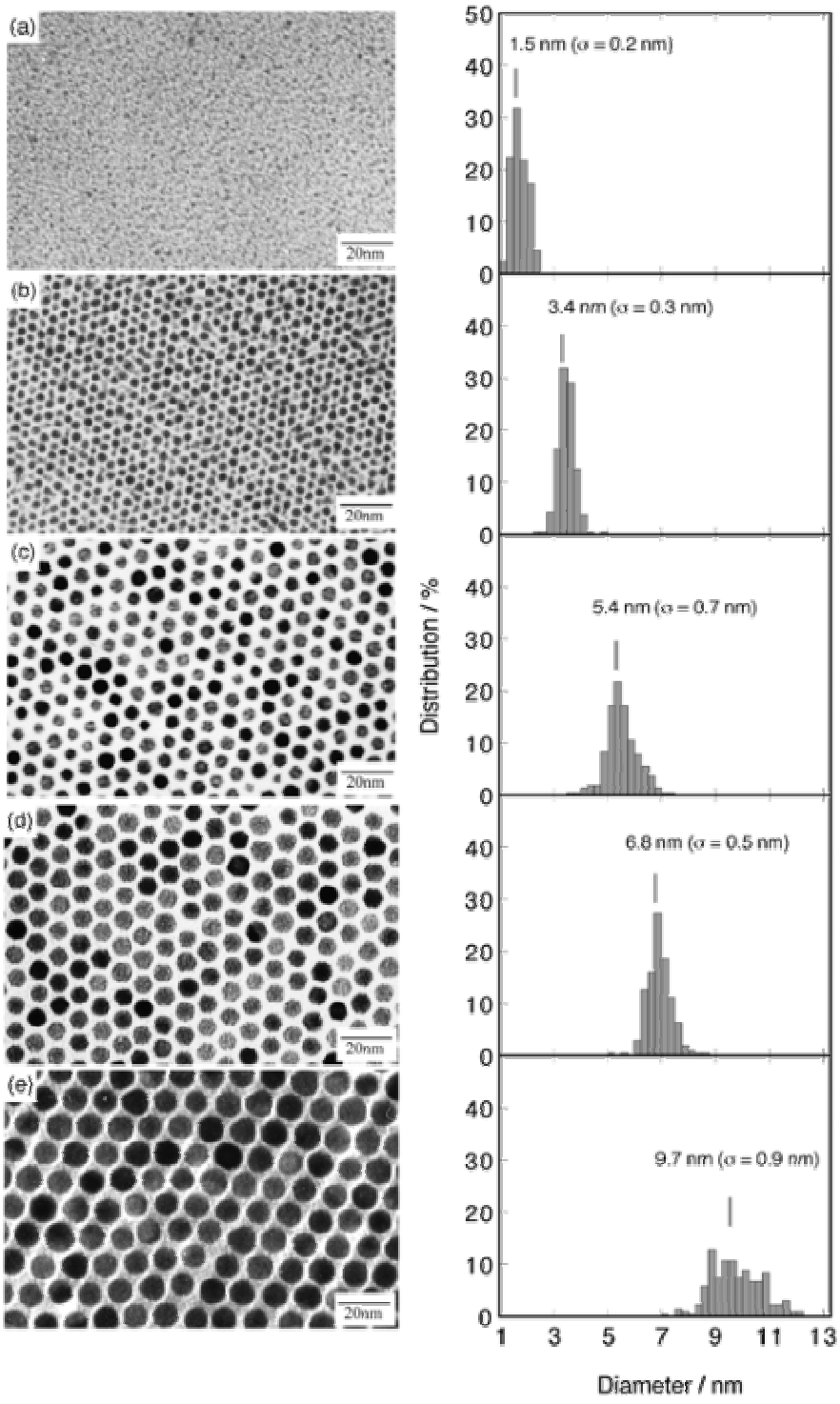

Figure 9. TEM images and size distributions of Brust two–phase method prepared dodecanethiol protected clusters(b) and following heat treatments in the solid state(c)150°C(d)190°C and (e) 230°C [143]

2.1.1.3.3 Nuclear Magnetic Resonance Spectroscopy

NMR studies also have proven useful in nanoparticle characterisation especially for the small MPCs prepared by the Brust method. Purity in terms of removal of ligand excess and phase transfer reagents may be determined given that the ligand atoms close to the gold core give

increasingly broadened signals as the core is approached and the signals from the atoms closest to the core (e.g. C1 and C2 of an alkane thiol) appear to disappear. This characteristic results from spin-spin relaxational (T2) broadening, variations in gold-sulphur bonding sites and gradient in packing density from close to the core out to the ligand peripheries [156,157]. Like NMR spectra for all compounds much structural information on the bound ligands can be deduced.

2.1.2 Nanoparticle-Biomacromolecule interface

The recognition of biomacromolecular surfaces is quite challenging due to the size and structural complexity of the interaction and so the use of scaffolds which can present surfaces with a scale similar to the biological represents an attractive strategy. As such, nanostructures such as nanoparticles, nanorods etc., on which a repertoire of functionalisation techniques has been developed, offer great potential based on this dimensional quality as well as the already mentioned nanoscale characterisation possibilities. One of the most accessible would be gold nanoparticles as they represent the most intensively investigated group of nanostructures with a number of techniques that have been developed allowing a level of size tunability and relatively broad funtionalisation range [158]. With this ability in hand to engineer the nanoparticle-biomacromolecule interface advanced medical applications can be envisaged.

2.1.2.1 Biocompatibility

Highly specific interactions have been demonstrated between functional gold nanoparticles and biomacromolecules including those of high affinity such as biotin-strepdavidin [159] as well as multivalently directed weak interactions involving carbohydrates, mimicking the cell adhesion and recognition processes (2.1.3). Gold nanoparticles appear highly appropriate for biomedical applications given as already stressed their functional tunability, but also their low toxicity. GNPs (gold nanoparticles) are generally found to exhibit very low toxicity in vitro and in vivo depending of course on the functionality but biofunctionalised particles generally show low toxicity [160].

2.1.3 Glyconanoparticles

Glyconanoparticle refers to nanoparticles decorated with saccharide moieties i.e; a metal core stabilised by either polysaccharide or oligosaccharides which as a result presents a biomimetic nanoscale surface with the accompanying properties associated with nanoscale objects.

The applicability of glyconanoparticles to the study of carbohydrate–carbohydrate and carbohydrate-protein interactions stems from their biomimetic nature. These interactions are characterised by high specificity and low affinity (see sections 1.3.2.1, 1.3.2.2) seldom showing association constants beyond 10^6 M^{-1}, the evident affinity of this interaction in nature is effected through multivalent presentation [46,161].

In the study of carbohydrate mediated interactions in a biomimetic manner glyconanoparticles stand out as having a powerful potential. Firstly their size range compares favourably with the biological entities with which they can interact and mimic. Also, their natural structure,that of a monolayer protected spherical platform, lends itself to polyvalent presentatuion of glycosyl moieties as exemplified by the glycolipid regions, glycoprotein presentation and glycocalyx in nature. Lastly with their optical properties they provide a means of interpreting nanoscale interactions quite readily using the simple technique optical spectroscopy as well as electron microscopy.

The present interest in glyconanoparticles appears to have begun around 2001 when the modified brust method for nanoparticle synthesis was developed by de la Fuente et al [121]. Particles functionalised with Le^x [121], lactose, maltose and glucose [162] were prepared using this method. Gold glyconanoparticles have been investigated recently by various groups as biomimetic nanostructures for lectin recognition [128,150] [149,163,164]. Colorimetric sensing of this type of carbohydrate-protein interaction goes back to Otsuka et al [149] where lactose functionalised nanoparticles were shown to bind reversibly to (*ricinus communis agglutin*) RCA_{120} lectin. Later examples of this type of sensing in solution looked at both Concanavalin A and RCA_{120} with mannose and lactose functionalised gold and silver nanoparticles respectively, the high selectivity of such structures was demonstrated for these particles by selective recognition from lectin mixtures [128]. Subsequent work demonstrated how the ligand surface density related to binding affinity in this system [163].
Lin et al. prepared mannose and galactose functionalised gold nanoparticles by a modified Brust method [112,118] and using SPR investigated their inhibitory effects on the binding of Con A to a mannose functionalised biosensor chip demonstrating the suitability of nanoparticles as multivalent ligand carriers and a dependency of the relative inhibition shown on particle size and ligand length and hydrophilicity [165]. Besides being applied for the study of the Lectin interaction glyconanoparticles have also been exploited in the study of the

carbohydrate-carbohydrate [121,166,167] interaction where polyvalency would seem to be even more critical. This interaction was shown to be highly divalent cation dependant through various studies [168,169].

2.1.3.1 Characterisation Techniques for Glyconanoparticle Activity

As already stated (see section 2.1.1.3) nanoparticles possess special optical properties which can be exploited for specific aggregation studies. Glyconanoparticles have been availed of in this manner for colorimetric lectin detection. In their preparation for this type of detection certain parameters are vital in order to optimise the response sought. The absorption spectrum profile is highly dependant on particle size with smaller particles < 8 nm being less suitable. This can be seen with the naked eye as they appear as brown or dark solutions not suited to a colorimetric assay as opposed to particles above 5 nm which form ruby red solutions with a clear optical absorption peak around 520 nm thus highly suited.

Preparation procedure is the determinant of glyconanoparticle core size. Particles prepared by the Penades method of reduction in methanolic solutions in the presence of glycoligand results in an average dimeter of ~2 nm. These particles can be prepared and are stable in in relatively high concentrations and so are amenable to NMR studies of the ligand function [162]. Being too small for NP Plasmon resonanace (nanoparticle surface plasmon resonance spectroscopy) investigation their carbohydrate-carbohydrate interactions have been investigated using surface SPR [166], AFM and isothermal titiration calorimetry [168].
For optical spectroscopy studies a larger nanoparticle is necessary as demonstrated for the same Ca^{2+} mediated carbohydrate-carbohydrate interaction by Russell et al. [167] 16 nm gold particles were prepare by a two step Turkevich reduction followed by ligand displacement giving particles of optimal optical core size. Their results were characterised using transmission electron microscopy along with optical absorption.

2.1.3.2 Glyconanoparticles,Multivalency and the Cluster Glycoside Effect

Returning to the discussion on multivalency and entropy it is accepted that a binding event is accociated with a free energy change ΔG .

$$\Delta G = \Delta H - T\Delta S$$

Eq 12

The Gibbs relation lends an understanding to the forces at play in the association-dissociation of matter when applied to biomolecular interaction. It can give a qualitative understanding based on a balance between the enthalpic contributions of supramolecular interaction (electronic interactions) and entropic contributions of tendency towards systems with increased number of microstates.

Aligning to previous argument on multivalency (see also section 1.3.2.1) the assumption is that in the case of a multivalent ligand interaction the enthalpic contribution will be equal to that of the corresponding sum of monovalent ligand interactions. It can also be considered that other entropic contributions such as “freeing” of water molecules from the binding site would remain consistent on increasing valency.

Biomolecular interactions occur with an entropic cost to the free energy. ”Clustering” of the saccharide moieties can lower this cost in protein-carbohydrate interactions. Glyconanoparticles present high valency saccharide surfaces in generally ordered monolayers. Following the Boltzman understanding of entropy where its value is proportional to the number of possible microstates for the given macrostate W (Eq 13) one could surmise that

$$S = k_B \ln W$$

Eq 13

the multivalent system exhibits a lower number of microstates as a result of ligand fixation while providing an equal or greater(chelate effect) enthalpic contribution hence larger ΔG represented by increased association (Eq 14).

$$\Delta G = -RT \ln K$$

Eq 14

2.1.4 Quartz Crystal Microbalance

2.1.4.1 Principle of Piezoelectric Sensing

QCM sensors work on the phenomenon of piezoelectricity. This mechanical-electrical effect was first reported in 1880 by the Curie brothers describing the generation of electrical charges on the surface of solids caused by pulling, pushing or torsion [170].

While a large number of crystals show piezoelectricity quartz provides the unique combination of mechanical, electrical, chemical and thermal properties that give it standout applicability. A shear strain is induced in an AT-cut quartz crystal when an alternating current

voltage is applied across it through opposing electrodes deposited on its surface. This generates a transversal acoustic wave propagating through the quartz to the contact media.

Initially it was demonstrated that there exists a linear relationship between mass adsorbed to crystal surfaces and the crystals resonant frequency in air or a vacuum [171]. Extension of this observation to study biological interactions was realised with the design of solution based systems and combination of these with microfluidics and controlled surface chemistry. Consequently, QCM has become a highly relevant analytical technique due to it sensitive solution-surface interface measurement capability. It possesses a wide detection range which at the low end can detect monolayer coverage by small molecules.

Sauerbrey provided the first treatment of the effect of mass loading on quartz resonators[171]. He showed that an ideal layer of foreign mass results in a frequency decrease that is proportional to the deposited mass where the resonator was operated in air or in a vacuum. Assuming the density of the crystal and the adsorbed layer were equal then the following equation applies.

$$\Delta F = \frac{-2 f_0^{\,2}}{A\sqrt{\mu_q \rho_q}} \Delta m = -S_f \Delta m$$

Eq 15

f_0 – resonant frequency(Hz)
Δf – frequency change (Hz)
Δm – Mass change (g)
A – peizoelectrically active crystal area (Area between electrodes, m^2)
ρ_q – density of quartz (ρ_q = 2.648 g/cm^3)
μ_q –Shear modulus of quartz for AT-cut crystal ($\mu_q = 2.947 \times 10^{11}$ $g/cm.s^2$)

This equation is valid for a thin, uniform, rigidly attached mass. Application of QCM to biological samples became possible when suitable oscillator circuits for operation in liquids were developed [172]. As the Sauerbrey relationship was formulated for thin rigid films in air or vacuum questions arose as to the validity of the Sauerbrey relationship in liquid media. For a long time it was postulated that a direct quantification of Protein adsorption at functionalised surfaces was possible based on this relationship. However frequency shifts

larger than those observed in air were frequently observed in aqueous media for equivalent proteins.

When used in liquid media other important frequency determining factors have to be taken into account. When in contact with a liquid, the frequency depends on the liquid density and also on its viscosity. This modified resonant frequency shift was treated theoretically by Kanazawa and Gordon [173] and their calculations are valid for rigid films immersed in liquid. However this work is not valid for non-rigid “soft” materials. For soft material layers it was even noticed that in applying Sauerbrey's equation the mass of the viscoelastic layer is underestimated and the result is a “missing mass” which was elucidated in calculations by Voinova et al. [174]. Alongside viscoelastic properties, electrolyte contributions, surface roughness and surface energy changes may have to be considered. For example changes in hydrophilicity can cause very large response changes in QCM as a function of surface roughness [175,176]. Rough and hydrophilic surfaces entrap liquids in small cavities contributing to the overall mass detected. Hydrophobic surface cavities may be unwetted and so contain air or vacuum cavities resulting in an artificially large frequency change on hydrophilisation of the surface. These problems can be kept to a minimum by optimising surface smoothness.

Although on analysing soft material adsorption in liquid environments the frequency shift cannot be translated directly to mass load according to Sauerbrey relationship, the quartz crystal microbalance can however be used for label free analysis of binding events. Concentration dependant measurements of the frequency shift together with the assumption of a linear relationship between ΔF and Δm allow thermodynamic and kinetic parameters of binding events to be determined as has been demonstrated in numerous examples.

2.1.4.2 . Quartz Crystal Microbalance Biosensing

2.1.4.2.1 QCM Biosensing surfaces by Monolayer Assembly

Application of QCM to the study of biologically evolved interactions has been ongoing for the past 20 years. The approaches used for the transduction of biological recognition processes by QCM are enabled through both covalent and physical surface chemistry techniques (see also section 1.4.2.1). Overall QCM has been used extensively in the areas of

DNA hybridisation, protein adsorption studies, immunological systems and also in the areas of protein-protein and protein-carbohydrate interaction which this work is directed towards [177]. In QCM detection of protein-carbohydrate interactions the two main approaches to surface functionalisation have been through self assembled monolayer and adsorbed polymer.

Self assembled monolayer formation based on the well understood gold surface-thiol chemistry remains a highly applicable approach considering the crystal sensor construction. There are many examples of thiol monolayers being used as a first step towards protein immobilisation for QCM measurements but surprisingly few with the direct covalent coupling of a biomolecular recognition element such as a carbohydrate. Examples prepared using carbohydrate SAMs to function as lectin biosensors are known since initially it was shown through investigation by quartz crystal microbalance that self-assembled monolayers of Gb3 mimics having different lengths of alkyl chains prepared on gold surfaces could interact with galactose-specific lectin *ricinus communis agglutin* (RCA_{120}) and Shiga toxins (Stxs) [65]. Later it was shown that the α-Gal carbohydrate antigen interacted in a specific manner with tri-Gal presenting SAMs [178]. ”Click chemistry” was introduced in a later work for the preparation of carbohydrate functionalised crystal surfaces which then showed selective lectin recognition [66] [179].

There are far more examples if one looks to oligonucleotide interactions with the first direct DNA detection using QCM back in 1988 [180]. Following this there were many more studies produced using immobilised oligonucleotide surfaces. These immobilisations were generally performed using biotin-avidin [181], or gold-thiol interactions [182] [183] with varying surface performances ensuing.

2.1.4.2.2 QCM biosensing surfaces by Polymer Adsorption

An alternative approach to SLM assembly is polymer adsorption whereby biofunctional thin films may be adsorbed on the crystal surface and which may be tuned by polymer composition to control non-specific binding. This approach proved successful as applied to carbohydrate-protein interaction by Matsuura et al. through adsorption of lactose bearing amphiphilic polymers on hydrophobic surfaces which then showed RCA_{120} and peanut lectin (PNA) affinity [184]. Carbohydrate surfaces prepared by photo insertion into an adsorbed polymer were tested by QCM and showed the predicted affinities [90] while in the same year a covalently bound glycopolymer demonstrated Concanavalin A detection ability [185].

2.1.4.3 .Advantages and Limitations of QCM for Biosensing

Advantages

QCM sensing eliminates the need for any labelling step to be part of the signal transduction mechanism. Signal transduction can operate in opaque solutions which may be limiting in optical techniques.The technique is capable of detecting subtle changes at the liquid-surface interface such as density-viscosity changes in the medium, viscoelastic changes in the bound layer and changes in the surface free energy.Also in its favour are its relative ease of use and cost-effectiveness and continually improving sensitivity

Limitations

Although improving on a continuous basis the main limitation of the QCM techniques as opposed to other established optical techniques such as SPR is actual sensitivity. A general limit of detection could be described as an alkanethiol monolayer. Therefore the case of small molecule detection falls outside this limit in terms of mass detection. Amplification approaches may be used to overcome this limitiation, either by mass amplification or surface area increase (porous films) (see also section 2.1.4.5).

2.1.4.4 Comparison between QCM and other techniques in Biosensing

In terms of the application of QCM technology to the study of biomolecular interactions the most relevant technique to compare would have to be surface plasmon resonance as they are both surface analytical techniques capable of in situ monitoring of interfacial processes. As described QCM is an acoustic wave device where the QCM oscillation frequency and quality are related to the mass loading and the viscoelastic properties of the adsorbed materials. On the other hand, Surface Plasmon resonance (SPR), another label-free detection technique, is based on the resonance coupling between incident light and a gold surface plasmon wave. In a classical SPR instrument, this occurs at a typical incident angle, causing a minimum in the reflectivity of the p-polarized light beam. The value of this critical angle depends on the thickness and refraction index of any layer adsorbed on the gold surface.
The measured signals are thus proportional to the molecular weight of the adsorbed materials, and can be used to quantify the number density of different types of adsorption [186]. SPR

measures “dry mass” meaning that the signal measured is not sensitive to water associated with macromolecules. This is not the case for QCM where the response may also contain an associated water contribution. Adsorbed molecular mass may thus be more directly discerned from SPR data.

It appears that in most cases the techniques are comparable in terms of resulting sensitivity. Whereas the SPR has the advantage in terms of real sensitivity the fact the QCM technique also measures entrapped water amplifies the gravimetric response and may render it sensitivity comparable in macromolecular binding experiments [187,188]. An added advantage of QCM over SPR is the availability of the QCM-D technique which is a measurement of the dissipation energy. A film that is viscoelastic or “soft” will not fully couple with the quartz crystal’s oscillation and in doing so will dampen it. This damping thus contains information as to the film’s viscoelastic properties and using these results viscosity, elasticity and a more correct thickness than may be estimated with the Sauerbrey relationship can be calculated on fitting to the so called Voigt model.

2.1.4.5 Quartz Crystal Microbalance Signal Amplification

As referred to earlier, a general limitation on QCM sensitivity is the mass of the analyte which is to be adsorbed from solution. At present QCM does not have single small molecule sensitivity The most common procedure for QCM detection of protein-carbohydrate interaction is immobilisation of the small molecule as the surface bound receptor as SAMs [66,178,189] or polymer films [90,103] followed by monitoring of the binding of the relatively large protein giving an easily measurable frequency change. Amplification methods may thus be employed in order to study certain biorecognition processes.

Two previously demonstrated ways in which to achieve amplification are mass increase i.e. the introduction of nanoplatforms such as nanoparticles, vesicles [190] and micelles to carry the recognising small molecule element, another way is by increasing recognising surface area e.g. porous films, MIP multilayers etc [191].
Nanoparticles as frequency change enhancement probes have already been demonstrated for the biotin-streptavidin interaction [192] and also for enhanced DNA detection by QCM. DNA –conjugated nanoparticles can be used to enhance the signal produced upon hybridization to a surface bound single-stranded template [193]. Also in a very recent work a lectin bound

glyconanoparticle layer was shown to act as an enhancer of lectin recognition response when compared to a glyco-SAM [194].

2.1.4.6 . Glycovesicle-Lectin Surface Binding Studies by QCM.

Vesicular aggregates exhibit an important advantage as a biological sensing platform in that they mimic the cell membrane-the site of molecular docking, ligand-receptor binding, and other vital processes (see section 1.1) in terms of progress in health and medical science. In the last two decades an interest has developed in these liposomal aggregates as drug delivery systems with their major advantage being the physiological origin of their components leading to high systemic tolerance. A third point is that they readily incorporate small molecular species either in their aqueous cavity or lipophilic wall. These traits taken together present the possibility of relatively synthetically accessible target directed drug delivery systems [195]. Surveying specifically protein-carbohydrate interaction studies the approaches used have been to modify the phospholipid building blocks [190] or to incorporate glycolipids in the bilayer [196-201]. Vesicles have been used to demonstrate molecular recognition on the QCM platform for interactions such as biotin-streptavidin driven adsorption [202] [203].

Referring specifically to lectin recognition by small unilamellar vesicles there are some noteworthy advantages to using this platform in QCM:
- the phospholipid surface is anti-adhesive towards lectin proteins [204] and so non-specific binding can be avoided.
- glycolipids should easily partition into phospholipids bilayer based structures [205].
- as alluded to earlier a limitation on the QCM technique is the analyte mass. A small unilamellar vesicle has an average molar mass of around $1.5x10^6$ [206].

Another interesting characteristic is the fluidity in the phospholipids bilayer which can allow microdomain formation as is the case for glycosphingolipids in the cell membrane where polyvalent carbohydrate presentation is fundamental to cell-cell interactions. Such fluidity may also confer responsiveness to the recognising vesicle when in the presence of a multivalent receptor.

2.1.5 Plan of Action

The present Project can be described as the investigation of nanoparticles as amplifiers for a Quartz Crystal Microbalance study of the carbohydrate-protein interaction and extension to exploring the dynamic nature of the particles.

It thus involved:

-Preparation and characterisation of glyconanoparticle library suitable for QCM technique (i.e. fully water/buffer soluble, stable, poly-sugar presenting.

-Optimisation of QCM running conditions for the experiments (buffer used, flow speed, surface properties)

-investigation of lectin layer formation

-Investigation of the specificity and affinity of glyconanoparticle interaction with adsorbed protein layers.

2.1.5.1 . Quartz Crystal Microbalance Setup Used

The setup uses a Thickness–Shear–Mode resonator which is composed of an AT-cut quartz crystal sandwiched between two gold electrodes deposited from vacuum. One face of the crystal is in contact with liquid while the other remains in contact with air.

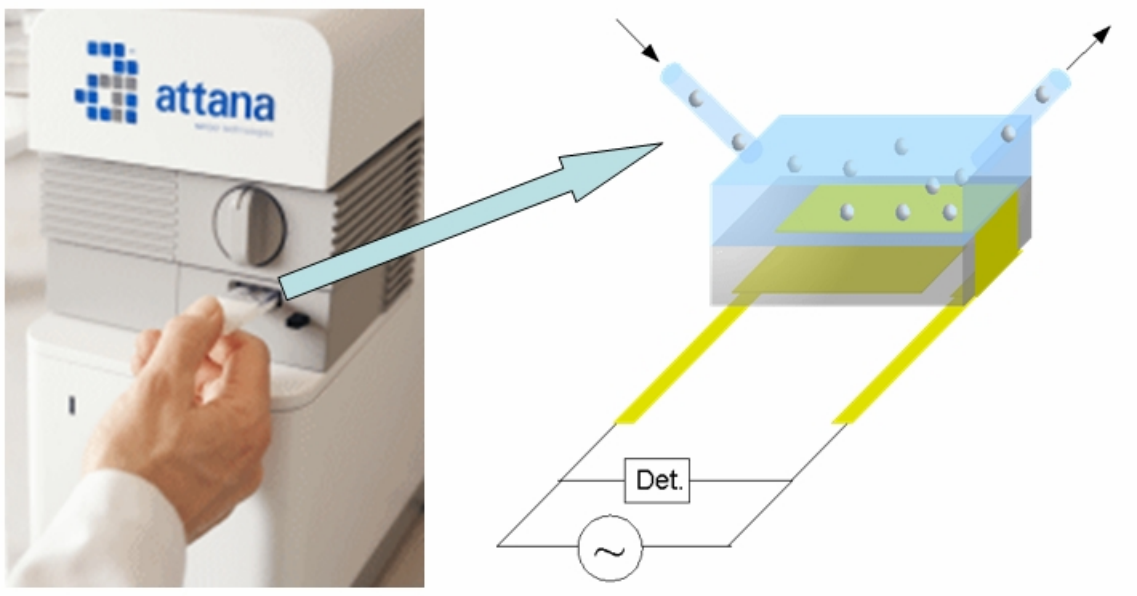

Figure 10 Representation of QCM Experimental Setup

The analyte is passed in a continuous flow in the liquid phase (normally buffer) over the functionalised surface and specifically adsorbed mass can be discerned by transduction to an

electrical signal as described. This combination of microfluidics and quartz crystal nanobalance allows the real-time label free measurement of molecular interactions.
The instrument used was the A100 from Attana Stockholm/Sweden (www.attana.com) where the crystal sensor is setup in a removable holder from which it itself can be removed and chemically modified.

2.2 Results/Discussion

2.2.1 Microscopy on Particles

2.2.1.1 Scanning Electron Microscopy (S.E.M.)

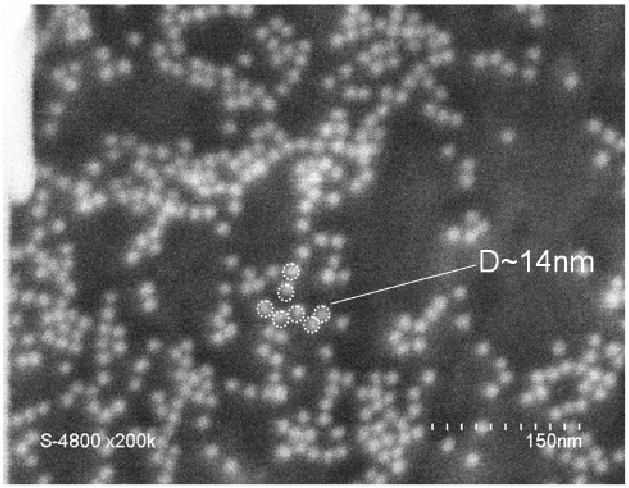

Figure 11 S.E.M. graph of MannoNP's evaporated on aluminium slide.

Highly dilute Glyconanoparticle solutions were evaporated on aluminium slides for scanning electron microscopy characterisation using a HITACHI S-4500 I instrument. The results indicated a homogenous particle size on observation of around 13-14nm (Figure 11). Higher resolution images by T.E.M. indicated a 12 nm diameter for the gold cores (Figure 12).

2.2.1.2 Transmission Electron Microscopy Results

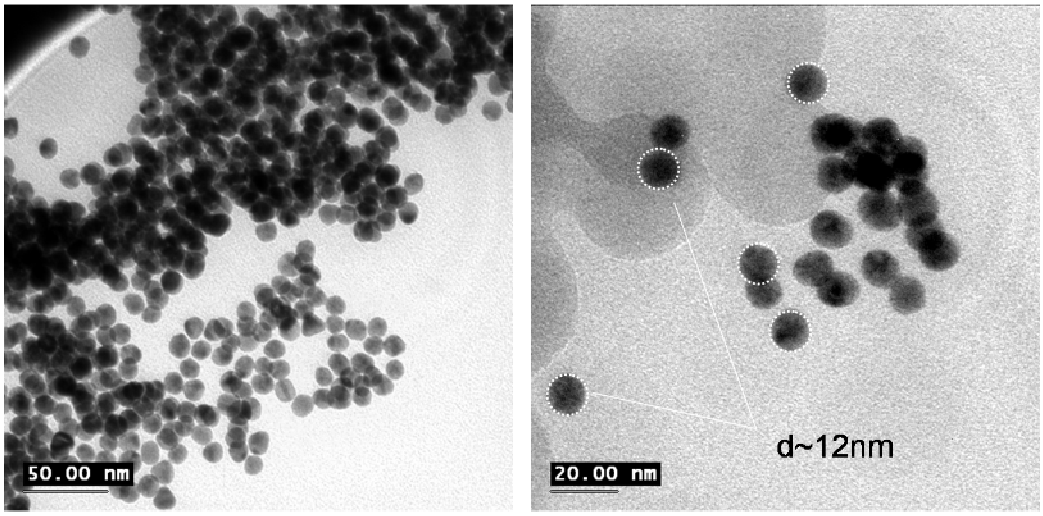

Figure 12 Con A agglomerated thiomannoside functionalised nanoparticles.

2.2.1.3 Dynamic Light Scattering Measurement of Hydrodynamic Radius

Dynamic light scattering measurements can give direct access to the hydrodynamic diameter of spherical nanoparticles. Using the Cordouan SL135 instrument a result of 16.9±1nm was determined. An estimated ligand length of 19Å based on perfect gas geometry optimisation would be in good agreement with a core size of 13nm considering the ligand shell.

2.2.2 Lectin Immobilisation on Quartz Crystal Surface

Concanavalin A was immobilised on gold coated quartz crystals by taking advantage of two types of interaction, a non-specific hydrophobic interaction and by specific mannoside recognition.

2.2.2.1 Lectin immobilisation by Hydrophobic Interaction

That Con A retains carbohydrate activity on hydrophobic immobilisation has been previously demonstrated [207,208]. Gold coated quartz crystals were rendered hydrophobic by cleaning in piranha (H_2SO_4/H_2O_2 7:3 (vol.)) for 30 seconds at room temperature followed by extensive rinsing with deionized water. They were then immersed in 1mM ethanolic solutions of octadecanethiol for 16hrs. Stable layers of Con A were then formed through immobilisation on these octadecanethiol functionalised gold coated crystals from phosphate (10 mM) buffered as well as Tris (10 mM) buffered saline (NaCl 0.1M) solutions (Figure 13). The advantage of this form of immobilisation is its simplicity, with an ease of surface regeneration apparent using surfactant solution SDS .3% w/v (Figure 14).

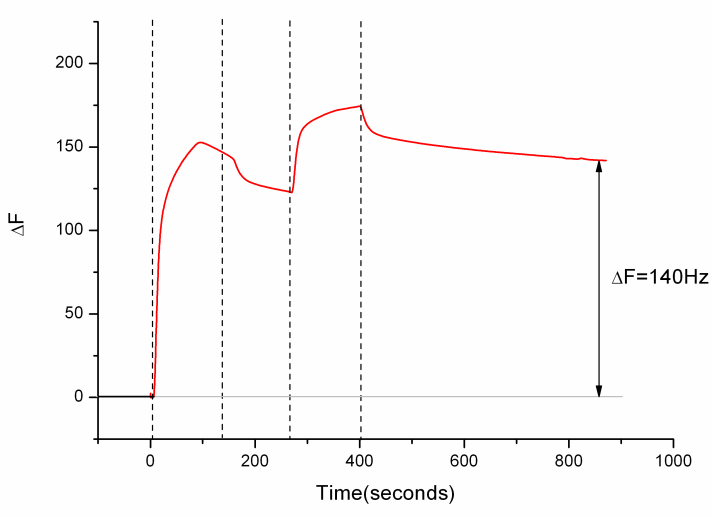

Figure 13 Con A immobilasation on ODT functionalised gold coated quartz crystal.

(Figure 13) and (Figure 14) show the reversible immobilisation of Concanavalin A on ODT functionalised gold surfaces. At t=0 the surface which is under a constantly flowing buffer is exposed to a Con A concentration of 1 μM upon which adsorption occurs as signified by the large frequency change of the quartz crystal setup. The second dotted line represents end of injection whereupon running buffer replaces the Con A containing stream. A second injection was then performed in order to saturate the surface after which the surface was left under the running buffer in order to equilibrate to a stable surface useful for further measurement with particles. Injection of aqueous SDS solutions (0.3%) resulted in complete removal of the lectin layers adsorbed in this manner, regenerating a clean hydrophobic surface (Figure 14).

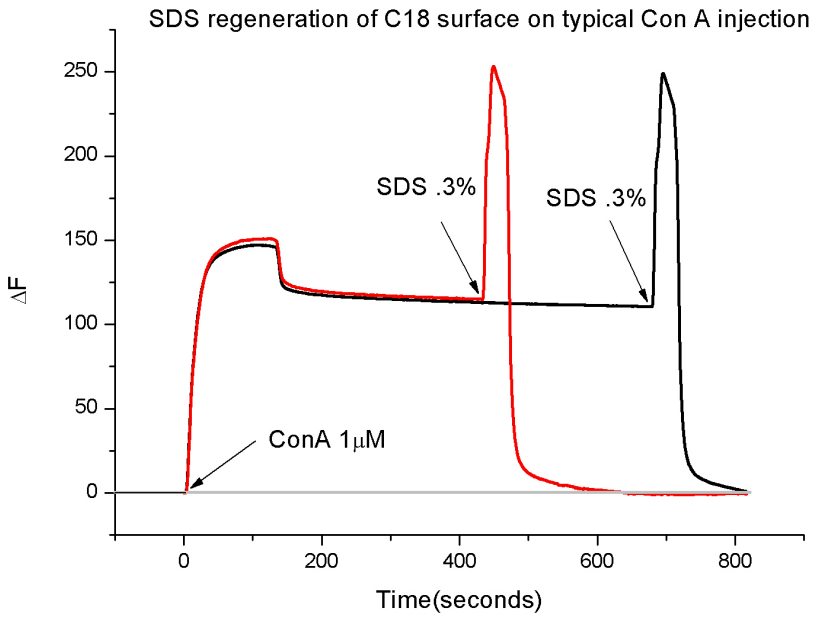

Figure 14 Surface regeneration with SDS solution 0.3%(w/v)

2.2.2.2 Specific adsorption on adsorbed polymer

Specific adsorption through mannoside recognition is another means of Con A immobilisation and can be accomplished with self assembled monolayers (SAMs) or adsorbed films of high specificity. Mannan adsorbed on polystyrene was demonstrated as an effective Con A immobilisation procedure in experiments by Pei et al [209]. By extension of this procedure to an even more hydrophobic surface in an octadecanethiol (ODT) monolayer the surface could be saturated with the polysaccharide giving a stable film through repeated injections at a low concentration (50 μg/ml) (Figure 15). Following this film deposition passing of buffered Con A solutions at 1μM concentration resulted in the formation of lectin layers which stabilised with time (20-30minutes). The mannan film could be regenerated with multiple injections of buffer at pH 1.5.

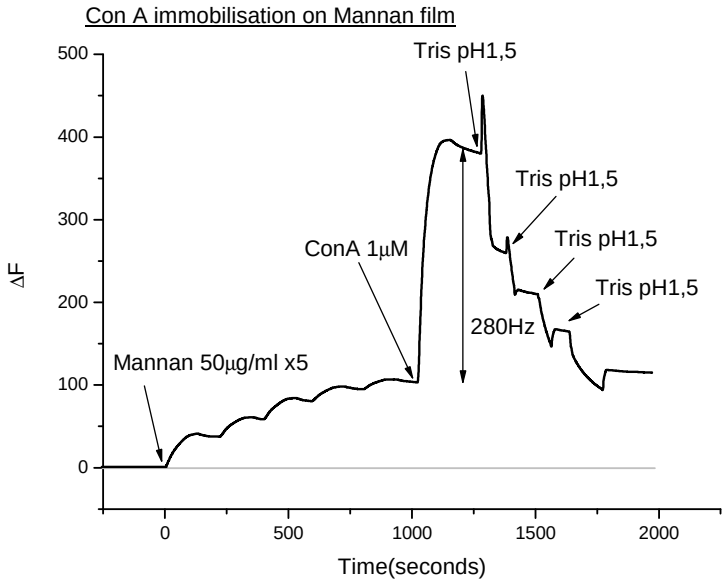

Figure 15 Mannan film immobilisation of Con A to form layer which could be removed through multiple acid injection.

The next goal was then to test the QCM response of these deposed films to glyconanoparticle solutions. The particles were prepared as described in the experimental section by a method similar to Russell et al [129]. These nanoparticles being of optimal size for colorimetric detection were then tested for reversible colorimetric response to selectively recognising lectins. Initially the mannoside functionalised particles were tested for Con A recognition in tris buffered solution (Figure 16). As described (see section 2.1.1.1.1.1) aggregation of nanoparticles based on specific recognition can be measured using UV-optical absorbance. A red-shift in λ_{max} allied to increased intensities at longer wavelengths indicates clustering of

nanoparticles to form larger aggregates due to plasmon coupling. It was shown to be concentration as well as time dependant as could be expected. The important thing was that it also proved to be reversible on addition of high-affinity ligand α-1-methyl-D-mannopyranoside indicating specificity (Figure 16).

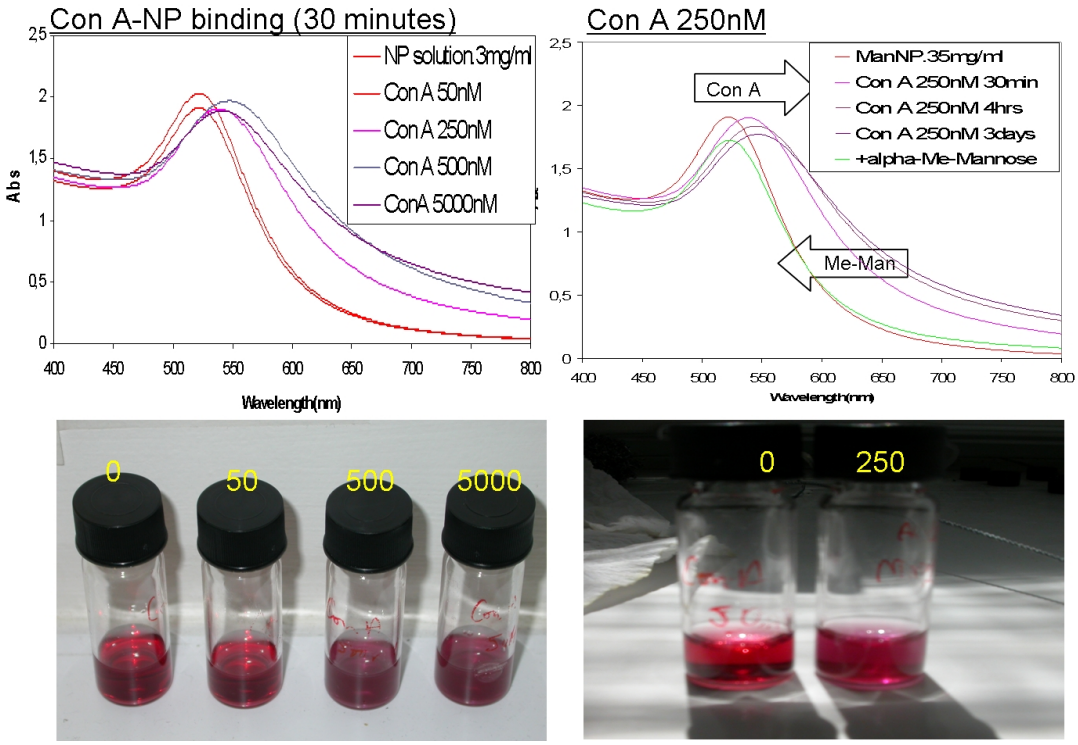

Figure 16 Optical absorption spectroscopy demonstrates reversible Con A driven ManNP agglomeration

This technique was also used to validate the galactoside particles which showed a reversible aggregation with the galactospecific RCA120 lectin (Figure 17).

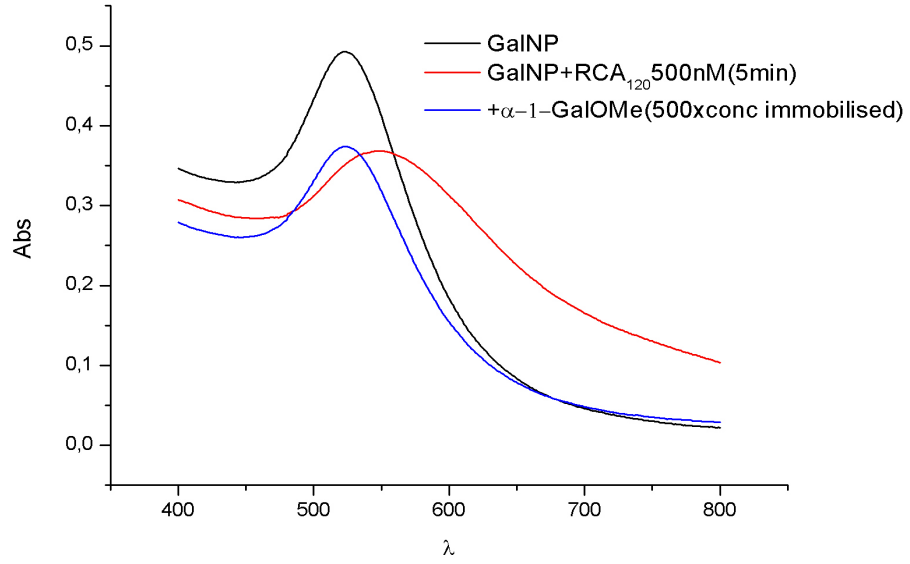

Figure 17 Reversible specific RCA_{120} recognition by GalNPs

Again aggregation was indicated by an increase in intensity at higher wavelengths which on addition of the α-1-methyl-D-galactopyranoside proved reversible as can be appreciated in the presented graph. Glyconanopartcle suspensions prepared and tested in this manner have been previously demonstrated as colorimetric lectin sensors [128] [129] [150] [167] [163].

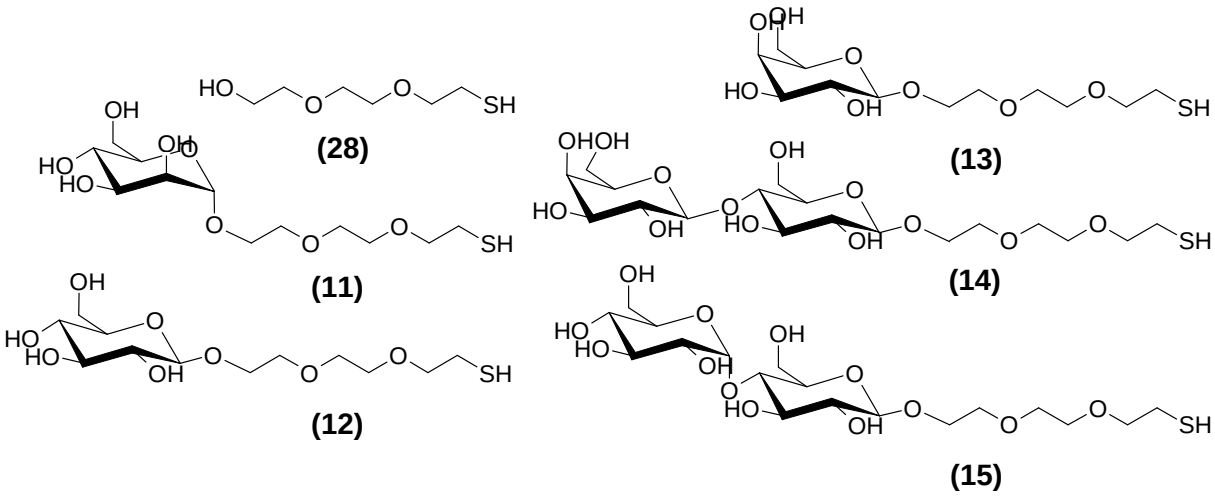

Figure 18 Ligand library synthesised for glyconanoparticle preparation.

The particle library was prepared from the six synthesised thioglycosides (Figure 18): mannoside **(11),** glucoside **(12),** galactoside **(13),** lactoside **(14)** and maltoside **(15)** as well as the 2-(2-(2-mercaptoethoxy)ethoxy)ethanol **(28)** functionalised control particles (see Experimental Section (6.1) for synthesis details). Glyconanoparticles prepared by surface self-assembly on citrate passivated particles of homogenous core size and purified by

centrifugation were diluted in tris buffer. The solution concentrations were diluted to an identical concentration according to optical absorbance measurements (Figure 19). The LactoNPs however appeared unstable and showed signs of precipitation and so were not tested. The concentration of gold cores in the solution could be calculated according to a theoretical study using multipole scattering theory developed by Haiss et al. [210].

$$N = \frac{A_{450} \times 10^{14}}{d^2\left[-0.295 + 1.36\exp\left(-\left(\frac{d-96.8}{78.2}\right)^2\right)\right]}$$

Eq 16

Knowing from T.E.M. images that the particle diameter is around 12nm and using the previous equation, where N represents the number density=N/V, nanoparticle molar concentration can be calculated for the NP dispersions.

$N = A_{450}$ x $5.5745.10^{12}$

$N = 5.2265 \times 10^{12}$

$C=N/N_A=8.679 \times 10^{-9}$ M

The number of ligands per particle can also be estimated assuming complete close-packed monolayer coverage [211] which gives a surface coverage of 196 pmol cm^{-2} . A 12 nm particle if perfectly spherical would have a surface area of $4.52x10^{-12}$ cm^2 giving $8.85x10^{-10}$ pmol. This number corresponds to 533 thiols per 12 nm particle.

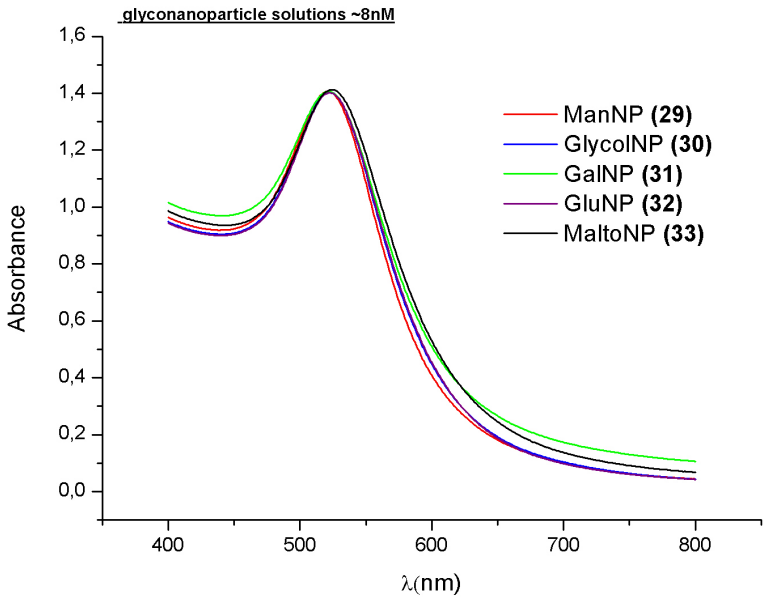

Figure 19 Optical absoption Spectrums of GlycoNP solutions adjusted with buffer to equal absorbance intensity.

2.2.3 Glyconanoparticle interaction Studies

The so prepared glyconanoparticle solutions at equal concentration and of identical gold core size (Figure 19) were injected. Concanavalin A films were prepared as described and the NP solutions were passed into the QCM flow in order to observe their surface interactions. It was noticed that Maltoside and Mannoside glyconanoparticles were bound selectively, with the protein layer being resistant to the other particles and with no signs of non specific adsorption (Figure 20). These results indicated that the present system was indeed highly specific based on sacharride form and that forming Con A layers by physical and specific adsorption resulted in layers which could still specifically recognise. This is presumably a result of Concanavalin A's tetrameric structure which due to shape constraints should only occupy two of its four binding sites upon surface immobilisation leaving two sites free presented to the liquid media for further interaction.

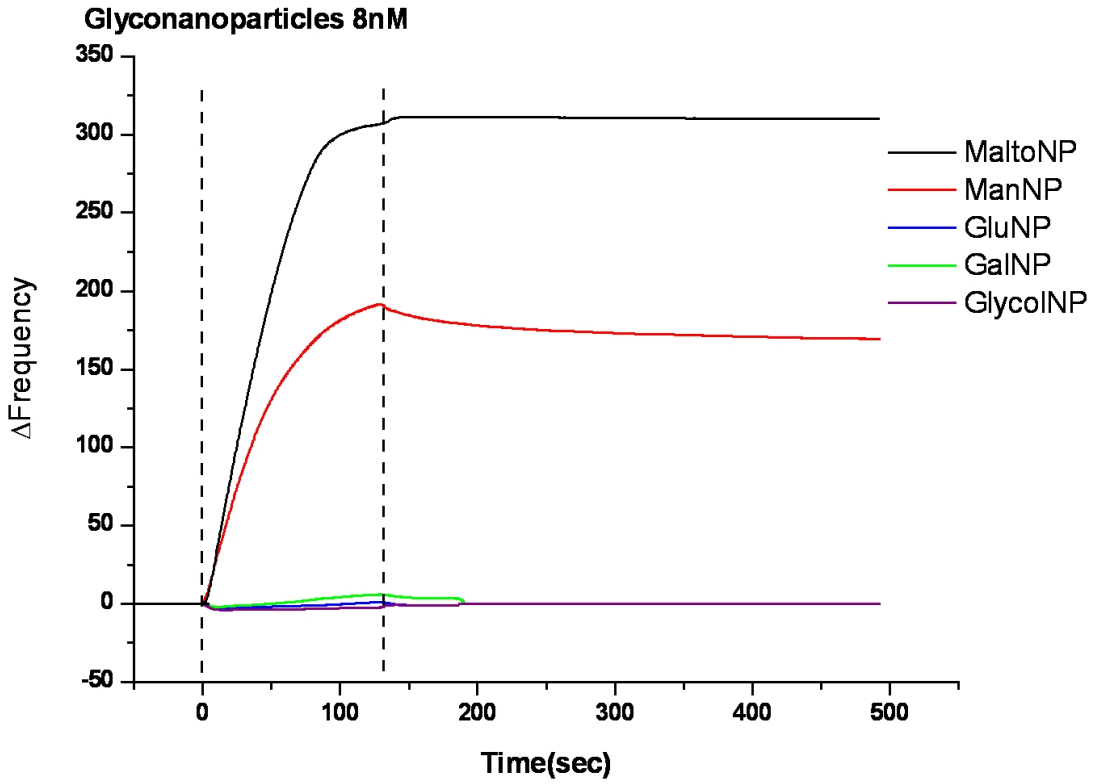

Figure 20 Comparison of different glycoNP solutions of identical concentration and core size

When the particles were tested on hydrophobically and galactomannan film immobilised RCA $_{120}$ (Ricinus Communus Agglutin) no affinity was observed for any particles. While the hydrophobic immobilisation may have a more detrimental effect on the RCA_{120} lectin's sugar recognising activity, an explanation for the lack of particle recognition by specifically bound lectin can be found in the tertiary structure. Unlike Con A, RCA_{120} possesses two and not four

active sugar binding sites on its homodimeric structure. It forms an elongated molecule of dimensions 12 nm x 6 nm x 4 nm [212] with two active sugar binding sites [213] 10 nm apart towards one side of the structure which would allow two sites to bind a 2-D surface. With such a structure, upon specific immobilisation this lectin can be rendered inactive to further specific carbohydrate interaction.

Further to this, a tetrameric galactose specific legume lectin PNA was tested in a similar fashion but again showed no affinity for particle library. This lectin, like Con A, exhibits a tetrameric structure at physiological pH and has four active saccharide binding sites [214] (Figure 1). It also showed galactose specific activity in solution by UV but when it immobilised did not. These lectins could be tested using covalent tethering for surface immobilisation in future work which could allow their activity be transferred from solution to the surface format.

2.2.4 Con A Immobilisation Method Dependant Binding Affinity

The immobilised lectin layers showed different affinity depending on the immobilisation procedure used (Figure 21, Figure 22).

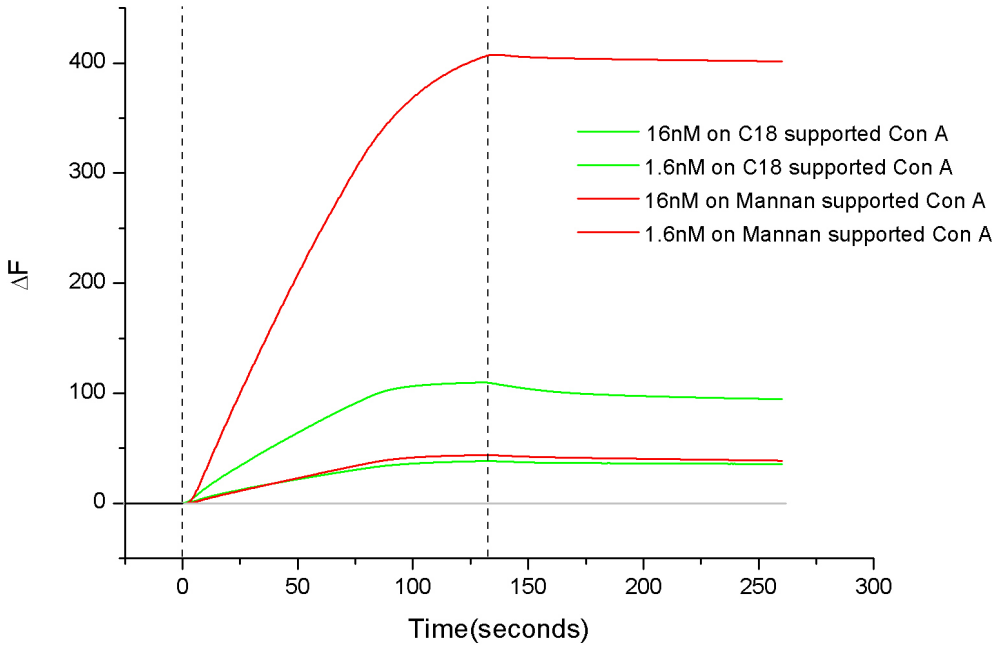

Figure 21 Mannoside nanoparticle injections (16nM and 1.6nM in nanoparticles) on immobilised Con A layers.

Con A adsorbed in a specific manner (i.e. on polymannoside) showed increased affinity, which was especially marked in the maltoside nanoparticle case. This could be expected as physical adsorption through the hydrophobic interaction may result in random orientation and have undesired structural effects lowering activity. On the other hand specific adsorption on a Mannan film should result in a favourable orientation and high activity for the Con A tetramer.

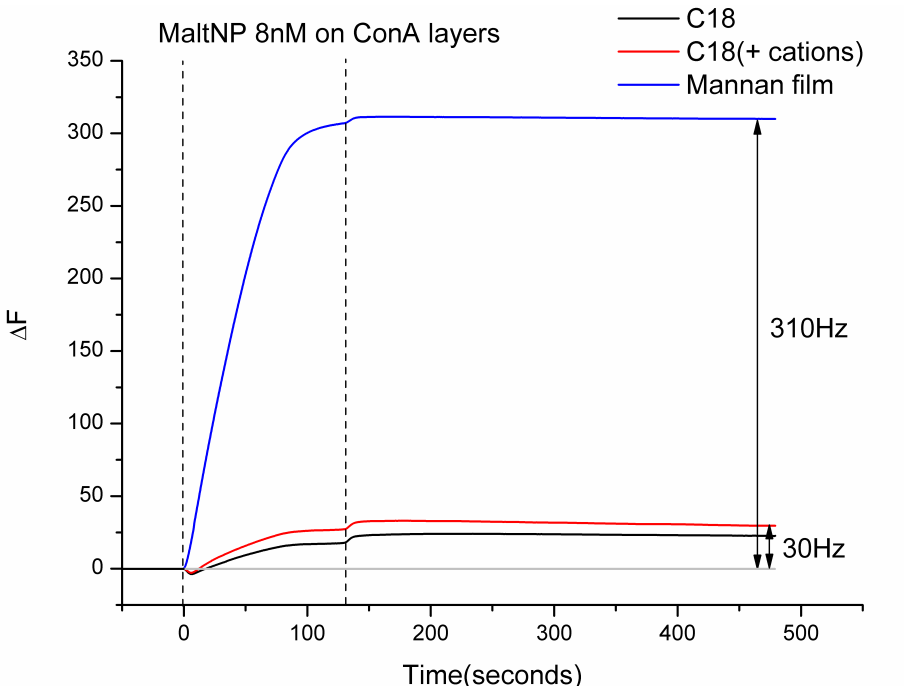

Figure 22 Maltoside nanoparticle injections on immobilised Con A layers.

2.2.5 Association Constant Estimation

In order to obtain apparent affinity constants of these glyconanoparticles for Con A a concentration assay was run with the results fitted to the Langmuir adsorption model [215]. The Langmuir adsorption model is commonly used for obtaining binding properties in surface based senor assays. It is based on the equilibrium relationship between the concentration of a compound adsorbing to binding sites from a liquid or gas and the resultant fractional occupancy of those binding sites limited by certain assumptions:

- A uniform surface.

- A single layer of adsorbed material.

- All sites are equivalent.

- Each site can hold at most one adsorbing molecule.

- There are no interactions between adsorbate molecules on adjacent sites.

- Constant temperature.

$$\theta = \frac{K_{eq}[C]}{1 + K_{eq}[C]}$$

Eq 17 Langmuir Adsorption Equation

Such a simple model is bound to have some limitations and so it does. In reality already adsorbed molecules may have some influence on their adsorbing neighbour, more than monolayer adsorption may also occur.

It is however valuable in that it gives access to an apparent binding constant and so allows the evaluation of surface affinity in at the very least a comparative manner. In terms of QCM measurements ϑ the fractional occupancy can be approximated by $\Delta F / \Delta F_{\max}$ giving

$$\frac{\Delta F}{\Delta F_{\max}} = \frac{K_{eq}[C]}{1 + K_{eq}[C]}$$

Eq 18

which can be rearranged to give :

$$\frac{1}{\Delta F} = \frac{1}{\Delta F_{\max} K_{eq}[C]} + \frac{1}{\Delta F_{\max}}$$

Eq 19

Plotting of $1/\Delta F$ against $1/\Delta C$ can thus give access to the association constant by fitting of a straight line (Figure 24).

2.2.5.1 ManNP Interaction

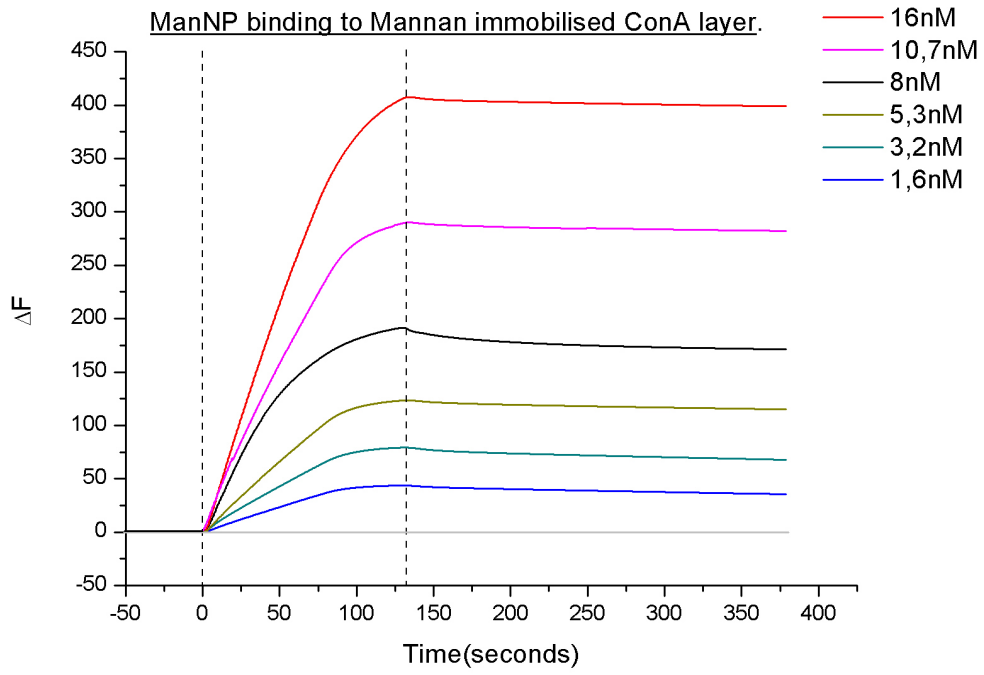

Figure 23 Concentration assay for ManNP (29) binding on specifically immobilised Con A layer.

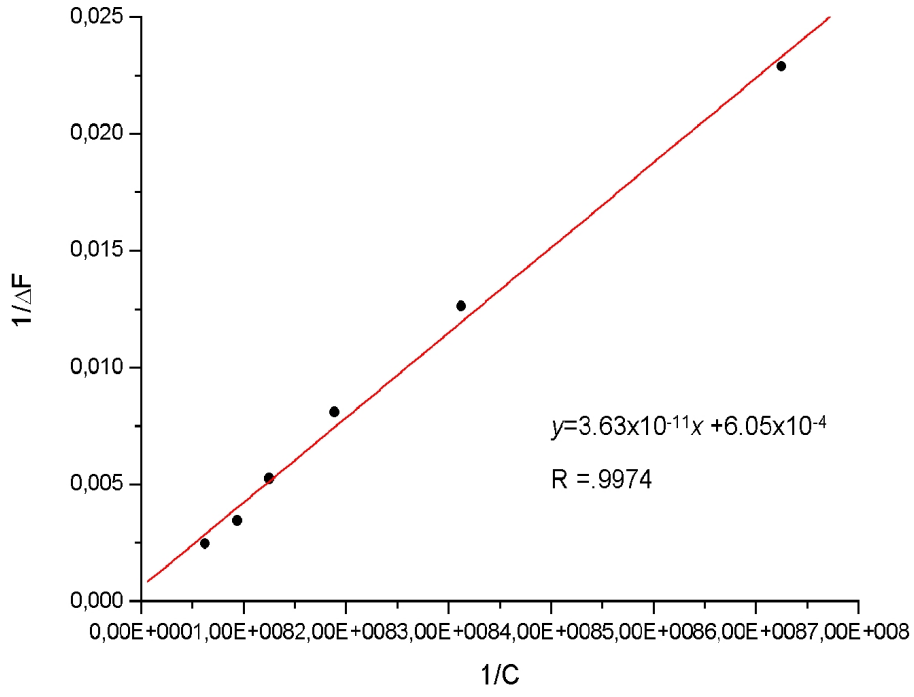

Figure 24 Plot of Langmuir relation allowing determination of K_{app} for ManNP (29).

Application of this model to the α-linked-mannose presenting nanoparticles gives an apparent binding constant: $K_{app} = 1.6 \times 10^{7} M^{-1}$

2.2.5.2 MaltNP Interaction

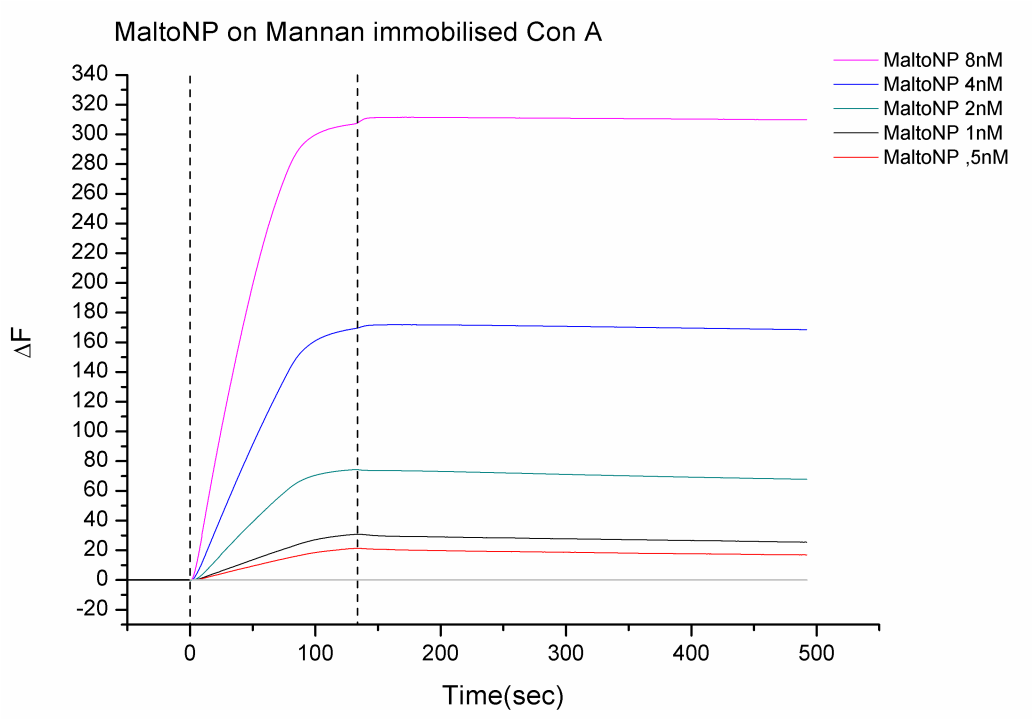

Figure 25 Binding Assay for MaltoNPs (33) on Con A layer.

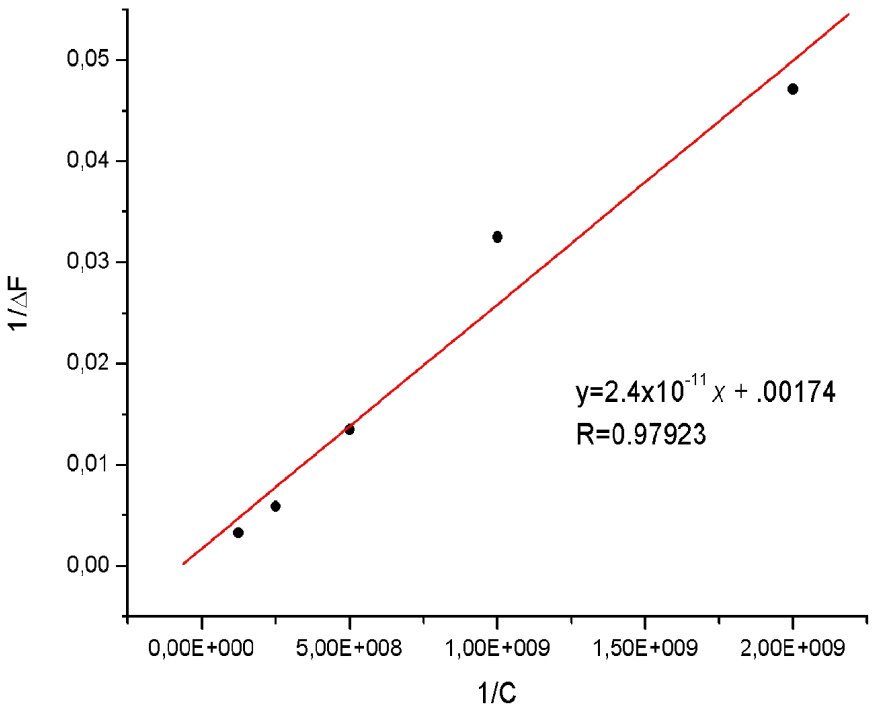

Figure 26 Plot of Langmuir relation allowing determination of K_{app} for MaltoNP (33).

$K_{app} = 7.2 \times 10^{7} M^{-1}$

The preference of Concanavalin A for a-configuration glycosides is exhibited by the high maltoside affinity against the lack of affinity fo glucoside nanoparticles. The glucose moieties are bound in the β-configuration on the glucoside nanoparticles **(30)** whereas the maltose (4-O-α-D-glucopyranosyl-D-glucose) moieties present a terminal α-linked glucose (**Erreur ! Source du renvoi introuvable.**) on **(33)**. Concanavalin A shows a selectivity for the α-configuration in its monosaccharide binding properties [216] and this can go some way towards rationalising this result. Such a glucose configuration dependant affinity difference has been demonstrated previously for polymer films [217] and by affinity chromatography [218] [219].

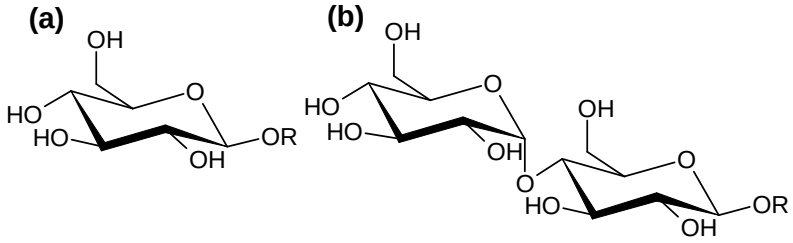

Figure 27 Glucoside (a) and Maltoside (b)

Somewhat surprisingly the maltoside functionalised particles appear to show a higher affinity than the mannoside ones. Looking to the literature, reports on colorimetric aggregation tests with Con A Maltose particles have shown a detection limit of (8.0×10^{-8} M) [164] for Concanavalin A in solution whereas Mannose particles of more or less equal diameter have shown a detection limit of ($4x10^{-8}$M) [128]. Searching affinity constant comparisons in structurally similar interactions in the literature, that is, multivalent presention of monosaccharide and disaccharide the following numbers can be found:

Table 1 Literature reported affinity constants (K_a) for Con A–Mannoside interaction in multivalent presentationsusing surface based characterisation techniques.

	QCM	**SPR**
glycoNP	$2.24x10^{7}M^{-1}$[194]	$4.3\ x10^{8}M^{-1}$ (diam 20nm) [165]
glycoSAM	$8.7x10^{5}M^{-1}$ [66]	$3.9x10^{6}M^{-1}$ [66] $5.6x10^{6}M^{-1}$ [220]

These reported figures agree quite well in range with the results presented for mannoside nanoparticles. The 2-D glycoside presentation show lower affinity constants than the 3-D nanoparticle presentations which could be rationalised in terms of surface area considerations [194] but some clustering causing deviation from the perfect monolayer assumption could not be ruled out which would lead to exaggerated binding constants in these mass sensitive techniques. This multivalent presentation brings the affinity into the range of neoglycoproteins (K_a =10 ^{8}) [221]. Considering that the relative affinity constants (K_a) of $8x10^3M^{-1}$ for MeαMan, $2.7x10^3M^{-1}$ for MeαGlu and affinity constants of $2.88x10^3M^{-1}$ [222], $1.1x10^3M^{-1}$ [223], $2.1x10^{-3}M^{-1}$ [224] and $1.6x10^{-3}M^{-1}$ [225] reported for D-Maltose it seems odd that the inverse ratio of affinity appears for the glyconanoparticles.

The concept of an extended binding site was introduced to explain the apparent 60-fold affinity increase on going from the MeαMan to the trisaccharide Manα1,6(Manα1,3)Man. A structural basis for this increased affinity can be described based on an increased number of favourable protein-saccharide contacts. The first Con A complex to be crystallographically determined was a tetramer of Con A with MeαMan at each of the four binding sites [36,226]. Subsequent determination of Con A in complex with the disaccharides, Man-α-(1→6)-Man-α-OMe and Man-α-(1→3)-Man-α-OMe [227] found the O-1-linked mannose to occupy the monosaccharide binding site in an analogous fashion to α-MeOMan. Similarly, the crystal structure of a trisaccharide, Man-α-(1→6)-[Man-α-(1→3)]-Man [40] found the 1→6 terminal mannose to occupy the monosaccharide site. The central reducing sugar in the core and the 1→3 terminal mannose occupied an adjacent extended region of the binding groove, also making direct polar and apolar contacts with the protein. A resultant affinity of $4.9x10^5M^{-1}$ [44] has been reported.

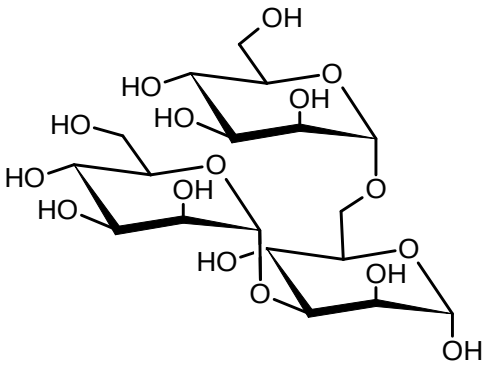

Figure 28 Trimannoside core Man-α-(1→6)-[Man-α-(1→3)]-Man

Extension of this extended binding enhanced affinity to maltosides does not appear to concur with the reported affinities where as stated MeαGlu shows higher affinity than maltose indicating a negative influence on the binding energy by the secondary glucose moiety. In a previous study on affinities of α-glucobioses by Oda et al. they noted that similar affinities to MeαGlu in all cases, the contribution of the second glucose residue being almost equal to that of a methyl group [219].

In reference to this apparent switch in selectivity, there are cases reported where the selectivity of a ligand can switch going from solution to a polyvalent format, as shown for the BP lectin (Bauhinia purpurea) [228]. It was noticed that this lectin bound to carbohydrate layer in a ligand density dependant manner showing a switch in selectivity as density was increased which led to the following proposition by the authors:

"It is even conceivable that different proteins may bind to the same carbohydrate ligand, albeit at different surface densities. We propose that changes in the expression levels of cell-surface carbohydrates may permit switching not just from an off state to an on state, but from one on state to another on state".

These results suggested that secondary interactions contribute greatly to protein avidity. In the present work the unusual results could be accounted for by appreciating that the structural organisation at the recognising interface may have an important impact on the results. In the case of maltoside NPs **(33)** the glucose moiety is separated by another glucose from the glycol linker, thus the recognising sugar may have more freedom or may enter the binding pocket more favourably with the second saccharide also interacting favourably with the protein as is seen in most lectin-carbohydrate intractions. This is as opposed to the anti-adhesive glycol groups for the mannoside NPs **(29).** However as Maltose have been shown to exhibit affinities similar to or slightly lower than MeαGlu this could be determined more by this anti-interaction glycol rather than increased favourable interaction.

2.2.6 Multilayers

Materials composed of 2-D an 3-D ensembles of nanoparticles are becoming increasingly important in analytical and material chemistry. Multilayers fabricated through layer by layer

assembly appear a promising route towards controlled film morphologies at the nanoscale. Previous examples are predominantly based on bifunctional covalent cross-linkers and electrostatically passivated particles [229-231]. Supramolecular layer by layer assembly based multivalent supramolecular interactions have been described for dendrimers and functionalised nanoparticles [232] with assembly using large biomolecules limited to a few cases such as nanoparticle–myoglobin multilayers based on electrostatic interaction resulting in highly stable multilayers [233] and later with the similar protein lysozyme and also following a LBL (layer by layer) electrostatic technique [84] [83]

Gold nanoparticle-biomacromolecule hybrid multilayer films have grabbed an interest again based on their colorimetric properties as well as electrochemical sensing capabilities [103] [234]. As plasmon coupling is a distance related phenomenon multilayers changing in physical composition,such as may occur on water absorbtion, may show colour changes due to changing interparticle distances which can be easily quantified using optical spectroscopy on for example a glass slide.

Accordingly the present system was examined for suitability in preparing nanoparticle–lectin composite multilayers organised through specific carbohydrate lectin recognition .The experimental conditions were as before to build the initial Con A layer on mannan (2.2.2.2). A Con A saturated surface once exposed to a ManNP solution and binding a stable layer of particles can then bind more Con A in the next injection and layers could be built up. Layers formed in situ could be easily broken down with an excess of the high affinity ligand (Methyl-α-D-mannopyranoside) (Figure 29). The plot shows initially three Concanavalin A injections on an adsorbed mannan film to give a saturated layer. This was followed by an injection of the mannoside nanoparticles **(29)** at a concentration of 16nM. A further Con A injection was followed by a 16nM nanoparticle which showed increased binding perhaps due to increasing surface area. Three injections of Methyl-α-D-mannopyranoside selectively broke down the layer to the original Con A on mannan film.

This observation was then extended to fully saturated lectin-nanoparticle-lectin multilayers (Figure 30).The initial layer was again a Mannan film followed by Con A until saturation then ManNP until saturation. An interesting point in the multilayer deposition is that ManNP saturation occurred at a ΔF of ~1600 which fits very well with the langmuir adsorption model where based on the ManNP concentration assay $\Delta F_{max} = 1652$.

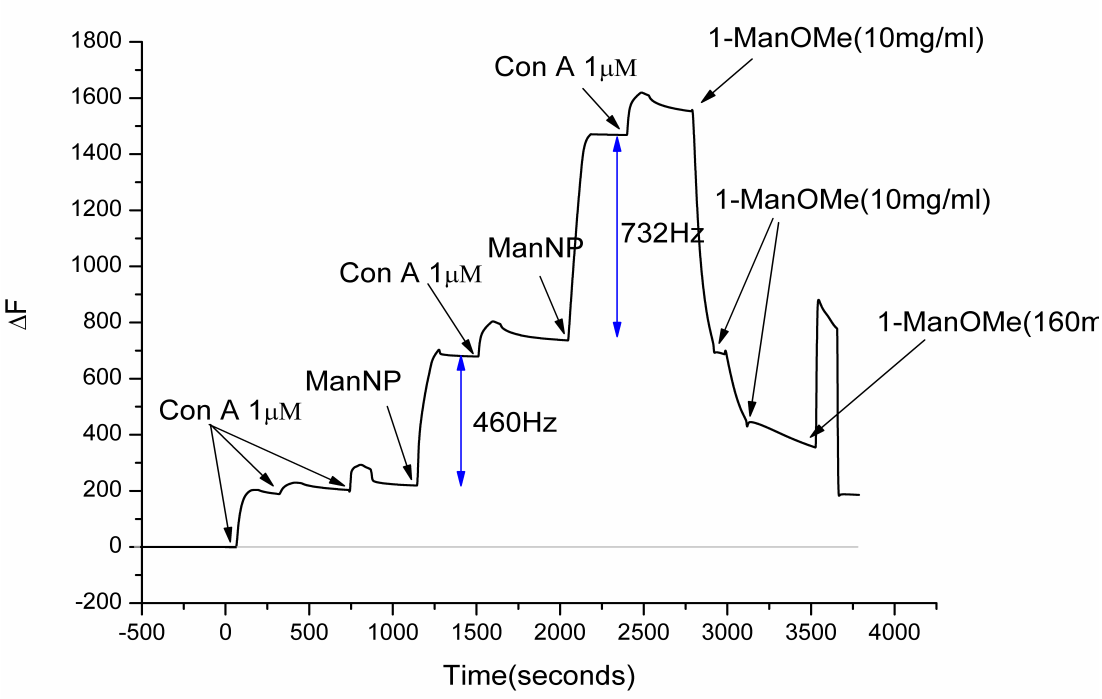

Figure 29 Frequency profile showing build up and specific removal of lectin- nanoparticle multilayer.

Based on this QCM measurement it appears that indeed multilayered structures can be built up in an LBL fashion.Stability in air or vacuum is a highly desirable factor in multilayer films and stability was the issue which caused problems in attempts at further characterisation through electron microscopy for the present work. The multilayer built from biospecific interactions had to be maintained in its buffer conditions and so some other type of in-situ measurement would be necessary to further characterize.

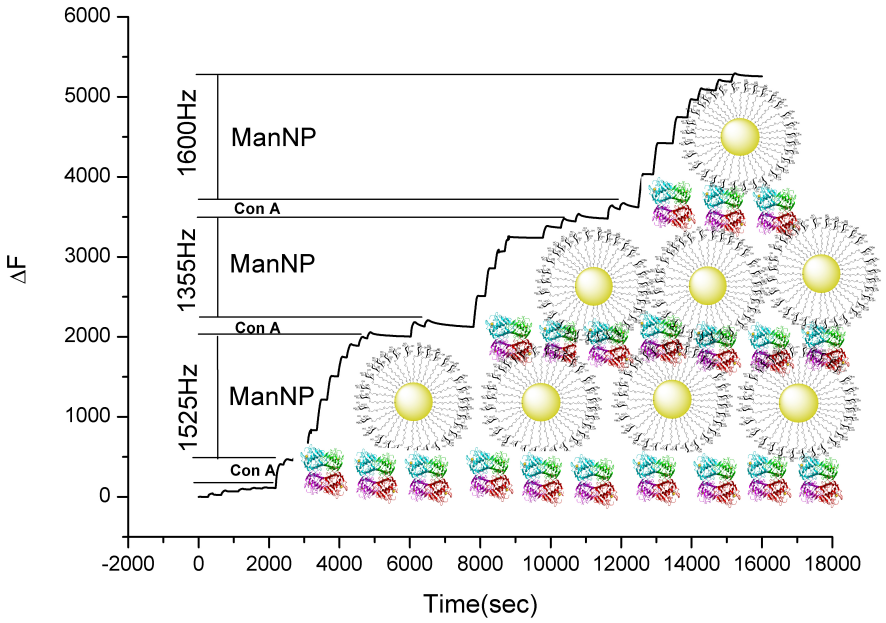

Figure 30 In situ QCM monitoring of LBL Multilayer construction by specific biomolecular recognition.

2.2.7 Alkylglycoside functionalised Small unilamellar vesicles

In a related investigation, small unilamellar vesicles having a range of alkyl glycosides partitioned amongst their phospholipid assemblies were tested for interaction with the said Con A layers by QCM. The ligands were prepared using a Huigsen 1,3-dipolar cycloaddition between glycosyl azides and tetradecyne.

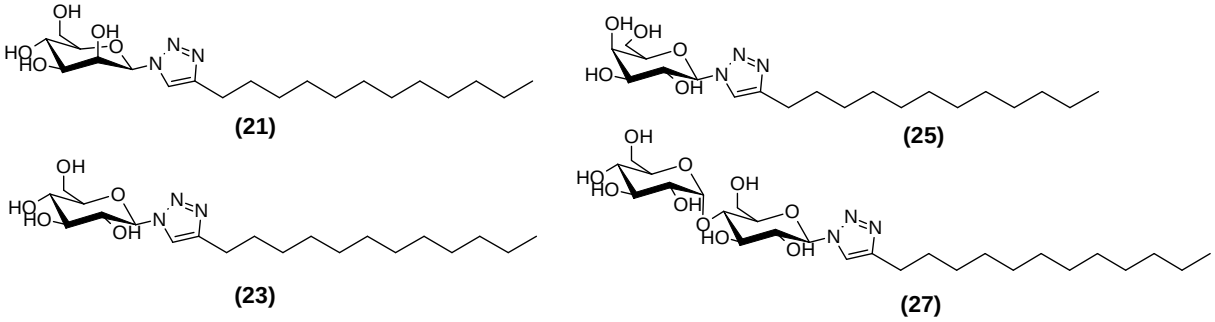

Figure 31 Alkyl glycosides for vesicle functionalisation : mannoside (21), glucoside (23), galactoside(25) and maltoside (27).

With Con A layers prepared as before (see section 2.2.2.2) vesicle solutions prepared by injection (see section 6.2.2) and incubated overnight at 4°C with the alkylglycoside type and concentration of choice were injected into the QCM setup (Figure 32). The vesicle solutions had a concentration of 200µM in POPC and various ratios of alkyl glycoside to phospholipid were tested. Of those tested only the alkyl maltoside vesicles showed surface recognition.

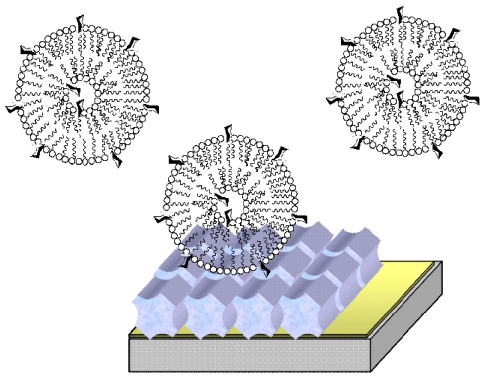

Figure 32 Cartoon representing specific recognition of Con A layer by "glycovesicles ".

As shown in (Figure 33) the "maltovesicles" adsorbed specifically while all the others including alkylglycoside free showed minimal adsorption. The results were fitted to the Langmuir model as before (2.2.5) giving an association constant $K_a = 8.4 \times 10^4$.

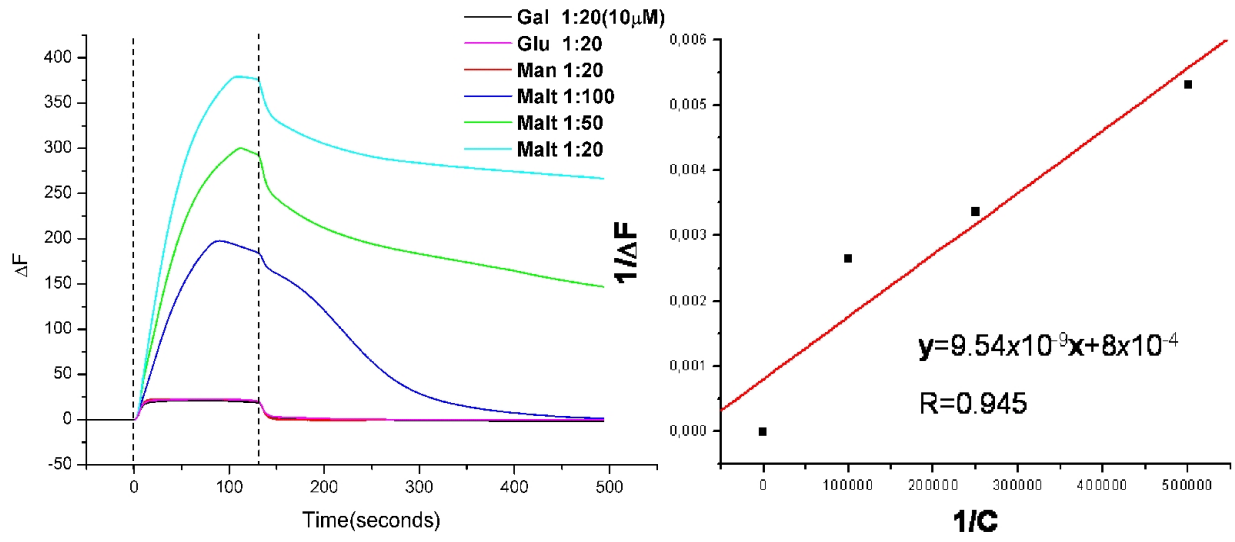

Figure 33 QCM adsorption profile for alkyglcoside functionalised vesicles.

The first point of interest to these results is that the "mannovesicles"show no apparent affinity whereas the "maltovesicles" do. A likely cause for this is the accessibility of the ligand at the bilayer surface.The maltoside bearing an extra sugar moiety can protrude more from the bilayer whereas the monosaccharide ligands may be buried in the external hydrophilic part phospholipid layer.

Again affinity enhancement is evident as Me-α-Glu moities show a Ka of $2.7x10^3$ M^{-1} [43]. This 40-fold increase can be attributed to multivalent effects allied to the fluidity within phospholipid bilayers. The scale of vesicles (25-35nm in diameter) may also allow them to access more than one binding site simultaneously.

2.3 Discussion

An overall conclusion would be that nanoparticles act as efficient signal enhancers in interaction measurement using QCM. This type of measurement could be applied to a whole range of interactions for which analyte mass is limiting, from biological protein-carbohydrate to cation mediated carbohydrate-carbohydrate and on to the library of known supramolecular interactions which could be investigated through combination of SAMs and NPs. The amplification is huge which is to be expected as there is an increase in the region of ~6000% in mass (considering 53000 gold atoms per 12 nm particle (Eq 20) [235]) when the 533 thioglycosides are fixed to a 12nm gold particle.

$$N = \frac{\pi \rho D^3}{6M} N_A$$

Eq 20

The interaction between these monolayer protected particles and the protein layer was also completely specific as there was no evidence of non-specific binding and layers could be removed by simply injecting excess solutions of the high affinity ligand, this being the case for both ManNP and MaltNP .

The question of the "cluster glycoside effect" in the apparent affinity constant is highly relevant. Lunquist and Toone surmised, based on solution experiments by calorimetry and inhibition studies, that enhancement in activity of multivalent carbohydrate presenting ligands over monovalent ligands results from aggregation and/or precipitation processes [55]. In the present work the Lectin is fixed in a layer structure on a chip surface and so protein aggregation of multivalent ligand could not be a factor in affinity enhancement. That leaves an intramolecular (chelate) effect or intermolecular (statistical effect). Assuming Concanavalin A as an 8 nm cube with its binding pockets located at 4 vertices then a thioglycoside functionalised 12nm particle could span at least 2 if not up to 4 monosaccharide binding sites on a saturated monolayer based on geometrical constraints. If two was the maximum span then

Applying the Whitesides rationale:

$$K_N^{poly} = \left(K_{avg}^{poly}\right)^N = \left(K^{mono}\right)^{\alpha N}$$

Eq 21

where α =1(the interactionis assumed non-cooperative

and where N=2(no. of interactions)

Then K_N^{poly} should equal to $(8X10^3)^2 = 6.4X10^7$ M^{-1}

That it does not reach this figure indicates negative cooperativity according to this approach with α =.924 although the results are not far from this model.

Assuming a non-cooperative association the concept of enhancement factor [46] may be applied as described in the general introduction.

$$\beta = \frac{K_a^{multi}}{K_a^{mono}}$$

Eq 22

For the present system this results in a β=2000 in the ManNP case and β=25000 for Malt NP (considering affinity constant of $2.88x10^3$ for D-Maltose [222]).

From a statistical point of view we could return to the reasoning of Kitov and Bundle [52] which seems to give a more complete treatment of the effect. As described in the general introduction (see section 1.3.2.1) they considered avidity binding energy to be made up of three components where although the second factor, a chelating effect, is of interest the last factor should be highly relevant to the present work and is termed the avidity entropy:

$$\Delta S^{O}_{avidity} = R \ln \Omega$$

Eq 23

where Ω is the number of accessible microstates.

In the present work the number of bound microstates of equal probability is huge given the valency of the multivalent scaffold and may therefore play the biggest role in enhancement.
Earlier thermodynamic treatment of the multivalent effect referred to in the general introduction (see section 1.3.2.1) considered the main driving force to be a reduced conformational entropy cost on the binding of a multivalent as opposed to a monovalent ligand [236].
In the present work the latter theory may also be highly applicable. The conformational entropic cost of for example binding to a Con A film from a solution of free ligands must be far larger than the case where these ligands are bound in large clusters with extremely restricted conformational entropy in the case of a SAM.

It can be proposed that overall affinity enhancement is an entropic effect. The enthalpic contributions for monovanent and individual contributions in multivalent binding can be considered equal. The restriction of a small molecule's motion on binding to a protein causes a loss of configurational entropy, and thus a penalty in binding affinity but again this would remain consistent in the multivalent scale-up as would the entropy change on freeing of water molecules on binding. Taking everything into account one could surmise that a combination of the following not entirely exclusive factors leads to affinity enhancement:

- Decreased conformational entropy cost.
- Large number of available multivalent ligand-receptor complex microstates.

- Chelating effect (when one site bound second one more favourable).
- Translational entropy cost (binding cost is lower for far larger nanoplatform, translational entropy depends primarily on (3/2)Rln(Mr), where M_r is the molecular weight).

2.4 Conclusion

The presented approach to QCM measurement has great potential, even using the present materials the carbohydrate–carbohydrate interaction can be investigated as well other lectin-carbohydrate interactions giving access to thermodynamic and kinetic parameters (for example using ClampXP fitting software). Nanoparticles and QCM can go hand in hand in order to expand the applicability of the QCM technique and investigate small molecule interactions in a real-time manner. More specifically in terms of the carbohydrate–protein interaction further work can investigate lead to a deeper understanding of this interaction with variation in carbohydrate distributions and particle size readily accessible.

In this work it has been shown that using nanoparticles in conjunction with QCM is a viable way in which to explore small molecule interactions. At present this technique does not demonstrate small molecule sensitivity and nanoparticles offer large signal amplification. This has been demonstrated in the present work where frequency changes in the region of up to 1600Hz were demonstrated for a complete nanoparticle layer while typical protein layers would show changes in the region of 100Hz.

Glyconanoparticles have been described as being biomimetic in their multivalent carbohydrate presentation and this work concurs. Large affinity increases with enhancement factors (β) of 2000 and 25000 for Mannoside and Maltoside respectively were shown.

Coupling of Vesicular aggregates with QCM as a signal amplification method has also been demonstrated as a versatile approach. Vesicles may prove to be even more applicable given their simple preparation and propensity to partition amphiphilic molecules. It could also be added that for the study of biomolecular interactions at cell interfaces etc. the vesicles biomimetic nature is highly attractive. This work showed ligand design is as expected an important feature and more ”natural” longer chain synthetic glycolipids could show even higher affinity amplifications due to accessibility. An enhancement factor of 40 was demonstrated for the Maltoside vesicles.

3 Polyoxomolybdates as Synthetic Ion Channels

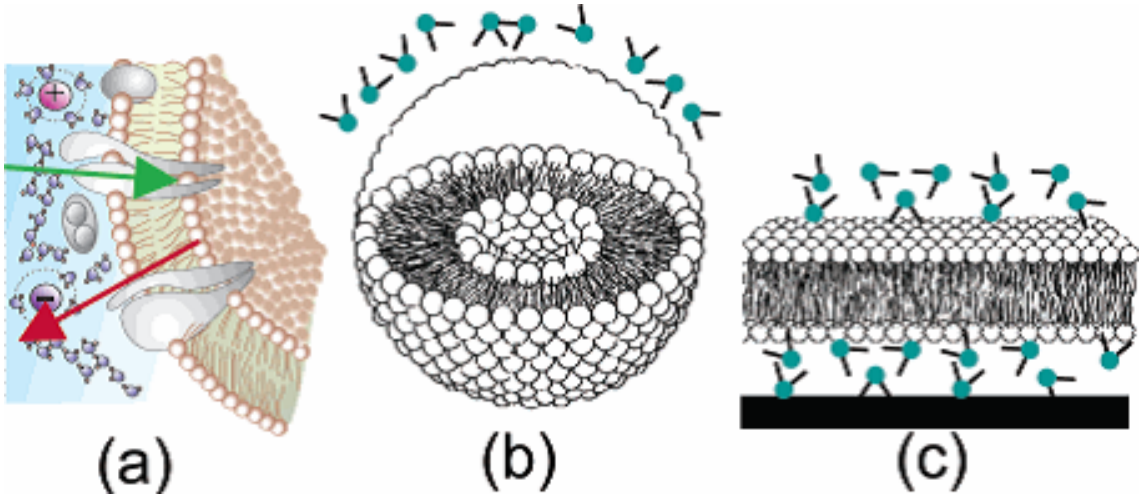

Figure 34. Bilayers from nature to measurement [237].

3.1 Introduction

3.1.1 Phospholipid bilayers

The phospholipid bilayer structure is essential to the existence of life. By the end of the nineteenth century scientists had come to believe that the substance separating the interior and exterior of the biological cell was comprised of something resembling oil [238]. During the study of anaesthetics Overton classified hundreds of organic solutes concluding that there permeability across cell membranes was determined not by their size but by their oil-water partition coefficient. He stated that the osmotic barrier must be a lipid impregnated boundary layer with properties similar to those of phosphatidylcholine and cholesterol [239].

It was not until 1925 that the actual structural thickness of the membrane was elucidated. Capacitance experiments by Fricke led to the conclusion of a layer thickness of 3.3 nm [240] which corresponded to the hydrophobic part of the bilayer with the fully hydrated polar head groups not showing up in these experiments. In the same year Gorter and Grendel correctly deduced a lipid bilayer structure when the area of a film of solvent extracted erythrocyte spread in a Langmuir-Blodgett trough was twice that of the cells original surface area [241]. With the development of Electron Microscopy the bilayer theory was confirmed in the late 1950's following work by Sjostrand and later Robertsons work and interpretation. [242] [243].

"About 1956 I applied two new developments in EM technique, permanganate fixation and epoxy embedding, and observed a triple-layered pattern in all cell membranes and membrane organelles studied. The membrane measured " ~7.5 nm in thickness and appeared as a pair of dense strata each "~ 2 nm thick bordering a light central zone. The work provided the first direct evidence that nerve myelin consisted only of Schwann cell membranes to the resolution of the sections ~2 nm), Partly on the basis of these observations I stated that the basic pattern resulted from the presence of one lipid bilayer as the fundamental core structure." J. D. Robertson

The current teaching, the "fluid mosaic model" (Figure 35), locates the proteins embedded within the bilayer ,some on one side or the other, some spanning the layer [244].

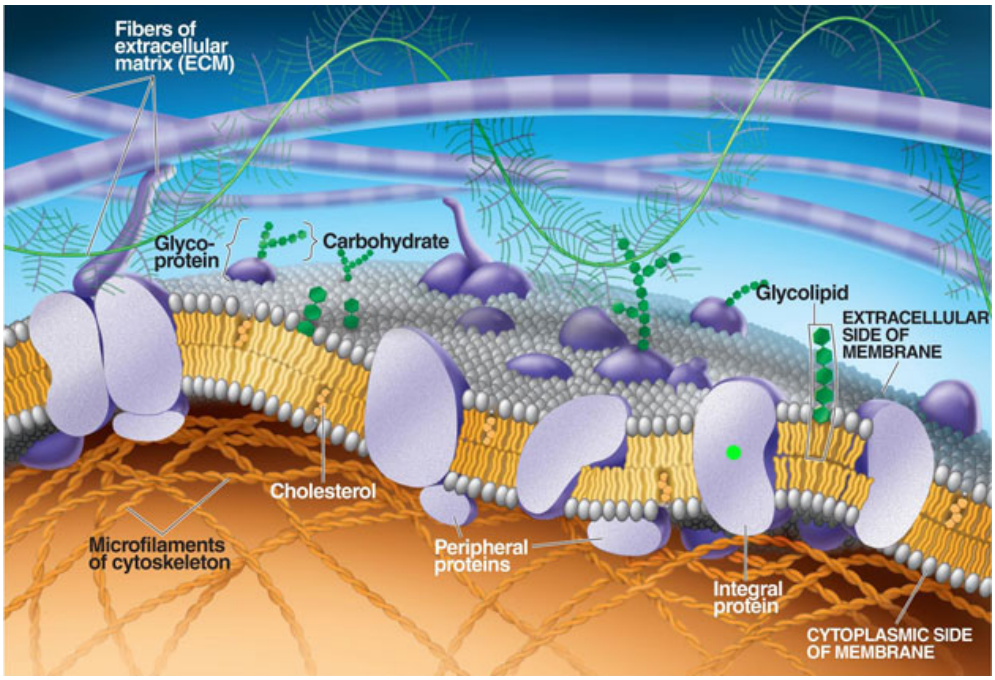

Figure 35. Fluid Mosaic Model of Cell Membrane [245]

3.1.2 Ion channels

Phospholipid bilayers act as diffusion barriers in biological systems being impermeable to ionic species. Transport across this barrier is facilitated either by transporters, channels and pores, or by low molecular weight carriers. Biological ion channels are passive transporters allowing the flow of ions across membranes close to their diffusion limit in water while at the same time exhibiting high specificities for ion conductance [246].

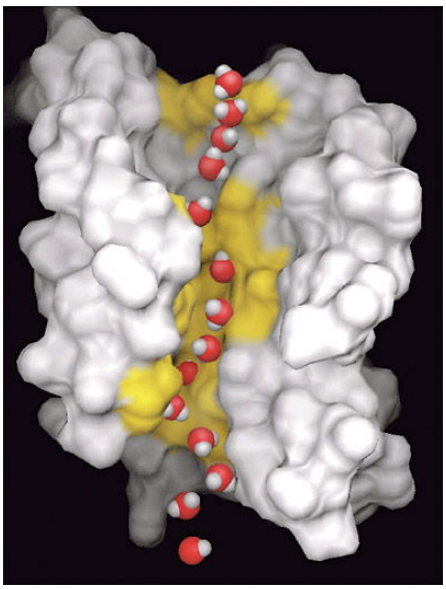

Figure 36 Aquaporin channel surface representation [247]

They are large protein complexes that regulate the key functions of cells and work by replacing the ion-water interaction with stabilizing ion–transporter interactions which can selectively permit movement across the high energy barrier that is the lipid bilayer. Ion channels are passive transporters. The flow is driven by the concentration gradient across the bilayer or by imposed electrochemical gradient. There also exist ion pumps, ATP driven transporters which can actively transport species against a gradient thereby creating gradients in biological systems. Both channels and pumps are highly selective with this selectivity based on supramolecular principles.

3.1.3 Basis for Ion Channel Seletivity in Nature

Biological ion channel function requires that there be a high rate of flux but also a selectivity which can discriminate between similarly sized cations such as K^+ and Na^+ .This has been accomplished through the evolution of channels where a small section is constricted to impart spacial selectivity (selectivity filter) whereas the rest of the channel is large enough to maintain rapid diffusion. This hypothesis was physically demonstrated with the determination of potassium ion channel structure [248]. Ion channel selectivity can be described in general as being effected in localized regions where the protein interacts strongly with the ionic species.

Cation selective channels that have been studied intensively have all shown a net negatively charged pore lining thus attracting cations and repelling anions [249]. For example Gramicidin, the first channel for which the structure was determined with atomic resolution although being neutral overall has a conducting pathway that is lined by polar regions of the protein with the partially negatively charged backbone carbonyl oxygens pointing slightly inwards towards the pore [250]. It has been shown hence for this channel that monovalent cations pass through the channel at high conductance, divalent cations block the channel conductance and anions neither permeate nor block the pore [251].

A similar asymmetric charge distribution appears to be behind the selectivity of most ion channels. K^+ channels have a group of carbonyl oxygen atoms lining their “selectivity filter”. As would be expected for anion selective channels it is the opposite case. Cl^- channels show a net positive charge along their conduction pathway judging from crystal structures [252].

Discrimination between monovalent and divalent cations appears to occur as a result of interaction strength [253-257]. It is thought that cations move along the channel due to being "knocked on" by coulumbic repulsion. This works well in the case of the monovalent cation but when a divalent cation enters the interaction is much stronger and this cation is immobilised relative to timescale [255]. The channel is not incapacitated however as the divalent cation will eventually leave the channel but over a timescale that is much longer than that of ion permeation.

When it comes to ions of similar size and charge such as K^+ (~1.38 Å) and Na^+(~1.02 Å) [258] the mechanism of selectivity shown is not as straight forward. It had been thought that it was basically a pore size effect, that, as the ions had to be fully desolvated to pass the selectivity filter, and that as this desolvation was fully compensated for by interaction with the carbonyl oxygen atoms within the pore, then K^+ could be stabilised sufficiently to overcome its desolvation energy whereas in the Na^+ case there would be insufficient interaction to accommodate desolvation.

This explanation requires that the structure of the protein be fairly rigid so that it cannot adjust to accommodate the smaller ion. This "snug-fit" model is based on crystal structures. There is likely going to be a "snug-fit" in the crystalline state between a K^+-channel and a K^+ cation coming from the corresponding salt solution. This fixed organised state however may not be a true reflection of the dynamic natural state of the working protein. Especially as proteins are relatively flexible structures that undergo rapid thermal fluctuations of a magnitude much greater than the size difference between Na^+ and K^+, it being .38Å in radius [259-261].

It also appears that the protein backbone is quite mobile as crystal structures obtained for low K^+ concentration show a large conformational change in the filter region as it adapts to this situation [262]. A further explanation has been put forward through theoretical study whereby the K^+ selectivity exhibited is proposed as being a consequence of coordination by dipoles of appropriate strength. Fluctuating carbonyl dipoles in the flexible binding site, with dipole between 2.5 and 4.5 debye, are K^+ selective whereas an increased magnitude would favour coordination of smaller ions and lower magnitude larger ones i.e. field strength selectivity [261]. Further dynamics studies have also aligned themselves to this approach [263].

The NaK channel is an interesting case in that it conducts both Na^+ and K^+ but has an almost identical structure to that of the K^+ channel except for the replacement of one tyrosine residue with aspartate. This channel is known to conduct most group 1A cations as well as Ca^{2+}.This raises the big question of how two channels with seemingly identical chemical environments can have different ion binding properties. In a recently published work analysis of the channel crystallised with a range of cations was performed [264]. For the four well defined binding sites in the NaK selectivity filter, sites 3 and 4, the two most intracellular are virtually identical to those of the K^+ channel, whereas 1 and 2 show a modified vestibular structure. The authors surmised that through increased mobility of water molecules in this vestibular part a greater flexibility on ion binding is imparted. However 3 and 4 which are identical to the K^+ channel surprisingly showed different binding properties. The explanation here was that through facilitative water complexation the Na+ ion is conducted through the selectivity filter in line with suggestions from recent computational studies on NaK channels [261,265].

Overall it appears that ion channel proteins are adaptive structures with exquisite selectivity (e.g. more then 1000-fold for K^+ over Na^+ in K-channels) based on and not in spite of their dynamic nature.

3.1.4 Rational design of Ion channels

Approaches towards the synthesis of ion channels of controlled functionality can be divided between the engineering of existing biological ion channels and de novo design of ion channels based on supramolecular approaches. The present work will concentrate on the latter approach. Completely synthetic ion channels based on this strategy have shown some success in recent times. As with many areas of interest in supramolecular chemistry evolution in naturally evolved systems has provided inspirational design concepts. Two such motifs for the design of synthetic ion channels are the gramicidin pentdecapeptide and the amphotericin molecule (Figure 37). In membranes and nonpolar solvents gramicidin forms a β helix with a hydrophilic interior and a lipophilic exterior bearing the amino acid side chains. The helix length is roughly half that of bilayer thickness so two gramicidin molecules span the bilayer connected by six intermolecular hydrogen bonds. The resulting structure creates a water filled tunnel that is an efficient channel for alkali ions. A second biological structure to influence rational design of synthetic ion channels is the antifungal amphotericin molecule which forms channels in sterol containing bilayer membranes [266].

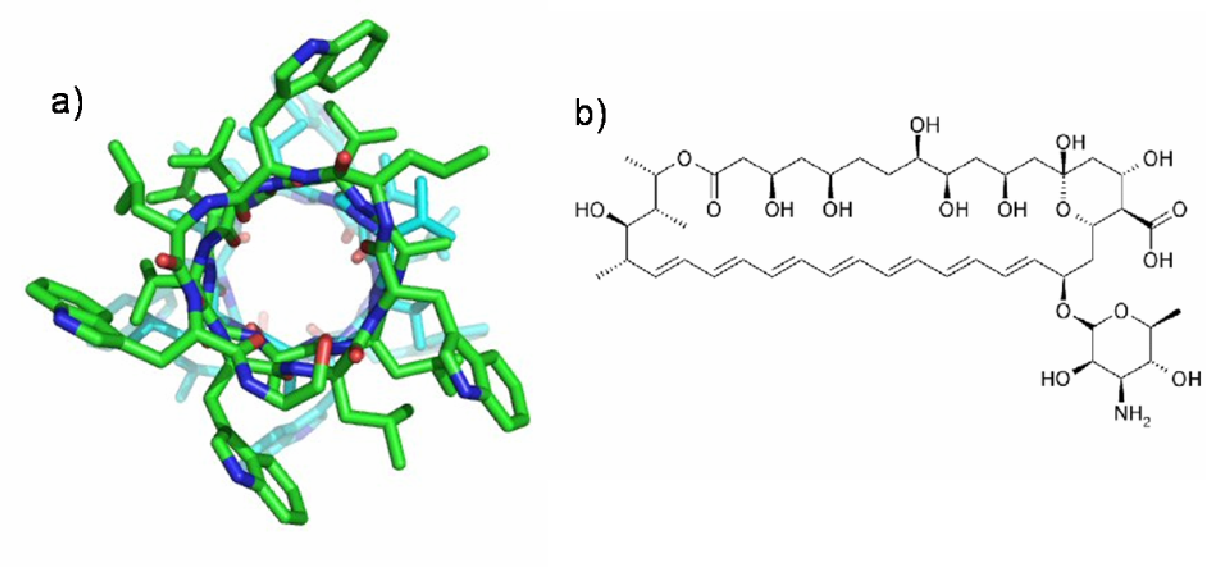

Figure 37 a) Gramicidin [267] and b) Amphotericin [268].

The mycosamine headgroup contacts with the aqueous phase giving directionality. With the polyene chain part in contact with the hydrophobic interior of the bilayer aggregation of these monomers builds a water filled channel structure, which being about half the width of a bilayer ,like gramicidin, requires that two such aggregates join end to end to span the membrane.

Through biomimetism, structural understanding and serendipity researchers have produced working synthetic ion channels. This goes back to crown ethers, which, since they were discovered have been used to transport cations through bulk liquid membranes. In the 1980s many groups began to contemplate the possibility of building synthetic cation channels that could function in bilayers. Most of the early designs were thus based on macrocyclic compounds. The first reported that demonstrated ion transport were by Gokel and coworkers [269] and Fyles and coworkers [270].

3.1.4.1 Unimolecular Synthetic Ion Channel Structures

3.1.4.1.1 Synthetic Unimolecular Ion Channels

The ‘hydraphiles’, a group of tris-macrocycles, are a relatively well characterised synthetic ion channel. Their intial design envisaged a co-facial structure forming a channel across the bilayer with the cental macrocycle acting as a cation relay (Figure 37). Subsequent results however have shown that it is more likely that the cations do not pass through the central macrocycle as variants with smaller central crown ethers also showed similar activity. Nevertheless the orientation and structure within the bilayer was supported by fluorescence

techniques [271]. Taken together with other work by the same group the enhanced transport activity would appear to be as a result a channel formation which allows water and partially hydrated cations to interact by Lewis base–cation and Lewis base-water-cation interactions [272].

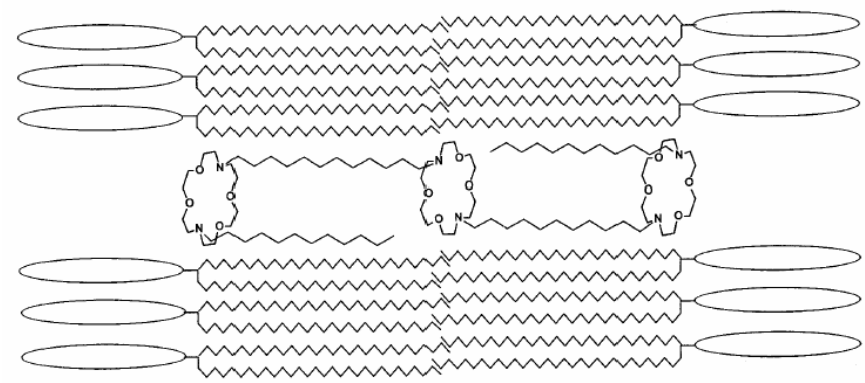

Figure 38 Design concept for 'hydraphile' channels [271].

The hydraphiles were also shown to be biologically active. A toxicity towards Gram-positive and Gram negative bacteria was shown correlating to their channel forming ability [273] [274]. Co-facial organisation of crown ethers has been a recurrent concept in channel design with many examples. Another early working example by Fyles et al. used an 18-Crown-6 as a central relay [275].

3.1.4.1.2 Semi-Synthetic Unimolecular Ion channels

Helical peptides have been used by Voyer et al. as scaffolds to support aligned crown ethers. The coupling of crown ethers to helix forming peptides with rationalized spacing to allow for macrocycle stacking has shown to generate membrane disrupting agents (Figure 39) [276].

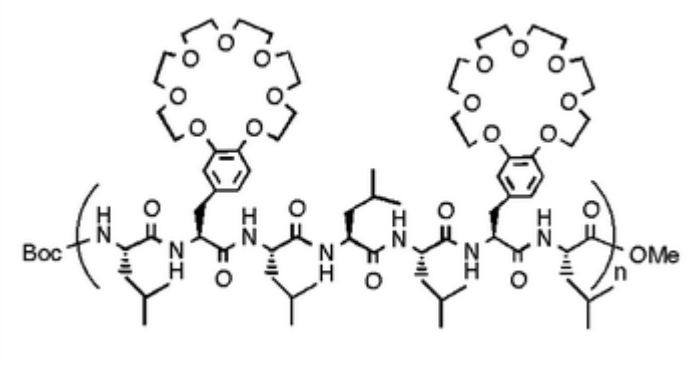

Figure 39. Synthetic ion channel incorporporating a helical peptide backbone and oriented crown ethers to form a unimolecular channel [276].

Another scaffold for the helical cylindrical type unimolecular channels was studied by Matile et al. based on the octiphenyl moiety. Modification of this structure with short sections of peptide resulted in the assembly of rigid rod β-barrels [277]. These large diameter channels allow the transport of large ionic species while the transport can also be controlled by modifying the internal functionality of the channel (Figure 40), [278].

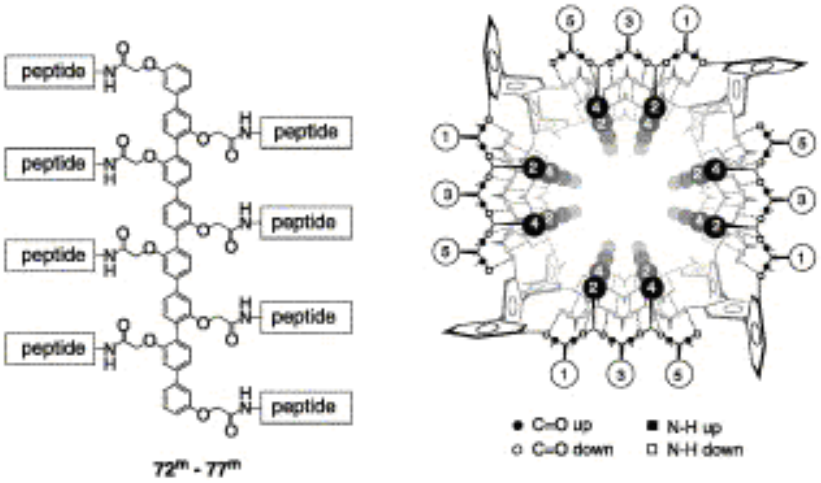

Figure 40 Octiphenyl based helical channels [277].

Other examples of unimolecular synthetic ion channels based on self-assembly by peptide hydrogen bonding have been demonstrated [279,280]. Cyclic peptides have also proven to be potent antibacterial agents, a property believed to result from membrane depolarisation [281].

3.1.4.2 Polymolecular ion-channels

As mentioned the amphotericin molecule provides another structural motif for ion channel formation, i.e. monomeric units which self-assemble within the bilayer forming channel structures. This approach has advanced around membrane spanning molecules which possess the tendency to aggregate in an edge to edge fashion within bilayers. Bolaamphiphiles (hydrophilic-hydrophobic-hydrophilic monomers), when membrane spanning in size, have been shown to form channels. Fyles et al demonstrated this for a series of compounds with varying head groups and bridge groups (Figure 41) [282] [283]. On variation of bridge group between (a) and (c) no activity difference was discerned and overall little selectivity is shown for channels of this form. Some selectivity may be introduced by headgroup modification with these headgroups then acting as electrostatic selectors. Their dynamic nature within bilayers leads to fluctuating polar regions within the layer allowing passage of water and hydrated ions. Results indicated that monomers remained inactive with dimers or trimers the active units. Their association is driven by phospholipid organisation hence an extension of

the hydrophobic interaction. These compounds also exhibited potential for voltage gating based on the formation of asymmetric channels leading to a dipole [282].

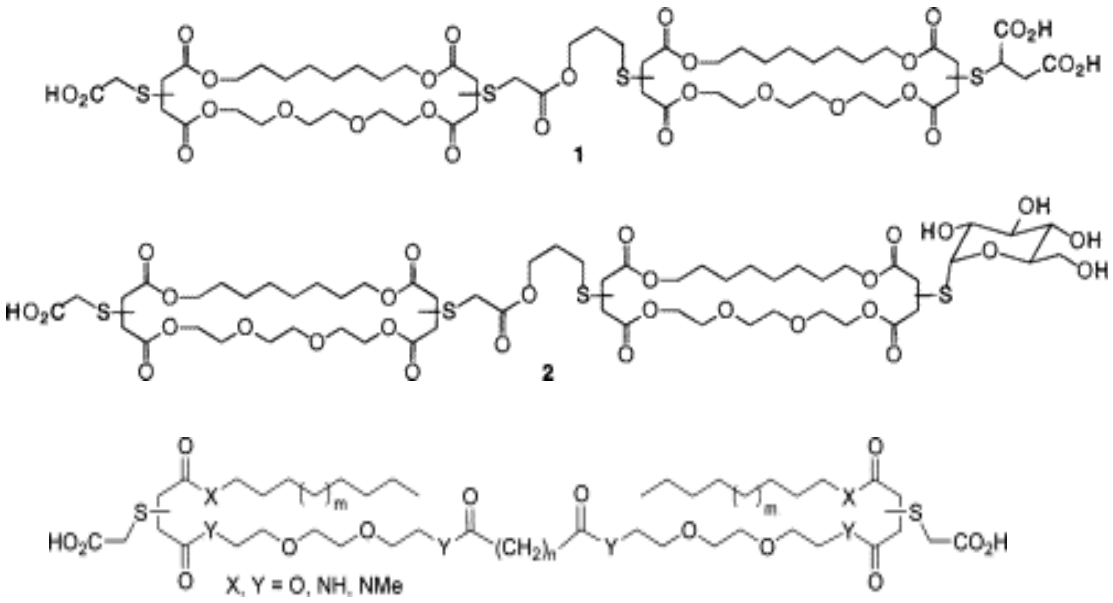

Figure 41 Ion channel forming bolaamphiphiles [282] [283].

Voltage-gated responses have also been observed in similar systems with bis-cholate amphiphiles. The symmetric compound (both end groups carboxylic acid) exhibited no such response whereas the non-symmetric gave a non-linear current-voltage response (Figure 42) [284].

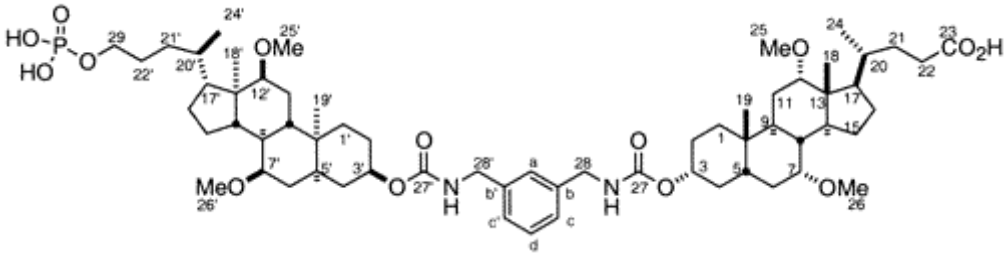

Figure 42 Voltage-gated ion channel forming Bis-cholate amphiphile [284].

Many common detergents show channel like activity [277]. However these are in general transient, irregular and poorly reproducible. There are simple compounds which appear to produce regular channel openings based on voltage clamp experiments (Figure 43) [277].

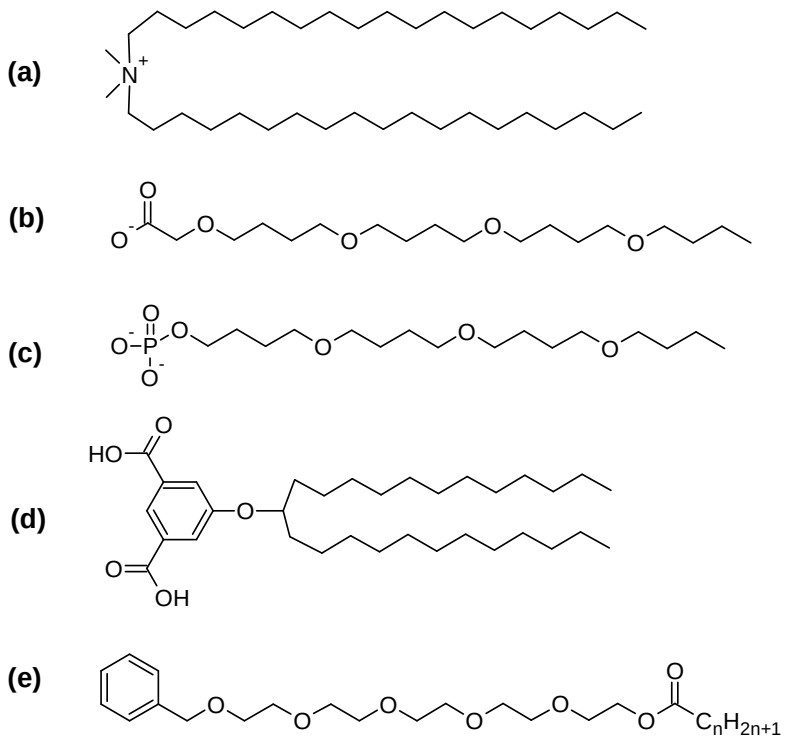

Figure 43 Detergents which have shown channel like activity.

3.1.4.3 Pre-assembled Metal-organic clusters as Ion transporters.

Most recently polyoxometallates have presented themselves as strong candidates for synthetic ion channels with tuneable transport properties. All the synthetic ion channels discussed so far have been constituted by organic molecules. There are few examples of metal-organic structures being investigated. Up to 2008 only one metal-organic compound was reported to facilitate ion transport this being a lipophilic ethylenediamine palladium complex reported by Fyles and Tong (Figure 44) [285].

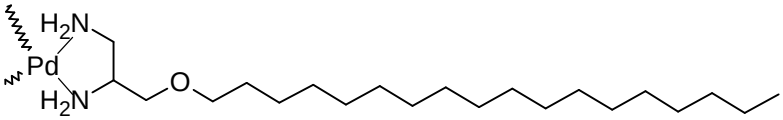

Figure 44 Ion channel forming lipophilic ethylenediamine palladium complex [285].

Following this Kim et al. reported synthetic ion channels based on metal-organic polyhedra [286]. The metal organic cage used was based on earlier work by Yaghi and co-workers [287,288]. The nanostructure is a 25Å cuboctahedron constructed from 12 $Cu_2(CO_2)(4)$ paddle-wheel building blocks. It contains a hydrophilic cavity of 13.8Å in diameter surrounded by eight triangular 3.8 Å and six square 6.6 Å windows. The overall diameter including the long alkyl chains surrounding the capsule is around 5 nm (Figure 45).

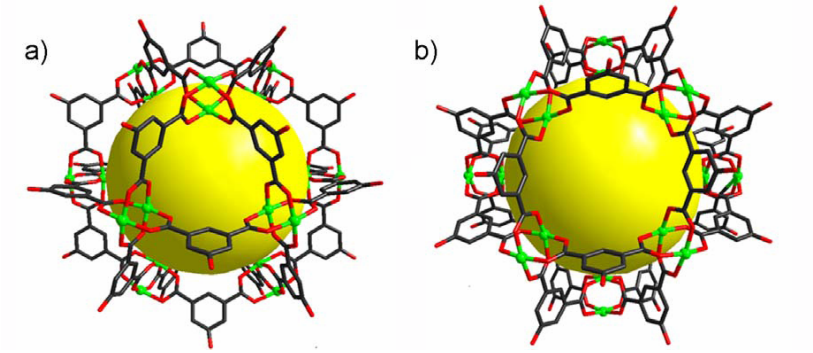

Figure 45 Metallo-organic nanocapsule ion channel showing hydrophilic cavity(yellow sphere) [286].

Using a Fluorometry protocol [289] alongside a voltage clamp method [246] they demonstrated proton and ion transport across lipid bilayers mediated by the cluster architectures.

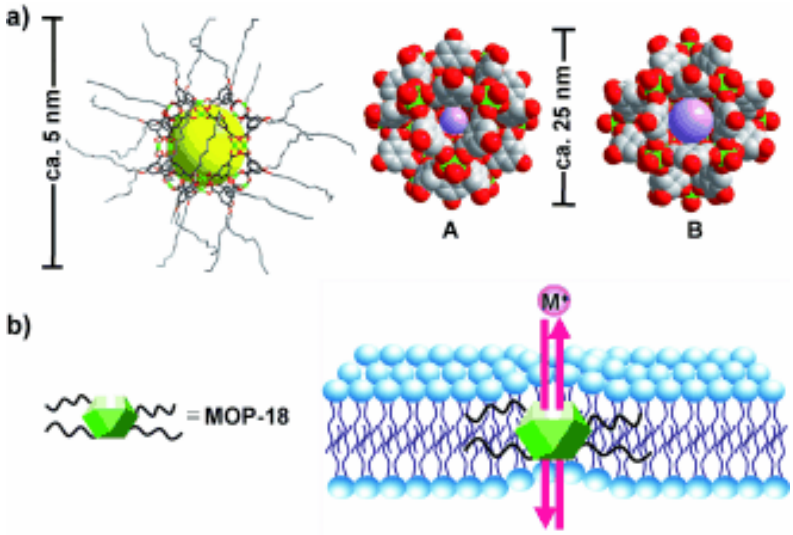

Figure 46 Scale of Capsule and Phospholipid bilayer [286].

Recent theoretical calculations have demonstrated the potential of surfactant encapsulated polyoxomolybdates to act as synthetic ion transporters [290]. More specifically a Mo_{132} type capsule complexed electrostatically with dimethyldioctadecylammonium bromide (DODA-Br) and its interaction with a palmitoyl-oleyl-sn-phosphatidyl-choline (POPC) bilayer was considered (Figure 47). These simulations concluded that water soluble structures are formed spontaneously through combination in aqueous solution of Mo_{132}, cationic surfactant (DODA) and model phospholipid (POPC) and that these liposome like structures insert spontaneously into lipid bilayers for given conditions. These POM's are particularly interesting candidates in that the capsule functionalities may be tuned through ligand variation as described in more detail in the next section.

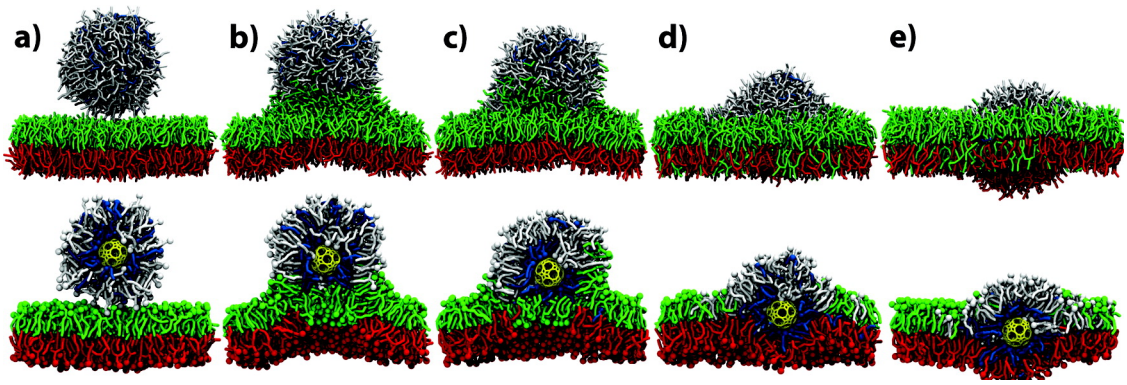

Figure 47 Snapshots of liposome(Mo_{132},DODA,POPC) fusion with bilayer [290].

3.1.5 Molybdenum Polyoxometalate Clusters

Molybdenum blue solutions are known of for more than 200 years since they were first reported in 1783 by Scheele. Pure crystalline samples of the these nanoclusters were then isolated by Müller et al. in 1995 where the synthesis and structural characterisation of the Mo_{154} cluster crystallised from a molybdenum blue solution was described [291].

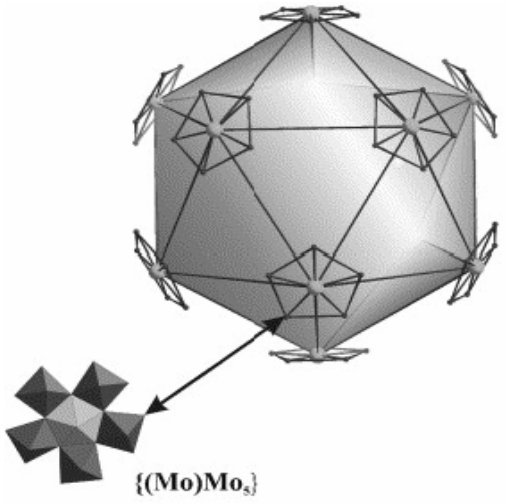

Figure 48 Keplerate clusters can be viewed as composed of pentagonal building blocks at 12 vertices of an icosahedron [290].

This work has been built upon by both the Müller group and others revealing varied nanoarchitectures including giant spherical or wheel shaped systems composed of {$Mo(Mo_5)$} pentagonal building blocks which are conserved between structures. These Mo based pentagonal building blocks allow the generation of large clusters with nuclearities between 36 and 368 metal atoms per cluster [291-293]. Reduction of anionic molybdenum salts (e.g. $Mo_7O_{24}^{6-}$) in acidic aqueous solutions results in self-assembly of theses higher order structures[292].

The clusters can be divided into groups, the keplerates and the big wheel types. The Keplerate clusters are all assembled from the pentagonal Mo(Mo_5) building blocks which in the case of the giant spherical clusters can be described as being placed at the 12 vertices of an icosahedron and linked by a set of 30 mono- or dinuclear spacers (Figure 48), such as $\{Fe(H_2O)\}^{3+}$ [294] and $\{Mo^{V}O(H_2O)\}^{3+}$ [295] or $\{Mo_2{}^{V}O_4(CH_3COO)\}^{+}$ [292]. Changing the linkers allows the size as well as the chemical characteristics of such nanoarchitectures to be adjusted. The big–wheel type polyoxomolybdates also incorporate the pentagonal unit as well as $\{Mo_2\}$ and $\{Mo_1\}$ type units. Composed of these building blocks, $\{Mo_{154}\}$ and $\{Mo_{176}\}$ "big-wheel" clusters were prepared by the Müller group[296].

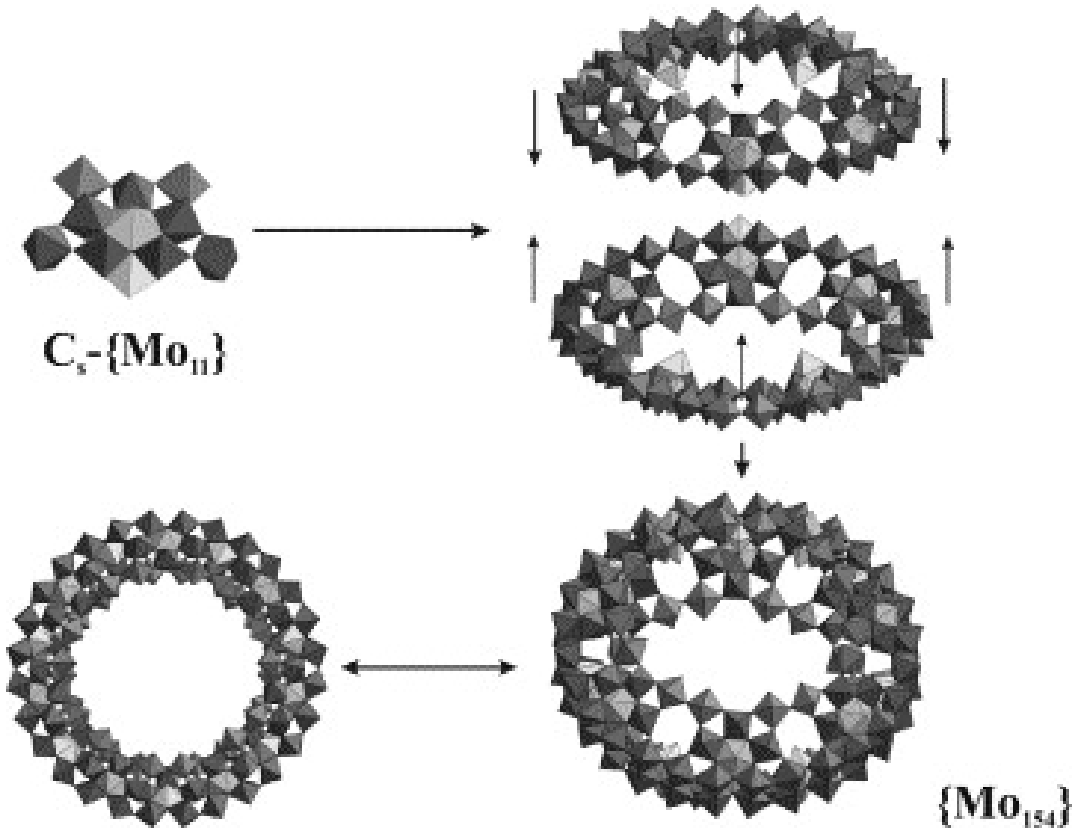

Figure 49 A formal building schme for an Mo_{154} ring starts from a C_s type Mo_{11} unit fourteen of which are fused ogether to form two Mo77 belts.Two of theses are fused together after one belt has been rotated by an angle of 360°/14 with respect to the other along the C_7-axis to form the wheel type species[296].

Another interesting development as regards the spherical kepelerates is that the 60 Mo^{v} linkers in the Mo_{132} can be replaced by 30 Fe^{III} ions, leading to the formation of $Mo_{72}Fe_{30}$ (Figure 50) which possesses novel magnetic properties [294].

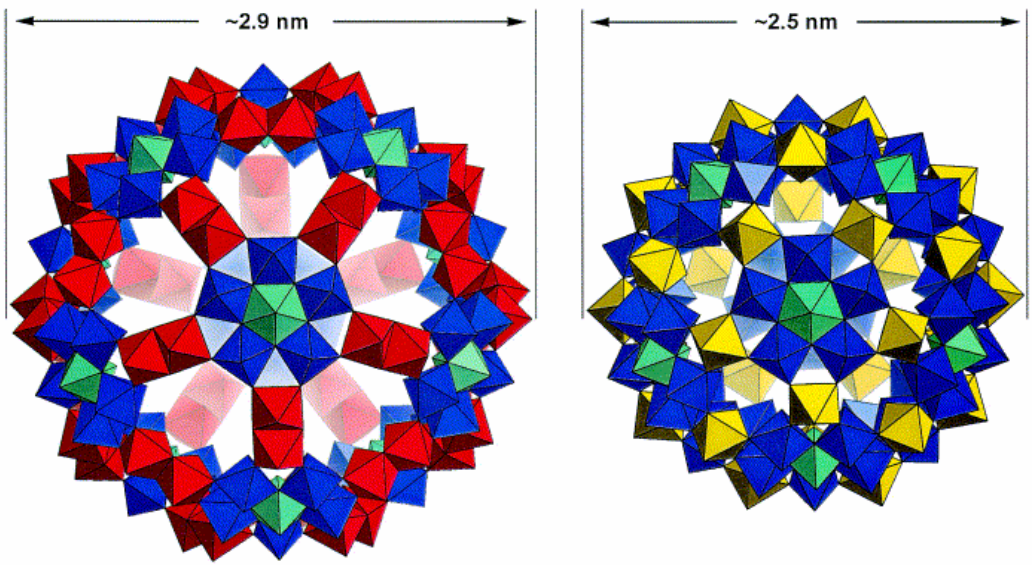

Figure 50. Structures of (Mo132) and ($Mo_{72}Fe_{30}$) [297].

In such cases with a mononuclear linker such as Fe^{3+} the pore size (Mo_6O_6 rings with receptor properties similar to that of crown ethers) is smaller in diameter which may have important influences on ion transport phenomena.

3.1.5.1 Self Assembly to higher ordered structures

These POM clusters have shown a propensity to form self assembled structures in aqueous solution. Large uniform aggregates with unknown structures were initially observed [298] which were later investigated by Dynamic and static light scattering techniques showing that these supramolecular structures were hollow spherical "blackberry" like vesicles [299]. Subsequent investigations also showed somewhat tuneable assembly processes for the spherical clusters Mo_{132} [300] and $Mo_{72}Fe_{30}$ [301-304] (Figure 51).

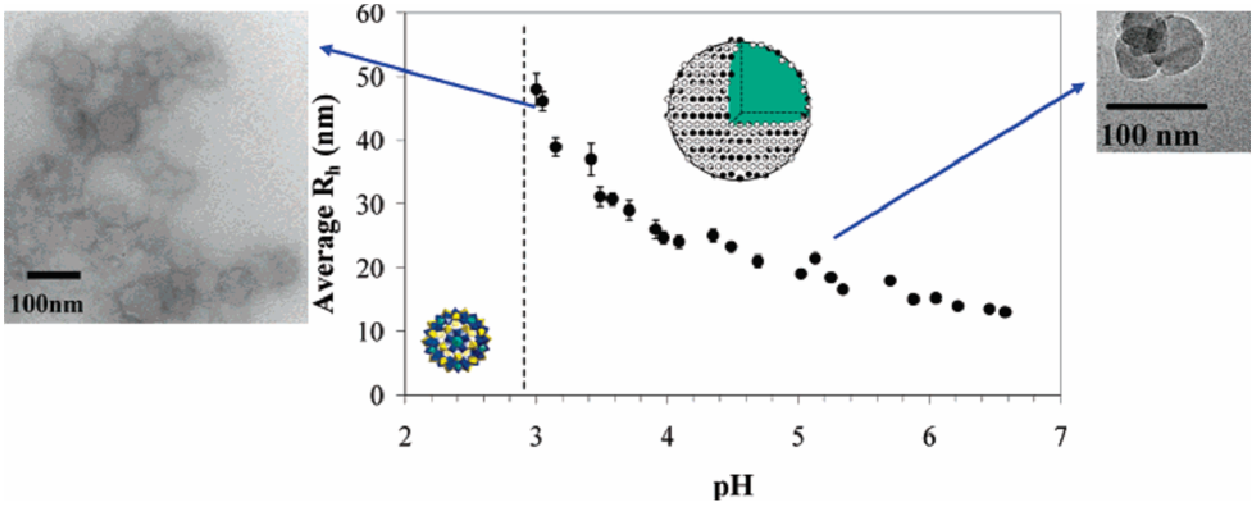

Figure 51 pH dependant vesicular organisation of $Mo_{72}Fe_{30}$ clusters.

3.1.5.2 Surfactant Encapsulated Clusters

Surfactant Encapsulated Clusters (SECs) as applied to poloxomolybdate clusters were initially described by Volkmer and Kurth around 2000. [305-307]. Mo_{132} kepelerate clusters prepared as had been previously reported by partially reducing Mo^{VI} to Mo^{V} via simple inorganic synthesis approaches [297] were encapsulated by DODA through simple electrostatically driven extraction into chloroformic solutions of dioctadecyldimethylammonium bromide (DODA-Br). These now electrostatically neutral assemblies altered in this manner would show an increased stability to fragmentation and new predictable surface chemical properties. The Mo_{132} polyoxomolybdates were shown to be stabilised by on average 40 DODA surfactant molecules.

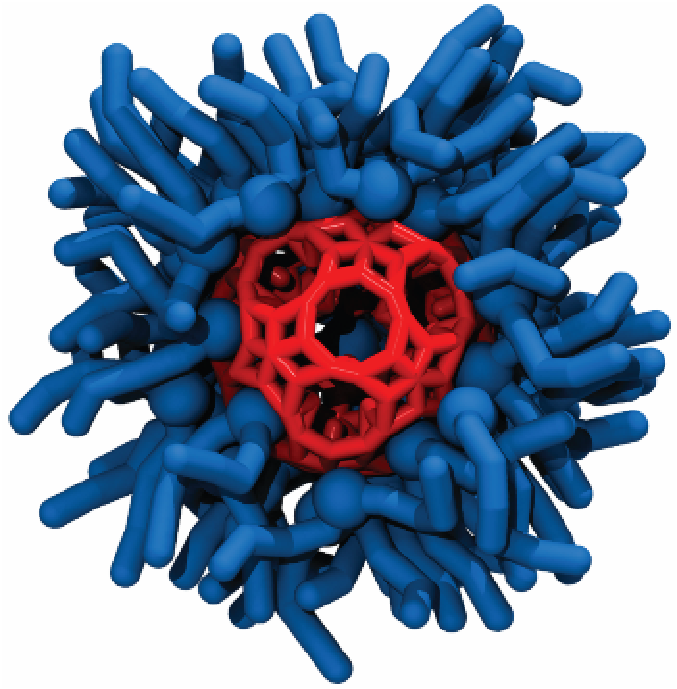

Figure 52 Model of SEC Mo_{132}. $DODA_{40}$ [290]

These nanocapsules were investigated by a variety of techniques both in solution and in film assemblies. Initially by small angle X-ray scattering (PDDF) which indicated similar hollow sphere structures for both the cluster and the SEC. Thin films cast onto water were prepared and examined by transmission electron microscopy showing dark cores with a 3nm diameter and an intercore distance of 4.5 nm. Ordered regions were observed with a packing best described as a fcc lattice with a cubic cell axis of approximately 6 nm [305].

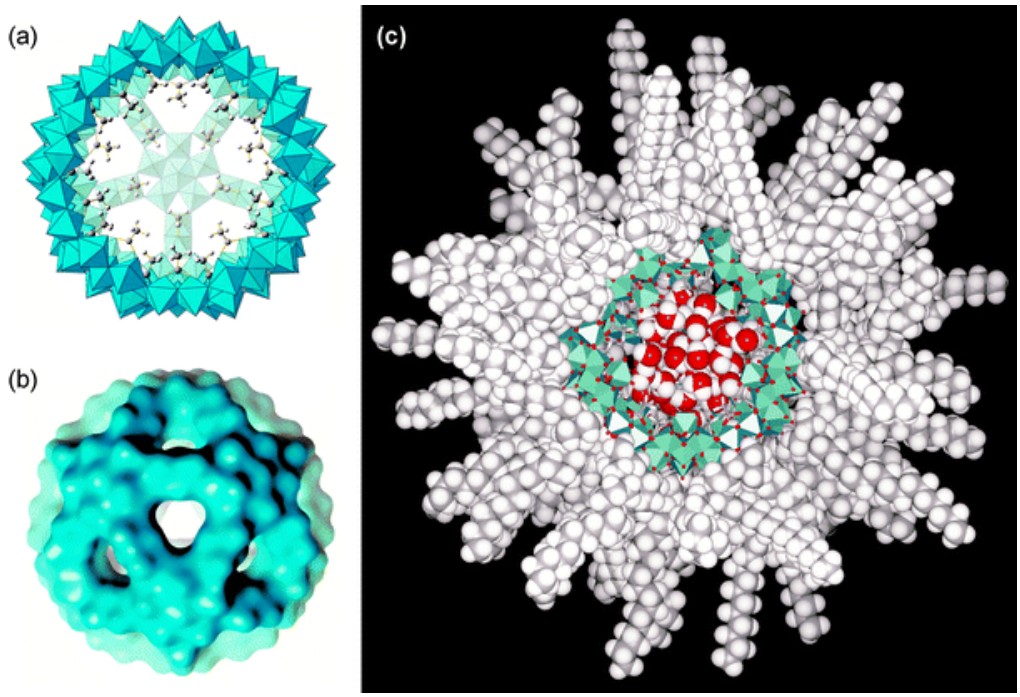

Figure 53 Model representations of keplerate Mo_{132} and $Mo_{132}DODA_{40}$ [307] (a) a polyhedral model of the Kepelerate Mo_{132} viewed in cross-section with the acetate ligands drawn in ball and stick representation. (b) the solvent accessible surface of the kepelerate cluster calculated for a 0.14nm surface probe. A MD snapshot of $Mo_{132}.DODA_{40}$ is shown in (c) in a pseudo cross-sectional format [307]. The diameter size of the polyoxometalate shell is 2.96 nm with the surfactant encapsulated cluster having an outer edge diameter of 6.18 nm.

NMR and IR studies indicated cationic headgroup–negative surface orientation of the surfactant as well as completely disordered alkyl chains attributed to the curvature of the structure. X-ray reflectance (XRR) showed that the core-shell architecture was preserved for Langmuir monolayers at the air-water interface. It was also shown by XRR spectra that this core–shell structure is fully preserved in 3-D highly ordered solid state structures formed by multilayer Langmuir-Blodgett transfer [307]. A similar extraction procedure was later applied to the $Mo_{72}Fe_{30}$ clusters which had been incubated in aqueous solution for a long period of time in order to allow for self assembly into the large unilamellar vesicles mentioned earlier [299,308]. On variation of the surfactant: cluster ratio used for the extraction to chloroform of "vesicular" cluster solutions it was observed by DLS that a low surfactant concentration (20:1) led to extraction with DLS particle size distribution intact, that is to say, vesicle like assemblies were stable enough to be extracted as one unit. However at high ratio (560:1) all clusters appeared to be in single cluster-surfactant assemblies with an intermediate case shown for a ratio of (100:1) revealing that electrostatics played a large role in the formation of these "giant" assemblies.

3.1.5.3 . Transport Properties of Polyoxomolybdate Capsules

3.1.5.3.1 POM Nanoarchitectures and Pore Size

The most interesting aspect as pertains to the present work is the porous nature of the clusters. As stated the Mo_{132} cluster is composed of 12 pentagonal molybdenum oxide ligand type groups. The connection of these groups forms 20 circular pores on the capsule surface. The resultant Mo_9O_9 pores have a crown-ether type structure and studies have shown that water and small inorganic cations can enter the capsule cavity through these pores [309-311]. Pore size can be modified as the linker between the $\{(Mo)Mo_5\}$ units is varied due to symmetry reasons . For example if the linker is a binuclear Mo_2 type unit the pore will then correspond to a Mo_9O_9 ring with a radius of around 2.25Å [312] whereas in the case of a mononuclear linker such as Fe^{III} the resulting smaller Mo_6O_6 ring is just large enough to capture K^+ ions, i.e. around 1.5 Å [309,313]. The crown ether like Mo_9O_9 pore geometry has been described by the Müller group for the cluster:

$[\{Mo^{VI}(Mo^{VI}_5O_{21})(H_2O)_6\}_{12}\{Mo^{V}_2O_4(SO_4)\}_{24}\{Mo^{V}_2O_4(CH_3COO)\}]^{64-}$ (Figure 54) [311].

Four of the 20 nanoscale pores can be seen on the surface. (Figure 54) (b) shows a lateral view of the coordination of an Na^+ ion to three sulphate groups on the interior surface. Figure 54(c) is a schematic presentation of ion uptake and release with Mo coloured blue and oxygen red. The distances relative to ion transport are represented in Figure 54(d).

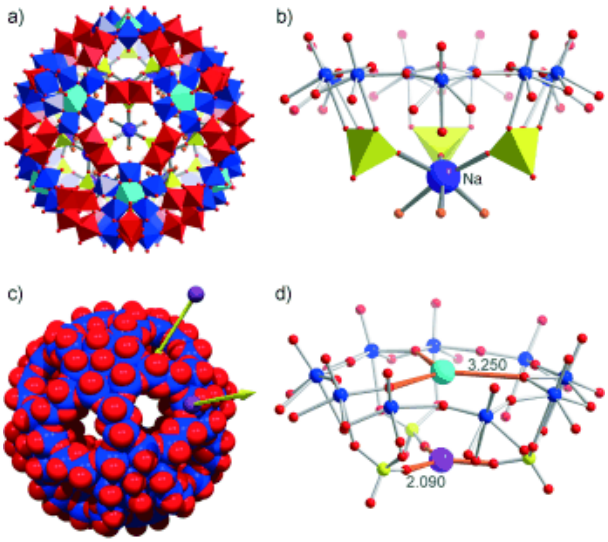

Figure 54 Structure of $[\{Mo^{VI}(Mo^{VI}_5O_{21})(H_2O)_6\}_{12}\{Mo^{V}_2O_4(SO_4)\}_{24}\{Mo^{V}_2O_4(CH_3COO)\}^{64-}$

The turquoise and lilac spheres represent the centre points for outer (Mo_9O_9) and inner (three sulphate groups) pores. The narrowest pore diameter is therefore around 2.1 Å which when taking into account a van der Waals radius of 1.5 Å for the O atom leaves an inner aperture of ~0.6 Å. With the ionic radii of the cations studied Li^+ (0.76 Å), Na^+ (1.02 Å), K^+ (1.38 Å) and Ca^{2+} (1.00 Å) flexibility of the sulphate groups in a dynamic process appears necessary to account for the fact that all four cations entered the capsule interior [311].

3.1.5.3.2 Cation Uptake by Aqueous Interior Cavity

Cation uptake studies have produced some very noteworthy results. In an investigation by X-Ray crystallography coupled with ^7Li and ^{23}Na NMR studies it was shown that cations Li^+ Na^+, K^+ and Ca^{2+} can all enter the cavity of the POMs [311]:

$$[\{Mo^{VI}(Mo^{VI}_5O_{21})(H_2O)_6\}_{12}\{Mo^{V}_2O_4(SO_4)\}_{30}]^{72-}\ \textit{(POM1)}$$
$$[\{Mo^{VI}(Mo^{VI}_5O_{21})(H_2O)_6\}_{12}\{Mo^{V}_2O_4(SO_4)\}_{24}\{Mo^{V}_2O_4(CH_3COO)\}^{64-}\ \textit{(POM2)}$$

It was also shown that the countercations are replaced preferentially from the capsules' interior surface. In the case of *POM1* Na^+ and K^+ ions to a large extent and Ca^{++} ions completely, replaced Li^+ counterions, whereas for *POM2* Li^+ ions did not replace the Na^+ counterions. This displacement took place despite the fact that these ions should be too large to enter the cavity of the capsule through a 'fixed' inner aperture of the channels, and hence indicating that the channel structure based on the sulfate ligands is sufficiently flexible to adapt to these specific cations. The extent to which the counter ion transport (intrusion of, e.g. Na^+; extrusion of Li^+) takes place depends on the concentration ratio of the two cations [311]. As suggested the ion channels formed by the Mo_9O_9 rings and internal ligands are flexible and adaptable with regard to the passage of different cations due to the remarkable local interactions between the weakly bound internal ligands such as sulphate and the entering cations [311].

3.1.5.4 Gating transport properties of Polyoxomolybdates (POMs)

"Gating" is described in later work on Pr^{3+} uptake into the highly negatively charged Mo_{132} (with SO_4^{2-} as ligand) POMs. The term gating was used, as, in high concentration conditions a certain amount of Pr^{3+} was taken up by the interior meanwhile displacing NH^{4+}.Further Pr^{3+} ions were then coordinated by the shell exterior [314]. Mimicking biological cation transport may require an adaptive ion flux controlling mechanism and to this end initial investigaions

were carried out on non-covalently bonded “molecular plugs”. Initially guanadinium chloride was seen to fit exactly within the pores of the Mo_{132} cluster (with $H_2PO_2^-$ as internal ligand) [309].

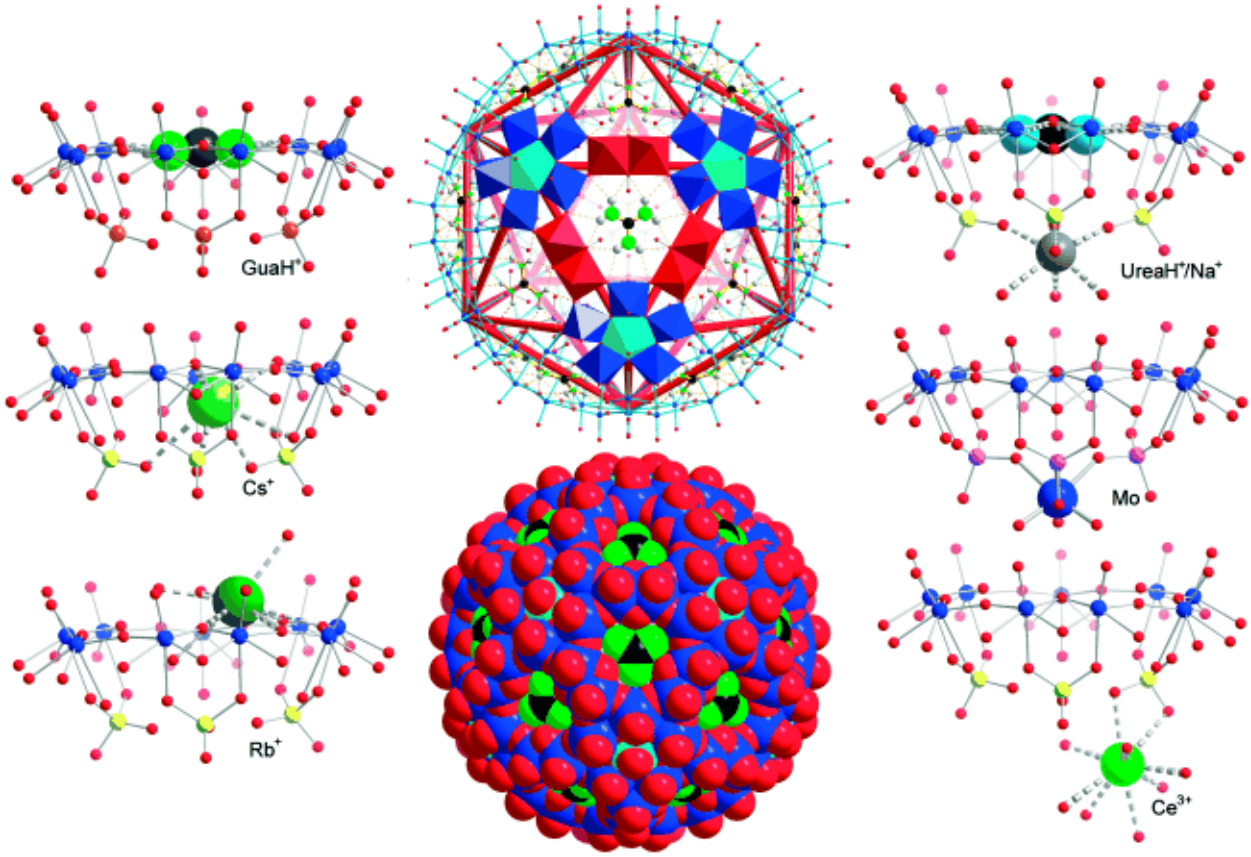

Figure55: Cations residing at well defined positions of capsule type $\{Mo^{VI}(Mo^{VI}_5O_{21})(H_2O)_6\}_{12}\{Mo^{V}_2O_4(ligand)\}$ [309].

Later other compounds were tested such as formamidinium and acetamidinium cations acting as supramolecular guests on the polytopic receptor capsule surface [310]. Formammidinuium was shown to inhibit Li^+ exhange processes with increasing concentration. Based on their supramolecular nature these blocked pores were shown to be unblocked by increasing temperature, as demonstrated by Ca^{2+} influx experiments. These summarized works give us a taste of the potential of POM’s acting as ion regulating nanoassemblies. Their behaviour can be engineered through simple ligand exchange syntheses which determine resultant pore size and coordinating properties of the inner pore aperture and inner surface.

3.1.6 Physical Methods to Measure Ion channel activity

Synthetic ion channels are studied mainly by two platforms, vesicles and planar bilayer membranes. Vesicles are prepared by dispersion of phospholipids in aqueous solution to

spontaneously form spherical closed-shell structures. They range in size from 20 nm to 1 μM and may be bounded by one or more layers of bilayer membrane.

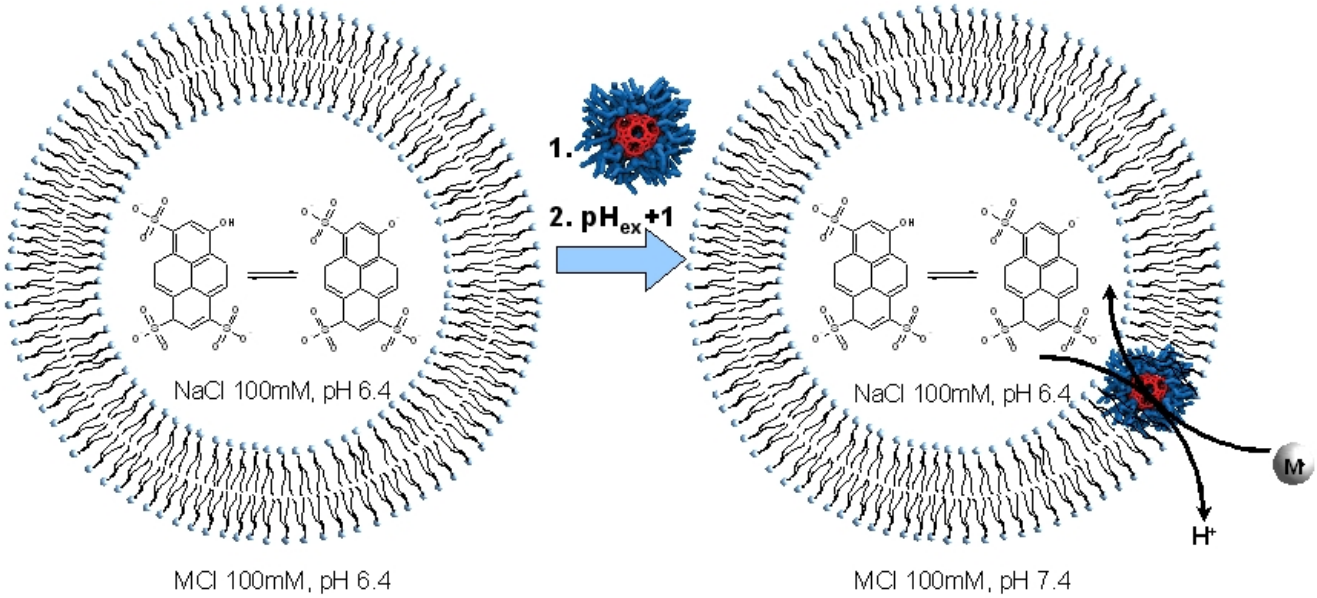

Figure 56 Scheme demonstrating principle of ion channel-cation interaction dependant pH gradient collapse measured with internal pH sensitive dye.

Flourescent dyes can be used to report a changing ionic composition in vesicle interiors. An example is HPTS (8-hydroxypyrene-1,3, 6-trisulfonic acid) which is a fluorescence sensor for quantifying pH in the range from 6.5 to 8.5. It can serve as an intravesicular pH meter that ratiometrically detects the collapse of an applied transmembrane pH gradient as well as the ability of synthetic ion channels to accelerate this process. The vesicles are prepared in the presence of HPTS with the excess then removed by gel filtration.

A pH gradient between the vesicle interior and external solutions is created by addition of an extravesicular NaOH solution (pH=6.4→ 7.4). This base pulse causes an H^+ efflux or OH^- influx facilitated by the synthetic ion channel. The charge translocations are compensated for by cation influx in response to proton efflux or anion efflux in response to hydroxyl influx. Therefore the increase in intravesicular pH, monitored by the entrapped pH-sensitive dye, HPTS, reflects the electrolyte exchange rate [315-318].

This technique may thus allow selectivity sequences to be established for synthetic ion channels. Changes in the increase of HPTS emission ratio (I_{460}/I_{403}) with time are measured in the presence of different external cations M^+. This method provides reliable results which are identical to those produced in bilayer lipid membrane conductance studies in terms of cation selectivity sequences [286,289,319-321].

Alternative methods include ^{23}Na NMR spectroscopy where a suitable paramagnetic relaxation agent, either inside or outside the vesicle causes a shift difference between external and internal sodium ions. [322].

Bilayer membranes supported in a pore have also been used for the voltage clamp technique in which a constant transmembrane potential is applied and current changes are then monitored with time [246].

3.1.7 Solid Supported bilayers

Biomimetic membranes on solid supports allow powerful analytical techniques to be used to study interactions at the surface such as AFM, QCM, SPR etc. These biosensor components can serve as model membranes in the study of cellular processes. One of such systems is the supported lipid bilayer which through incorporation of other elements may constitute a biological membrane mimic. These layers have been prepared by two general methods. One way uses the Langmuir-Blodgett technique to transfer the lower leaf to the solid support with the second leaf then added by horizontal dipping, using the Langmuir-Schaefer method [77]. A more versatile method involves the fusion of small unilamellar vesicles to the solid support [323,324] which is a spontaneous process affected by factors such as phospholipid chemistry, pH and ionic strength of solution and also surface and vesicle properties [325-327]. The SUV's themselves can be prepared by different methods namely the extrusion method [328,329] or by sonication coupled with centrifugation [330].

3.1.7.1 QCM and Supported Bilayers

QCM based techniques have been previously used to study the interaction between unilamellar vesicles and surfaces [331-334]. Keller et al. looked at phospholipid vesicle adsorption on oxidised gold, silica and alkanethiol SAM surfaces. The results indicated bilayer formation on silica, single layer deposition on the SAM and intact vesicle adsorption on oxidised gold [331]. Later they observed the progression in the vesicle fusion process on SiO_2 by combining QCM and SPR [332].

Ha et al studied the behaviour of such vesicles when exposed to hydrophobic surfaces, specifically ODT funtionalised gold. They studied the adsorption by both ellipsometry and QCM where ellipsometry results were consistent with a monolayer deposition the QCM frequency change when correlated with the Sauerbrey equation suggested 30 layers which

they put down to adsorbed intact vesicles adsorbed on the hybrid bilayer [333] or in the light of the inapplicability of this equation to such measurements (see section 2.1.4) could be due to water molecules and viscosity changes.

3.1.7.2 Solid Supported Hybrid Bilayers

Another class of biomimetic lipid interface is the hybrid bilayer membrane. Pioneered by Plant et al. [79,335] this type of bilayer consists of a inner leaf of alkanethiol covalently bound to a solid support with an outer leaf of phospholipids and may act as a more stable biomimetic membrane than the supported bilayer due to the strong covalent interaction between the lower leaf and the substrate while showing less fluidity in its exposed leaf due to the increased crystallinity of the alkanethiol leaf [336]. On gold substrate the first step is self-assembly of an alkanethiol layer usually octadecanethiol (ODT) due to its well studied propensity to form close packed well ordered SAM's from ethanolic solutions. The phospholipid layer can then be added by transfer from the air-water interface or more commonly vesicle rupture and organisation.

3.1.7.3 Supported Bilayer Membrane Formation and Structure

It has been shown that in some cases vesicle adsorption occurs with the vesicles remaining intact on the surface [325,337]. The surface properties, lipid type and solution composition play critical roles. The driving force it would appear is the electrostatic interaction between the phospholipid head groups and the surface overcoming the vesicle stability. Hence vesicle adsorption and whether or not SBMs will form may be tuned by phospholipid type [338] (i.e. vesicle charge). By extension condition parameters such as pH and ionic concentration are also structure determining. Calcium ions seem to play a special role as they appear to interact with surfaces and phospholipids and tend to promote the adsorption and rupture of vesicles [338-342]. A level of surface roughness is well tolerated by this process and little affected by roughness in the nanometer range. Lipid bilayers will follow the topography of the underlying substrate [343] with the attraction for the surface enough to overcome the bending energy of the bilayer.

3.1.7.3.1 Critical vesicular Coverage

A cooperative effect on the interaction of surface and vesicle was first reported by Kasemo et al. [331,332] where they showed using SPR, QCM and simulation that:

- Isolated vesicles remain intact when bound to a silica support

- A certain density (critical coverage) is required to initiate decomposition of surface bound vesicles into bilayer patches.

3.1.7.3.2 Asymmetry

Another interesting aspected of the vesicle to supported bilayer transition is that of asymmetry. The lipid configuration is not necessarily conserved upon transition due to differences in surface affinity [344,345].

3.1.8 Mo clusters and Therapeutics

Studies have indicated that POM's present potent antiviral, antibacterial; and anti-tumor activities [346]. Their biological activity was first noted over 30 years ago where they exhibited activity against various non-retro RNA and DNA viruses in vitro and in vivo. $[NH_4]_{17}Na[Na(SbW_7O_{24})_3(Sb_3O_7)2]\cdot 14H_2O$ (HPA-23) and other polytungstates inhibited RNA –dependant DNA polymerases of retroviruses.

3.1.8.1 Poloxometallate Antiviral Properties

Research on POM antiviral activity has focused on the polyoxotungstates since as mentioned the polyoxotungstate HPA-23 was shown to active against HIV-1 in cell culture. It eventually proved to be too toxic and ineffective for clinical doses but consequently a range of new poloxometalates were developed showing lower toxicity and higher activity [347-349] [350].
Nb substituted polyoxotungstates were demonstrated as anti-HIV agents by Kim et al. [351]. Other Nb containing polyoxotungstates were shown to strongly inhibit HIV-1 Protease. The mode of inhibition was indicated by molecular modelling studies to be not by the normal route of other known inhibitors i.e. binding to the active site but by binding to a cationic pocket on the "hinge" region of the flaps covering the active site [348].
Relatedly an electrostatic recognition was proposed for Keggin structured tungsten polyoxometalates which were shown to selectively bind and aggregate the Prion protein PrP^{Sc} which causes bovine spongiform encephalopathy [352]. The Polyoxometallate-protein interaction has also been investigated for human serum albumin (HSA) [353] [354].

3.1.8.2 Poloxometallate Anti cancer Properties

In terms of potent *in vivo* anti-tumor activity the Molybdenum containing POMs have shown great potential. Polyoxomolybdates have shown anti-cancer activity for a range of tumors

since 1988 when anti tumor activity was shown against murine mammary cell line, Meth A sarcoma and MM46 adenocarcinoma [355-357]. The results indicated that the Mo_7O_{24} is a critical structure for antitumor activity. DNA ladder formation and DNA fragmentation were observed in the treatment of human pancreatic cancer cells [358] and proceeding thought on the mechanism of action is that the activity is a result of activation of the apoptotic pathway. It has been proposed that the electron transfer system in the mitochondria of the tumor cells, which preferentially take up the $[NH_3Pr_i]_6[Mo_7O_{24}]\cdot 3H_2O$ (PM8), reduce it to a more cytotoxic species PM17 [359]. The reduced species $[NH_3Pr_i]_6[H_2Mo_{12}O_{28}(OH)_{12}(MoO_3)_4]\cdot 2H_2O$ (PM17) has been shown to exhibit more potent anti-tumor activity than PM8 against difficult to treat pancreatic cancers [360].

3.1.8.3 Nucleotide-POM interaction

Interest in the interactions of molybdate and nucleotides was stimulated by the the anticancer, antiviral and antibiotic activity of polyoxometalates. The molecular origins of the biological activity of polyoxomolybdates remained poorly understood and was further complicated by the dynamic nature of Mo clusters. Polyoxomolydates have long been known to show a weak non-specific interaction with DNA [361] [362]. Hill et al. concluded that complexation between molybdates and a range of nucleotides occurred though the phosphate moiety [362]. Studies on the hydrolysis of ATP→ADP catalysed by polyoxomolybdates showed that these clusters were highly efficient catalysts even at room temperature in contrast to divalent metal ion catalysts which required elevated temperatures [363].

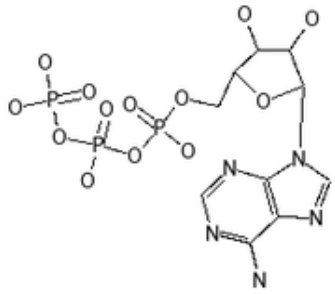

ATP

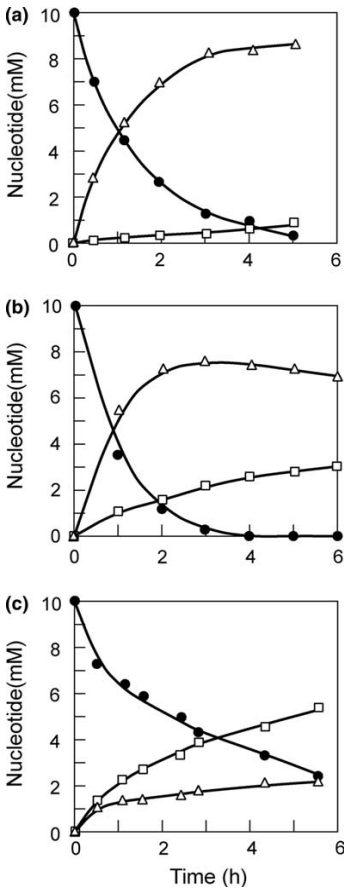

Time-profile of the ATP hydrolysis followed with HPLC at pH 6 (a), pH 4 (b), and pH 2 (c). Initial concentration is 10 mM Na2ATP Æ 3H2O and 200 mM Na2MoO4 Æ 2H2O (ATP = ●, ADP =Δ , and AMP =□).

Figure 57 Molybdates showing hydrolytic activity on ATP [363]

Prompted by these discoveries Cartuyvels et al. discovered unprecedented hydrolytic activity of the $[Mo_7O_{24}]^{6-}$ towards phosphodiesters [364]. On a DNA model substrate bis(p-nitrophenyl)phosphate (BNPP) they noted that hydrolysis rates were nearly four orders of magnitude higher in the presense of $[Mo_7O_{24}]^{6-}$than the uncatalysed cleavage (Figure 58).

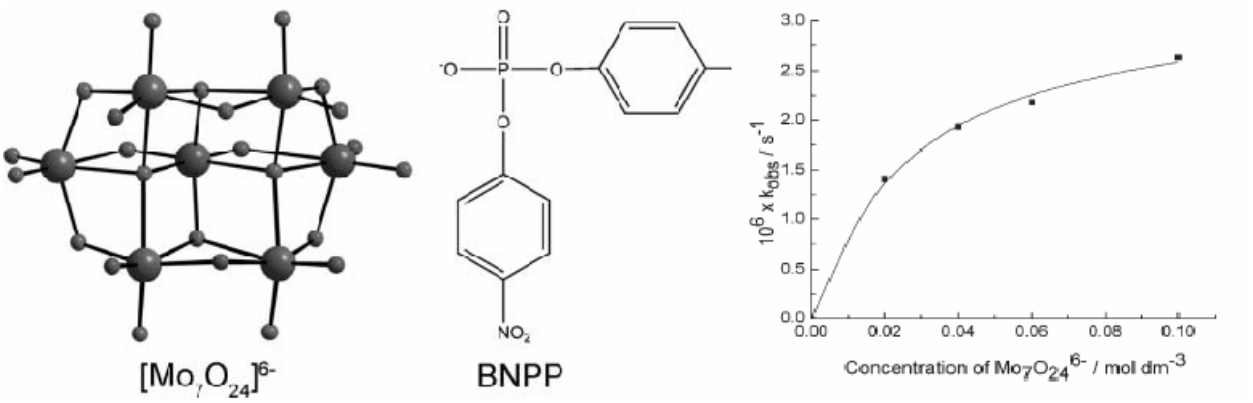

Figure 58 Influence of $[Mo_7O_{24}]^{6-}$concentration on k_{obs} for cleavage of BNPP(20mM,pH=5.3, T=50°C) [364]

Generally it was positively charged metal species which would presumably interact favourably with the negatively charged phosphate group that had been shown to act as

artificial phosphoesterases and not large negatively charged clusters with one other known exception [365]. A model for the cleavage process of NPP (nitrophenyl phosphate) was proposed based on ^{31}P and DOSY NMR data based on the incorporation of the phosphoester group into the polyoxomolybdate skeleton and sharing of oxygen atoms with Mo^{IV} centres (Figure 60).

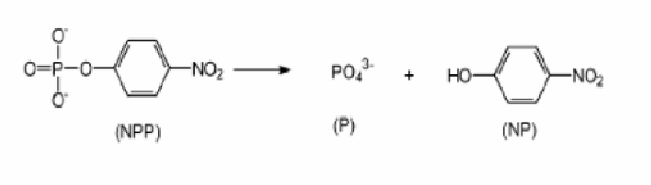

Figure 59 Phosphoester cleavage [364].

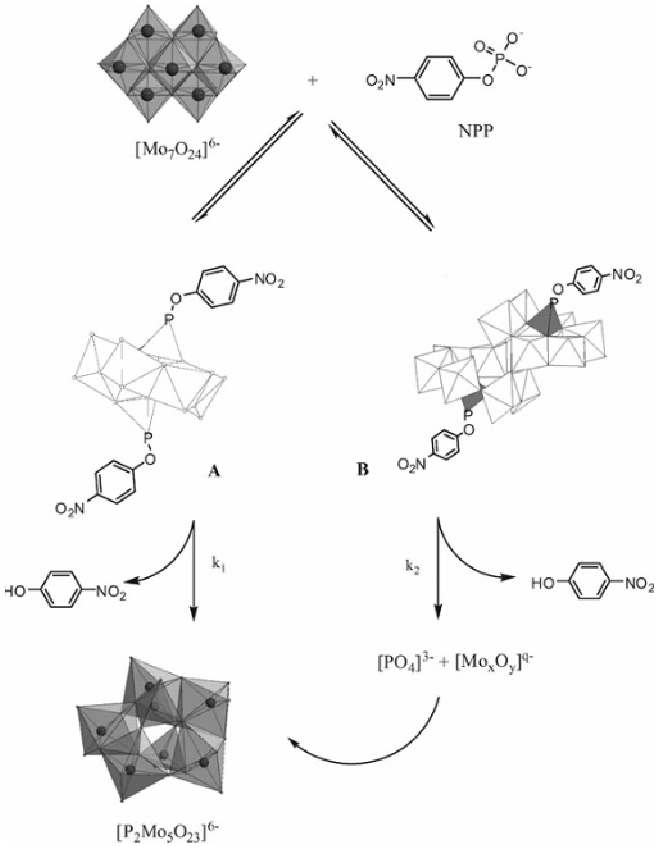

Figure 60 Proposed mechanism of phosphoester cleavage by polyoxomolybdate [364].

Related later work involved cleavage of an RNA model HPNP (Figure 61) where tests with strikingly structurally similar Tungsten clusters showing no hydrolytic activity led the authors to the belief that the inherent lability or dynamic aspect of the Mo clusters had a large part to play in their cleaving behaviour. They propose that this lability effect incorporation into the MoO skeleton of the phosphodiester group straining the P-O bond making it increasingly susceptible to hydrolysis by nucleophilic sovent water molecules [364].

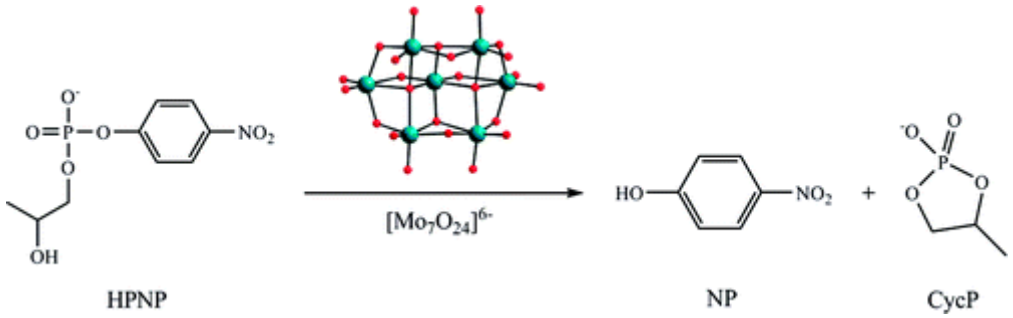

Figure 61 Hydrolysis of RNA model HPNP with $[Mo_7O_{24}]$ [364].

3.2 Results/Discussion

3.2.1 Supported Lipid Bilayers by Vesicle Deposition from Unbuffered NaCl (100mM) solution, Tris pH 7.4 and Pure water

It was noticed during the early experiments that the Tris buffer and NaCl presence seemed to have an interference or screening effect on an adsorption observed for Mo clusters on supported bilayers. It is highly favourable if not completely necessary to maintain a constant flow of a consistent buffer throughout a QCM experiment and so the possibility of forming supported bilayers from water or buffer free NaCl solutions were explored (Figure 62). In the time period marked injection solution (130 seconds long) the surface is exposed to the vesicular solution. The frequency profiles strongly suggest the adsorption of intact vesicles to a critical coverage point followed by rupture to form the supported bilayer [331] [332]. The bilayer is completed, stable and saturated. This change in sign of df/dt can be assigned to the release of trapped water on vesicle rupture [325]. In all cases the adsorption of vesicles is observed as a frequency change due to adsorbed mass corresponding to the Sauerbrey equation (see section 2.1.4).

Buffer composition has a direct effect on whether or not bilayers are formed (3.1.7.3). The NaCl concentration plays a direct role as previously reported for the DMPC lipid with an optimal concentration of 150mM [366]. In the present work a Ca^{2+} facilitation of vesicle rupture was noted for the buffer system (Tris 10mM) and also for brine solutions. This calcium effect has been previously noted [366-368].

It is known that phospholipids vesicles have a strong electrostatic interaction with Ca^{2+} and that divalent cations are known to accelerate membrane fusion processes in general by

bridging interactions between the phosphate head groups and the negatively charged SiO_2 surface [338]. When PBS was used here as buffer this effect was not observed which may be due to the phosphate ions themselves acting as bridging entities.

In (Figure 62) this "calcium effect" can be discerned on observation of curves (a) and (b). In the absence of calcium (a) it appears that a build up of intact vesicles occurs with rupture not favoured. However in the presence of calcium (1mM) SBM formation was observed in both the equivalent Tris, NaCl (pH7.4) buffer (b), (c), in NaCl solutions (d), (e) and with pure

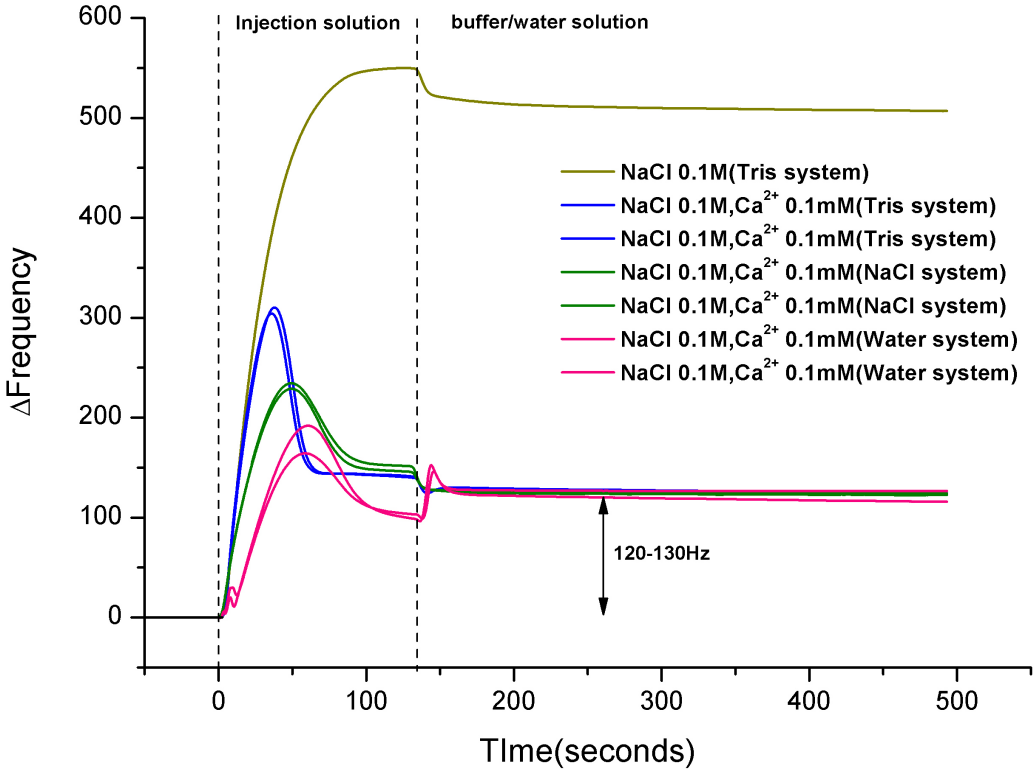

Figure 62 SBM formation from different conditions on SiO_2 layers.

water as running buffer **(f)**, **(g)**. The adsorption profile disparities as a result of varying solution viscosities are also apparent as is expected in QCM. The supported phospholipid bilayers could be removed and regenerated on the silica surfaces repeatedly in a reproducible manner. The bilayer removal was performed by injecting ethanol/water 1:1 mixtures and/or sodium dodecyl sulphate solutions (0.3%w/v).

3.2.2 Investigation of Cluster Interaction with Supported Phospholipid Bilayers

3.2.2.1 Incorporation of Surfactant Encapsulated Clusters's studied by QCM

In order to investigate SEC incorporation in the phospholipid bilayer following the theoretical study previously described [290], SBM formation from SUV's equilibrated with the synthetic ion channel components and their controls were examined by QCM. The experiments were performed with UHP water as running buffer with the vesicle injections containing NaCl 100mM and $CaCl_2$ 1mM. (Figure 63) shows evidence for SEC incorporation and transfer to the supported bilayer structure. The larger dF observed for POPC with unencapsulated anionic clusters (green line) can be assumed to be a result of electrostatic interactions between phospholipid headgroups and the anionic clusters as reported in the next section (see section 3.2.2.2).

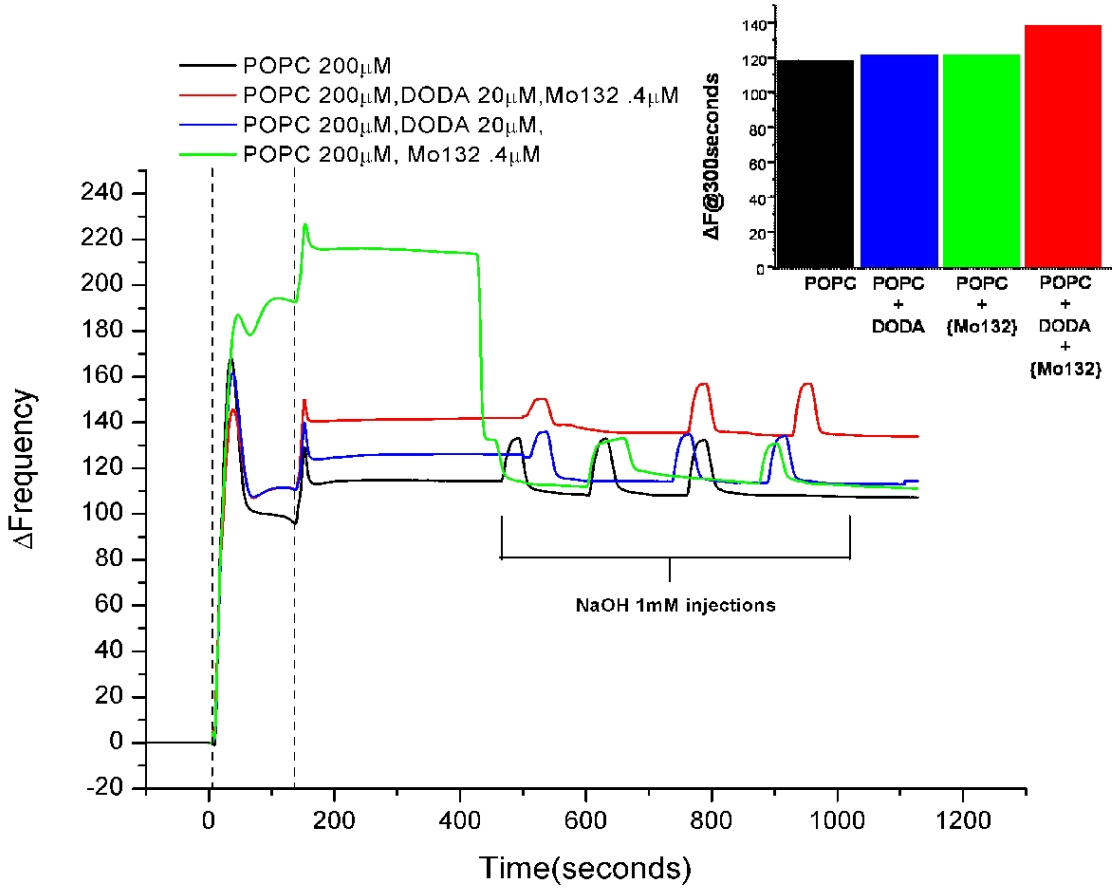

Figure 63 Supported bilayer formation from vesicles incorporating incorporating SECs on silica surfaces.

Bilayer formation appears to be unaffected as upon addition of NaOH (1mM) a stable frequency corresponding to the supported bilayer only is produced indicating cluster removal (Figure 64).

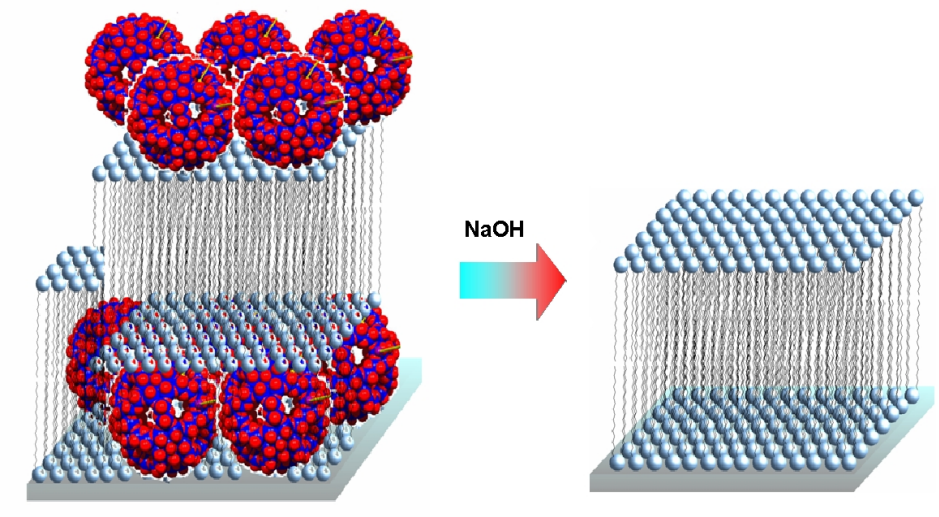

Figure 64 Representation of case where DODA-Br surfactant is absent (green line above)

This contrasts with the case with DODA surfactant present in a >40:1 ratio (red line) where a stable frequency of higher value is observed which is also stable towards NaOH (1mM).This increased frequency represents a greater deposited mass indicating that the clusters are associated with the surface and bilayer while their stability to the NaOH solution indicates protection by supported bilayer membrane incorporation (Figure 65).

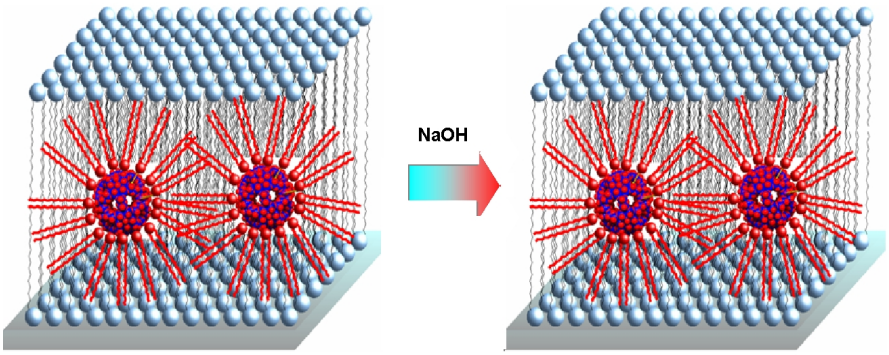

Figure 65 Representation of case when DODA-Br is present (red line above)

3.2.2.2 Interaction of Supported Bilayers and Molybdenum Clusters "Mo132 "and "Mo72Fe30"

It was noticed during the course of the experiments that the negatively charged molybdenum clusters were adsorbed on SBMs with this adsorption affected by factors such pH and ionic

strength. They adsorbed to the phospholipid head groups in a manner cleavable by aqueous base whereby they could be removed from the bilayer through injection of a 1mM or 10mM NaOH solution depending on cluster type. The tests were performed for both the Mo_{132} and $Mo_{72}Fe_{30}$ type clusters, which are known to show different surface properties, from aqueous solutions with pure water as running buffer. Both cluster types showed different adsorption responses dependant on pH and presence or non-presence of NaCl. This may be expected given the differing surface electrostatic properties of both clusters. The frequency changes observed can be viewed as being determined by cluster surface properties and also interpreted with reference to cluster vesicle formation characteristics [298]. The clusters are negatively charged in solution balanced by small counterions and can be categorised into two groups, strong electrolyte and weak electrolyte based on their solution behaviours.

The strong electrolytes ("molecular conductors") exhibit a delocalized negative surface charge and as a result are highly soluble in water. Some of these macro-ions tend to self-assemble into single-layered spherical, hollow, vesicle-like structures due to attractive forces thought to result from the presence of countercations (alkaline metal and/or H+). An example of this type of higher level assembly is demonstrated by the anionic wheel cluster "Mo_{154}" [301] as well as the spherical keplerates.

The "Mo_{132}" cluster falls into the category of strong electrolyte but its self assembling properties are not apparent in aqueous solutions. No vesicle formation was observed in 100% aqueous solutions at 1mg/ml by Liu et al. but could be driven by lowering the polarity of the solvent with water /acetone mixtures [369] where they proposed a solvent tunability of vesicle size.

The "$Mo_{72}Fe_{30}$" on the other hand falls into the weak electrolyte ("molecular insulator") category. It has a localized charge distribution due to the presence of hard centres Fe^{III} and Mo^{VI}. It can also be considered a nanoacid as it possesses 30 $Fe^{III}(H_2O)$ surface groups which can undergo pH dependant deprotonations. Surprisingly it shows assembly properties at 1mg/ml in water. It assembles to form blackberry type vesicular structures as has been previously noted (Figure 51) [308]. The aggregation process was relatively very slow however as vesicular aggregation of the $Mo_{70}Fe_{30}$ required several weeks showing less than 1% by DLS after 4 days and taking 72 days to be judged complete [299,308]at RT. This is compared to 3-5 days for solvent driven Mo_{132} assembly [369].

The supramolecular assemblies formed by the latter are thought to be different in nature to the types formed for the "Mo_{154}" wheels. The strong electrolyte types are thought to associate in solution due to Van der Waals interaction as a result of their high polarizability. The $Mo_{72}Fe_{30}$ as well as possessing much lower polarizability possesses less electrostatic bonding and hydrogen bonding possibilities. Experiments have shown however that the vesicle formation is still very much charge related showing pH dependence, with larger aggregates forming going from pH6 to pH3. At H<2.9 however, no supramolecular structures were observed due to the clusters as weak acids becoming almost neutral in solution [304]. Above pH2.9 the varied deprotonation configurations result in varied thermodynamically favoured vesicular structures while decomposition of the anionic cluster itself may occur above pH6.6. In comparison, the $Mo_{72}Fe_{30}$ cluster shows increased skeletal stability in solution between pH 2 and 6.6 when compared with the parent Mo_{132} [304]. Supramolecular assemblies of polyoxomolybdate (POM) clusters have been previously realised based on their negatively charged surfaces ,directly by electrostatic LBL assembly [307,370,371], and indirectly through the surfactant encapsulated form where assembly has been demonstrated driven by the hydrophobic effect at the air-water interface for LB transfer [307]. Ionic effects on vesicle formation by $Mo_{72}Fe_{30}$ has also been investigated with larger vesicles forming with increased ionic strength presumably by decreasing the interparticle repulsion interaction [303].

The experiments were performed by initially forming supported bilayers following the vesicle fusion method (sees section 6.2.3) from an aqueous solution (NaCl 100mM, CaCl2 1mM) of POPC (200μM) vesicles. POM solutions in pure water were then passed over the surface adsorbing to form stable layers which were stable to acidic solutions (1mM and 10mM HCl) but were removed with NaOH solutions (1mM for Mo_{132} and 10mM for $Mo_{72}Fe_{30}$).The results were recorded and frequency change after 300 seconds was taken as stable response time for plotting of concentration against frequency change.

The reversible nature of the adsorption is shown for $Mo_{72}Fe_{30}$ and Mo_{132} type clusters in (Figure 66) and (Figure 67) respectively. The clusters were adsorbed from solutions at varied pH levels where upon injection end (130 seconds) the setup was under a constant flow of H_2O. Initially it was noticeable that the adsorbed $Mo_{72}Fe_{30}$ clusters required a stronger NaOH solution to regenerate the supported bilayer surface as opposed to the Mo^{132} indicating a stronger interaction. This may be expected given the as previously noted differing surface properties. The "weak electrolyte" $Mo_{72}Fe_{30}$ exhibiting localized charge on its surface may be

showing a more spatially specific and hence stronger interaction when compared with the delocalized surface charge of the Mo_{132}. This difference in layer stability of the two POM types investigated could also be accounted for by hydrolysis of the clusters back to their molybdenum oxide fragments with the $Mo_{72}Fe_{30}$ noted as a more stable species.

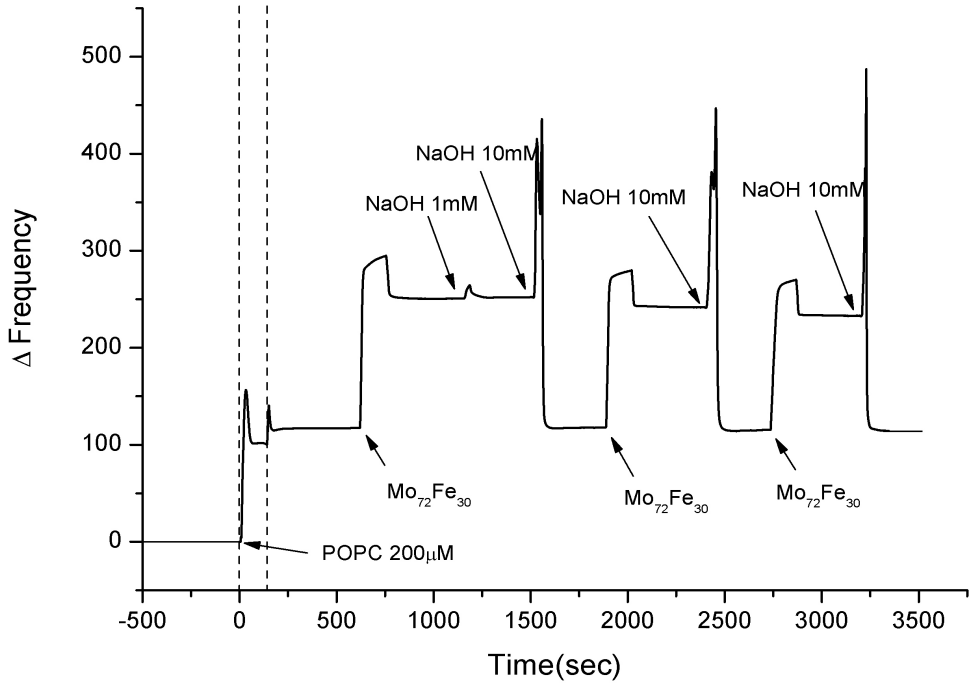

Figure 66 Reversible adsorption of "$Mo_{72}Fe_{30}$"(of lowering concentration) on supported phospholipid bilayers by QCM for pH2.5 .

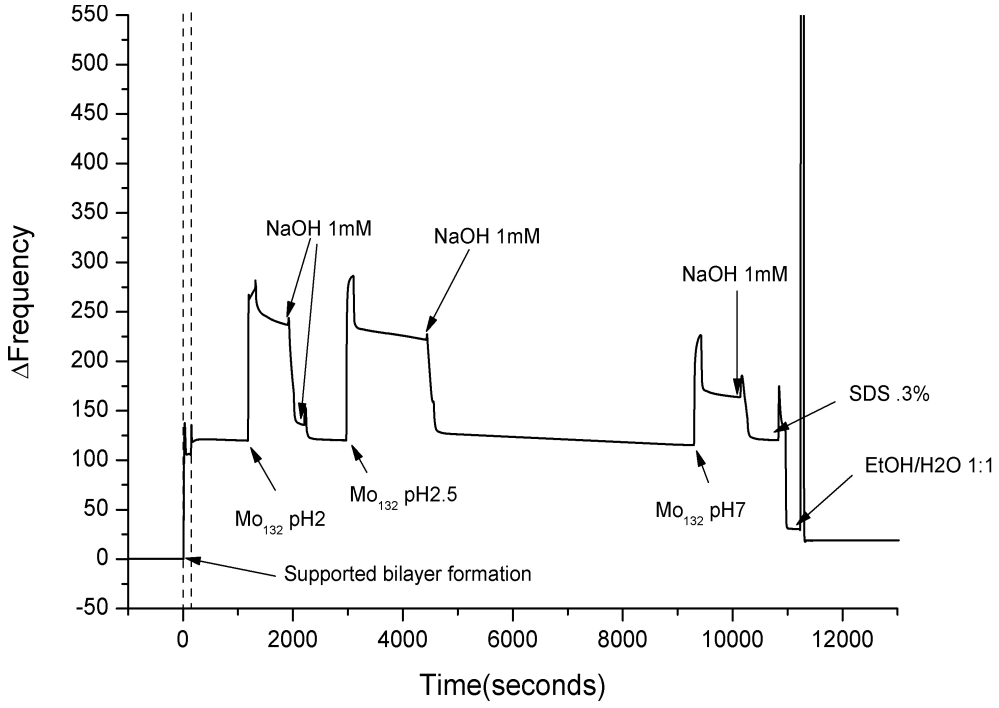

Figure 67 Reversible adsorption of "Mo_{132}" on supported phospholipid bilayers by QCM.

The POPC bilayer presents a zwitterionic head group terminated by a cationic choline group which could directly interact with the negative clusters. This aspect of supported bilayers has been previously demonstrated for polyelectrolyte-phospholipid bilayer multilayers using negatively charged polyelectrolytes [372-374].

3.2.2.2.1 pH Effects on POM cluster adsorption

Solution pH greatly affects adsorption response especially in the case of the Mo_{132} clusters. At pH below 2.5 there is a large increase in the response which was accompanied by a blue colour in the solution. This blue colour corresponds to a surface oxidation of the Mo_{132} clusters from Mo^{V} to Mo^{VI} resulting in altered surface electronic properties [375]. This blue colour change was noticed in a study by Müller and co-workers [295] and was attributed to oxidation of the $\{Mo^{v}_{2}\}$ linkers of spherical Mo_{132} keplerate to O=Mo(H2O) i.e. oxidation in acidic solutions of:

$$(NH_4)_{42}[Mo^{VI}_{72}Mo^{V}_{60}O_{372}(H_2O)_{72}(CH_3COO)_{30}].c.a.300H_2O.10CH_3COONH_4 \textbf{(35)}$$

Work by the same group has shown that in "molybdenum blue" solutions this colour corresponds to the prototype "Mo_{154}" wheel structure [375]. At low pH oxidation of Mo^{V} to Mo^{VI} results in a reconstitution of the kepelerate to a wheel structure which contains only 28 Mo^{V} units as opposed to 60 Mo^{V} in the case of $Mo_{132.}$ The blue colour results from compartmentalisation of the 28 delocalized 4d electrons within the wheel structure.
The solutions used in theses experiments were aged by three days before use which was enough time for Mo132 in solutions < pH2.5 to reconstitute by surface oxidation.

The resulting adsorption results from the change in nanoobject surface properties correlated to the brown-blue colour change (Figure 68). In aqueous solutions the nanowheels are disposed towards forming single walled vesicular aggregates [376], with equilibrium being reached after two weeks in water, whereas the Mo132 nanoclusters are not at concentrations examined [300]. Self association is thought to be stabilised by the highly hydrophilic surface templating structured water assemblies and cation mediated attraction between the discrete clusters [377].This property of the wheels may be reflected in the increased adsorption values evident at low pH (Figure 68) i.e. increased electrostatic stabilisation.

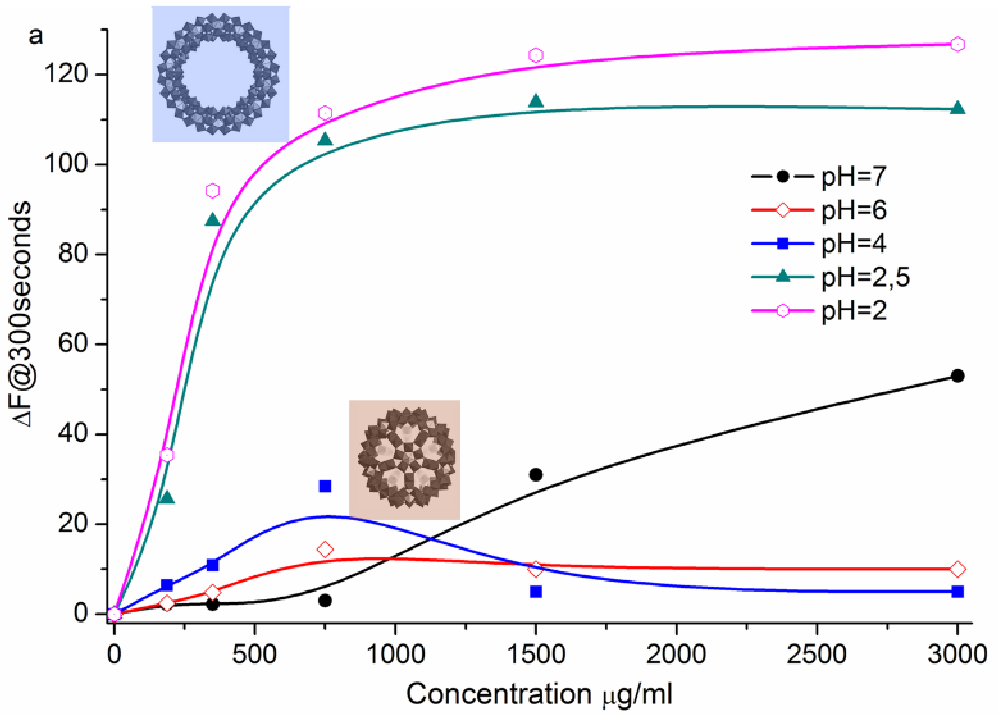

Figure 68 pH dependant adsorption versus concentration profiles for anionic clusters from (35).

The $Mo_{72}Fe_{30}$ clusters from **(37)** adsorb more favourably at lower concentrations than the Mo132 case (Figure 69). It appears that their disposition toward higher level assembly may be mirrored by that of adsorption on POPC bilayers. The micellar-like self-assembly of this cluster is far slower and believed to be different in nature to that of the Mo154 wheels. Its surface is comparably less hydrophilic with only partially deprotonated Fe coordinated H_2O ligands at the surface.

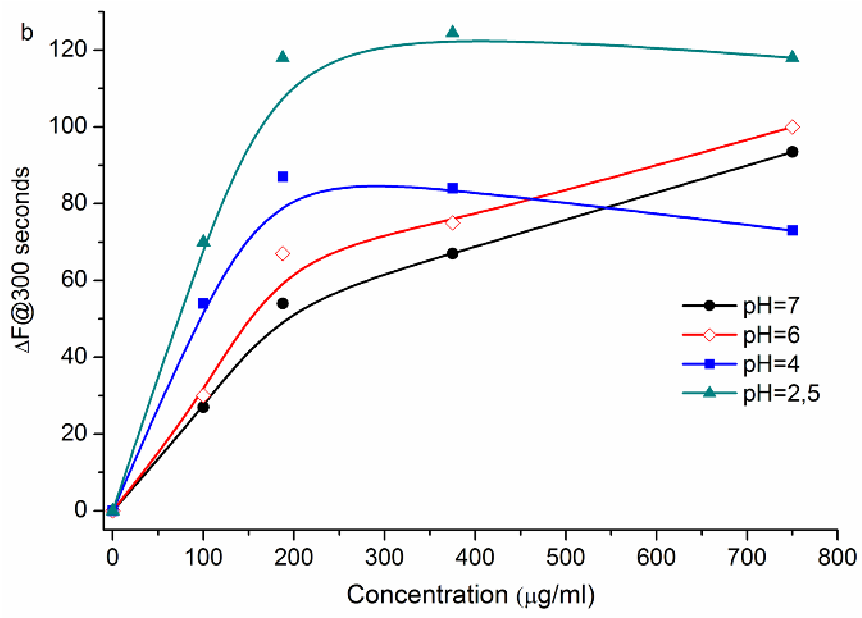

Figure 69 pH dependant adsorption versus concentration profiles for [$Mo_{72}Fe_{30}$] clusters.

However its interaction with POPC bilayers appears stronger and results in a more stable layer. Surprisingly, even at lower pH (<2.5), where it would be expected that the cluster surface be neutral and thus show less adsorption, an increased level is observed across the concentration range. This neutral surface at pH<2.5 averts vesicular assembly however it shows continued affinity for the bilayer.

The lowering of cluster hydrophilicity appears to be a determing factor in cluster adsorption as a parallel can be drawn between propensity for assembly to higher order vesicular structures in solution and bilayer adsorption. This is demonstrated by the Mo_{154} and the $Mo_{72}Fe_{30}$ surface configurations' disposition toward interaction.

3.2.2.2.2 Salt Effects

When an NaCl solution 100mM was used as running buffer and for dissolving the clusters surface adsorption was observed in the case of Mo132 for all pH values which were not observed in the case of pure water even at far lower concentrations (Figure 70). The small electrolyte appears to stabilise Mo132 layer formation also showing increasing adsorption with salt concentration.

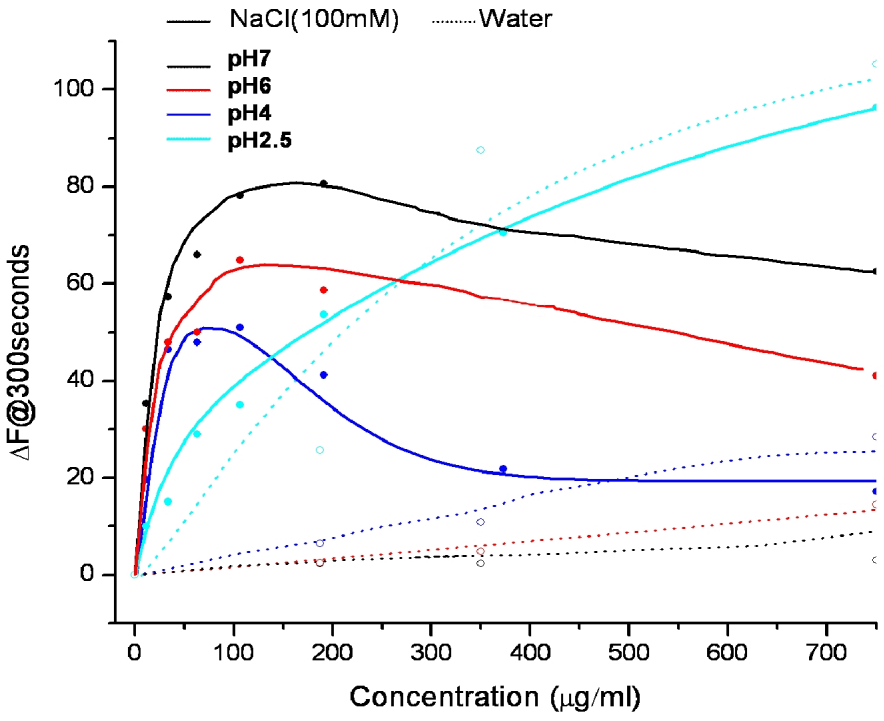

Figure 70 Comparison of [Mo132] adsorption on supported bilayers from 0.1M NaCl and pure water.

Ionic strength has been shown to effect POM macroion surface properties before .For example NaCl concentrations above .3% are known to accelerate blackberry formation for the $Mo_{72}Fe_{30}$ macroions leading to a precipitation.

Ionic effects on vesicle formation by $Mo_{72}Fe_{30}$ have also been investigated with larger vesicles forming with increased ionic strength presumably by decreasing the interparticle repulsion interaction. [378] [379] [380].

In the present study, compared to the Mo_{132} macroion, NaCl concentration up to 0.1M has minimal effects on the already strongly adsorbing $Mo_{72}Fe_{30}$. Presence of NaCl however greatly effects the interaction of the "Mo_{132}" with SBMs especially at higher pHs where the cluster retains it highly charged surface (Figure 70).

The overall picture appears to be that the more hydrophilic the surface the less the adsorption as evidenced by the increased adsorption and stability for $Mo_{72}Fe_{30}$ and the surface oxidised version of Mo_{132} **(38)** compared with the more hydrophilic Mo_{132} species (anion of **(35)**). This strong electrolyte type with its highly charged surface surrounded by layers of water ligands adsorbs to a much greater degree in the presence of salt perhaps due to a screening effect.

3.2.3 Cation Transport by Surfactant Encapsulated Clusters

Following the studies on POM-SBM interaction by QCM which supported the theoretical proposal of bilayer incorporation, the next step was an investigation of the appliance of these porous nanocontainers as selective cross bilayer channels.

Traditionally in terms of the discussion on ion channel selectivity the Eisenman sequences are used to give some interpretation of the results and by extension the channel properties. The Eisenman sequences cover cation selectivity arising solely from dehydration penalties and cation coordination strength and so runs from weak field strength site ($Cs^+>Rb^+>K^+>Na^+>Li^+$) to high field strength site ($Li^+>Na^+>K^+>Rb^+>Cs^+$) [381].

	K^+	Na^+	Li^+	Ref.
r_{ionic} (nm)	0.138	0.102	0.074	
$r_{hydrated}$ (nm)	2.01 2.7	1.78 2.4	1.55 1.95	[382] [383]
$\eta_{hydr.}$	6.6 6	5.9 5-6	4.5 4	[384] [383]
$\Delta G_{hyd.}$(kJ/mol)	295	364	474	[384]
$Vol_{hydration\ shell}$	180	160	110	[385]

Table 2 Cation physical properties

In channels with larger radii the ion-water interaction is the predominating selectivity determining factor over ion-pore interaction and so the largest ion with the lowest hydration energy will be selected. This is the case in the gramicidin channel which follows sequence II ($Cs^+ > Rb^+ > K^+ > Na^+ > Li^+$) On the other hand at a strong field site (corresponding to a site with a small effective radius) the smallest cation will be preferred due the strength of interaction overcoming dehydration energy. Ion transport can be considered, as was discussed in the earlier section, to be determined by:

- a dimensional contribution (pore size)
- electrical field strength contribution
- ion-water interactions

However binding selectivity could hardly be directly proportioned to channel conductance. One could imagine that the higher the affinity of a binding site then the less time spent in flux hence, lower gradient driven conductance. This problem is overcome by thinking of the channel as a barrier, like the K-channels selectivity filter where the dimensional contribution of the pore restricts larger cations, but the field strength in the filter is optimal for K^+ with dehydration and dipole interaction required to pass the filter.

3.2.3.1 Capsule Pore Aperture and Internal Cavity surface function

The Mo132 type keplerates have been proposed as models for cellular cation transport as a result of the biomimetic nature of their 20 pores. The pore size as well as functionality matches up quite well. The biological transbilayer cation channels are lined with carboxylate and/or carbonyl oxo groups attached to the peptide backbone whilst the Mo132 capsules can contain a range of co-ordinating ligands similar to natural channel representatives such as sulphates or carboxylate.

This work was performed on the Mo132 type capsules having formulas:

$(NH_4)_{42}[Mo^{VI}_{72}Mo^{V}_{60}O_{372}(H_2O)_{72}\ (CH_3COO)_{30}].ca.300H_2O.ca.10CH_3COONH_4$ **(35)**

$(NH4)_{72}[Mo^{VI}_{72}Mo^{V}_{60}O_{372}(H_2O)_{72}(SO_4)_{30}].ca.\ 280H_2O$ **(36)**

The anions summarised by $\{Mo^{VI}_{72}Mo^{V}_{60}L_{30}\}^{n-}$ may contain a range of stabilising ligand functionalities on their inner surface thus permitting tuning of their transport properties if

electrostatics interactions play an appreciable role in the transport process. This can be considered given the previous studies which showed cation complexation on the inner surface by sulfate ligands [312]. The Mo_9O_9 crown-ether type pores are lined with functional ligands which may impart selectivity [386] based, like in the natural ion channels, on electrostatic interaction and size effects.

Müller and co-workers performed NMR experiment to demonstrate cation selectivities of $\{Mo^{VI}_{72}Mo^{V}_{60}(SO_4)_{30}\}^{72-}$ and $\{Mo^{VI}_{72}Mo^{V}_{60}(SO_4)_{24}(CH_3COO)_6\}^{62-}$ anions [311]. The fundamental skeleton remains the same across the Mo132 type clusters with the 20 pores showing an average ring aperture of 0.45nm in diameter [312]. Evidence suggests that cations can compete for complexing sites on the capsule surfaces. As shown in (Figure 71), in the case of the $\{Mo^{VI}_{72}Mo^{V}_{60}\ (SO_4)_{30}\}^{72-}$ capsule, the inner ligand organisation can dictate the complexing ability as demonstrated by the three way symmetrical complexing of Na^+ [309] but unsymmetrical complexing of Li^+ due to the interligand distance [312].

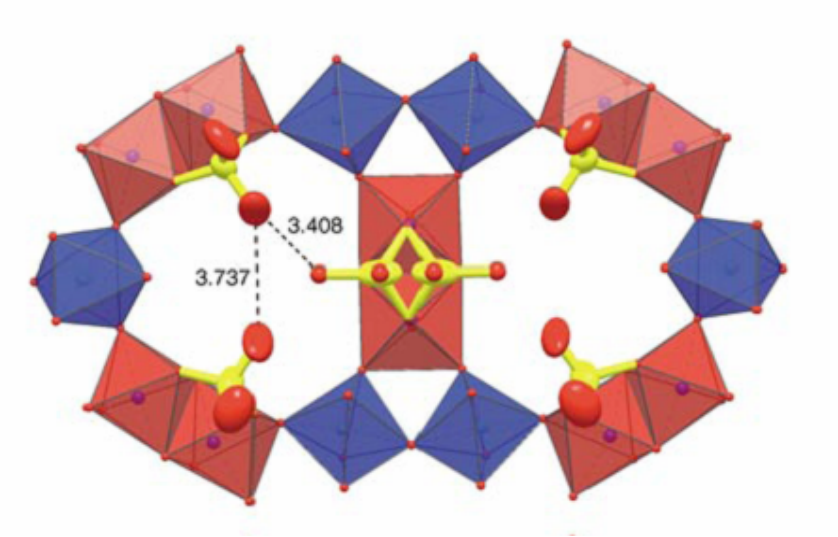

Figure 71 Two of the twenty pores if anion $\{Mo^{VI}_{72}Mo^{V}_{60}(SO_4)_{30}\}^{72-}$ [312]

The inner pore aperture formed by the associated ligands is approximately 0.6Å taking into account the van der Waals radius of the O atoms but yet the capsules take up cations with ionic radii larger than this indicating a level of flexibility at the pore, demonstrating properties similar to the biological ion channels (see section 3.1.3).

Li^+, Na^+, K^+, and Ca^{2+} have all been shown to enter the capsule interior by NMR. These results would appear to indicate that the internal surface of the aforementioned capsules complex preferentially Na^+ and K^+ over Li^+. This deduction is based on cation uptake from solutions where Na^+ and K^+ can mostly, and Ca^{2+} can fully (demonstrating its high affinity for

sulphates), replace Li^+ from the cluster internal surface whereas the Li^+ does not displace Na^+ in the reverse experiment. The extent to which the counter ion transport (intrusion of, e.g. Na^+, extrusion of Li^+) takes place depends on the concentration ratio of the two cations.

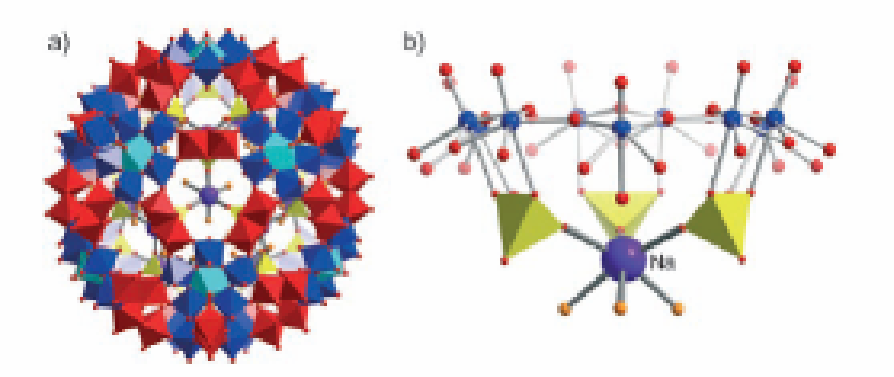

Figure 72 Polyhedral representation based on structure of { $Mo^{VI}_{72}Mo^{V}_{60}(SO_4)_{24}(CH3COO)_6\}^{64-}$ with sulphate (yellow tetrahedrons) oxygens (red) and water oxygens (orange) coordinated to sodium cation [311].

On going from the original cluster $\{Mo^{VI}_{72}Mo^{V}_{60}(CH_3COO)_{30}\}^{42-}$ to $\{Mo^{VI}_{72}Mo^{V}_{60}(SO_4)_{30}\}^{72-}$ the internal surface is modified with an increase in hydrophilicity allowing water molecules to form ordered contained nanoclusters as opposed to the disordered water assemblies present in the hydrophobic capsules' internal cavity [309]. The presence of these oxygen donor sites on the capsules inner surface can lead to cation complexation in a selective manner based on size-charge principles [387].

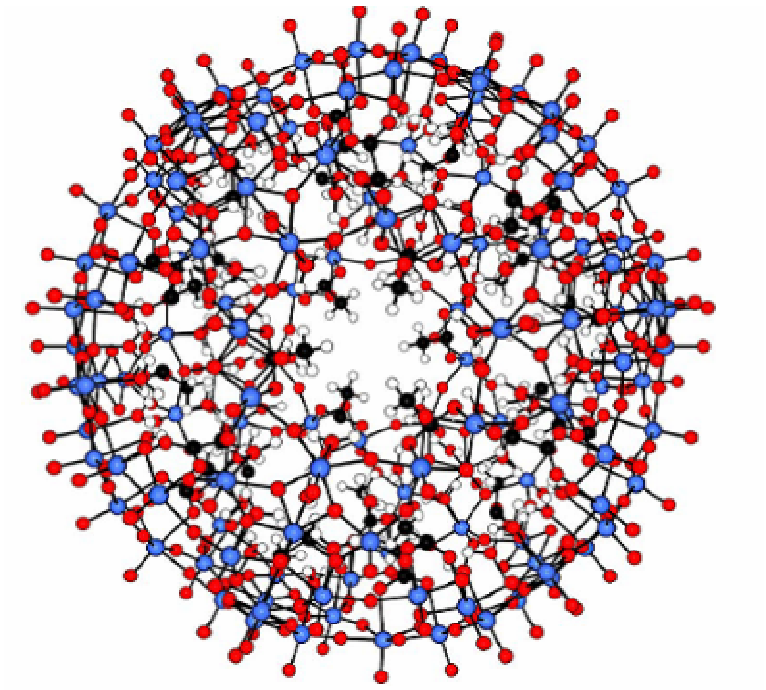

Figure 73 Ball and stick representation of { $Mo^{VI}_{72}Mo^{V}_{60}(CH3COO)_{30}\}^{42-}$ cluster showing acetate methyl groups in black and white [388].

The inner pore diameter would be expected to have a fundamental influence on transport properties. For the acetate function cluster it is difficult to define, in this case, the radius could be, at its narrowest, 0.84 Å if all H-atoms point towards the channel, but not larger than 2.36 Å in the case where the H-atoms point away (Figure 73) [388]. The Mo_9O_9 pore acts as a selectivity filter where with the maximum inner pore opening state could allow partially hydrated cations of Na^+, K^+ and Li^+ to enter the cavity or, as in the present investigation, cross a lipid bilayer .The second level of selectivity is introduced by inner surface functionalisation through ligand replacement represented here by the $\{Mo_{132}(SO_4)_{30}\}$anion. In the case of the sulphate clusters the inner pore radius at its narrowest formed by the sulphate ligands is estimated to be 0.6 Å and so ligand coordination becomes a crucial step [311].

3.2.3.2 Surfactant encapsulation effects

Can these properties hold upon surfactant encapsulation? Upon encapsulation by cationic surfactant DODA the cluster surface becomes charge neutral. The water accessible surface extends into the central cavity through each of the 20 crown like pores where as many as 50 H_20 molecules may reside indicating the validity of theses structures as ion transporters [306]. The internal surface remains partially hydrophobic due to the methyl groups of the acetate ligands pointing towards the centre of the cavity in the case of "$Mo_{132}(CH3COO)_{30.}DODA_{40}$".

The keplerates in water exhibit dynamic aspects structurally which are absent for the SECs (surfactant encapsulated clusters) as it is thought that the electrostatically adsorbed surfactant shell may confer increased stability in addition to hydrophobic surface properties.

3.2.3.3 SEC Assembly and Bilayer Inclusion Shown by Fluorimetry.

In (Figure 74) further evidence for SEC incorporation is presented. Both POM and DODA-Br need to be present for the facilitated cation transport to occur. In the control measurements where only anionic POMs or only DODA-Br surfactant were added facilitated transport of cations was not observed.

As mentioned the measurement of cation transport was investigated by observing the collapse of a pH gradient across a vesicular phospholipid bilayer. The basic concept can be viewed in (Figure 75).

An initial intravesicular pH of 6.4 is present up to 60 seconds. At this point the external solution is brought to pH7.4 resulting in an efflux of protons over 440 seconds. This is the point at which addition of a Triton solution ruptures the vesicles resulting in a fluorescence ratio corresponding to pH 7.4.

The rate of change of this internal pH was used to give pseudo first-order rate constants for cation transport as the proton efflux is balanced by cation influx as described (see section 3.1.6).

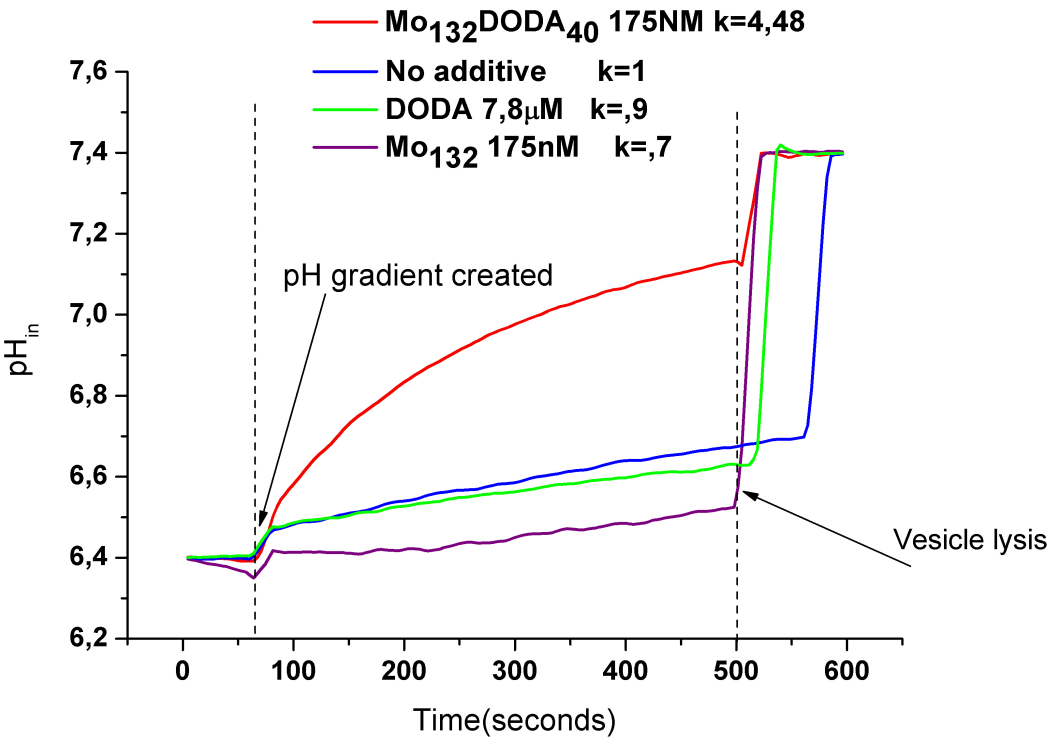

Figure 74 POM mediated cation transport with control experiments.

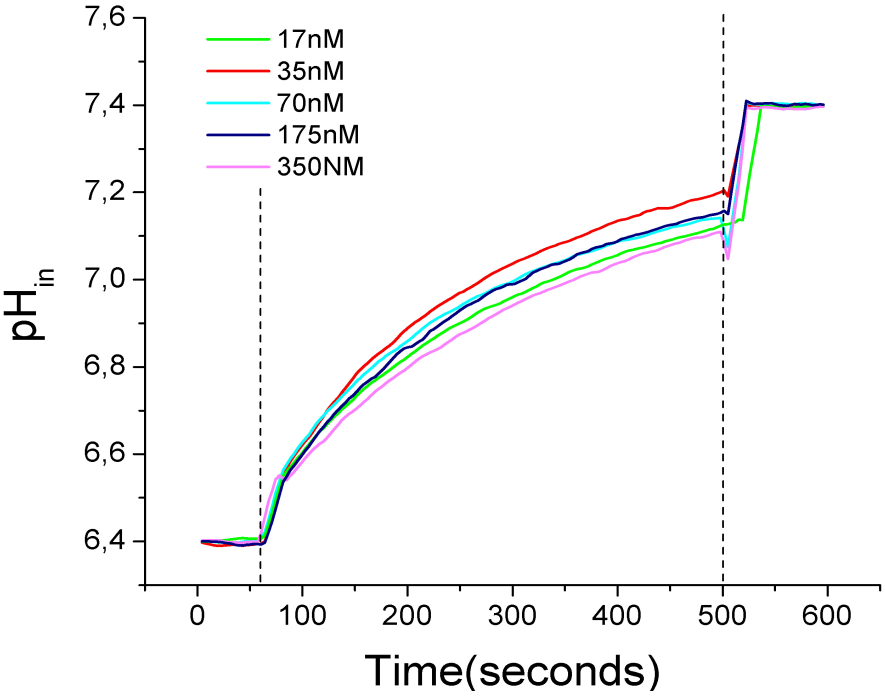

Figure 75 Typical experiment→change in intravesicular pH with time monitored by fluorescent probe

There is an overall difference between the two capsules in that the acetate capsule consistently shows higher transport rate constants. This can be visualised qualitatively in (Figure 76) where the general trend of higher cationic flux in the acetate clusters is quite apparent.

This difference was apparent for all three cations (Figure 77).Transport selectivity however was not shown clearly by each capsule. The basic difference in transport rate between each type of capsule can be attributed to pore size effect. As described the capsule exhibiting the acetate internal surface depending on ligand orientation can show a pore radius of 2.36Å which would allow all three cations pass in their hydrated form. Considering the similarity in

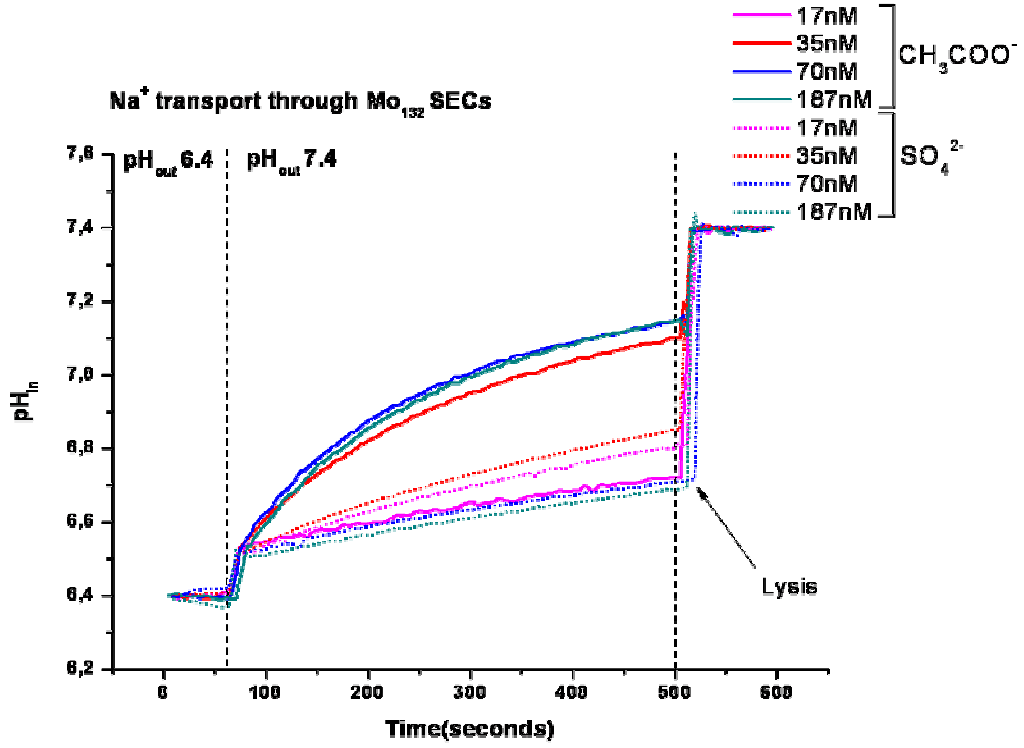

Figure 76 Comparison of Na^+ transport with coordinating (SO_4^{2-}) and hydrophobic (CH_3COO^-) clusters

this value across the three cations it would not be expected to impart much selectivity. The sulphate functionalised capsule on the other hand exhibits a functional pore which could be expected to show both size and coordinative selectivity. The results show that the modified pore structure indeed inhibits cation flux. With a pore radius of 0.6 Å it is thought that dynamic coordinative behaviour allows the the incorporation of cations with radius larger than this as K^+, Na^+ and Ca^{2+} have all been shown to enter this capsule in its non-surfactant encapsulated form. Coordinative behaviour is also expected to impart selectivity with K^+ and Na^+ coordinated preferentially over Li^+. This type of tight fit ligand directed selectivity is reminiscent of the "selectivity filter" of the natural monocation channels.

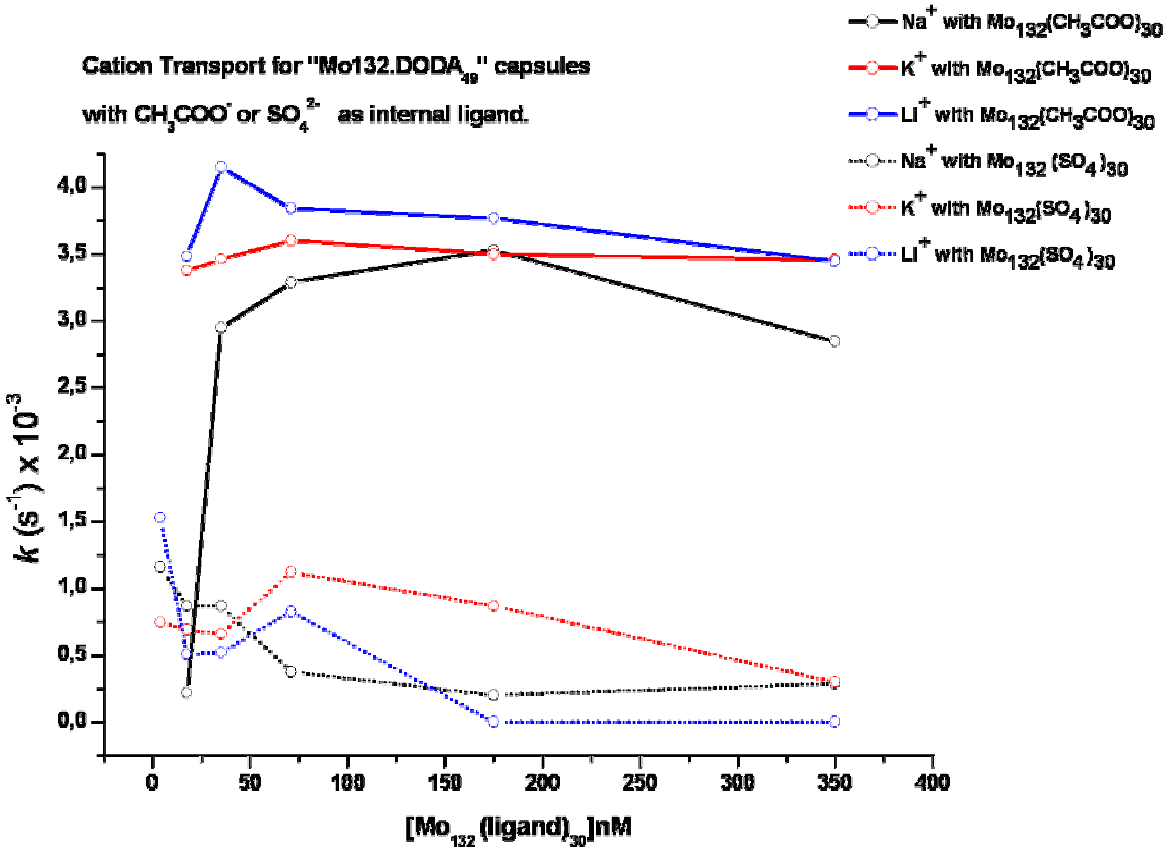

Figure 77 Plot of transport rate constants against Mo_{132} capsule concentration.

$Mo_{132}(CH3COO)_{30}$						
Conc(nM)	**4nM**	**17nM**	**35nM**	**70nM**	**187nM**	**375nM**
Na^+	-	0.2	2.95	3.29	3.53	2.85
K^+	-	3.38	3.46	3.6	3.5	3.5
Li^+	-	3.48	4.15	3.88	3.77	3.5
$Mo_{132}(SO_4)_{30}$						
Na^+	1.16	0.87	0.88	0.39	0.2	0.29
K^+	0.75		0.66	1.12	0.87	
Li^+	1.53	0.51	0.52	.83	0	0

Table 3 Initial Pseudo-first Order Transport Rate Constants($x10^{-3}$ s^{-1})

3.3 Discussions/Conclusions

With an eye toward novel synthetic ion channels of a tunable nature, recent progress in polyoxomolybdate research has demonstrated selective ion complexation by anionic POM clusters, while in parallel theoretical studies have described spontaneous inclusion of surfactant encapsulated clusters in phospholipids bilayers. The present work has gone some way towards demonstrating the potential of theses nanoarchitectures as novel synthetic ion channels

It was shown that surfactant encapsulated polyxomolydate clusters can act as viable ion channel structures allowing cation flux across bilayers: Investigations by the techniques used, Fluorimetry and QCM, both suggest cluster incorporation. The dependence of both the cation transport and cluster incorporation demonstrated on the presence of DODA-Br, with neither operational in its absence, can be viewed as an affirmation of the feasibility of simultaneous assembly and bilayer incorporation of SECs in aqueous solutions.

The transport experiments showed that the non-coordinating $Mo_{132}(CH_3COO)_{30}.DODA_{40}$ mediates a much higher cation transport rate than the coordinating $Mo_{132}(SO_4)_{30}.DODA_{40}$. Going on previous studies the $Mo_{132}(CH_3COO)_{30}.DODA_{40}$ cluster is essentially a non-interacting cluster where any selectivity would be derived from a limiting pore diameter. The transport properties of surfactant encapsulated $Mo_{132}(CH_3COO^-)_{30}$ show a general order of $Li^+ > K^+ > Na^+$ which could be rationalised in terms of dehydration effects at the pore. The Mo_9O_9 pore which has been shown to be around 0.45nm is quite similar in size to the 27-crown-9. Going by the values in (Table 2) displayed selectivity can be attributed to dehydration effects. Hydrated lithium ions with one shell of 4 water molecules have a hydrated diameter no greater than 0.4nm and so can pass the pore aperture without interaction on the other hand Na^+ and K^+ show hydrated diameters close to or greater than this pore diameter and my require partial dehydration through oxygen stabilisation to enter the pore. This can explain the higher transport rate shown by K^+ as a result of its lower ΔG_{hyd} i.e. less tightly bound water molecules.

While such a level of selectivity may reside on the outer surface pore it is thought that a second level exists on the inner pores through ligand coordination. As shown previously by the Müller group ligand coordination in the case of sulphate internal ligands can stabilise cations selectively based on size and charge similar to the function displayed by the natural channels. In the present work however the capsule with interior coordinating function showed

lower transport capability. A possible explanation for this observation comes from the charge of the cluster. Both Mo_{132} can take a maximum of around 40 DODA surfactant molecules electrostatically stabilised on their surface. While the $Mo_{132}(CH_3COO)_{30}$ has a charge of 42- the $Mo_{132}(SO_4)_{30}$ has a charge of 72- and so with size constraint on DODA stabilisation the other charges are counteracted by NH_4^+ on the surface. This positively charged shell may negate cation uptake acting as an electrostatic barrier.

A novel procedure for controlled cluster immobilisation was also demonstrated. It was observed that that the parent anions can adsorb electrostatically to bilayer headgroups in a reversible manner. Furthermore the adsorption properties can be controlled with pH and ionic strength modifications. The promise of this discovery lies in the fact that controlled layered assemblies of clusters may be formed for further investigation of POM properties. As well as nanoscale multilayered assemblies this pertains in particular to the biological properties demonstrated for smaller molybdenum clusters including anti-cancer and anti-bacterial properties discussed in an earlier section (see section 3.1.8). Using QCM in conjunction with a technique such as liquid atomic force microscopy the biological interactions of these large cluster layers could be extensively analysed in-situ structurally and quantitatively.

4 .Amplification by Selective transport: Amplification effect on a Glycosyl Disulfide Dynamic Combinatorial Library by Selective Transport across a Supported Liquid Memebrane

4.1 Introduction

4.1.1 Dynamic Combinatorial Chemistry

"Dynamic Covalent Chemistry" refers to a branch of chemistry which exploits reversible covalent chemistry to impart an adaptive nature on molecular ensembles. A range of different known reversible reactions have been adopted towards this goal as presented in (Table 4) taken from [389].

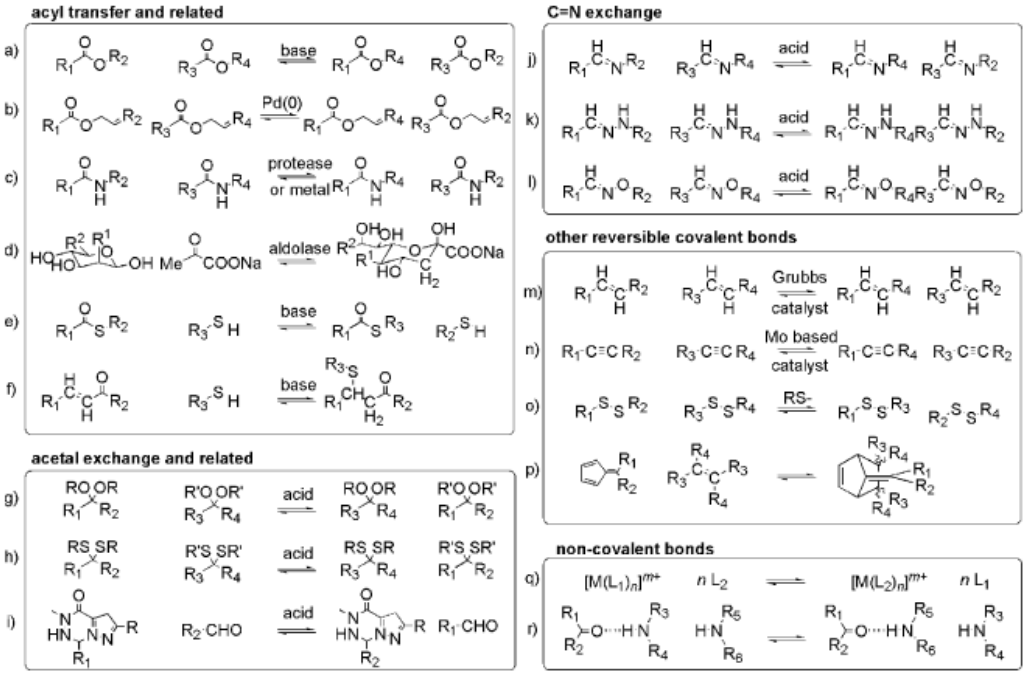

[a] (a) Transesterification; (b) transallylesterification; (c) transamidation; (d) aldol exchange; (e) transthioesterification; (f) Michael/retro-Michael reactions; (g) acetal exchange; (h) thioacetal exchange; (i) pyrazolotriazone metathesis; (j) transimination; (k) hydrazone exchange; (l) oxime exchange; (m) alkene metathesis; (n) alkyne metathesis; (o) disulfide exchange; (p) Diels−Alder/retro-Diels−Alder reactions; (q) metal−ligand exchange; (r) hydrogen-bond exchange.

Table 4 List of reversible covalent reactions adopted for "Dynamic Covalent Chemistry" [389].

Combinatorial chemistry involves the synthesis of a large number of molecules in a combinatorial fashion with non-reversible reactions preferred. Dynamic Combinatorial Chemistry however aims to exploit reversibility in covalent interactions to assemble libraries under thermodynamic control which may be influenced by external parameters such as temperature, solvent etc as ell as molecular recognition. Molecular recognition of such libraries could be of great importance in applications such as drug discovery where targets could select their highest affinity ligand from an adaptive combinatorial library (Figure 78). By introducing controlled reversible covalent chemistry one can access a virtual library whose constituents comprise all possible component combinations [389-392]. Target driven

amplification [393] of the highest affinity species from exchanging components is the ongoing goal of such investigations.

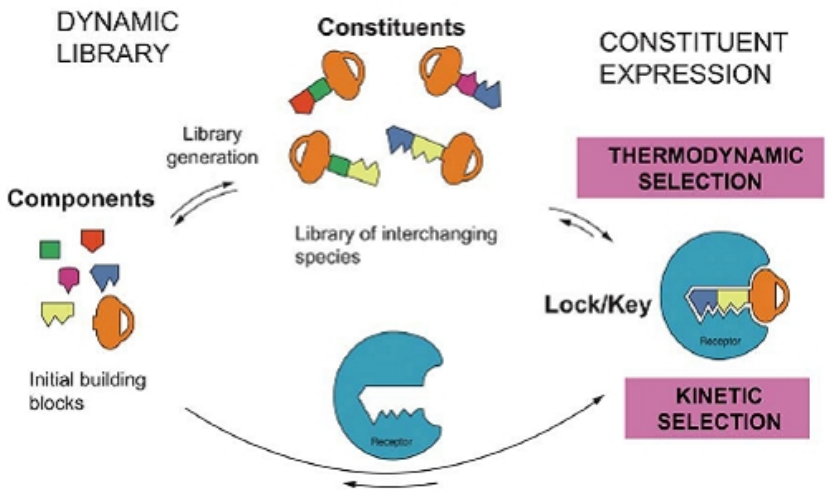

Figure 78 DCC concept : target driven assemby and amplification [390].

The choice of reversible reaction introduced in a DCL is of great importance. For the study of biomolecular interactions in biological conditions there is a considerable limitation. Reversible covalent chemistry which occurs naturally in living systems would appear highly convenient and so disulfide exchange is without doubt the most popular choice for such systems [394-405] while other reversible reactions such as imine exchange [406-415], thioester exchange [416,417] and aldol reactions [418,419] have also been utilized.

4.1.1.1 Disulfide exchange

In the generation of DCLs in biological conditions the disulfide exchange reaction holds many advantages over others such as imine where water drives the equilibrium toward hydrolysis giving very little yield of imine adducts.

Disulfide bonds are formed by the oxidation of thiol groups (Figure 79).This oxidation can be realised by atmospheric oxygen (stirring of open container) as well by a range of oxidising reagents such as H_2O_2, I_2, Br_2, NaI and other metal salts, and transition metal catalysts in air exposed solutions [420,421].

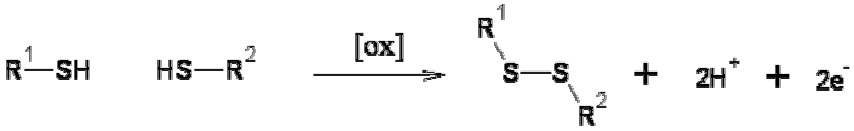

Figure 79 Disulfide bond results from thiol oxidation.

For disulfide exchange to proceed some thiolate anion is necessary as desribed by the mechanism scheme (Figure 80). Exchange can thus be controlled by pH, where, at pH below 6 exchanges can be arrested while pH above 7 is adequate to provide sufficient thiolate concentrations.

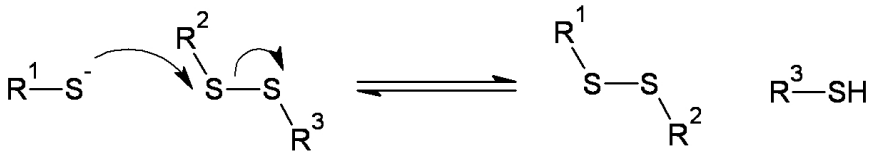

Figure 80 Disulfide exchange mechanism.

Consequently there have been two approaches towards disulfide DCL approaches:

- Thiols in an open aqueous solution at a pH above 7.5 which undergo simultaneous oxidation and exchange due to residual thioates which is a slow process, with the fixed library being reached at complete oxidation.
- Disulfides in solution with exchange initiated by a catalytic amount of a reagent such as DTT or some free thiol in conditions amenable to thiolate generation.

4.1.1.2 Saccharide Recognition and Dynamic Combinatorial Chemistry

Returning to earlier discussions (see section 1.3), lectins have been described as tools in carbohydrate chemistry and as models for the protein-carbohydrate interaction based on their known specificities and characterised structures in a number of cases. In dynamic combinatorial chemistry this application has not gone unappreciated. Concanavalin A was used to demonstrate the DCL principle for disulfide disaccharide libraries with its mannoside specificity used as driving force [394,422-424].

Other examples based on lectin-carbohydrate recognition include iron coordination and peptide decorating strategies. An early relevant example, granted it is supramolecular in nature, shows a dynamic lectin recognising structure based on Fe-bipyridine coordination which adapts its orientation through affinity for the GalNac specific lectin *Vicia Villosa B4* [425,426].

Sando et al. reported a DCL made from peptide and glycoside building blocks again using disulfide chemistry which they intended to screen against lectins [395] and disulfide chemistry was again employed for glycopeptide amplification by the WGA lectin which was demonstrated by the Davis group [427].

Returning to the carbohydrate dimers around which Ramström and co-workers based their Concanavalin A interaction investigations, they demonstrated initially a slight amplification from a library of UV active compounds (Figure 81). Using an immobilised receptor (gel bound ConA) they monitored the unbound species after equilibration as well as the bound species by removal from the gel. DTT was used as an exchange initiator at pH7.4 and equilibration was run for two weeks. The aqueous mixtures were analysed using RP-HPLC and showed evidence of amplification of the Man-Man ligand.

*Table 1. Structures of the disulfide-linked carbohydrate dimers **1**–**6**.*

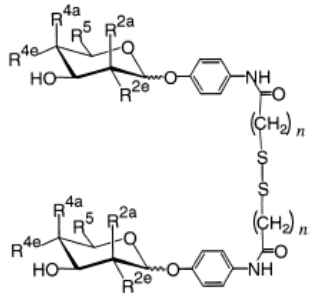

Compound[a]	α/β	R^{2a}	R^{2e}	R^{4a}	R^{4e}	R^5	n
1 (Man/Man)	α	OH	H	H	OH	CH_2OH	3
2 ($GalC_2$/$GalC_2$)	β	H	OH	OH	H	CH_2OH	2
3 ($GalC_3$/$GalC_3$)	β	H	OH	OH	H	CH_2OH	3
4 (Glc/Glc)	β	H	OH	H	OH	CH_2OH	2
5 (Ara/Ara)	β	H	OH	OH	H	H	2
6 (Xyl/Xyl)	β	H	OH	H	OH	H	2

[a] Man = D-mannose; $GalC_2$ = D-galactose, $n = 2$; $GalC_3$ = D-galactose, $n = 3$; Glc = D-glucose; Ara = L-arabinose; Xyl = D-xylose.

Figure 81 Disulfide linked carbohydrate library used by Ramstrom et al. [394].

This biorecognition was also used in the screening of acylhydrazone built di and tritopic saccharide presenting receptors with the best binder discovered by a deconvolution process [423].

In later work they turned to the simpler glycosyldisulfides, revealing their suitability as mimetics for the di and trisaccharide moieties which have been shown to exhibit greater affinity for Con A than monosaccharides while incorporating, in the disulfide bond, a dynamic aspect. Based on a Mannan film adsorbed on a quartz crystal shown to bind Con A specifically [428] they studied the inhibition of this process with a range of thiosaccharides and glycosyldisulfides (Figure 82) noticing an inhibition in the cases of Man-Man(1-1), Glu-Glu (2-2) and even Gal-Gal (3-3) with the latter two's inhibitory effects non-existent in the presence of calcium [429].

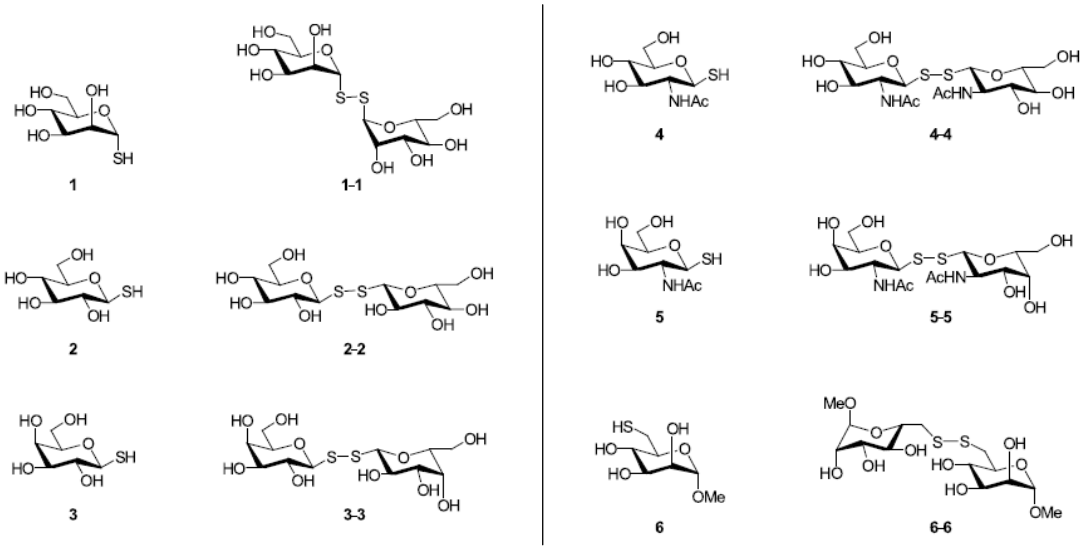

Figure 82 Library of glycomimics studied for Con A binding inhibition on Mannan film [429].

This Mannan film Con-A system was again used to screen a 14 member thiol DCL with the expected result of the ManMan dimer (Figure 83, **1-1**) proving to be the best inhibitor.

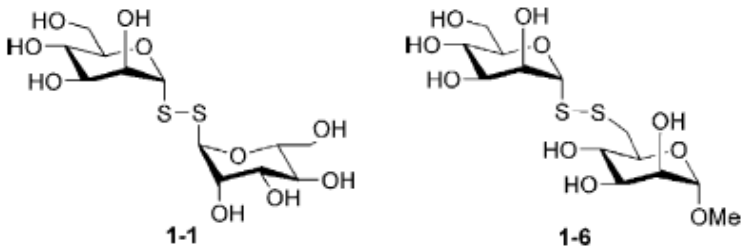

Figure 83 Best Inhibitors of specific Concanavalin A polymannoside recognition [429].

This work showed that such glycosyl disulfides are effective as glycomimetic structures for the oligosaccharide moieties involved in natural processes. They display enhanced affinity when compared to the corresponding monosaccharide structures related to their structural similarities with the highest affiniy ligand trimannoside, a property that has also been demonstrated in other studies with dimannosides [40,44]. By incorporation of the dynamic disulfide linkage there is also the possibility of selection from interchanging species in exchange conditions resulting in a real time amplification of the best binding species.

4.1.2 DCL limitations and Amplification Approaches

In general for DCL amplification it has been noticed that there are some very important parameters if one is to realise an amplification of the best binder:

Isoenergetics

It is highly favourable in DCL experiments that the library members exist in equal concentration distribution at equilibrium in absence of the target. If for example the concentration of certain components was highly biased then any observed shift in equilibrium distribution on target introduction may be greatly outweighed by the original bias.

No. of Library members

Most works up to the present have involved small libraries in "proof of principle" or highly simplified systems. As an eventual practical aim of this concept is drug discovery by target amplification from large compound libraries it is vital to take into account thermodynamic considerations as the number of members increases. The mean yield of the most highly amplified host decreases with increasing library size although the upper limits of usefulness has been postulated to be 10^6 members given the right conditions [430,431].

Importance of target concentration

A low target concentration is preferable .The higher the target concentration then the poorer the correlation between affinity and amplification [393,432,433].

How to find amplification

Looking specifically at library amplification by molecular recognition their have been some elegant approaches towards discerning such an occurrence.

Molecular recognition induces a shift in product distribution and it is this modified distribution which it is desirable to characterise. The libraries may be analysed directly by NMR, mass spec, HPLC etc. but there are also some ways in which to realise a "cleaner" analysis. Tailored choice of reversible covalent reaction plays a large role.

Dynamic Freezing

Freezing *or* fixing of the target instructed distribution can be accomplished for certain chemistries such as thiol-disulfide. In this case dynamic behaviour occurs only at pH>7 where some thiolate anion exists and so thermodynamically shifted libraries may be "frozen" by acidifying the solution. Imine chemistry offers this possibility through library trapping by reduction to amine.

Evolutionary Systems

The evolutionary perspective in DCC alludes to refining library selections in an iterative process. There have been two approaches towards this end. In the first method molecular recognition and equilibration processes are separated (Figure 84) [434]. Initially the conditions in which an equilibrated library resides are changed to a slow exchange regime. An immobilized target is then added and once removed with the bound library members the non-bound members are reequilibrated in solution under a fast exchange regime. The reequilibration may lead to the formation of high affinity members which are then removed in the next cycle with the target

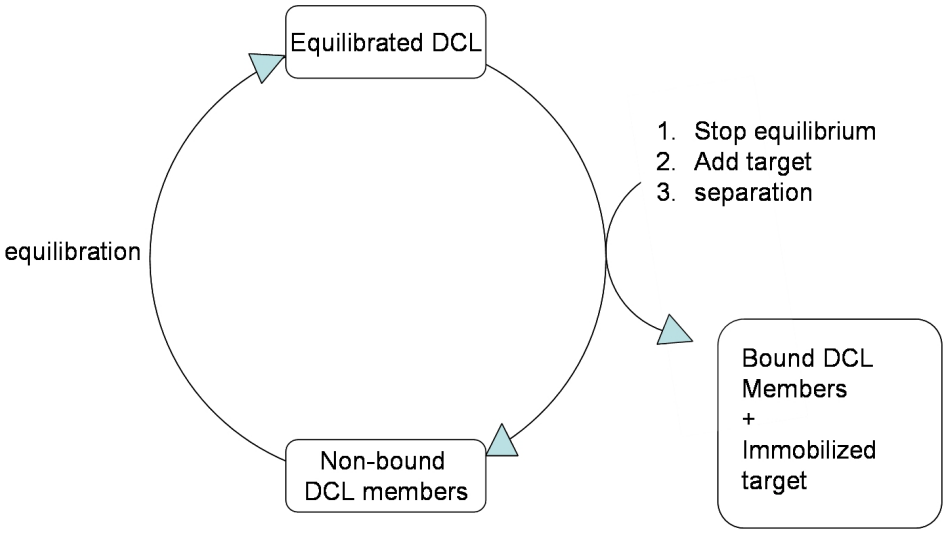

Figure 84 Evolutionary approach to library amplification with equilibration and recognition separated.

A second type of evolutionary approach is depicted in (Figure 85) where a DCL and immobilised target are contained under exchanging conditions. When the new distribution is at equilibrium the mixture is “frozen” and the bound and non-bound members are separated by filtration. The bound members and target are then returned to the cycle with the relative concentration of the best binding increasing per cycle.

The aim of the present work forms an extension of these evolutive systems in coupling selective transport and molecular recognition of a DCL. By constantly transporting the highest affinity species from an equilibrating library one could expect amplification of the best binder from the building block ensemble. If the best binder is continually removed, the library under exchange conditions will re-adjust it member distribution forming more of this binder within statistical limitations, amplifying its concentration.

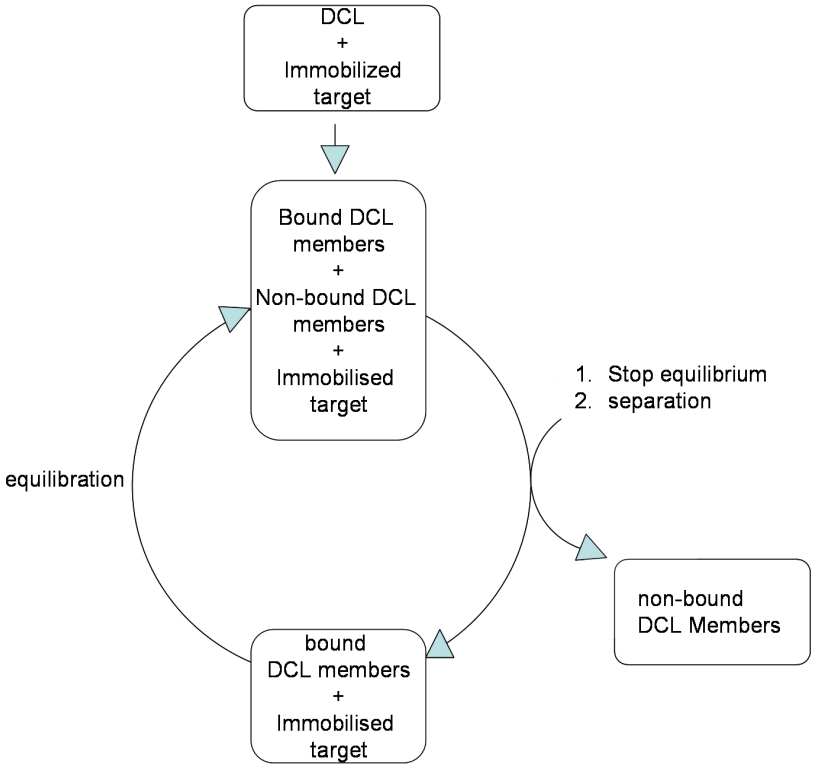

Figure 85 Amplification of best binder by iterative selection and separation.

4.1.3 Membrane for three phase amplification

Using concentration gradient as a driving force the barrier is formed by a hydrocarbon phase separating two aqueous phases. In keeping with the theme of Carbohydrate-protein interaction this molecular recognition study was performed on a simple three member glycosyl disulfide library with Concanavalin A as model Lectin adopting the approaches discussed earlier used by Ramström and co-workers (see section 4.1.1.2).

The considerations regarding the membrane phase were that it:

- Contains the Lectin which would act as selective transporter based on its monosaccharide binding selectivity.
- be hydrophobic in nature so as to act as a barrier across which a diffusion gradient could be set up.
- Allows appreciable transport in a relevant timeframe.

In order to reconcile these properties Con A would have to be contained within an organic phase. One way in which this has been demonstrated is by surfactant stabilisation [435].

4.1.4 Proteins in microemulsion phase

When oil, water and surfactants are mixed they can, depending of course on proportions, form stable dispersions known as microemulsions. These microemulsions can exhibit different types of structures such as spherical water droplets, interconnected bicontinuous water channels, interating rods and so on. The simplest microstructure may be the spherical water droplet in oil stabilised by a surfactant layer and know as a reverse micelle.

The classical reverse micelle forming system is the water-AOT-Isooctane system. Aerosol OT (Sodium dioctyl sulfosuccinate) (Figure 86) was recognised as forming reverse micelles in hydrocarbon oil 60 years ago [436]. The AOT isooctane system can form reverse micellar phases with pool diameter dimensions up to 10nm and standard deviation of average size of less than 10% at room temperature [437].

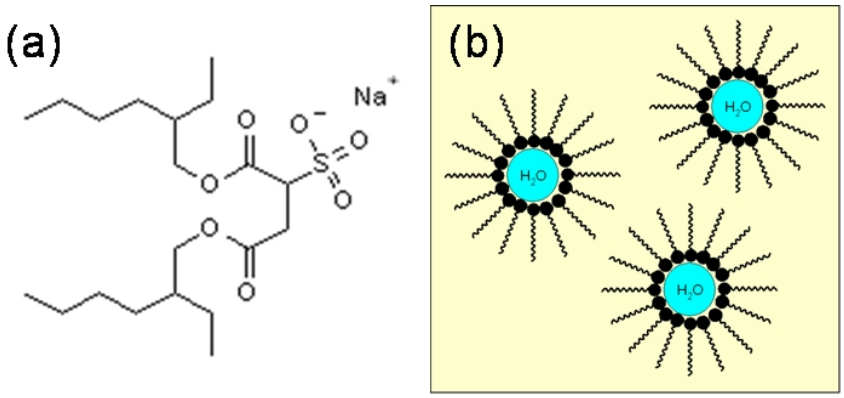

Figure 86 (a) AOT (Sodium dioctyl sulfosuccinate) and (b) Reverse Micelle cartoon.

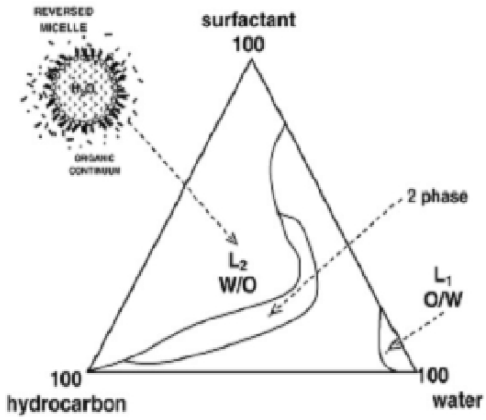

Figure 87 Phase diagram for oil-water-AOT mixture [438].

There are many examples of solubilisation of proteins in reverse micellar phases for tasks such as the investigation of enzyme activity in theses nanopools [438-442] as well as purification procedures by selective reverse micellar extraction [438,441]. These

investigations have produced such notable results as super activity in enzyme catalysed processes, a concept first introduced by Hilhorst et al. [443] as well as many applications in food technology and pharmaceutical purification based on reverse micellar separating and extracting properties [438].

4.1.4.1 Procedures for Preparation of Protein Occluding Reverse Micellar Phases

Generally there are three ways in which to solubilise proteins in a reverse micellar phase

- Injection method
- Phase transfer method
- Solid phase extraction method

4.1.4.2 Injection Method

The injection method simply involves the addition of the protein in aqueous buffer to the surfactant-alkane solvent mixture with gentle shaking giving a clear solution.W_0 which is defined as $[H_2O]/[AOT]$ for the present system is determined by the concentration and volume of the injected aqueous buffer.

4.1.4.3 Extraction Method

A second procedure to prepare protein in reverse micellar phase solutions is by extraction. Protein in an aqueous solution is contacted with the surfactant containing organic phase. The two phases can be shaken together to speed up transfer with a spontaneous transfer occurring dependant on factors which affect electrostatic and hydrophobic interactions. The disadvantage of this approach is that W_0 cannot be as easily controlled and it may take some time to reach an equilibrium state (hours), however, this equilibrium state will likely correspond to the optimal conditions for protein solubilisation and perhaps activity. The mechanism of solubilisation by extraction is generally thought of as mass transfer controlled by ion exchange between the protein surface and surfactant head group at the interface [444]. This theory was backed up in numerous studies with small molecules [445,446] as well as small proteins [447] although when it comes to larger proteins as well as this solubilisation resistance, a diffusion resistance in the aqueous boundary layer has also been reported which may be the rate limiting factor [448]. Electrostatics has been the most commonly exploited driving force for phase transfer of biomacromolecules. There is proven correlation between

pH, surfactant charge and extraction yield [449,450]. Generally speaking a negatively charged surfactant such as AOT extracts favourably a protein with positively charged surface intimating a solution pH below it's pI whereas a cationic surfactant could be utilized at a pH higher than its pI [451].

Ion effects

Ionic strength of the aqueous stripping solution plays a crucial part in extraction efficiency as would be expected for an electrostatically driven process. It appears to affect transfer in two ways, the interfacial transfer kinetics and secondly the overall protein distribution across the phases at equilibrium directed by surfactant-protein electrostatic interaction strength and surfactant-surfactant interaction. The effect of salt concentration and type has been investigated by various groups with the resulting trends showing that as you increase the ionic strength or ionic charge you decrease the protein solubilisation capacity of the organic phase. Going back to 1987 the work of Goklen and Hatton can be cited where cytochrome C, lysosyme and Ribonuclease A were transferred at 0.1M KCl but no transfer was observed from 1M KCl [452]. The interfacial nature of the transfer kinetics was later backed up given the rate limiting dependence on salt concentration and pH which should not greatly effect bulk transfer processes [447].

As well as affecting protein transfer ionic strength also influences micellar radius in accordance with Debye electrostatic screening. Basically the higher the ionic strength the smaller the reverse micelles formed which can have a detrimental effect on enzyme activity for example where the greater water uptake at lower ionic strength enhances activity. This ionic strength effect on W_0 appears only up to 0.1M ionic strength after which it is absent [438]. Protein surface electostatics appears to be the major driving force in protein take-up by theses solutions as proteins can be easily extracted at conditions which favour reverse micelles of smaller radius than the proteins themselves and it has been shown that this reverse micellar radius changes upon protein inclusion. They are adaptive structures, so favoured micellar radius for a given ionic strength may be less determining of equilibrium protein distribution than protein surface electrostatic interactions.

A similar postulation was put forward by Kinugasa and co-workers when they looked at a range of ion species' effects on lysosyme, cytochrome C and Ribonuclease A extraction. The

cation series produced showed increased protein inclusion in the organic phase with increased water structurating ability of cation according to the authors [453].

Protein size

Size plays an important role in relation to charge as was demonstated by Wolbert et al. [454] where a linear correlation of (pH_{ext} - pI) to protein size was discovered .The higher the molecular weight of the protein the greater the shift in pH from pI for optimal extraction.

Flexibility and Hydrophobicity

As the hydrophobicity is increased there is a concomitant increase in ease of extraction and proteins with hydrophobic areas have shown some anomalous behaviour outside of the purely electrostic model. It has been proposed that this is due to interactions with the hydrophobic interface and /solvent [451].

4.1.4.4 Reverse Micelle Contained Concanavalin A

Con A may be contained in aqueous microdomains within an organic phase through reverse micellar extraction based on an Aerosol OT/Isooctane system. Its extraction into AOT/isooctane has been extensively studied by Hatton and co-workers [455] [456] and has partition coefficients ranging from 0.2 to 20. This figure is dependant on factors such as pH, ionic strength of aqueous solution and surfactant concentration. The partition coefficient $[\mathrm{Pr}otein_{rev.micelle}]/[\mathrm{Pr}otein_{aq}.]$ of 20 for Con A was realised for an aqueous phase pH of 5.4 and a surfactant concentration of 0.025M for Con A solutions of 1mg/ml (~10 μM, $\therefore$ 2500 x surf.) [456]. The optimum conditions for such an extraction according to Chen and co-workers who studied reverse micelles containing affinity co-surfactants is pH5.6 and an ionic strength of 0.1M. [457].

This optimisation is based on the surface charge of Con A which has a (isoelectric point)pl >8, [458] which makes it positively charged at acidic pH's (5-5.5) and, therefore, extractable into micelles formed by the negatively charged AOT surfactant as a function of pH and salt screening effects.

4.1.4.5 Structural features of Protein Occluding Reverse Micelles

In terms of how the system works and interpretation of results the actual structure and transport properties of reverse micelles containing proteins is of great interest. Taking initially reverse micellar structure without biomacromolecule inclusion we have already noted some determinants of micellar radius such as ionic strength and pH with the fundamental one being W_0, the surfactant to water ratio which for extraction approaches should be at a thermodynamically stable value.

Researchers have been interested in the changes in reverse micelle structure and properties on protein inclusion. It was reported that on protein extraction into a phase which included reverse micelles of radius greater than that of the protein that the subsequent volume increase was never more than 10% of the original micellar volume. When the reverse micellar radius was of smaller size than the protein, on extraction, a reverse micelle of larger size was assembled to incorporate it.
As alluded to previously (see section 4.1.4.3) protein solubilisation is not strongly determined by the preordained reverse micellar radius as determined by W_0. For example using the injection method it appears that proteins induce the reverse micellar structure distribution driven by their own favourable incorporation [459-462].

4.1.4.6 Effect of Protein Occlusion on Micelle Structure

When proteins are solubilised in a reverse micellar phase the relationship between W_0 and R_{rm} (reverse micelle radius) as well as occupancy ([no. of RM occluding proteins]/[total no. of RMs], RM= Reverse Micelle) comes into question especially when the aim is to use it as a transport medium for small molecule species. Christ and Shurtenburger looked for the effect of protein addition to AOT microemulsions on the scattering intensity and the droplet size using optical contrast variation technique [463]. They also noticed only a very small hydrodynamic radius change on α-chymotrypsin inclusion. In terms of occupancy i.e. filled versus unfilled vesicles they followed an earlier model by Hatton et al. [464] whereby there is a categorisation of two different micelle types in the emulsion. The filled vesicles retained a constant R_{rm} with increasing W_0 and increased water concentration was accommodated amongst unfilled micelles through R_{rm} and N_{rm} adjustement. Thus for extraction procedures percentage occupancy can be affected by protein concentration in the aqueous phase prior to

extraction resulting in filled micelles of rather constant size with unfilled ones responding to changing conditions such as salt concentration.
Using the injection method similar results were noted where again filled micelle radius remained independent of W_0. Concurrent to the observation of minor changes in microemulsion structure a change in microemulsion dynamics namely enhanced shape fluctuation was later reported by Hirai and co-workers working with α-chymotrypsin [465].

4.1.4.7 Transport Properties of Reverse Micellar Phases

Reverse micelles are dynamic entities which fuse and exchange their contents including water, surfactant and contained materials. This dynamic equilibrium can be divided up into:

- The exchange of water between the bound and free state on the inner surface.
- The exchange of counterions between the ionic head groups of the surfactant and core water.
- The exchange of co-surfactants among the interfacial film, the continuous phase and the dispersed phase if soluble in the phase.
- The exchange of surfactants between the interfacial film and the aqueous phase.
- Droplet-droplet interactions.

Of these processes the last one is of most interest as regards transport properties of such a phase. Experiments have shown that mass-exchange, mass transfer and chemical reactions can occur through interdroplet fusion in w/o microemulsions in a rapid redistribution process. A transient dimer model was proposed by Eicke et al. [466]. This idea was supported by later investigations [467] where studies on limiting factors of the rate of exchange supported the idea that in a small fraction of encounters, two droplets temporarily coalesce and in this way exchange their core contents in a reversible process thus forming two daughter micelles [468-470]. Intermicellar exchange of reactants (k_{ex}) occurs in the order of $10^6 – 10^8$ $M^{-1}.s^{-1}$ [471] indicating that 1 in 1000-10000 collisions results in content exchange [472]. There exist also other mechanisms of transfer, interfacial transfer, where collision of micelles is sufficient for exchange and also interfacial transport for oil soluble small molecules. Protein transport across reverse micellar phase has been shown to be at least three orders of magnitude slower than small molecule as well as other macromolecule transport where the coalescence process may be inhibited by strong protein surfactant interaction and highly dependant on W_0 [473].

Nishii et al. reported on the transport behaviour of lysozyme through a bulk liquid membrane of AOT reverse micelles through variation of salt type and concentration and pH between feed and strip phase using high pH (>pI) in the strip phase [474]. Tsai et al. [475] looked at reverse micellar protein extraction across a supported liquid membrane again using pH 12 in the strip phase

4.1.4.8 Structural Properties of Proteins Contained in Reverse Micelles

Proteins when contained in a reverse micellar solution maintain their activity or may even show signs of superactivity as has been demonstrated for some enzymes. The W_0 may affect this activity whereby it may be restricted at values below the equilibrium W_0, on the other side there is also evidence of increased activity when W_0 is increased by lower salt concentration. This super activity for catalytic enzymes has been explained in terms of increased local concentration effects in the water-pool [476], water structuration properties in the nanodroplets [477,478] and increased enzyme rigidity leading to higher bioconversion efficiency [443] [442].

Protein location plays a dominant role in the structural effects of micellar incorporation which are largely determined by the hydrophobicity of the protein. The hyrdrophobicity can dictate whether the protein resides in the centre of the water pool(highly hydrophilic) or interacts with the interface [479]. The favourability of such environments for protein activity is further reaffirmed by work which demonstrates that reverse micelles can actually be utilised to refold denatured proteins [480].

4.1.4.9 Stability of Concanavalin to Back-extraction

For such a three phase transporter concept the stability of Con A within the organic phase is a major point of interest and in order to avoid back transfer to the aqueous phase one can look to the techniques used to cause deliberate back-transfer.

The most common method used for back extraction was stripping with aqueous solution which reduces the electrostatic interactions i.e. a high pH and high ionic strength [481]. This process is however mainly ineffective for proteins such as Con A which interact strongly with the water-surfactant interface. In such cases an amphiphilic alkanol can be used [482]. Alkanols can be used to change the interfacial properties of reverse micelles thus destabilizing them at the oil-water interface leading to back extraction. For example according to Chen et al. the back extraction of AOT stabilised Con A was performed with a 12.5% isopropanol aqueous solution releasing 88% of the protein [457].

The use of other alcohols such as 1-butanol has been reported to release proteins when added directly to the water- in- oil phase in some cases releasing the protein as a solid [483].
Temperature increase has also proven effective for protein expulsion as first reported by Hilhorst et al. [449].

Normally the back extraction of Con A into aqueous solution would require a high salt concentration (~1M) and a pH well above the pI which is 8 for ConA, therefore under the conditions utilised the Con A should remain in largely in the reverse micellar- isooctane phase with perhaps some minor interfacial transport.
Also as alcohols are frequently used in back extraction procedures the use of t-Butanol as an internal NMR reference may be a concern. In previous examples polar alcohols which may disrupt the hydrophobic interaction between the protein and surfactant have been used [484] but at much larger concentrations such as 12.5%(2M) for isopropanol [457] or 0.43M [485] as opposed to $8.7x10^{-4}$M in this case.

4.1.5 Supported Liquid Membranes (SLMs)

Liquid membranes can be classified into bulk, emulsion and supported liquid membranes. Supported liquid membranes are microporous supports which are impregnated with a carrier containing liquid phase. The liquid is held inside by capillary forces. Due to its low loading capacity, when compared with BLMs (bulk liquid membranes), it allows the use of very small amounts of sometimes expensive carrier molecules as well as demonstrating higher diffusion rates [486,487]. A common configuration for SLMs is the flat sheet SLM and typical examples such as those produced by Celgard or Accurel are composed of hydrophobic material polypropylene and exhibit pore sizes from 0.2-0.5 μM.

4.1.5.1 Microemulsions and SLMs

The use of SLM technology in conjunction with micro or nanoemulsion for membrane transport numbers few examples but yet had been demonstrated as a viable process. As mentioned Tsai et al. looked at protein diffusion across such membranes [475] and lysozme diffusion was again observed in a later example [488]. There are also examples explained in more detail in the next section where biomacromolecules are contained in the supported organic media by surfactant encapsulation [489-491].

4.1.5.2 Bioactive Supported Liquid Membranes

Examples of bioactive membranes based on surfactant protein complexes in an organic separating phase have shown up in the past few years. Miyako and Goto describe the separation of the optically active compounds (*S*)-ibuprofen and L-phenylalanine from their racemic mixtures based on a surfactant encapsulated protease (lipase from *Candida Rugosa*) in a supported liquid membrane [489] (Figure 88).

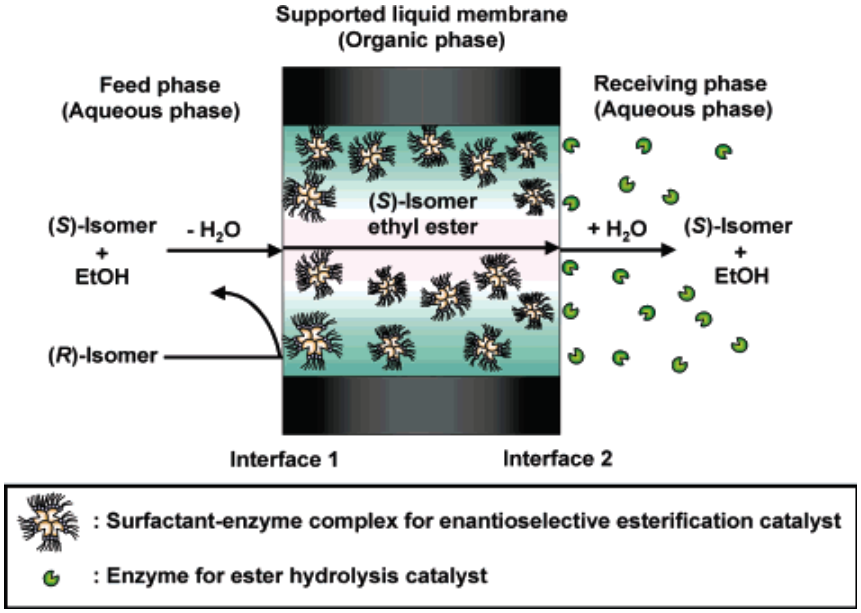

Figure 88 Scheme demonstrating enantioselective tensport mediated by protein-surfactant complex [489].

This system relies on an enantioselective esterification at the feed interface which renders the small molecule soluble in the organic membrane where it then crosses the membrane to the second interface where hydrolysis occurs catalysed by the same lipase in the strip phase to water soluble products with the whole process concentration gradient driven. They later extended this system to separation a range of organic acids based on their ester product solubilities in the organic phase coupled to substrate specificity at the interface [490]. Another example demonstrated the chiral resolution of various amino acids with α-chymotrypsin [491].

4.2 Results/Discussion

In order that this system provides a suitable transport profile to demonstrate adaptive library evolution a prerequisite is selectivity of transport and so it was the initial goal to demonstrate selective transport from a “non-dynamic” library. The opening experiments were aimed

transport of the individual disaccharides in the hope of demonstrating firstly transport across the organic barrier and secondly selectivity in the permeability of the membrane.

4.2.1 Individual Transport Measurements

Applying a mathematical model for solution-diffusion based transport previously developed by Palmeri and Barboiu et al [492] we can access relative values for membrane permeability: This model assumes that the chemical potential gradient across the membrane is only due to a concentration gradient. The flux of the solute " i " can be expressed as follows :

$$J_i = -D_i \frac{dc_i}{dx}$$

Eq 24

By integrating over the thickness l of the membrane, the flux of solute " i " is :

$$J_i = -\frac{D_i}{l}(c_i^{m,s} - c_i^{m,f})$$

Eq 25

with $c_i^{m,s}$, $c_i^{m,f}$ the concentrations of the solute in the membrane at the strip and the feed phase interfaces, respectively.

The concentration gradient in the membrane can be deduced by assuming thermodynamical equilibria at the interfaces :

$$c_i^{m,s} = K_i^s * c_i^s$$

Eq 26

$$c_i^{m,f} = K_i^f * c_i^f$$

Eq 27

with c_i^s and c_i^f the concentrations of the solute " i " in the strip and feed phases, respectively, and K_i^s and K_i^f the partition coefficients at the strip and feed phase interfaces with the membrane, respectively

By combining equation 24 with equations 25 and 26, we obtain the flux according to the concentrations in the feed and the strip phases :

$$J_i = \frac{D_i}{l}(K_i^f c_i^f - K_i^s c_i^s)$$

Eq 28

D_i and K_i, the effective diffusion and partition coefficients of this macroscopic approach, can be correlated with the physical and chemical structure of the dense membrane.

If we suppose that the transport rate is governed by diffusion and that the complexation-decomplexation reactions are kinetically rapid, then the accumulation of the solute in the membrane can be neglected. In a quasi-stationary regime (Figure 89) the transport rate across each interface becomes approximately equal to:

$$-J_1 = a\frac{dc_i^f}{dt} = -\frac{D_i}{l}(K_i^f c_i^f - K_i^s c_i^s)$$

Eq 29

$$J_2 = a\frac{dc_i^s}{dt} = \frac{D_i}{l}(K_i^f c_i^f - K_i^s c_i^s)$$

Eq 30

with a = V/A the compartment length (we suppose a simple geometry), V the compartment volume, and A the active surface of the membrane. The solute flux density across the membrane is then simply $J_m \cong J_1 = J_2$

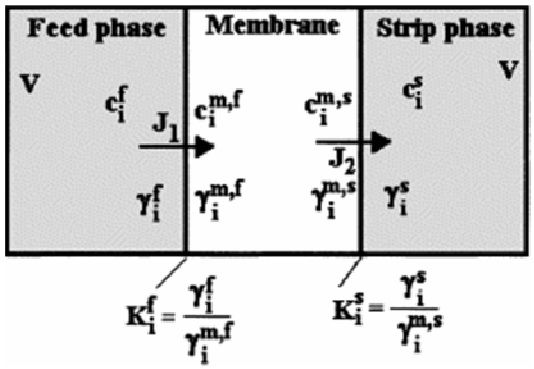

Figure 89 3-phase setup scheme.

With $\frac{D_i K_i^f}{al} = \lambda$, $\frac{K_i^s}{K_i^f} = \alpha$ and the initial conditions ($c_{1,\,t=0} = c_1^0$ and $c_{2,\,t=0} = 0$) equations (28) and (29) yield :

$$c_2(t) = \frac{c_1^0}{1+\alpha}\left[1 - e^{-\lambda(1+\alpha)t}\right]$$

Eq 31

Note that as $\alpha \to 0$, (i.e., $K_i^s << K_i^f$), $C_2(\infty) \to C_1^0$

and as $\alpha >> 1$ (i.e., $K_i^s >> K_i^f$), $C_2(\infty) \to 0$.

where :

$\alpha = \frac{K_i^s}{K_i^f}$ K is the partition coefficient at each liquid membrane interface, feed and strip

$P_i = D_i K_i^f = \lambda \times a \times l = .04\lambda cm^2$

as

$a = \frac{V}{A}$ (A =active membrane area =0 .785 cm^2 , V= compartement volume= 2 cm^2) = 2.548 cm

l= membrane thickness= 160μM

$c_1^0 = 10^{-2} M$ *(initial feed concentration)*

Levenberg-Marquardtof fitting the experimental data from the strip phase with

$y = a(1 - e^{-bx})$

Eq 32

with (Eq 31)can thus give direct access to partition coefficient ratio “α “and the permeability ”P_i” values based on the preceeding model.

4.2.2 Competitive Transport Measurements

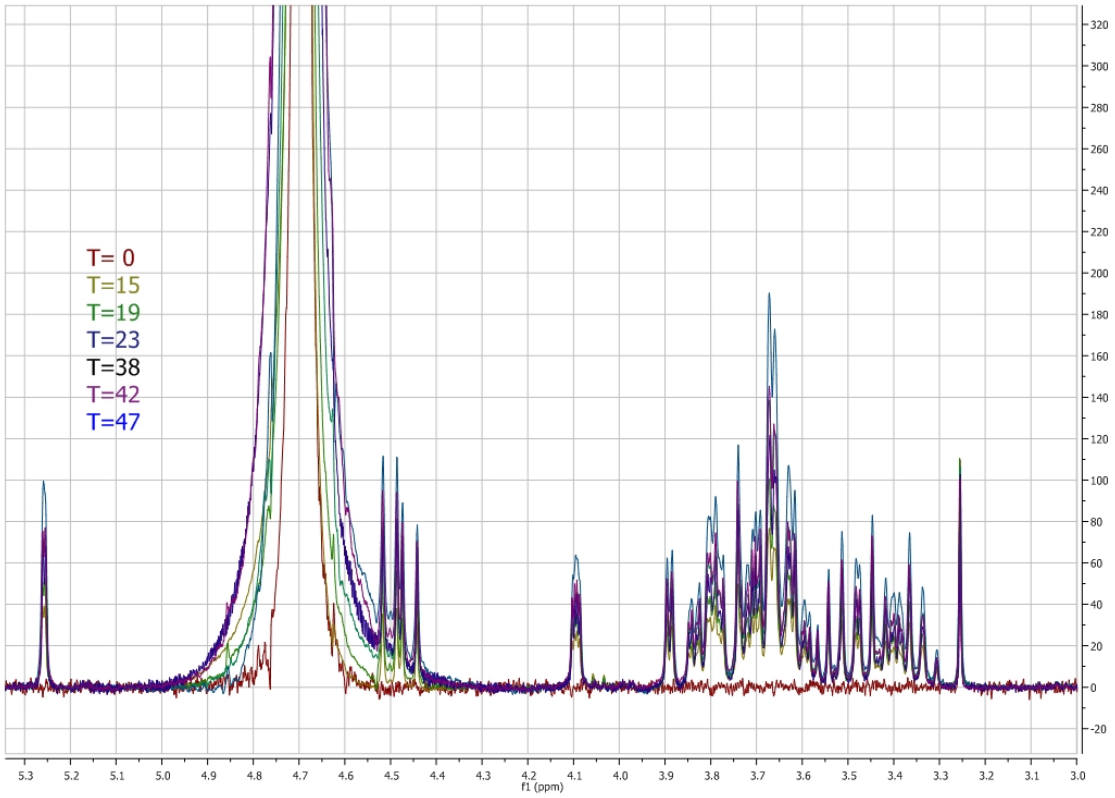

Figure 90 typical ^{1}HNMR series for competitive transport.

(Figure 90) shows the concept behind the measurement of the transport properties. As the area under a peak in an NMR spectrum is proportional to the proton molar concentration by using an internal standard of known concentration throughout the system changes in concentration with time could be calculated. The internal standards used were DMSO or t-BuOH, non-volatile substances with a high number of protons.

The initial experiments on single species transport presented some differences in permeability and partition coefficient ratio which indicated some selectivity but perhaps well outside the bounds of error while the setup and procedure was being established.

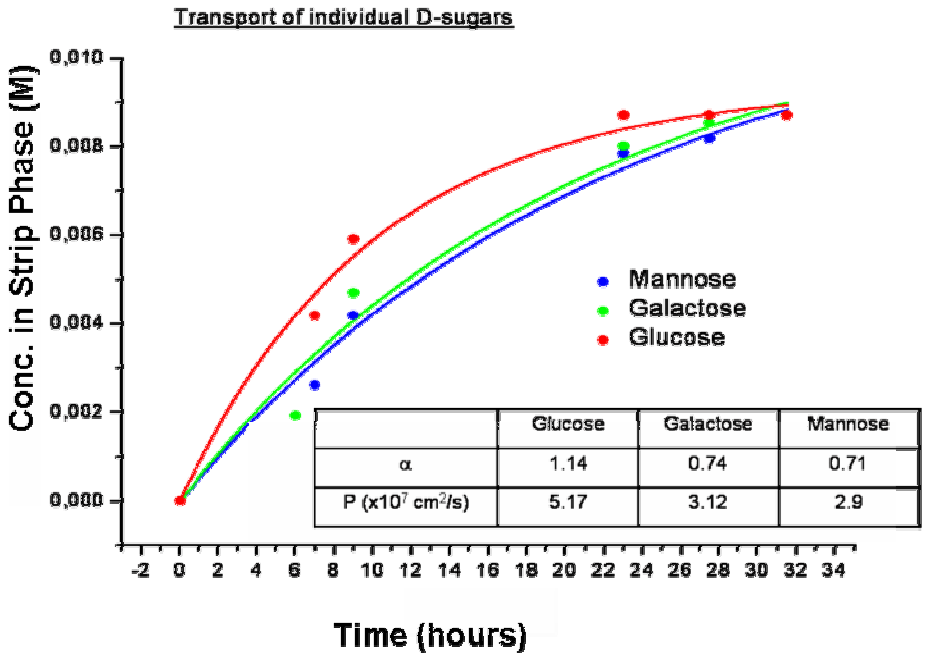

Figure 91 Transport results for simple monosaccharides.

The partition coefficient ratio can give an indication as to the activity of the membrane. As $\alpha = K_i^s / K_i^f$ a value >1 would indicate a higher partition coefficient at the strip interface than the feed interface. This in turn could indicate a lowering of solute activity across the membrane from feed to strip interface if activity coefficients are considered equal in both phases. On the other hand if activity throughout the membrane was considered equal a variable α could be ascribed to a variation in activity coefficients in the feed and strip phases.

In the simple monosaccharide transports (Figure 91) the permeability results show an order of Glu>Gal>Man which would indicate that acts like chromatography separation with the highest affinity species being retained by molecular recognition and the others passing.

Following this experiments were run on transport of the glycosyl disulfides (Figure 92). Again in this case the retention of the mannosyl disulfide was noted although the galactosyl and glycosyldisulfides had reversed their trend position. The lower α for the mannoside **(41)** indicates membrane retention by a lowering of the partition coefficient at the strip interface. Overall it appeared that the membrane was most permeable to galactosyl disulfide and glucosyl disulfide where an $\alpha > 1$ indicated enhanced transport. This led to the belief that the membrane may selectively slow the mannoside transport through affinity with the other species passing more freely through diffusion and the droplet coalescence mechanism.

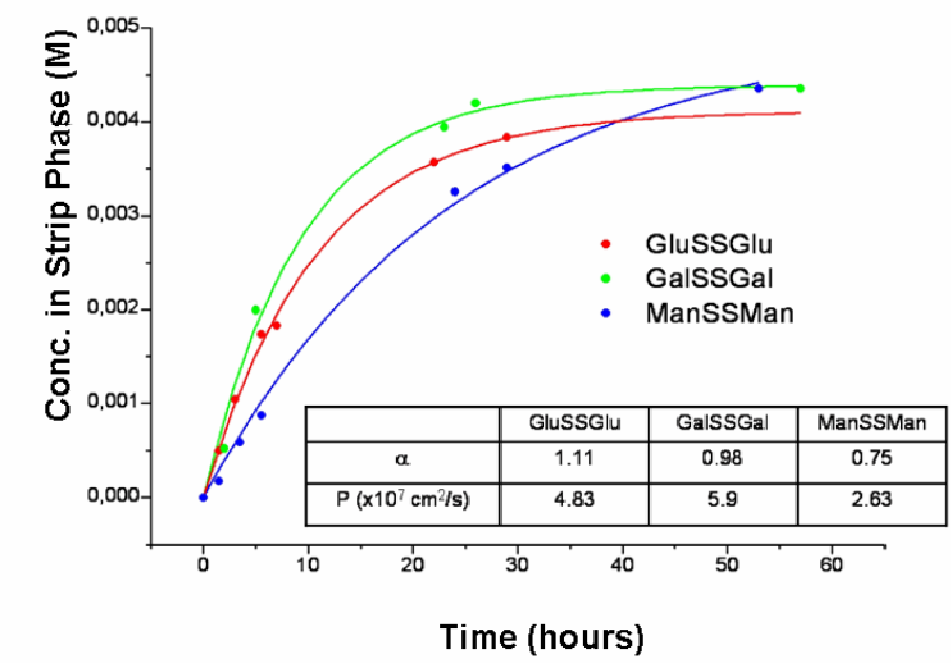

Figure 92 Transport results for glycosyl disulfides from individual experiments.

In any case it appears that disaccharide take up at the feed interface is not greatly influenced by lectin specificity.

The next step was the testing of competitive scenario in which biomolecular recognition based selectivity could show greater influence. However the membrane proved quite equally permeable to all three glycosyl disulfides (Figure 93) in repeated experiments for the given Con A concentration (~8 µM in isooctane).

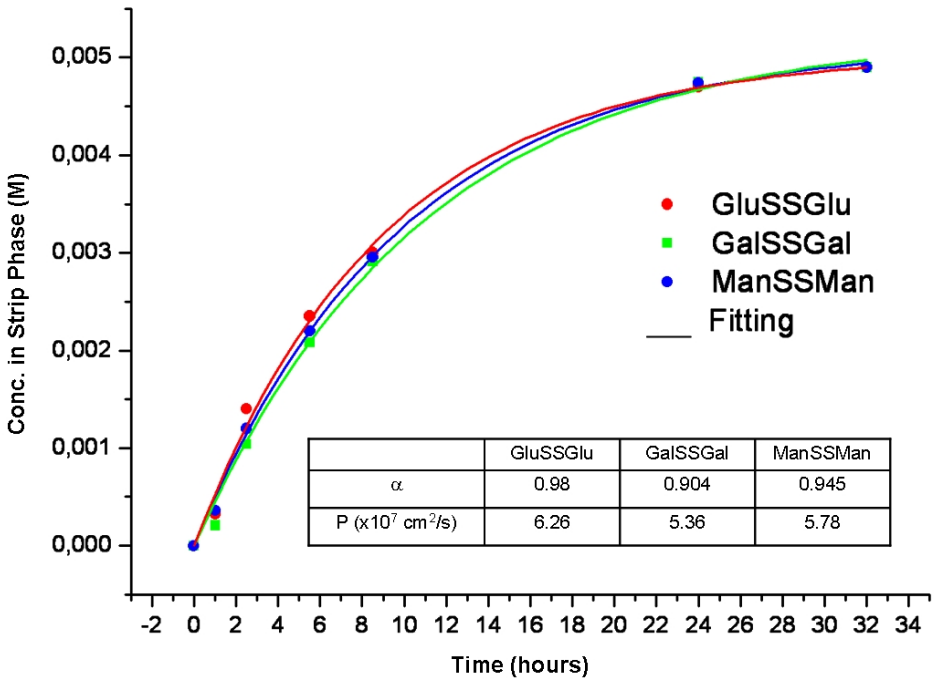

Figure 93 Transport results for glycosyl disulfides in competitive transport.

4.2.3 Con A concentration dependency

The Con A concentration of the supported nanoemulsion was then adjusted to check if this parameter could induce selectivity based on increasing the number of occupied versus unoccupied reverse micelles (see section 4.1.4.6). Variation of the Con A concentration did indeed affect transport properties of the membrane but did not show an appreciable selectivity influence (Figure 94), (Table 5). An increase in this concentration resulted in higher permeability as well as a small change in partition coefficient ratio. This greater permeability could be due to a change in the nanoemulsion dynamics on protein incorporation as the ratio of filled to unfilled RMs is altered as has been previously reported.

The influence of Ca^{2+} across these three states was also tested as it has been shown in multiple cases to influence Con A–carbohydrate recognition [493-496].It was introduced at a concentration of 1mM across all aqueous phases. Calcium proved to have some influence on overall transport but not noticeably on selectivity for the low concentration state. For the higher concentration membrane it did not have a pronounced effect.

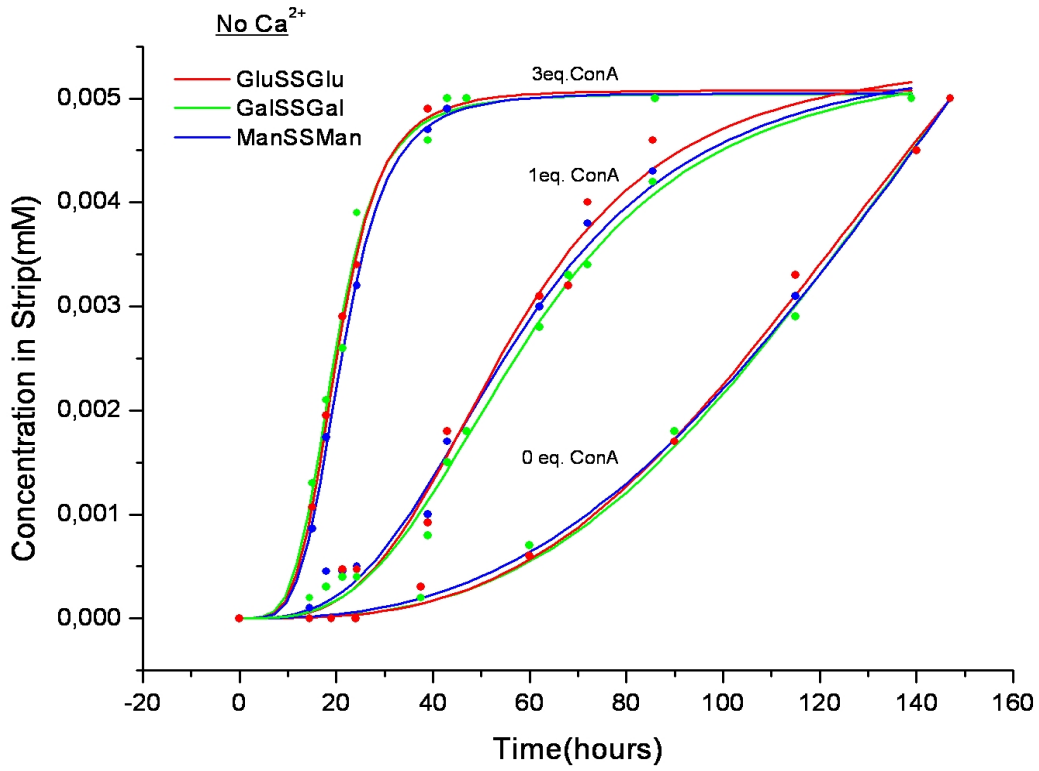

Figure 94 Effect of variation of Con A concentration in nanoemulsion (1eq = 2µM in Isooctane)

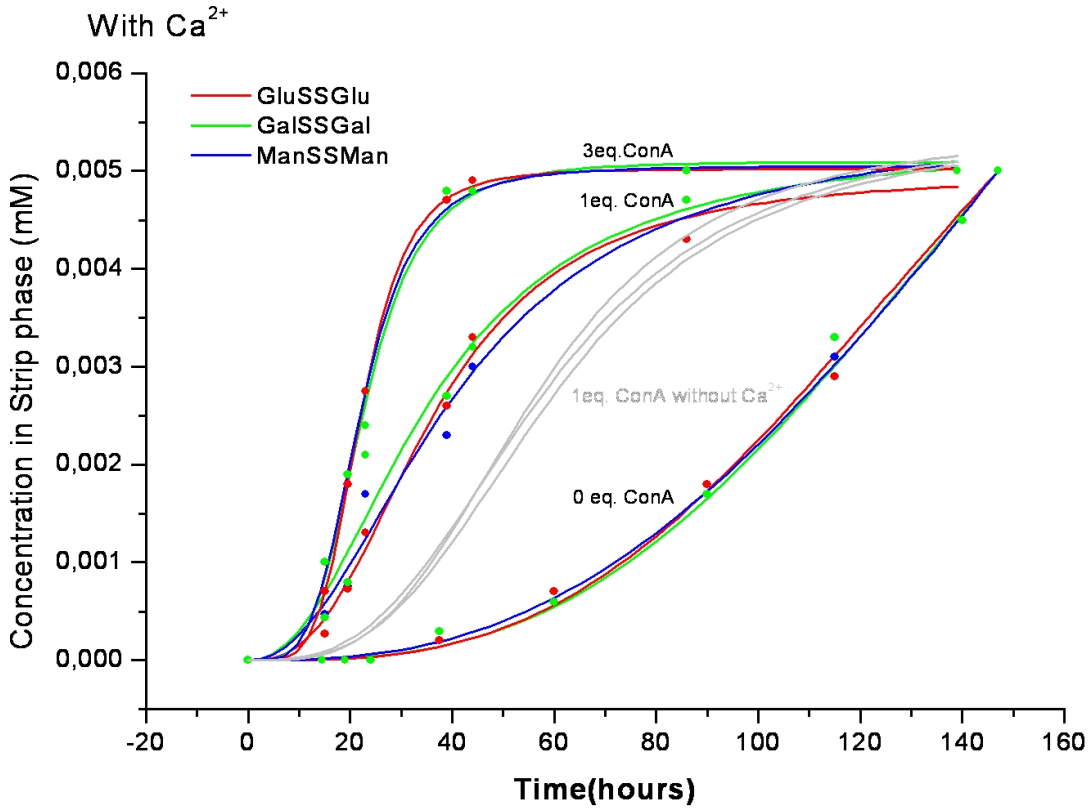

Figure 95 Effect of variation of Con A concentration in nanoemulsion (1eq = 2μM in Isooctane) with Ca^{2+} in all aquous phases.

	Con A 1eq.			ConA 1eq.+ Ca^{2+}			Con A 3eq			Con A 3eq +Ca^{2+}		
	Man	Gal	Glu	Man	Gal	Glu	Man	Gal	Glu	Man	Gal	Glu
α	0.58	0.57	0.48	0.75	0.8	0.84	0.86	0.87	0.89	0.89	0.87	0.88
P(x $10^7$$cm^2$/s)	0.8	0.8	0.72	1.16	1.17	1.35	3.2	3.3	3.3	2.7	2.7	2.7

Table 5 Permeability and α values measured for competitive glycosyl disulfide transports.

The results in Table 5 show how Con A concentration affects the membrane permeability with an increase in permeability as the lectin concentration is increased. Calcium present in equal concentration throughout the system aqueous phases increased permeability in the 1 equivalent case.

4.2.4 Test with non-specifically recognising species

For the sake of comparison a transport experiment was run with two water-soluble non-specifically lectin recognising compounds Uridine and Thymidine. Again in this case Con A inclusion in the nanoemulsion phase resulted in increased permeability. The permeability values were also of a similar range as the disaccharide samples.

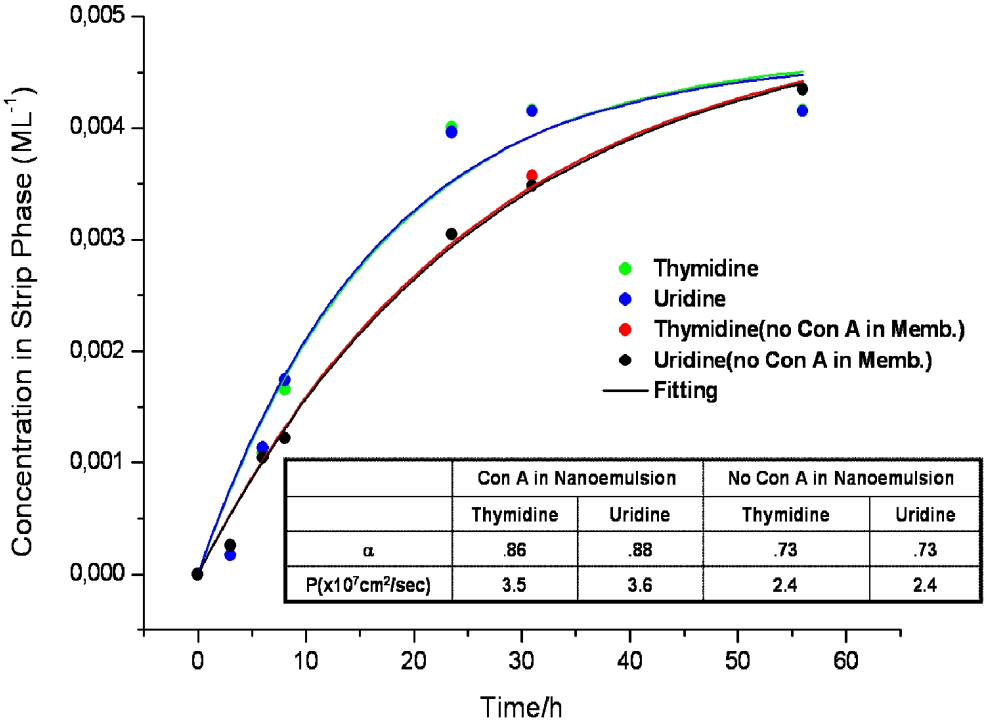

	Con A in Nanoemulsion		No Con A in Nanoemulsion	
	Thymidine	Uridine	Thymidine	Uridine
α	.86	.88	.73	.73
P(x10^{7}cm^2/sec)	3.5	3.6	2.4	2.4

Figure 96Transport Results for competitive transport of non-recognising species

Although transport selectivity was not demonstrated there are some interesting features to the results obtained such as:

- Enhanced transport when protein present
- Calcium effect on transport

As shown in (Figure 94, Figure 95) the concentation of Protein had a large influence. This influence can be reasoned based on the dynamic properties of the reverse micelles. As has been previously noted increasing the protein concentration increases the ratio of filled to unfilled micelles [465].

As the analysed disaccharides are fully water soluble species we can assume that transport can only occur through droplet coalescence with each other or the interfaces. This being the case transmembrane movement would then be mediated by a combination of micellar diffusion and coalescence with also some reports of tubular transporting structures formed by AOT in isooctane at a percolation threshhold [497,498].

Hirai et al. report on a D_{eff} (effective diffusion coefficient) in the range 10-15 x10^7 cm^2/sec measured with neutron spin echo comparing protein containing and protein free emulsions which tended to become higher with increased protein concentration.

Studies have also been performed based on the percolation phenomenon. The RMs represent conducting spheres floating in a non-conducting background which on variation of parameters such as temperature or W_0 form a macroscopically connected series indicated by a sharp increase in conductivity [499]. This threshold can be used as an indicator of micelle-micelle interaction and it has been shown that protein inclusion has a profound effect. Evidence has shown that BSA inclusion causes an increase in the electrical percolation threshold indicating decrease in micelle-micelle attraction ,whereas, cytochrome c inclusion has the opposite effect lowering the threshold [500,501] which indicates an increase in attraction. Added Cytochrome C which has been shown to interact strongly with the surfactant layer, which concurs with the line of thought that strongly interacting proteins effect this phenomenon by reducing the electrostatic repulsion between micelles, hence, the strength of protein micelle interaction will be determining.

Previous models for reverse micellar transport in liquid membranes have considered the protein-micelle complex transport as a pure diffusional process with inclusion at the feed interface, diffusion in membrane to strip interface and exclusion [475]. If it is considered that in order to maintain the thermodynamic equilibrium across the three phase system in the current investigation droplet coalescence at a certain point on the interface must be counteracted by droplet formation at another point on the interface. In this scenario we could say that the small molecule diffusion is limted by micellar diffusion after equilibration.

Applying the following simple empirical equation which relates W_0 to hydrodynamic radius :

$$R_h^0 = 1.5 + 0.175W_0$$

Eq 33 [502]

we get a diameter of 10 nm for W_0 = 20(the optimum Con A waterpool).This model is in very good agreement with dynamic light scattering results (Figure 97) which showsalmost 50% of the particles present to be 10nm in diameter although the distribution extends from 8→14nm:

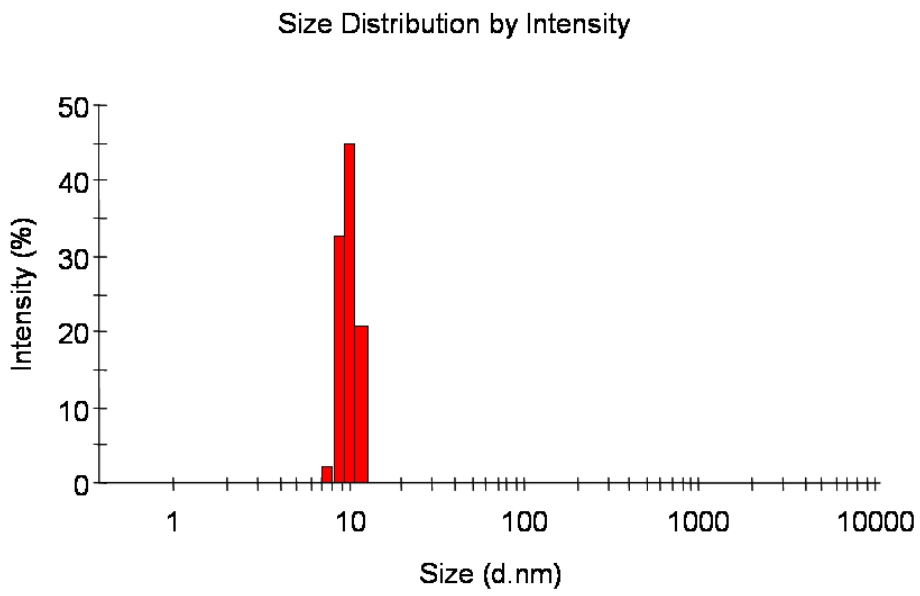

Figure 97 Dynamic Light Scattering analysis of Con A-Reverse Micellar Solution with W_O=20.

If we then estimate a diffusion constant based on the Stokes-Einstein-Sutherland equation:

$$D = \frac{k_B T}{6\pi\eta R_h}$$

Eq 34

the diffusion of radius 5nm objects in isooctane can be estimated at 8x10^7 cm^2/sec with $\eta = .503$ cP for isooctane [503]. In the simple model applied to the transport the P(permeability value) is related to diffusion by $P_i = D_i K_i^f$ [492] where K is the activity coefficient ratio at the feed interface. The permeabilities observed are of a similar order to the diffusion constant for such a micelle and so it appears that this may be the limiting factor for transport with interfacial exchange a rapid process.

Diffusion of AOT reverse micelles has been investigated experimentally by voltammetry where a value of 6.13x10 $^{-7}$ cm^2/sec was established for W_0 =10. It was also noticed that this value indicated a particle with double the radius determined experimentally indicating that this “sticky” attraction between reverse micelles had an inhibiting effect on diffusion. [504]

Taking the different reports as indicators we could say that Concanavalin A appears to interact with the surfactant layer in a way that lowers its stability, increasing coalescence successes on micelle-micelle contact as well as micelle-interface contact. Such a destabilisation has been observed experimentally in other cases such as small protein Cytochrome C. This strong protein-surfactant interaction hypothesis is further backed up by the observation of the difficulty of back extraction for such a system at neutral pH. Another

reason could be a size effect whereby Con A inclusion results in a greater proportion of larger micelles with increased shell curvature increasing unfavourable interactions [456]. Further investigation of such a system would be necessary to discern transport mechanisms and thermodynamics.

4.3 Conclusions/Perspectives

The aim of this work was selective amplification of a DCL by selective transport. In order to realise this proof-of-principle idea selective transport was a prerequisite which the present system did not accomplish. In using a nanoemulsion phase the possibility of transport exists for all the species in solution through droplet coalescence and formation at the interface. Based on the results obtained biomolecular recognition is not a vital component for transport and may have little or no effect.

The Con A biomacromolecule is contained in a water pools distributed amongst a unfilled nanopools with this ratio governed by protein concentration given the favourable interactions between protein surface and surfactant. The unfilled nanopools will find their own equilibrium size which may be different from that of the filled. Another question which raises its head is that if for the present conditions protein back extraction into aqueous solution does not occur why coalescence of Con A containing RMs at the interface would occur where complete coalescence would liberate the protein in the aqueous phase. Perhaps as part of theses dynamic processes reversible interfacial exchange of protein is occurring but with the partition coefficient lying heavily in favour of the membrane side.

In previous related work by Goto and co-workers demonstrated selective transport using as transporter what they called a surfactant-lipase complex which is a reverse micellar lipase containing phase which is lyophilised to produce a white powder which they then dissolve in isooctane before loading the membrane. This system would presumably equilibrate in contact with aqueous strip and feed phases however contrary to the aim of the present work the selectivity in this case was induced at the interfaces and not in the transport. Esterification by the lipase catalyst at the interface rendered the species increasingly soluble in isooctane and the accompanying hydrolysis by PPLipase dissolved in the aqueous receiving occurred at the strip interface giving the water- soluble products [489].

In order to attain a selective transport mediated by Concanavalin A a way in which to make molecular recognition a vital step for transport to occur is necessary.

5 General Conclusion and Perspectives

Biological processes can be described on a supramolecular level. By taking advantage of the ongoing progress in the synthetic side of supramolecular chemistry allied to the supramolecular understanding of biological processes we can design functional systems which can interact in a biomimetic way. This has powerful relevance towards the future trends in medicine and medical technology where already bionanotechnology is applied in the fields of diagnostic imaging and targeted drug delivery.

The presented work has backed the viability of this approach by demonstrating interaction between biomimetic components, such as supported bilayers, vesicles and lectin layers, and synthetic nanoassemblies.

The future could introduce higher levels of function to nanoassemblies such as those exhibited by the natural immune system where by rational design and chance such systems could even present an enhanced immuno-performance. An example of this can already be seen with targeted drug delivery by functional liposomes known as rector targeted liposomes whereby biorecognition is coupled with delivery of the active agent which performs the second function [267,505-507] [508].

In part I the applicability of nanoparticles in the study of molecular recognition based interactions by QCM was also demonstrated.
Gold nanoparticles functionalised with biomolecular recognition motifs were shown to greatly amplify QCM sensitivity with monolayer nanoparticle recognition showing a frequency change of 1600Hz.
The carbohydrate–protein interaction studied by this approach exhibited high specificity and and no evidence of non-specific surface binding. The biomimetic aspect of glyconanoparticles as regards multivalent presentation was displayed with affinity enhancements (β) of 25000 for maltoside glyconanoparticles and 2000 for mannoside particles. An unexpected feature was

the higher affinity of maltoside nanoparticles for a Concanavalin A layer than the Mannoside presenting ones which may be related to ligand density determined selectivity.

Glycoparticle biorecognition was demonstrated as a way in which to build reversibly assembled protein-nanoparticle multilayers. These multilayers were constructed in situ with QCM analysis of the layer by layer assembly and were selectively broken down by the high specifity ligand for the lectin. Such layers are of great interest due to their molecular recognition construction principle which, due to its lability, may allow higher levels of organisation to present in the resulting material. The optical properties of such organised materials can be exploited in the development for photonic devices due to the sensitivity of optical absorption to interparticle distance.

Allied to this work vesicle amplification was also demonstrated as a means in which to adapt QCM for small molecule -biomacromolecule interactions. Unilamellar vesicles incorporating synthetic alkylglycosides were shown to selectively recognise lectin layers. Enhanced affinity was demonstrated for these multivalent structures.
Amphiphilic assemblies such as vesicles or supported bilayers can be used as cell membrane mimics for the study of biomolecular processes. This facile approach demonstrates the applicability of QCM to biomimetic platforms with, by natural extension, future potential in the study of specific interactions at actual biological cell surfaces.

Synthetic ion channels are of great interest medicinally due to ion channels' crucial biological role as well as involvement in a range of debilitating illnesses. This work presented experiments on the applicability of metal-organic nanoclusters as synthetic ion channels. Their chemistry tunable properties make them highly attractive candidates for applications such as sensors while they can also model natural ion channels lending a greater understanding of their function mechanism. Evidence presented showed the viability of these nanoarchitectures as ion channels through spontaneous insertion and ion transporting capability.
Using QCM as a platform for supported lipid bilayers, spontaneous polyoxomolybdate capsule embedding was demonstrated .Following this, the capability of such nanocapsules as synthetic ion channels was shown by fluorimetry measurement of cation flux across vesicle

bilayers. They displayed a selectivity attributable to dehydration-coordination effects reminiscent of natural ion channels.
Electrostatic adsorption of POM layers on supported phospholipid bilayers was discovered and showed dependence on parameters such as pH and ionic strength. Such platforms may be applied in the study of the biological activity of POMs specifically their reported interactions with DNA and proteins.

In the final project presented a protein containing supported liquid membrane was developed as a novel means of dynamic combinatorial library amplification. This membrane transported disaccharide species across a recognising nanoemulsion at rates limited by micellar diffusion where the dynamic properties of the reverse micelles were heavily influenced by protein concentration. Selectivity was demonstrated for individual experiments but in competitive transports was not apparent indicating perhaps a cooperativity effect in transport or a low influence for molecular recognition.

Cross disciplinary research in what could be termed nanobiotechnology such as expressed in this work can lead improved to understanding of biological workings combined with the ongoing development of novel biointeractive nanomaterials.
Collectively this work demonstrated the development and applicability of bioactive nanomaterials through rational design and bottom-up assembly from molecular level synthesis through surpramolecular assembly and incorporation in organised systems with function conveyed from the molecular to the material level.

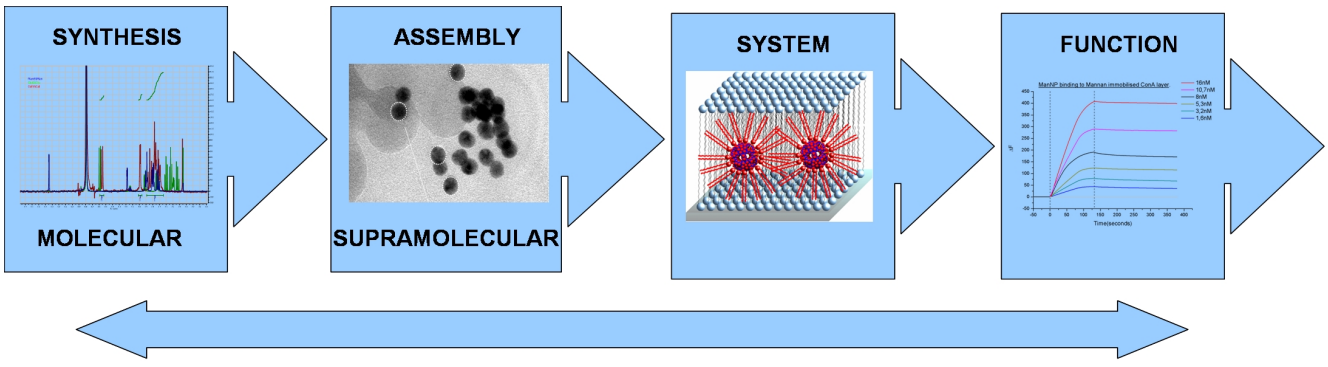

6 Experimental

6.1 Section 2 Experimental

6.1.1 General Remarks

All materials used were obtained from commercial sources and used without further purification. gold(III) chloride trihydrate (CAS : 16961-25-4), 2-oleoyl-1-palmitoyl-sn-glycero-3-phosphocholine (CAS : 26853-31-6), 2-[2-(2-chloroethoxy)ethoxy]ethanol (CAS: 5197-62-6), sodium citrate tribasic dihydrate, borontrifluoride-diethyletherate (CAS: 109-63-7), 1-tetradecyne (CAS: 765-10-6), sodium azide (CAS: 26628-22-8), tetrabutylammonium hydrogensulfate (CAS: 32503-27-8), hydrogen bromide in acetic acid, thioacetic acid (CAS: 88620), copper(II) sulfate pentahydrate (CAS: 7758-99-8), ascorbic acid sodium salt (CAS: 134-03-2), 1-octadecanethiol (CAS: 2885-00-9), methyl-alpha-D-glucopyrannoside (CAS : 97-30-3), mannan (CAS: 9036-88-8) were all purchased from either Sigma-Aldrich or Fluka. Analytical TLC was performed on silica gel 60-F_{254} (Whatman) with detection by immersion in 5% methanolic H_2SO_4 followed by charring or by fluorescence.Column chromatography was performed with silica gel 60 A C.C 70-200 µm. 2-(2-(2-mercaptoethoxy)ethoxy)ethanol **(28)** was prepared following a known protocol [509]. ^{1}H NMR spectra were recorded with a Bruker Avance 300 MHz instrument at 25°C. Chemical Shifts in ppm were referenced to the relevant solvent residual peaks. Mass spectrums were recorded using ESI. QCM measurements were performed using the A100 instrument from Attana Biosensors. The experiments were run in the continuous-flow QCM system at a flow rate of 20 µL/min. The experiments were performed in a Tris buffer at pH 7.4. All species were dissolved in this medium so as to ensure buffer effects be kept to a minimum

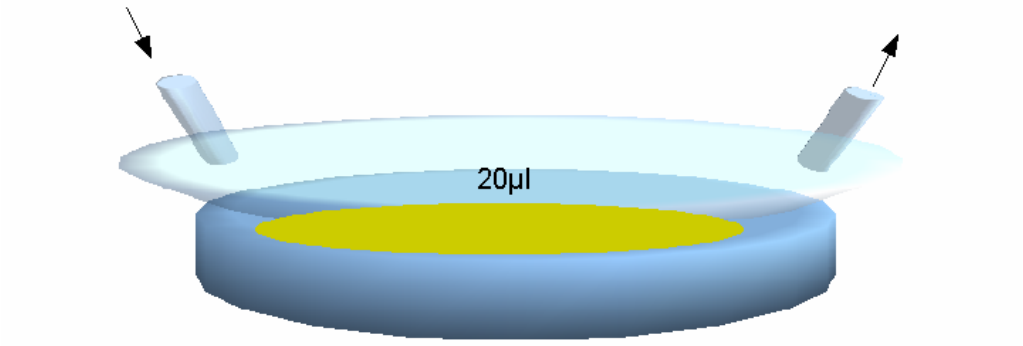

Figure 98 The instrument passes a continuous buffer flow through a 20 µl chamber over the crystal surface.

Dynamic light scattering measurements were performed with the Cordouan SL135 and S.E.M. measurements with a HITACHI S-4500 I instrument.

6.1.2 Glyconanoparticle Preparation

The nanoparticles were prepared by self assembley of thiol ligands on citrate stabilised gold colloid solutions. The ligands were prepared in a three step synthesis from the simple sugars.

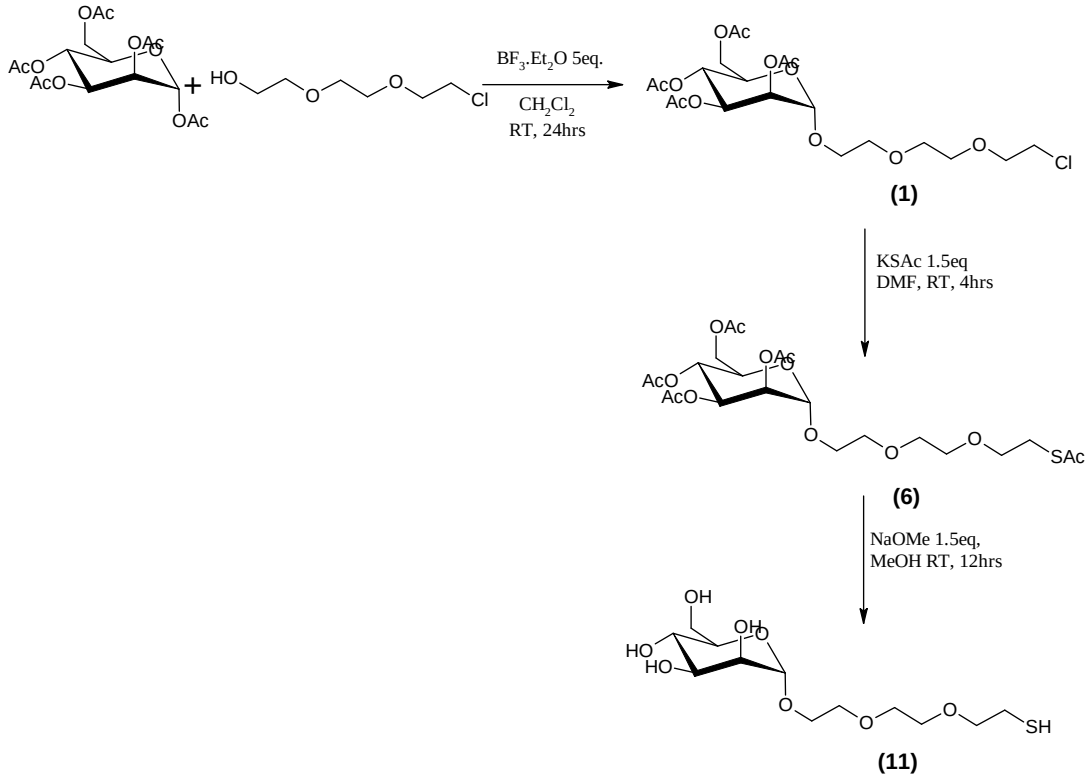

Figure 99 Reaction scheme for preparation of α-D-Mannopyranoside2-[2-(2-mercaptoethoxy)ethoxy]ethyl.

Peracetylation was followed by Lewis acid catalysed glycosylation with $BF_3.Et_2O$ [510-512] giving the α-anomer in the case of mannose peracetate due to the neighbouring group participation and anomeric effect and β-anomer for the other peracetates as it to be expected due to neighbouring C2 acetoxy group participation [37]. The chloroglycol glycosides thus prepared were then treated with potassium thioacetate in DMF to give the thioacetates in high yield followed by deacetylation with NaOMe in MeOH with some presence of disulfides also in the products which are equally suitable for the next step of glyconanoparticle preparation.

6.1.2.1General Synthesis of D-Glycopyranoside, 2-[2-(2-chloroethoxy) ethoxy]ethyl, 2,3,4,6-tetraacetates.

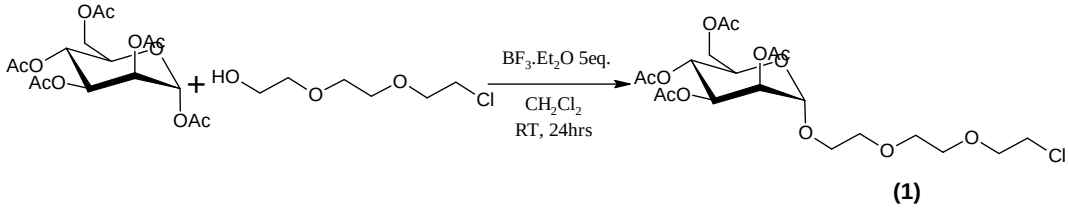

(1)

Figure 100 Glycosylation Step.

7.74 ml of $BF_3.Et_2O$ (min 46.5% w/v BF_3) (3.6 g, 5 equiv., 25.6 mmol) was added dropwise to a solution of 2-[2-(2-chloroethoxy)ethoxy]ethanol (1.3 g, 1.5 eq., 7.68 mmol) and the peracetylated carbohydrates (1 eq., 5.12 mmol) in dry dichloromethane (25 ml) stirring at 0 °C. The mixture was allowed to warm to RT and then stirred for a further 24 hrs in the case of the mannoside preparation and 72 hours for the other glycosides. The product was extracted with dichloromethane and washed with $NaHCO_3$ sat. (x3) and then dried over Na_2SO_4. The product was purified by flash column chromatography using EtOAc/Hexane as eluent (1:1) to afford the glycosylated products in the form of pale residues.

*6.1.2.1.1 α-D-Mannopyranoside, 2-[2-(2-chloroethoxy)ethoxy]ethyl, 2,3,4,6-tetraacetate **(1)***

Yield 45%. ^{1}HNMR(300MHz, $CDCl_3$, 25°C): δ=1.98 (s, 3H, CH_3CO), δ2.05 (s, 3H, CH_3CO), δ2.12 (s, 3H, CH_3CO), δ2.16 (s, 3H, CH_3CO), 3.6-3.76 (m, 12H, OCH_2CH_2O) 4.04-4.07 (m, 1H, H-6), 4.1 (dd, 1H, *J* = 12.3, 2.5Hz, H-6), 4.3 (dd, 1H, *J*= 12.3, 5.1 Hz, H-5), 4.88 (d, *J*= 1.5 Hz,1H, H-1), 5.27 (m, 2H, H-2, H-3), 5.36 (dd, 1H, *J*= 12.3, 3.3 Hz, H-4). ^{13}C NMR (300MHz, $CDCl_3$): δ=20.6, 20.7, 20.8, 21.0 (4s, 4×*C*H_3CO), 42.255 (CH_2Cl), 62(C6), 65.7, 66.9, 68.58, 69.11, (4s, C-2 to C-5), 67.94, 69.56, 70.17, 70.24, 70.90 (5s, 5×*C*H_2O), 97.22(C1), 169.2, 169.35, 169.5, 170.1 (4s, 4×CH_3*C*O).

6.1.2.1.2 β-D-Glucopyranoside, 2-[2-(2-chloroethoxy)ethoxy]ethyl, 2,3,4,6-tetraacetate **(2)**

Yield 40%. ^{1}HNMR(300MHz, $CDCl_3$, 25°C): δ=2.0 (s, 3H, CH_3CO), 2.019 (s, 3H, CH_3CO), 2.04 (s, 3H, CH_3CO), 2.08 (s, 3H, CH_3CO), 3.6-3.8 (m, 12H, OCH_2CH_2O), 3.9-4.0 (m, 1H, H-6), 4.1 (m, 1H, H-6), 4.26 (dd, 1H, *J*= 12.3, 5.1 Hz, H-5), 4.6 (d, 1H, *J*= 8 Hz, H-1), 4.98 (dd, 1H, *J*= 9.3, 8 Hz, H-2), 5.1 (dd, 1H, *J*= 9.3, 9.3 Hz, H-3), 5.2 (dd, 1H, *J*= 9.3, 9.3 Hz, H-4). ^{13}C NMR (300MHz, $CDCl_3$): δ=20.1, 20.12, 20.18, 20.25 (4s, 4×*C*H_3CO), 42.25 (CH_2Cl),

61.47 (C6), 67.93, 68.56, 71.3,72.34 (4s, C-2 to C-5), 69.91, 70.18, 70.79, 70.88, (4s, 6×CH_2O), 100.33 (C1),168.87, 168.92, 169.78, 170.18 (4s,4×CH_3CO).

6.1.2.1.3 β-D-Galactopyranoside, 2-[2-(2-chloroethoxy)ethoxy]ethyl, 2,3,4,6-tetraacetate **(3)**

Yield 31%. ^{1}HNMR (300MHz, $CDCl_3$, 25°C): δ=1.98 (s, 3H, CH_3CO), 2.04 (s, 3H, CH_3CO), 2.05 (s, 3H, CH_3CO), 2.14 (s, 3H, CH_3CO), 3.6-3.8 (m, 12H, OCH_2CH_2O), 3.9-4.0 (m, 1H, H-6), 4.1 (m, 1H, H-6), 4.55 (d, 1H, *J*= 8 Hz, H-1), 5.0 (dd, 1H, *J*= 10, 3 Hz, H-3), 5.2 (dd, *J*= 10, 8 Hz, 1H, H-2) 5.4 (d, 1H, *J*= 3 Hz, H-4). ^{13}C NMR (300MHz, $CDCl_3$): δ=20.09, 20.17, 20.28, 20.54 (4s, 4×*C*H_3CO), 42.27(CH_2Cl), 60.8(C6), 66.58, 68.33,68.57 70.89 (4s, C-2 to C-5), 69.65, 69.9, 70.18, 70.42 (4s, 6×CH_2O), 100.87(C1),168.98, 169.66,169.76, 170.09 (4s, 4×CH_3CO).

6.1.2.1.4 β-D-Glucopyranoside, 2-[2-(2-chloroethoxy)ethoxy]ethyl 4-O-(2,3,4,6-tetra-O-acetyl-β-D-galactopyranosyl)-, 2,3,6-triacetate **(4)**

Yield 35%. ^{1}HNMR (300MHz, $CDCl_3$, 25°C): δ=1.97(s, 3H), 2.05(m, 12H), 2.12(s, 3H) 2.16 (s, 3H)7×CH_3CO, 3.6-3.8 (m, 12H, OCH_2CH_2O), 3.8-3.95 (m, 2H, CH), 4.05-4.15(m, 4H, CH2), 4.47-4.58 (m, 2H, CH2), 4.56 (d, 2H, *J*=7.8, CH), 4.89 (t, 1H, CH), 4.95 (dd, 1H, *J*= 10.5, 3.3Hz, CH), 5.1 (dd, 1H, *J*=10.5, 7.8, H-2,), 5.195 (t, 1H, *J*= 9.3 Hz, CH) 5.34 (d, 1H, *J*= 3.3 Hz, CH).

6.1.2.1.5 β-D-Glucopyranoside, 2-[2-(2-chloroethoxy)ethoxy]ethyl 4-O-(2,3,4,6-tetra-O-acetyl-α-D-glucopyranosyl)-, 2,3,6-triacetate **(5)**

Yield 29%. ^{1}HNMR (300MHz, $CDCl_3$, 25°C): δ=1.95-2.09 (m, 18H), δ2.1 (s, 3H), 2.14 (s, 3H)7×CH_3CO, 3.6-3.8(m, 12H), 3.9-4 (m, 3H, CH), 4.05(dd, 1H, *J*= 12,3 Hz, CH), 4.25 (m, 2H, CH2), 4.49 (dd, 1H, *J*=12, 3Hz, CH), 4.63 (d, 1H, *J*= 7.8Hz, CH), 4.8-4.9 (m, 2H, CH), 5.05 (t, 1H, *J*= 10), 5.25 (t, 1H, *J*= 9 Hz, CH) 5.35 (t, *J*= 10 Hz,1H, CH), 5.4 (d, 1H, *J*= 3.9 Hz, CH).

6.1.2.2Synthesis of α-D-Mannopyranoside, 2-[2-(2 (acetylthio)ethoxy)ethoxy] ethyl, 2,3,4,6-tetraacetate.

The following protocol was used for all ligands. α-D-Mannopyranoside 2-[2-(2-chloroethoxy)ethoxy]ethyl,2,3,4,6-tetraacetate (200 mg, 0.4 mmol, 1 eq) and potassium thioacetate (138 mg, 0.6mmol, 3 eq.) were taken and dissolved in DMF (10 ml). This solution

was then stirred at room temperature for 4 hrs. Ethyl acetate (40 ml) was then added to the reaction mixture which was then washed with H_2O(x2), $NaHCO_3$ and finally saturated NaCl. This organic phase was then evaporated off leaving a colourless oil.

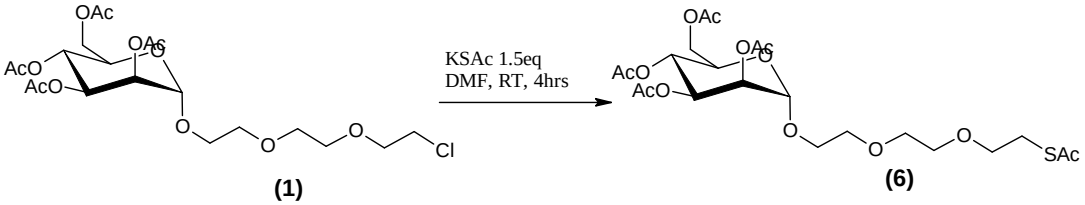

(1) **(6)**

Figure 101 Thioacetate Substitution.

6.1.2.2.1 α-D-Mannopyranoside, 2-[2-(2-(acetylthio)ethoxy)ethoxy]ethyl, 2,3,4,6-tetraacetate **(6)**

Yield 82%. ^{1}HNMR (300MHz, $CDCl_3$, 25°C): δ=1.95 (s, 3H), 2.01 (s, 3H), 2.06 (s, 3H), 2.12 (s, 3H) 4×CH_3CO, 2.3 (s, 3H, CH_3COS), 3.1(tr, 2H, J= 6Hz, CH_2CH_2S), 3.55-3.76(m, 10H), 4.04-4.07 (m, 1H, H-6), 4.1 (dd, 1H, J= 12.3, 2.4Hz, H-6), 4.25 (dd, J= 12.3, 1H, 5.1 Hz, H-5), 4.88 (d, 1H, J= 1.5 Hz, H-1), 5.23 (m, 2H, H-2, H-3), 5.36 (dd, 1H, J= 12.3, 3.0 Hz, H-4). ^{13}C NMR (300MHz, $CDCl_3$): δ=20.6, 20.7, 20.8, 21.0 (4s, 4×CH$_3$CO), 28.28(CH_2CH_2S), 29.97 (CH$_3$COS), 42.255 (CH$_2$Cl), 62(C6), 65.7, 66.9, 68.58, 69.11, (4s, C-2 to C-5), 67.94, 69.56, 70.17, 70.24, 70.90, (5s, 5×CH_2O), 97.22 (C1) 169.2, 169.35, 169.5, 170.1 (4s,4×CH_3CO), 194.84 ($CH_3$$C$OS). Lit: [163]

6.1.2.2.2 β-D-Glucopyranoside, 2-[2-(2-(acetylthio)ethoxy)ethoxy]ethyl, 2,3,4,6-tetraacetate **(7)**

Yield 86%. ^{1}HNMR (300MHz, $CDCl_3$, 25°C): δ 1.988 (s, 3H), 2.01 (s, 3H), 2.044 (s, 3H), 2.09 (s, 3H) 4×CH_3CO 2.35 (s, 3H, CH_3COS), 3.1(tr, 2H, J= 6Hz, CH_2CH_2S), 3.55-3.7 (m, 12H, OCH_2CH_2O), 3.9 (m, 1H, H-6), 4.1 (dd, 1H, J= 12.3, 2.3 Hz, H-6)), 4.25 (dd, 1H, J= 12.3, 4.8 Hz, H-5), 4.61 (d, J= 8 Hz, 1H, H-1), 5.01 (dd, 1H, , J= 9, 8.1 Hz H-2), 5.08 (t, 1H, J= 9.5 Hz, H-3), 5.2 (tr, 1H, J= 9.5 Hz, H-4). ^{13}CNMR (300MHz, $CDCl_3$): δ=20.1, 20.12, 20.18, 21.25 (4s, 4×CH$_3$CO), 28.28(CH_2CH_2S), 30.07 (CH_3COS), 61.48(C6), 67.93, 68.56, 71.3, 72.34 (4s, C-2 to C-5), 69.91, 70.18, 70.79, 70.88, (4s, 6×OCH_2CH_2O), 100.35 (C1), 168.87, 168.92,169.78, 170.18 (4s,4×CH_3CO), 194.03 ($CH_3$$C$OS) .

6.1.2.2.3 β-D-Galactopyranoside, 2-[2-(2-(acetylthio)ethoxy)ethoxy]ethyl, 2,3,4,6-tetraacetate **(8)**

Yield 78%. ^{1}HNMR(300MHz, $CDCl_3$, 25°C): δ=1.98 (s, 3H), 2.04(s, 3H), 2.05(s, 3H), 2.14 (s, 3H) 4×CH_3CO, 2.35 (s, 3H), CH_3COS, 3.08(tr, 2H, J= 6Hz, CH_2CH_2S), 3.55-3.76 (m, 12H), 3.9-4.0 (m, 2H, H-6), 4.1 (m, 1H, H-5), 4.55 (d, 1H, J= 8 Hz, H-1), 5.0 (dd, 1H, J= 10, 3 Hz, H-3), 5.2 (dd, 1H, J= 10, 8 Hz, H-2) 5.4 (app d, 1H, J= 3 Hz, H-4). ^{13}CNMR (300MHz, $CDCl_3$): δ=20.09, 20.17, 20.28, 20.54 (4s, 4×CH_3CO), 27.4 (CH_2CH_2S), 29.7 (CH_3COS), 60.8(C6), 66.58, 68.33, 68.57, 70.89 (4s, C-2 to C-5), 69.65, 69.9, 70.18, 70.42 (4s, 6×CH_2O), 100.87(C1), 168.97, 169.65, 169.76, 169.89 (4s,4×CH_3CO), 194.03 (CH_3COS). Lit: [163]

6.1.2.2.4 β-D-Glucopyranoside, 2-[2-(2-(acetylthio)ethoxy)ethoxy]ethyl 4-O-(2,3,4,6-tetra-O-acetyl-β-D-galactopyranosyl)-, 2,3,6-triacetate **(9)**

Yield 81%. ^{1}HNMR(300MHz, $CDCl_3$, 25°C): δ=1.855 (s, 3H), 1.935 (s, 3H), 1.941 (m, 6H), 1.955 (s, 3H), 2.014 (s, 3H), 2.046 (s, 3H) 7×CH_3CO, 2.23 (s, 3H, CH_3COS), 2.92(tr, J= 6.3Hz, 2H, CH2S), 3.6-3.8 (m, 12H), 3.85 (m, 2H, CH), 4.01 (m, 2H, CH) 4.38(dd, 1H, J= 1.8Hz , 12.6Hz, CH), 4.42 (d, 1H, J=7.8Hz, CH), 4.49 (d, 1H, J= 7.8Hz, CH), 4.78 (dd, 1H, J= 7.8hz , 9.3Hz, CH), 4.86 (dd, 1H, J= 10.5, 3.3Hz, CH), 4.9 (dd, 1H, J= 10.5, 7.8Hz, CH), 5.1 (t, 1H, JH = 9.3 Hz, CH), 5.24 (d, 1H, J= 3.6 Hz, CH). ^{13}C NMR (300MHz, $CDCl_3$): 19.920, 20.049, 20.049, 20.079, 20.130, 20.22, 20.27 (7 x CH_3CO), 28.212 (CH_2CH_2S), 29.982 (CH3COS), 60.298 (C6Gal), 61.526 (C6Glu), 66.131 (C-4Gal), 68.497, 68.580 (CH2), 69.139 (C-2Gal), 69.72, 70.28, 70.07 (CH2) 70.409 (C-5Gal), 70.77 (C-3Gal), 71.1 (C-2Glu), 72.0 (C-5Glu), 72.271 (C-3Glu), 75.75 (C-4Glu), 100.01 (C-1Gal), 100.458 (C-1Glu), 168.452, 168.99, 169.12, 169.37, 169.51, 169.68, 169.7 (CH_3CO), 194.7 (CH_3CS).

6.1.2.2.5 β-D-Glucopyranoside, 2-[2-(2-(acetylthio)ethoxy)ethoxy]ethyl 4-O-(2,3,4,6-tetra-O-acetyl-α-D-glucoopyranosyl)-, 2,3,6-triacetate **(10)**

Yield 85%. ^{1}HNMR(300MHz, $CDCl_3$, 25°C): δ=1.966 (s, 6H), 2.006 (s, 3H), 2.009 (s, 3H), 2.028 (s, 3H), 2.087 (s, 3H), 2.12 (s, 3H) (7×CH_3CO), 2.32 (s, 3H, CH3COS) 3.08 (tr, 2H, J= 6.3Hz, CH_2CH_2S), 3.6 (m, 8H, OCH_2CH_2O), 3.95 (m, 2H, CH), 3.8-3.9 (m, 2H), 4.2 (m, 2H, CH), 4.47 (dd, 1H, J= 12Hz, 3Hz, CH), 4.61 (d, 1H, J= 8 Hz, CH), 4.8 (m, 2H, CH) , 5 (tr, 1H, J= 10 Hz, CH), 5.242 (t, 1H, J= 9Hz), 5.34 (t, 1H, J= 10Hz, CH) 5.4 (d, 1H, J= 3 Hz, CH). ^{13}C NMR (300MHz, $CDCl_3$): δ=20.08, 20.08, 20.1, 20.16, 20.18, 20.35, 20.4 (7x CH_3CO), 28.25 (CH_3COS), 30.118 (CH_2CH_2S), 61.1, 62.3, 67.5, 68.03 (CH), 68.65, 68.89,

69.35, 69.56, 69.828(O*C*H$_2$*C*H$_2$O) 70.08, 71.76, 72.3, 74.87, 95.087 (C1α), 99.92 (C1β), 168.929, 169.212, 169.443, 169.738, 169.931, 170.02, 170.03 (7x CH$_3$*C*O), 195(CH$_3$*C*OS).

6.1.2.3Deprotection to give α-D-Mannopyranoside, 2-[2-(2-mercaptoethoxy)ethoxy]ethyl.

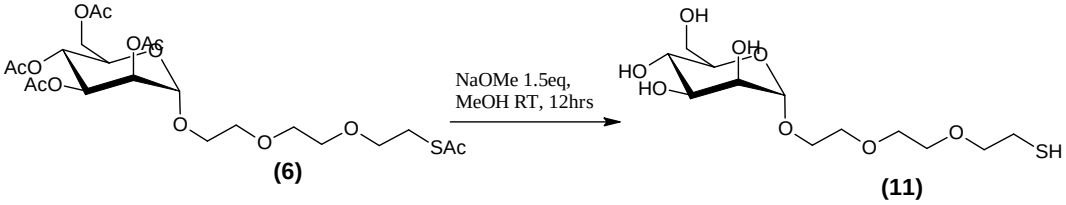

(6) **(11)**

Figure 102 Deacetylation.

α-D-Mannopyranoside, 2-[2-(2-(acetylthio)ethoxy)ethoxy]ethyl, 2,3,4,6-tetraacetate (200mg, 0.37mmol, 1eq.) was taken and dissolved in anhydrous methanol (5ml). Sodium Methoxide (30mg 0.055mmol, 1.5eq) was added and the solution was stirred at room temperature for 12 hrs. Acidic Ion exchange resin (Amberlite IR-120) was then added and at neutralisation was filtered off and washed with MeOH. The solvent was then evaporated off to afford the corresponding thiol in high yields (>80%). The initial ^{1}H NMR spectrums indicated the thiol as the main product with disulfide also formed. The amount of disulfide increases over time due to oxidation by atmospheric oxygen. Both thiol and disulfide product forms will interact in the same manner with gold nanoparticles and so no purification is necessary.

6.1.2.3.1 α-D-Mannopyranoside, 2-[2-(2-mercaptoethoxy)ethoxy]ethyl **(11)**

^{1}HNMR(300MHz, MeOD, 25°C): δ=2.7 (tr, 1H, *J*= 6.6Hz), 2.96 (tr, 1H, *J*= 6.6Hz), 3.6-3.79(m, 10H), 3.8-3.95(m, 4H), 4.0 (dd, 1H, *J*= 3, 1.5Hz, H-2), 4.9 (d, 1H, *J*= 1.5Hz, H-1). ^{13}C NMR (300MHz, MeOD, 25°C): δ=24.334, 39.469, 62.387, 67.926, 68.353, 70.485, 71.315, 71.364, 71.538, 71.983, 72.417, 74.433, 101.694. ES-MS calcd. for $C_{12}H_{24}O_8SNa$ $[M+Na]^+$: 351.1090, found 352.0; for $C_{24}H_{45}O_{16}S_2Na$ $[M+Na]^+$ 676.7335, found 676.5. Lit: [163]

6.1.2.3.2 β-D-Glucopyranoside, 2-[2-(2-mercaptoethoxy)ethoxy]ethyl **(12)**

^{1}HNMR(300MHz, MeOD, 25°C): δ=2.7 (t, 2H, *J*H =6.6Hz), 3.32 (tr, 1H, H-4) 3.4-3.7 (m , 2H, H-5, H-3, H-4), 3.7-3.9 (m, 10H), 3.95 (dd, 1H, *J*=12.3, 2.1Hz, H-2), 4.1 (m, 1H, H-6), 4.52 (d, *J*= 1H, H-1). ^{13}C NMR (300MHz, MeOD, 25°C): δ=102.366, 76.096, 76.016, 73.245, 73.144, 71.885, 71.543, 70.588, 69.812, 69.704, 69.480, 69.458, 69.278, 68.599, 67.761,

66.025, 60.751, 37.462, . ES-MS calcd. for $C_{12}H_{24}O_8Sna$ $[M+Na]^+$: 351.1090, found 352.1; for $C_{24}H_{45}O_{16}S_2Na$ $[M+Na]^+$ 676.7335, found 676.5.

6.1.2.3.3 β-D-Galactopyranoside, 2-[2-(2-mercaptoethoxy)ethoxy]ethyl **(13)**

^{1}HNMR (300MHz, MeOD, 25°C): δ=2.7 (t, 1H, *J*=6.6Hz), 3.6 (dd, 1H, *J*= 10, 8Hz), 3.65-3.9(m, 12H), 3.95 (m, 2H), 4.1 (m, 1H), 4.45 (d, *J*=8Hz, 1H, H-1). ^{13}C NMR (300MHz, MeOD, 25°C): δ=23.961, 43.954, 62.786, 67.667, 69.960, 71.082, 71.151, 71.201, 71.442, 72.409, 100.184. ES-MS calcd. for $C_{12}H_{24}O_8SNa$: 351.1090, found 352.1; for $C_{24}H_{45}O_{16}S_2Na$ $[M+Na]^+$ 676.7335, found 676.6. Lit: [163]

6.1.2.3.4 β-D-Glucopyranoside, 2-[2-(2-mercaptoethoxy)ethoxy]ethyl 4-O-β-D-galactopyranosyl **(14)**

^{1}HNMR (300MHz, MeOD, 25°C): δ=2.8 (t, 2H, *J*=6.6Hz), 3.35 (2H, s), 3.5-3.8 (20H, m), 3.9 (d, 2H, *J*H=3.3Hz, H-4), 4.1 (2H, m), 4.45(d, 1H, *J*H =7.8Hz, H-8 (H-1Gal)), 4.51 (1H, d, *J*H =7.8Hz, H-1Glc). ^{13}C NMR (300MHz, MeOD, 25°C): δ=102.54, 101.65, 77.82, 74.88, 73.89, 72.29, 70.41, 69.25, 68.27, 60.6, 59.61, 48.51, 42.79. ES-MS calcd. for $C_{18}H_{34}O_{13}SNa$ $[M+Na]^+$: 513.5198, found 514.4.

6.1.2.3.5 β-D-Glucopyranoside, 2-[2-(2-mercaptoethoxy)ethoxy]ethyl 4-O-α-D-glucopyranosyl **(15).**

^{1}HNMR (300MHz, MeOD, 25°C): δ=2.82 (2H, m), 3.25(2H, m), 3.35-4 (20H, m), 4.39(d, 1H, *J*=7.8Hz, H-1(H-1β-Glu), 5.275(d , 1H, *J*=3.6Hz, H-1α-Glc). ^{13}C NMR (300MHz, MeOD, 25°C): δ= 102.300, 99.851, 77.176, 76.331, 74.781, 73.198, 73.064, 72.910, 71.889, 69.905, 69.743, 69.553, 68.884, 68.615, 60.967, 60.715, 37.539, 20.574. ES-MS calcd. for $C_{18}H_{34}O_{13}SNa$ $[M+Na]^+$: 513.5198, found 514.3.

6.1.3 Alkylglycoside Synthesis

Alkyl glycosides were prepared to act as synthetic glycolipids which would then be partitioned into phospholipid vesicles to look at lectin recognition in a biomimetic manner. They were prepared using the "click chemistry" i.e. a Huisgen-type azide-alkyne cycloaddition to give a 1,4-di-substituted 1,2,3-triazole unit [513-515].

6.1.3.1 General Preparation Procedure for Glycosyl Azides.

The glycosyl azides were prepared from the glycosyl bromides in a two-phase reaction. The glycosyl bromides were prepared as follows:

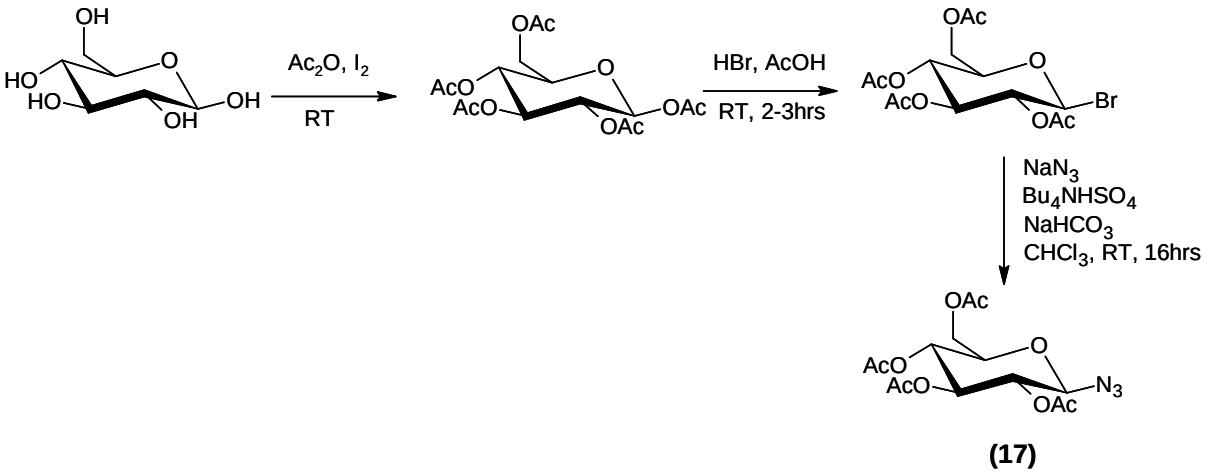

Figure 103 1-Azido sugar peracetate synthesis.

To 2 gr of sugar peracetate in glacial acetic acid (10ml) stirring under inert conditions was added HBr (33% in acetic acid) (5ml) dropwise. The mixture was stirred at room temperature for another 3 hours before being diluted with dichloromethane (40 ml) and poured into ice-water. The layers were separated and further washing with sat.$NaHCO_3$ (3x20 ml) was followed by drying over sodium sulphate and evaporation of the solvent to yield yellow oil. This oil was used directly in the next step, phase transfer azidation. The crude glycosyl bromides were weighed before being dissolved in chloroform (20ml). A saturated $NaHCO_3$ solution (20 ml) was then added to the stirring chloroformic solution followed by NaN_3 (5 eq.) and the phase transfer catalyst tetrabutylammonium hydrogen sulphate (1 eq.). This two phase mixture was stirred at room temperature overnight. The work-up was by washing of the chloroformic phase with water x 1, sat. $NaHCO_3$ x1 followed by a brine wash. After drying over sodium sulphate the solvent was then evaporated of to yield white solids which could be recrystallised form methanol to yield anomerically pure azides.

6.1.3.2 Coupling and Deprotection to give Alkylglycosides

A suspension of $CuSO_4$.5H2O (0.2 eq.) and Na ascorbate (0.4 eq.) dissolved in H_2O (5ml) was added to a stirring suspension of glycosyl azide (1 eq. 500 mg) and 1-Tetradecyne (1 eq.) in t-butanol (5 ml). The cloudy mixture was heated to 70°C and stirred at this temperature for

typically 48 hours. On cooling slowly to 4°C the product precipitated from solution and could be filtered off.

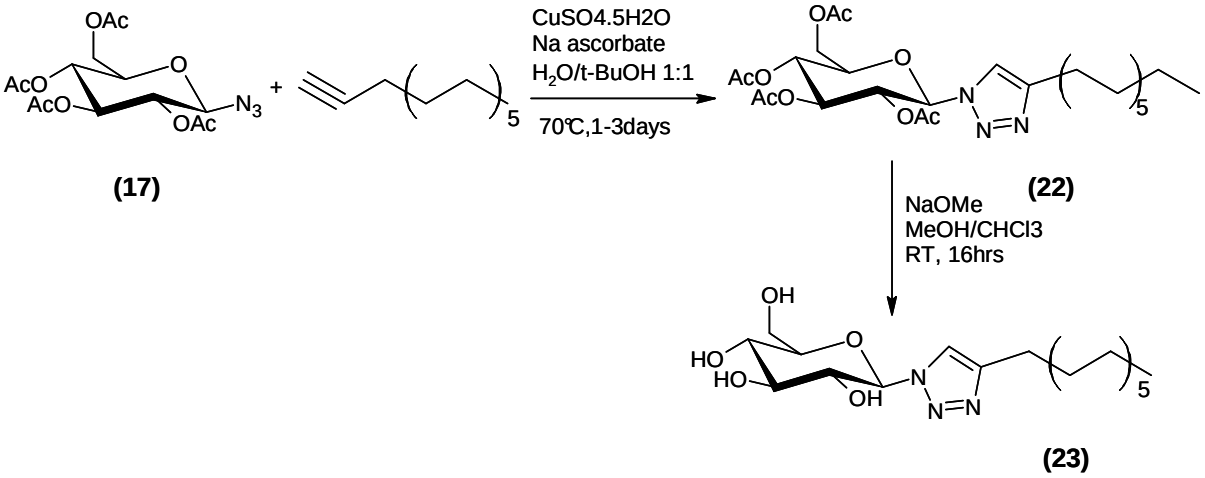

Figure 104 Alkyl glycoside by "click chemistry".

The peracylated products were then deprotected using the classic sodium methoxide in MeOH method (1 eq.) stirring at room temperature for 16 hours. Chloroform was used as a co-solvent in some cases. Acidic ion-exchange resin (Amberlite IR-120) was then added and at neutralisation was filtered off and washed with MeOH. The solvent was then evaporated off to afford the products **21, 23, 25** and **27**. They were further purified by crystallisation from $CHCl_3$/MeOH.

6.1.3.3Characterisation by ^{1}HNMR.

6.1.3.3.1 1-Azido-1-deoxy-α-D-mannopyranoside tetraacetate **(16).**

1H NMR (300MHz, $CDCl_3$ 25°C): δ= 1.988 (s, 3H), 2.052 (s, 3H), 2.107 (s, 3H), 2.202 (s, 3H), 3.75 (m, 1H), 4.19 (dd, 1H, *J*=12.3, 2.7 Hz), 4.28 (dd, 1H, *J*=12.3, 5.4 Hz), 4.73 (d, 1H, *J*=1.2 Hz), 5.03 (dd, 1H, *J*=9.9, 3.3 Hz), 5.26 (t, 1H, *J*=9.9), 5.4 (dd, *J*=3.3, 1.2 Hz).13C NMR (300MHz, $CDCl_3$, 25°C): *δ*=20.47, 20.55, 20.58, 20.68, 62.11, 65.62, 68.20, 69.13, 70.62, 87.41, 169.52, 169.61, 169.72, 170.45.

6.1.3.3.2 1-Azido-1-deoxy-β-D-glucopyranoside tetraacetate **(17)**

1H NMR (300MHz, $CDCl_3$, 25°C): *δ*=1.99 (s, 3H), 2.022 (s, 3H), 2.068 (s, 3H), 2.092 (s, 3H), 3.75 (m, 1H), 4.15 (dd, 1H, *J*=12.5, 2.4 Hz), 4.26 (dd, 1H, *J*=12.5, 4.8 Hz), 4.63 (d, 1H, *J*=8.7 Hz), 4.95 (t, 1H, *J*=9.6 Hz), 5.093 (t, 1H, *J*=9.6 Hz), 5.212 (t, 1H, *J*=9.6 Hz). ^{13}C NMR

(300MHz, $CDCl_3$, 25°C): δ=20.5, 20.5, 20.5, 20.7, 61.6, 67.8, 70.6, 72.5, 73.6, 87.9, 169.2, 169.3, 170.1, 170.6.

6.1.3.3.3 1-Azido-1-deoxy-β-D-galactopyranoside tetraacetate **(18)**

1H NMR (300MHz, $CDCl_3$, 25°C) δ = 1.98 (s, 3H), 2.05 (s, 3H,); 2.08(s, 3H,), 2.16 (s, 3H, CH_3), 4.00 (t, 1H, *J*=6.6 Hz); 4.14-4.17 (m, 2H),) 4.59 (d, 1H, J = 8.7 Hz), 5.02 (dd, 1H, J =10.3, 3.3 Hz), 5.15 (dd, 1H, J = 10.4, 8.7 Hz), 5.41 (d, J = 3.3 Hz, 1H). ^{13}C NMR (300MHz, $CDCl_3$, 25°C) δ =20.65, 20.74, 20.78, 20.80, 61.3, 66.9, 68.1, 70.8, 72.9 , 88.4, 169.5,170.1, 170.3, 170.5.

6.1.3.3.4 1-Azido-1-deoxy-β-D-Maltopyranoside heptaacetate **(19)**

^{1}HNMR (300MHz, $CDCl_3$, 25°C): δ=1.99(s, 3H), 2.009(s, 3H), 2.024(s, 3H), 2.039(s, 3H), 2.048(s, 3H), 2.1(s, 3H), 2.152(t, 3H), 3.78(m, 1H), 4.0(m, 2H), 4.25 (m, 2H), 4.5 (dd, 1H, *J*=12.3, 2.4 Hz) 4.7 (d, 1H, *J*=8.4 Hz), 4.78 (t, 1H, *J*=8.6 Hz), 4.85 (dd, 1H, *J*=9.9, 3.6 Hz), 5.05 (t, 1H, *J*=9.9 Hz), 5.25 (t, 1H, *J*=8.6 Hz), 5.29 (s, 1H), 5.35 (t, 1H, *J*=10.2 Hz), 5.4 (d, 1H, *J*=3.9 Hz). ^{13}C NMR (300MHz, $CDCl_3$, 25°C) δ=20.5, 20.5, 20.6, 20.6, 20.7, 20.8, 20.8, 60.4, 62.5, 67.9, 68.6, 69.2, 70.0, 71.4, 72.3, 74.2, 75.1, 87.5, 95.7, 169.4, 169.5, 169.9, 170.1, 170.4, 170.5, 170.5.

*6.1.3.3.5 1H-1,2,3-Triazole,4-dodecyl-1-(2,3,4,6-tetra-O-acetyl-β-D-mannopyranosyl)-***(20)**

1H NMR (CDCl3, 300 MHz): δ=0.87 (t, 1H, *J*=6.3Hz), 1.25 (m 22H), 2.0 (s, 3H), 2.09 (m, 12H), 3.95 (m, 1H), 4.19 (dd, 1H, *J*=12.6, 2.4 Hz), 4.33 (dd, 1H, *J*=12.6, 6 Hz), 5.26 (dd, 1H, *J*=9.9, 3.3 Hz), 5.35 (t, 1H, *J*=9.9Hz), 5.7 (dd, *J*=3.3, 1.5 Hz). 6.1 (d, 1H, *J*=1.2 Hz) 7.48 (s, 1H).

*6.1.3.3.6 1H-1,2,3-Triazole- 4-dodecyl-1-α-D-mannopyranosyl-***(21)**

1H NMR (300 MHz, CD_3OD) : δ=0.82 (t, 3H, *J*=6.7 Hz), 1.22 (m, 18H), 1.6 (t, 2H, *J*=7.2 Hz), 2.65 (t, 2H, *J*=7.8 Hz), 3.32 (t, 1H, *J*=1.5 Hz), 3.45 (m, 1H), 3.65 (dd, 1H, *J*=9.6, 2.1 Hz), 3.73-3.9 (m, 2H), 4.17 (d, 1H, *J*=2.1 Hz), 5.76 (s, 1H), 7.85 (s, 1H). ^{13}C NMR (300MHz, $CDCl_3$, 25°C) δ=14.5, 23.4, 26.1, 30.1, 30.14, 30.18, 30.4, 32.7, 62.0, 67.2, 71.7, 74.4, 80.7, 87.6, 122.6. ES-MS calcd. for $C_{20}H_{36}N_3O_5Na$ $[M+Na]^+$: 421.513, found 421.3.

*6.1.3.3.7 1H-1,2,3-Triazole,4-dodecyl-1-(2,3,4,6-tetra-O-acetyl-β-D-glucopyranosyl)-***(22)**

1H NMR (300MHz, $CDCl_3$, 25°C): δ=0.87(t, 3H, *J*=6.6Hz), 1.255(m, 18H), 1.67 (t, 2H, *J*=7.2Hz), 1.877 (s, 3H), 2.007 (s, 3H), 2.043 (s, 3H), 2.219 (s, 3H), 2.714 (t, 2H, *J*=7.8Hz), 4.2 (m, 3H), , 5.22 (dd, 1H, J =10.3, 3.3 Hz), 5.55 (m, 2H), 5.8 (d, 1H, J = 9.3 Hz), 7.55 (s,1H).

*6.1.3.3.8 1H-1,2,3-Triazole- 4-dodecyl-1-β-D-glucopyranosyl-***(23)**

1H NMR (300 MHz, CD_3OD) : δ=0.81 (t, 3H, *J*=6.7 Hz), 1.2 (m, 18H), 1.57 (t, 2H, *J*=7.2 Hz), 2.63 (t, 2H, *J*=7.8 Hz), 3.48 (dd, 1H, *J*=9, 9 Hz), 3.56 (m, 2H), 3.71 (dd, 1H, *J*=12.0, 5.0 Hz), 3.85 (m, 1H), 5.244 (s, 1H), 5.37 (d, 1H,*J*=9.0 Hz), 7.53 (s, 1H). ^{13}C NMR (300MHz, CD_3OD, 25°C) δ=14.4, 23.7, 149.26, 26.31, 30.3, 30.45, 30.48, 30.5, 30.66, 30.73, 30.75, 33.05, 62.42, 70.94, 73.99, 78.6, 81.12, 89.5, 122.34. ES-MS calcd. for $C_{20}H_{36}N_3O_5Na$ $[M+Na]^+$: 421.513, found 421.4.

1H-1,2,3-Triazole,4-dodecyl-1-(2,3,4,6-tetra-O-acetyl-β-D-galactopyranosyl)- **(24)**

1H NMR (300MHz, $CDCl_3$, 25°C): δ=0.87(t, 3H, *J*=6.6Hz), 1.255(m, 18H), 1.67 (t, 2H, *J*=7.2Hz), 1.877 (s, 3H), 2.007 (s, 3H), 2.043 (s, 3H), 2.219 (s, 3H), 2.714 (t, 2H, *J*=7.8Hz), 4.2 (m, 3H), 5.22 (dd, 1H, *J*=10.3, 3.3 Hz), 5.55 (m, 2H), 5.8 (d, 1H, *J*= 9.3 Hz), 7.55 (s,1H).

*6.1.3.3.9 1H-1,2,3-Triazole- 4-dodecyl-1-β-D-galactopyranosyl-***(25)**

1H NMR (300 MHz, CD_3OD) : δ=0.89 (t, 3H, *J*=6.7 Hz), 1.3 (m, 18H), 1.68 (t, 2H, *J*=7.2 Hz), 2.7 (t, 2H, *J*=7.8 Hz), 3.68 (dd, 1H, *J*=9.6, 3.3 Hz), 3.74-3.9 (m, 3H), 3.98 (d, 1H, *J*=3.3 Hz), 4.12 (t, 1H, *J*=9.3 Hz), 5.5 (d, 1H, *J*=9.0 Hz), 7.96 (s, 1H). ^{13}C NMR (300MHz, CD_3OD, 25°C) δ=14.448 (CH_3), 23.755 (all CH_2) , 26.392, 30.310, 30.494, 30.540, 30.708, 30.776, 30.803, 33.098, 49.050, 62.518 (C-6) , 70.485, 71.487, 75.443, 79.979, 90.224 (C-1), 121.859, 149.448. ES-MS calcd. for $C_{20}H_{36}N_3O_5Na$ $[M+Na]^+$: 421.513, found 421.2.

6.1.3.3.10 1H-1,2,3-Triazole,4-dodecyl-1-(2,3,4,6,8,9,10,12-hepta-O-acetyl-β-D-maltopyranosyl) **(26)**

1H NMR (300 MHz, $CDCl_3$, 25°C) : δ=7.423 (s, 1H), 5.845 (d, 1H, *J*=9.3 Hz), 5.45–5.40 (m, 2 H) 5.34 (d, 1 H), 5.05 (dd, 1H, J= 10.3, 7.8 Hz), 4.87 (dd, 1 H, J=10.4, 3.4 Hz,) 4.47 (dd, 1 H, J=12.4, 2.4 Hz), 4.25 (m, 2 H), 4.0–3.93 (m, 3H), 2.67 (t, 2H, *J*=7.8 Hz), 2.11 (s, 3H), 2.09 (s, 3H), 2.05 (s, 3H), 2.02 (s, 3H), 2.014 (s, 3H), 1.99 (s, 3H), 1.82 (s, 3H), 1.63 (t, 2H, *J*=7.4 Hz), 1.24 (m, 18H), 0.86 (t, 3H, *J*=6.6 Hz).

*6.1.3.3.11 1H-1,2,3-Triazole- 4-dodecyl-1-β-D-maltopyranosyl-***(27)**

1H NMR (300 MHz, $CDCl_3$, 25°C): δ=0.82 (t, 3H, J=6.6 Hz), 1.22 (m, 18H), 1.68 (t, 2H, J=7.2 Hz), 2.71 (t, 2H, J=7.2 Hz) 3.3 (t, 1H, J=9.3 Hz), 3.5 (dd, 1H, J=9.3 Hz), 3.7(m, 4H), 3.85 (m, 3H), 3.95 (t, 1H, J=9Hz), 5.25 (d, 1H, *J*=9 Hz), 5.6 (d, 1H, J=3.6 Hz), 7.95(s, 1H). ^{13}C NMR (300MHz, CD_3OD, 25°C) *δ*=14.39, 23.38, 25.92, 29.80, 29.98, 30.02, 30.06, 30.20, 30.27, 32.63, 62.09, 70.90, 73.36, 73.48, 74.31, 74.53, 77.93, 78.76, 79.02, 88.74, 101.87, 122.73, 149.56. ES-MS calcd. for $C_{26}H_{46}N_3O_{10}Na$ $[M+Na]^+$: 583.655, found 583.6

6.1.4 Glyconanoparticle Preparation

6.1.4.1Self-assembly on citrate stabilised particles

$HAuCl_4$ (12.5 mg 0.21mM) was dissolved in H_2O (mQ)(100 ml) and heated to 60°C with constant rapid stirring. Sodium citrate (50 mg, 1.3mM) was dissolved in H_2O (mQ)(50ml) and was also heated to 60 °C upon which it was added to the vigorously stirring gold salt solution in order to keep temperature and concentration variance to a minimum. The temperature was then changed to 85°C and the solution was stirred for another two hours. The initially pale yellow solution gradually turned red indicating colloid formation. The solution was then allowed to cool to room temperature before the next step.

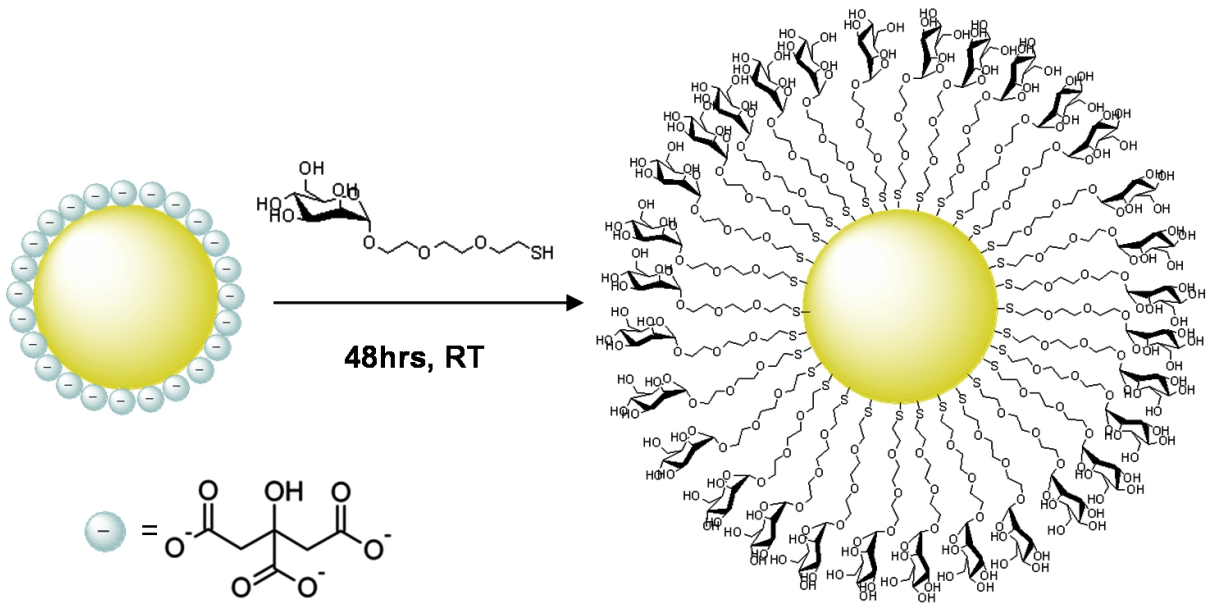

Figure 105 Two step glyconanoparticle preapration procedure.

To 25 ml of this gold sol (0.21 mM in gold) was added excess of the thiol ligand (50 mg, 6 mM) giving a final ligand to gold ratio of around 30:1. This solution was then allowed to stir at room temperature for 48 hrs before being diluted (x5) with pure water and being

centrifuged (14000 r.p.m for 10 minutes) down to remove excess ligand and citrate followed by resuspension in mQ water. This purification procedure was repeated twice followed by resuspension of the particles in Tris buffer. Using this procedure mannoside **(29)**, triethyleneglycol **(30)**, galactoside **(31)**, glucoside **(32)** and maltoside **(33)** nanoparticles were prepared.

6.1.4.2One step direct method (Penades Method [162])

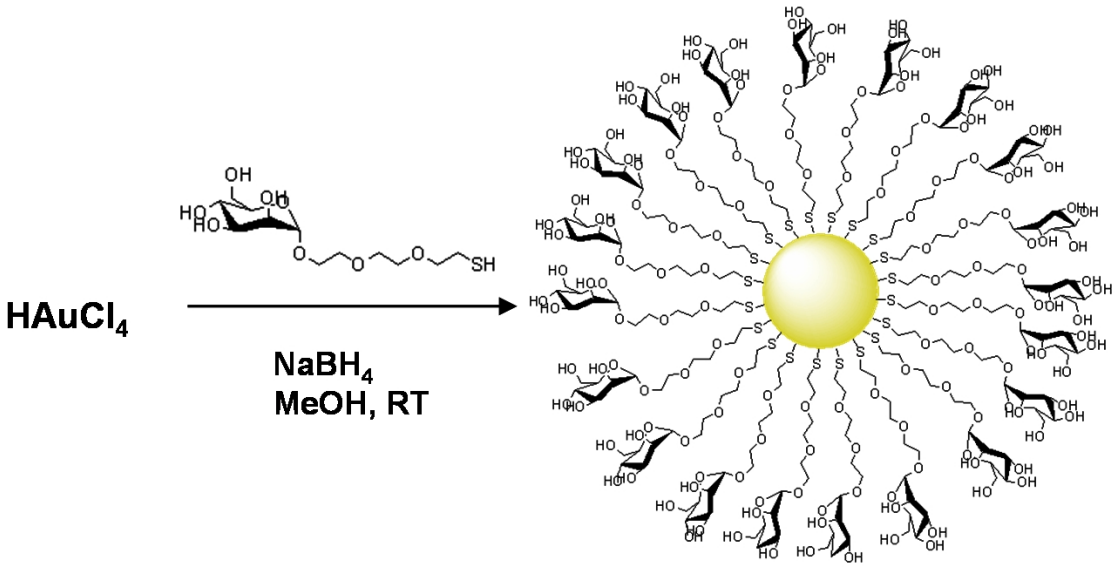

Figure 106 One step modified brust method for glyconanoparticle preparation

To a solution of glycoligand (20 mg, 5eq.) in MeOH (5 ml) under vigorous stirring was added a solution of $HAuCl_4.3H_2O$ (8 mg, 1 eq. in H_2O (0.5 ml). After 1 minute a sodium borohydride solution (1M) was added dropwise and the solution changed colour from pale yellow to black. The solution was then left to stir for a further 2 hours with a dark precipitate forming in each case. Each solution was then centrifuged at 4400 r.p.m. for 30 mins followed by removal of the supernatant. The precipitate was dissolved in 1ml of water followed by 4ml of methanol then recollected by centrifugation at 4400 r.p.m. for 15 minutes. This purification process was then repeated twice more. The purified particles were then dried and dissolved in the Tris buffer (10 mM, pH 7.4, NaCl 0.1M).

6.1.5 Quartz Crystal Surface Preparation

Hydrophobic self-assembled monolayers were prepared directly on gold coated quartz crystals acquired from Attana. The crystals were firstly immersed in a freshly prepared piranha solution (H_2SO_4 / H_2O_2 7:3) for 1 minute and then washed thoroughly with pure water. They were then dried under a nitrogen stream and immersed in a 1mM octadecanethiol

solution (EtOH:Hexane 9:1) for at least 16 hours followed by extensive rinsing with ethanol followed by hexane and then more ethanol and lastly water before being blown dry with a nitrogen stream and being placed in the QCM chip setup.

6.2 Section 3 Experimental

6.2.1 General Remarks

Polyoxomolybdate Clusters "$Mo_{132}(CH_3COO)_{30}$" **(35)**, $Mo_{132}(SO_4)_{30}$ **(36)** and "$Mo_{72}Fe_{30}$"**(37)** were obtained from the Achim Müller group:

$(NH_4)_{42}[Mo^{VI}_{72}Mo^{V}_{60}O_{372}(H_2O)_{72}(CH_3COO)_{30}]$.c.a.$300H_2O.10CH_3COONH_4$ **(35)**
$(NH4)_{72}[Mo^{VI}_{72}Mo^{V}_{60}O_{372}(H_2O)_{72}(SO_4)_{30}]$.ca. $280H_2O$ **(36)**
$Mo^{VI}_{72}Fe^{III}_{30}O_{252}(CH_3COO)_{12}\{Mo_2O_7(H_2O)\}_2\{H_2Mo_2O_8(H_2O)\}(H_2O)_{91}]\cdot$ca.$150H_2O$ **(37)**

EYPC (3-sn-Phosphatidylcholine solution, CAS:8002-43-5), POPC (1-palmitoyl-2-oleoyl-sn-glycero-3-phosphocholine), HPTS (8-Hydroxypyrene-1,3,6-trisulfonic acid trisodium salt) and Tris base (2-Amino-2-(hydroxymethyl)-1,3-propanediol) were purchased from Sigma-Aldrich.

QCM experiments were run on the A100 instrument from Attana (www.attana.com).

Fluorescence experiments were run on the LS 55 Flourescence spectrometer from Perkin-Elmer. Nuclepore™ track-etched polycarbonate membranes (pore size 0.1 μM) (cat no. 800319) from Whatman were used for vesicle extrusion

For QCM the instrument used was the Attana A100 QCM balance. Frequency changes were recorded for a quartz crystal with a deposited SiO_2 layer (500Å) on a TiO_2 adhesive layer (15Å). The experiments were run under a continuous flow of buffer/water of 20μl/min at 25°C.

6.2.2 POPC SUV (small unilamellar vesicle) Preparation.

The vesicle solutions were prepared following a known protocol [79] for SUV's: 1.5 mg of POPC was dissolved in iso-propanol (50 μl). This solution was then injected into 1 ml of Buffer (PBS or Tris) (pH 7.4) (NaCl 100 mM) with rapid shaking on a "paramix II" shaker

for one minute resulting in a clear solution. This solution was then ultrasonicated for 30 minutes at 0°C before being diluted (x10) with buffer giving a final concentration of 200μM in POPC.

6.2.3 Supported bilayer formation by Vesicle Fusion

Supported bilayers were formed following the vesicle fusion method [323-326]. Silica functionalised gold coated quartz crystals were pre-cleaned by immersion in Piranha solution (H_2SO_4/H_2O_2, 7:3) for 30 seconds followed by extensive rinsing with UHP water after which they were blown dry and placed in the QCM chip setup. They were then, under a constant buffer ((Tris 10mM, NaCl 100 mM, $CaCl_2$ 1mM) or (PBS 10 mM NaCl 100 mM)) flow of 20 μl/min exposed to 200 μM POPC SUV solutions for 130 seconds. The bilayer formation was monitored in situ by QCM frequency response.

6.2.4 POPC Small Unilamellar Vesicles incorporating $Mo_{132}DODA_{40}$ (m.w.≈43,900). for QCM Supported Bilayer Measurements

SUV solutions prepared as described and at a concentration of 200μM were incubated for 5 minutes with Mo_{132} anionic clusters and DODA-Br before being injected into the QCM chamber for vesicle fusion investigation. For example to prepare a 400 nM $Mo_{132}DODA_{40}$ SEC concentrations represented in (Figure 63) 6 μl of a 1mg/ml "$Mo_{132}.(CH_3COO)_{30}$" (m.w. ≈28616 g/mol) in buffer was added to 500 μl of the POPC solution followed by 6.5 μl of an 1mg/ml aqueous DODA-Br solution.

6.2.5 EYPL (3-sn-Phosphatidylcholine) Large Unilamellar Vesicles

600ul of 3-sn-Phosphatidylcholine solution (100mg/ml in chloroform) was dried under vacuum overnight. To this dried film was added HPTS (20 μl of a 1mM solution (PBS pH6.4, NaCl 100mM)) and the solution was then brought up to 2ml with buffer (PBS pH6.4, NaCl 100mM). After shaking the suspension was then sonicated at 60°C for 30 minutes giving a milky solution which was then extruded at least 20 times through a polycarbonate membrane (pore size 1μM) giving a translucent solution. In order to remove external HPTS from the solution it was then passed through a column of sephadex (G-50) with the resultant fractions collected and diluted up to 8ml (final conc. 10mM). Vesicles prepared in this manner were analysed by dynamic light scattering presenting a highly homogenous vesicular solution with vesicle diameter of 94.5 nm (Figure 107).

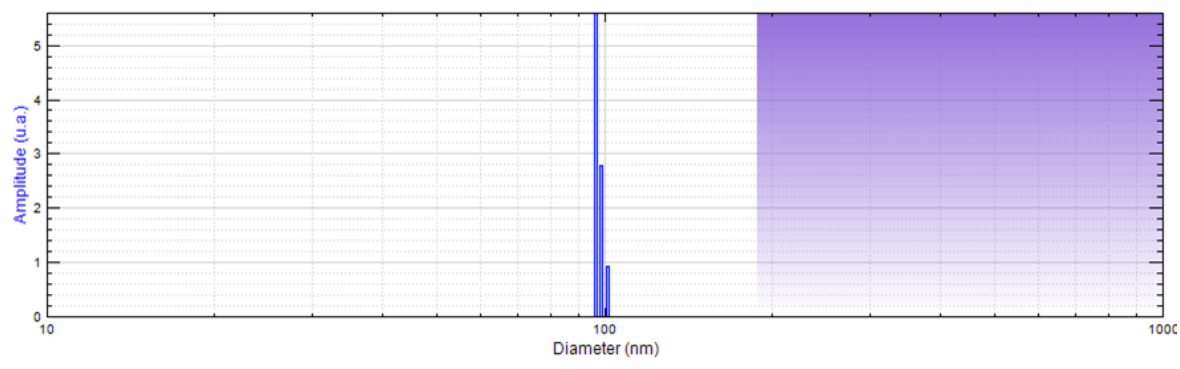

Figure 107 DLS analysis of HPTS containing LUV solution showing size distribution.

6.2.6 Cation Transport Measurements by Fluorescence.Spectroscopy

The experiments were performed by monitoring the emission intensity of HPTS at 510nm. HPTS is a pH-sensitive fluorescent dye with a pKa of 7.3 and one excitation maximum at 405 nm which decreases and another one at 450 nm which increases ,with increasing pH. The ratio in emission intensities resulting from excitation at these wavelengths can be calibrated to solution pH.

Entrapped in vesicles, HPTS can serve as intravesicular pH meter that ratiometrically detects the collapse of an applied transmembrane pH gradient as well as the ability of synthetic ion channels to accelerate this process [516,517].

The prepared LUV solutions were taken and diluted with buffer (PBS 10 mM, pH 6.4, MCl, M=Na, K or Li) up to 2 ml in a quartz cuvette (final conc. 500 μM in phospholipid) and the measurement was immediately commenced under agitation. After 60 seconds an NaOH (0.5 M) (29 μl) solution was injected to cause a pH shift in the external medium 6.4→7.4. The fluorescence emission intensity ratio was monitored for a further 440 seconds upon which the vesicles were lysed by injection of a 5% Triton X-100 (40μl) solution giving the maximal change in dye emission.

6.2.6.1 In situ preparation and inclusion of SECs for Fluorescence Measurements

To 1977ml of the LUV solution prepared as stated and stirring in situ was added a freshly prepared solution of Mo_{132} in buffer (15 μl of relevant concentration of "Mo132.$(CH_3COO)_{30}$" (m.w. ≈28616 g/mol) or "Mo132.$(SO_4)_{30}$ " (m.w. ≈28237.2 g/mol)) followed by DODA Br in UHP water (8 μl of relevant concentration) with measurement commenced immediately. For example a 70 nm concentration required that 15ul of a 9.3 μM cluster solution and 8μl of a 870μM DODA-Br solution (50 equivalents) be added to 100 ul of 10mM EYPC vesicular

solution in 1877 µl of buffer. After stirring for 60 seconds 29ul of NaOH (0.5 M) was added to create the pH gradient.

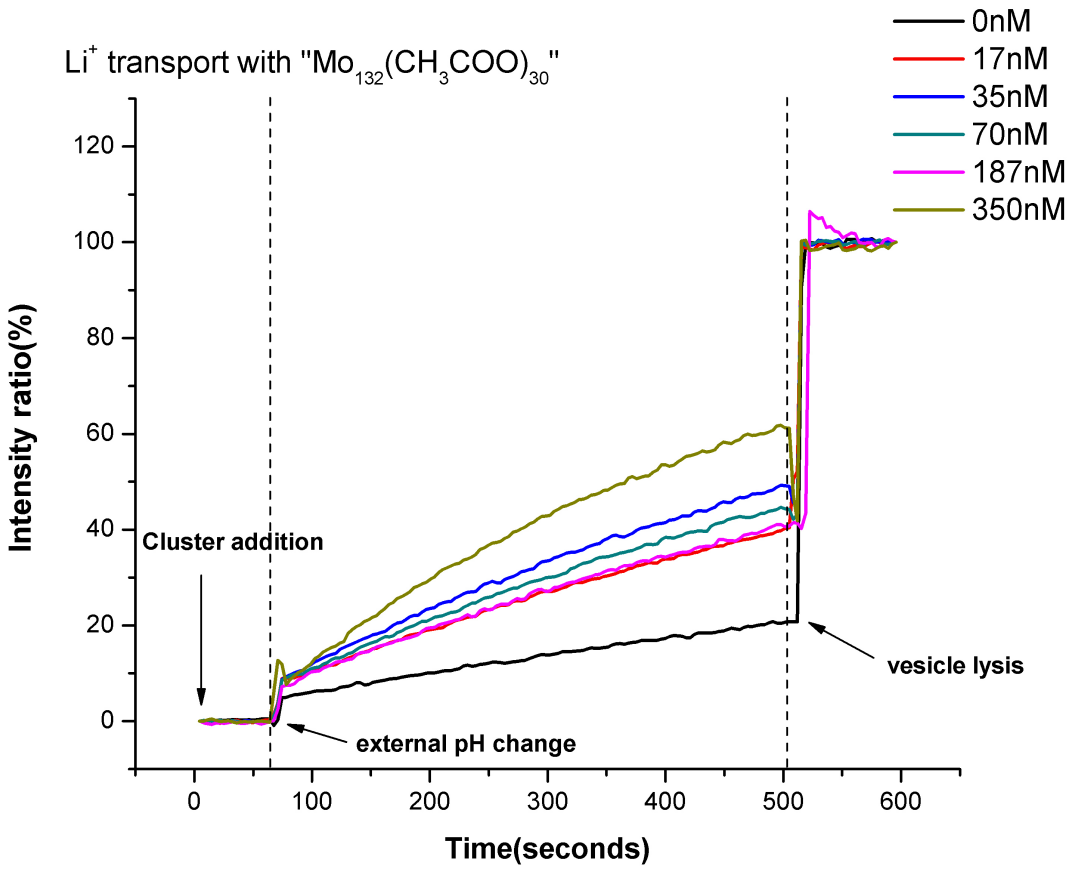

Figure 108 Typical experimental run for fluorescence measurements.

Pseudo first-order rate constants were calculated by calibration of fluorescence intensity ratio change to vesicle internal pH following a method previously demonstrated by Davis and co-workers [318]. Then assuming a constant external pH of 7.4 the rate constants could be calculated from the slope of $\ln\left([H^+]_{in} - [H^+]_{out}\right)$ plotted against time.

$$\ln\left([H^+]_{in} - [H^+]_{out}\right) = -kt + \ln\left([H^+]_{in} - [H^+]_{out}\right)_{t=0}$$

6.3 Section 4 Experimental

6.3.1 System setup

Taking the different factors described as regards protein containing nanoemulsion stability, pH favourable to thiol exchange etc. the system was set up as depicted in (Figure 109).

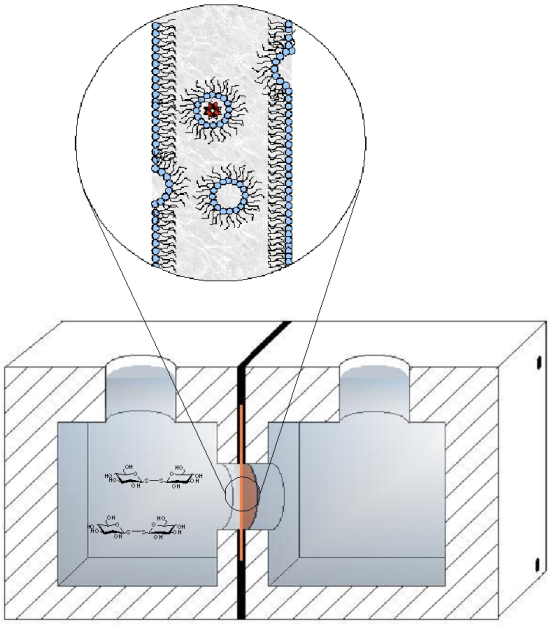

Figure 109 Three-phase transport setup with SLM contained between two teflon cells.

It consisted of a three phase system of D_2O-isooctane-D_2O with the isooctane phase contained by a porous polypropylene membrane. The source phase contained the relevant disaccharide or disaccharides dissolved in 2 ml of D_2O at a concentration of 10^{-2} M and also buffered to pH 7.3 using deuterated phosphoric acid (10 mM) and NaOD. The strip phase contained buffered D_2O (2 ml) and both phases contained t-BuOH (10^{-3}M) or DMSO (10^{-3}M) as an internal concentration standard.

6.3.2 General Remarks

The membrane used was Accurel® PP 2E-HF which had a thickness of 160µm, an average pore size of 200 nm and a Porosity *(θ) of .75.* Concanavalin A from *Canavalia ensiformis* was obtained from Sigma (L7647). Aerosol OT was also obtained from Sigma (D4422). ^{1}H NMR spectra were recorded with a Bruker Avance 300 instrument in D_2O using the residual signal from H_2O as an internal standard.

6.3.3 Membrane Preparation

Extraction Method

Close to complete extraction of Con A may be accomplished at pH 5.3 with AOT concentration of 40 mM. An aqueous Concanavalin type (iv) soln. was initially prepared at a concentration of 1.5 mg/ml from an 10mM acetate buffer soln. pH 5.26 also containing NaCl (100 mM), $CaCl_2$ (10 mM) and $MnCl_2$ (10mM).

The extraction was performed by stirring, at 800rpm for 5mins, 1ml of this Con A solution with 1.5 ml of a 40 mM AOT in isooctane solution. The resulting two-phase mixture was left to sit for 12 hours resulting in a clear two phase system which was then centrifuged for 5 minutes at 2000 r.p.m. A control solution was prepared in an identical manner but without the Con A, hence resulting in a water in isooctane micoemulsion.

Injection Method

Con A containing nanoemulsions were also prepared using an injection method whereby Con A (1mg) in buffered D2O(pH7.4) (50µl) + H_2O(20µl) was injected into a 40mM AOT solution (5ml) giving a W_0 value of 19.4 which based on a reported calculation [518] is optimal for Con A activity:

$$w_0^{optimal} = 0.47\sqrt[3]{M_p} - 2.7$$

Eq 35 [518]

$$w_0^{optimal}(ConA) = 19.4$$

However in other reports on Con A nanoemulsions formed by the extraction procedure W_0 values of 30 have been reported [519].

The supported liquid membranes were then loaded by submersion in these reverse micellar solutions for 48hrs before being placed in the transport setup.

6.3.4 Disaccharide Library

The glycosyl disulfides were synthesised following a one step procedure initially reported by Defaye et al. [520]. 1-Thioglycosides were prepared in collaboration with Remi Caraballo at the Ramström group at KTH Stockholm. The following general procedure as described for 1-thiomannoside was used for all three sugars.

Synthesis of 2,3,4,6-Tetra-O-acetyl-1-S-acetyl-1-thio-d-mannopyranose.

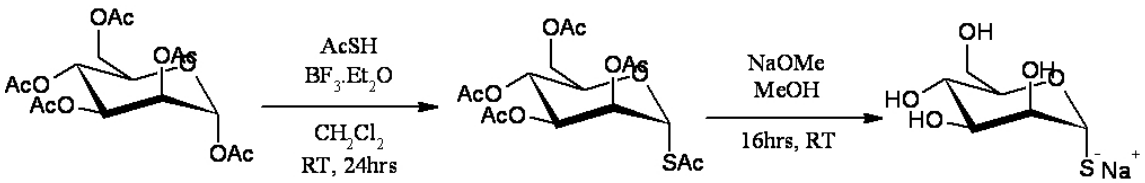

1,2,3,4,6-Penta-*O*-acetyl-d-mannopyranose (0.78 g, 2 mmol) and thioacetic acid (0.305 g, 4 mmol) were dissolved in dry dichloromethane (8 mL) at 0 °C, and $BF_3 \cdot Et_2O$ (1.4 mL, 8

mmol) was added dropwise over a period of 10 min. The reaction mixture was allowed to warm to ambient temperature and stirred for 24 h under nitrogen protection. The resulting reaction mixture was diluted with dichloromethane (20 mL), poured onto ice-cold water, and extracted with dichloromethane. The combined organic phases were washed with saturated $NaHCO_3$, water and brine, dried over Na_2SO_4, and filtered. The crude product was purified by flash chromatography on silica gel (eluent: Hexane/EtOAc 2:1) to give product (yield 51%).

^{1}H NMR ($CDCl_3$, 400 MHz) δ = 5.94 (d, 1H, $J_{1.2}$ = 1.9 Hz, H-1), 5.33 (t, 1H, $J_{4,3}$ = 10.1, $J_{4,5}$ = 10.1 Hz, H-4), 5.31 (dd, 1H, $J_{2,3}$ = 3.4 Hz, H-2), 5.08 (dd, 1H, H-3), 4.27 (dd, 1H, $J_{6a,6b}$ = 12.5 Hz, $J_{6a,5}$ = 4.7 Hz, H-6a), 4.05 (dd, 1H, $J_{6b,5}$ = 2.27 Hz, H-6b), 3.91 (ddd, 1H, H-5), 2.42 (s, 3H, SAc), 2.17 (s, 3H, OAc), 2.07 (s, 3H, OAc), 2.03 (s, 3H, OAc), 1.98 (s, 3H, OAc); ^{13}C NMR ($CDCl_3$, 125 MHz) δ = 192.0 (SAc), 171.1, 170.3, 170.0 (3 × OAc), 79.7 (C-1), 77.2 (C-5), 72.2 (C-3), 71.0 (C-2), 65.6 (C-4), 62.7 (C-6), 31.0 (SAc), 21.2, 21.1, 21.0, 20.9 (4 × OAc); $[\alpha]_D^{22}$ = +70 (*c* = 1.0 in $CHCl_3$); Anal. Calcd (%) for $C_{16}H_{22}O_{10}S$: C 47.29, H 5.46; found: C 47.39, H 5.38.

2.6.2. 1-Thio--d-mannopyranose sodium salt

Compound (0.101 g, 0.25 mmol) was dissolved in methanol (2 mL) at room temperature, and sodium methoxide (0.014 g, 0.26 mmol) in methanol (3 mL) was added dropwise. The reaction mixture was stirred under nitrogen protection resulting in a white precipitation, which was washed with cold methanol to give product 1 (yield 90%).

^{1}H NMR (D_2O, 400 MHz) δ = 5.34 (d, 1H, $J_{1,2}$ = 1.3 Hz, H-1), 4.20 (dd, 1H, $J_{3,4}$ = 9.5 Hz, H-3), 4.04 (m, 1H, H-5), 3.80 (m, 1H, $J_{2,3}$ = 2.6 Hz, H-2), 3.69 (m, 2H, H-6), 3.52 (t, 2H, H-4); ^{13}C NMR (D_2O, 125 MHz) δ = 82.8 (C-1), 77.4 (C-2), 71.6 (C-5), 70.5 (C-3), 68.0 (C-4), 61.4 (C-6); $[\alpha]_D^{22}$ = +52.5 (*c* = 0.1 in MeOH); Anal. Calcd (%) for $C_6H_{11}NaO_5S$: C 33.03, H 5.08; found: C 33.01, H 5.05.

The disaccharides were then prepared by oxidation using hydrogen peroxide (2 equivalents) of the 1-thio-pyranose sugars which may be already partially oxidised by exposure to air at pH7.4. A more controlled faster technique for complete oxidation was later used whereby the thiosaccharides were dissolved in a small amount of methanol (2ml) a concentrated methanolic iodine solution was then added dropwize until a faint colour remained indicating

complete oxidation. The solvent was then evaporated followed by redissolution in 1-2ml of dry methanol and precipitation of the white product with ethyl acetate (30ml) with the disaccharide product then filtered off with vacuum and dried under vacuum immediately.

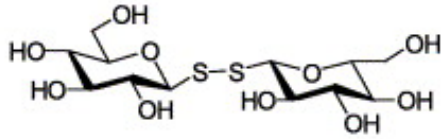

6.3.4.1 β-D-Glucopyranose, 1,1'-dithiobis[1-deoxy- (9Cl) ***(39)***

^{1}H NMR (D_2O, 300 MHz, 25°C) δ= 4.6 (d, 2H, *J*= 9 Hz, H-1), 3.94 (dd, 2H, *J*= 12.6,2.1 Hz) , 3.75 (dd, 2H, *J*= 12.6, 5.4 Hz), 3.626 (tr, 2H, *J*= 9 Hz), 3.55 (tr, 2H, *J*= 9 Hz), 3.51 (dd, 2H, *J*= 5.4, 2.1 Hz), 3.47 (app d, 2H, *J*= 9Hz). ^{13}C NMR (D_2O, 500 MHz, 25°C) 89.401, 80.268, 77.011, 71.171, 69.183, 60.814.

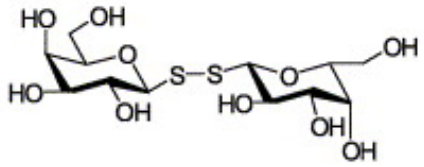

6.3.4.2 β-D-Galactopyranose, 1,1'-dithiobis[1-deoxy- (9Cl) ***(40)***

^{1}H NMR (D_2O, 300 MHz, 25°C) δ= 4.51 (d, 2H, *J*= 9.3 Hz, H-1), 4(d, 2H, *J*= 3.3 Hz H-4) , 3.85 (t, 2H, *J*= 9.3 Hz), 3.76 (m, 4H,), 3.71 (dd, 2H, *J*= 9.3, 3.3 Hz), 3.65 (dd, 2H, *J*= 5.4, 2.1 Hz H-3) ^{13}C NMR (D_2O, 500 MHz, 25°C) δ= 89.950, 79.604, 73.911, 68.840, 68.724, 61.149.

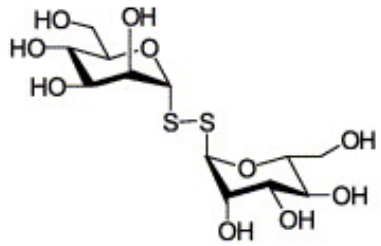

6.3.4.3 α-D-Mannopyranose, 1,1'-dithiobis[1-deoxy-(9Cl) ***(41)***

^{1}H NMR (D_2O, 300 MHz, 25°C) δ= 5.37 (d, 2H, *J* = 1.5 Hz, H-1), 4.2 (dd, 2H, *J* = 3, Hz *J* = 2.1 Hz) , 3.92 (m, 4H), 3.82 (m, 4H), 3.75 (d, 2H, *J* = 9 Hz). ^{13}C NMR (D_2O, 500 MHz, 25°C) δ= 90.090, 74.687, 70.803 (2C), 66.800, 60.693.

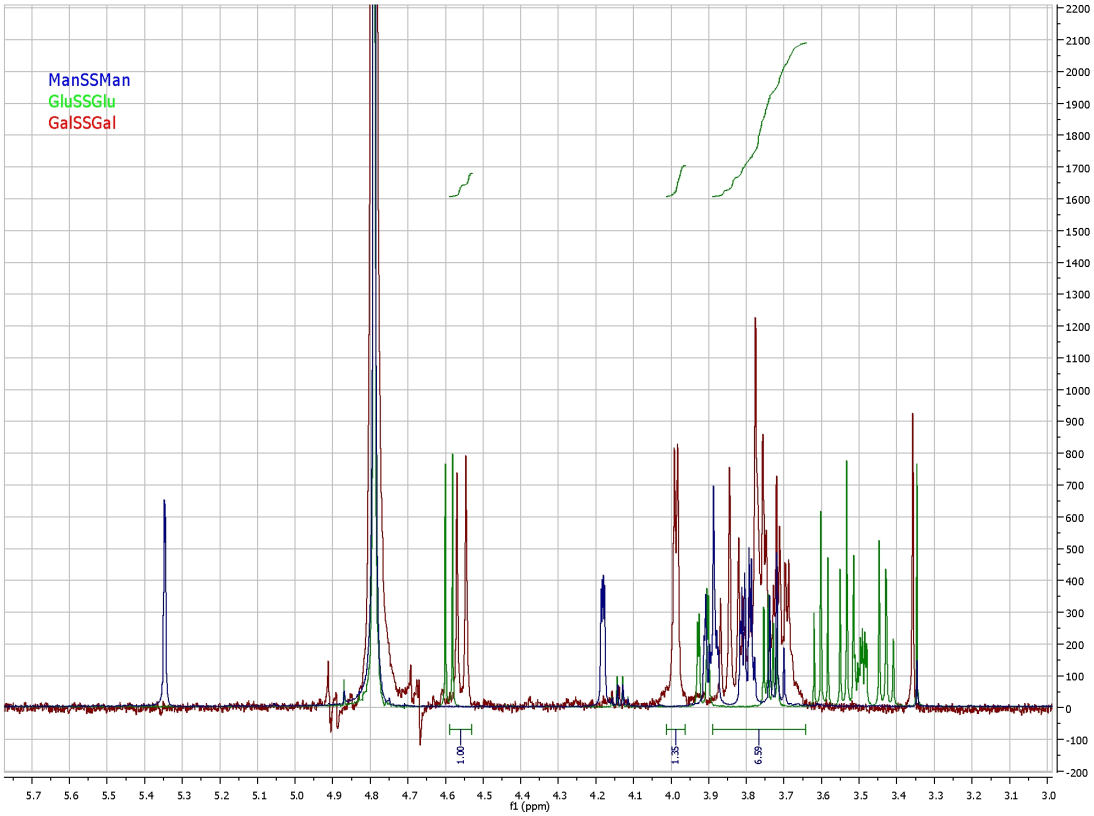

Figure 110 ^{1}H NMR spectrum was used to quantify saccharide concentrations.

The transport was monitored at time intervals by taking NMR samples of equal volume from the feed and strip phases. As represented in (Figure 110) showing a superimposition of the ^{1}HNMR spectra competitive transport of the three member library could be monitored by integration of the H-1 or other pyranose protons.

A small 3-member disaccharide library was thus chosen to test this system based on the selective recognition of the Concanavalin A lectin.

1. Buzas EI, Gyorgy B, Pasztoi M, Jelinek I, Falus A, Gabius HJ: **Carbohydrate recognition systems in autoimmunity**. *Autoimmunity* 2006, **39**:691-704.
2. Cohen M, Joester D, Geiger B, Addadi L: **Spatial and temporal sequence of events in cell adhesion: From molecular recognition to focal adhesion assembly**. *Chembiochem* 2004, **5**:1393-1399.
3. Vogler O, Barcelo JM, Ribas C, Escriba PV: **Membrane interactions of G proteins and other related proteins**. *Biochimica Et Biophysica Acta-Biomembranes* 2008, **1778**:1640-1652.
4. Mackinnon R: **Determination of the Subunit Stoichiometry of a Voltage-Activated Potassium Channel**. *Nature* 1991, **350**:232-235.
5. Long SB, Campbell EB, MacKinnon R: **Crystal structure of a mammalian voltage-dependent Shaker family K+ channel**. *Science* 2005, **309**:897-903.
6. Veselovsky AV, Ivanov YD, Ivanov AS, Archakov AI, Lewi P, Janssen P: **Protein-protein interactions: mechanisms and modification by drugs**. *Journal of Molecular Recognition* 2002, **15**:405-422.
7. Keskin O, Tuncbag N, Gursoy A: **Characterization and prediction of protein interfaces to infer protein-protein interaction networks**. *Current Pharmaceutical Biotechnology* 2008, **9**:67-76.
8. Lehn JM: **Perspectives in Supramolecular Chemistry - from Molecular Recognition Towards Molecular Information-Processing and Self-Organization**. *Angewandte Chemie-International Edition in English* 1990, **29**:1304-1319.
9. Ariga K, Ji QM, Hill JP, Kawazoe N, Chen GP: **Supramolecular approaches to biological therapy**. *Expert Opinion on Biological Therapy* 2009, **9**:307-320.
10. Roco MC: **Nanotechnology: convergence with modern biology and medicine**. *Current Opinion in Biotechnology* 2003, **14**:337-346.
11. Derakhshan M, Ansarian HR, Takafuji M, Sakurai T, Ihara H: **The impact of self-assembly in medicine and pharmacology**. *Current Pharmaceutical Analysis* 2006, **2**:79-83.
12. Ravishankar R, Suguna K, Surolia A, Vijayan M: **Structures of the complexes of peanut lectin with methyl-beta-galactose and N-acetyllactosamine and a comparative study of carbohydrate binding in Gal/GalNAc-specific legume lectins**. *Acta Crystallographica* 1999
55:1375-1382.
13. Gabius HJ: **Biological information transfer beyond the genetic code: The sugar code**. *Naturwissenschaften* 2000, **87**:108-121.
14. Dwek RA: **Glycobiology: Toward understanding the function of sugars**. *Chemical Reviews* 1996, **96**:683-720.
15. Varki A: **Biological Roles of Oligosaccharides - All of the Theories Are Correct**. *Glycobiology* 1993, **3**:97-130.
16. Bourne Y, Vantilbeurgh H, Cambillau C: **Protein Carbohydrate Interactions**. *Current Opinion in Structural Biology* 1993, **3**:681-686.
17. Lee YC, Lee RT: **Carbohydrate-Protein Interactions - Basis of Glycobiology**. *Accounts of Chemical Research* 1995, **28**:321-327.
18. Ritchie GE, Moffatt BE, Sim RB, Morgan BP, Dwek RA, Rudd PM: **Glycosylation and the complement system**. *Chemical Reviews* 2002, **102**:305-319.
19. Rojo J, Morales JC, Penades S: **Carbohydrate-carbohydrate interactions in biological and model systems**. In *Host-Guest Chemistry*. Edited by: Springer-Verlag Berlin; 2002:45-92. Topics in Current Chemistry, vol 218.]

20. Hakomori S: **Carbohydrate-Carbohydrate Interaction as an Initial Step in Cell Recognition**. *Pure and Applied Chemistry* 1991, **63**:473-482.
21. Sharon N, Lis H: **Lectins as Cell Recognition Molecules**. *Science* 1989, **246**:227-234.
22. Ashwell G, Harford J: **Carbohydrate-Specific Receptors of the Liver**. *Annual Review of Biochemistry* 1982, **51**:531-554.
23. Ashwell G, Morell AG: **Role of Surface Carbohydrates in Hepatic Recognition and Transport of Circulating Glycoproteins**. *Advances in Enzymology and Related Areas of Molecular Biology* 1974, **41**:99-128.
24. Sharon N: **Bacterial Lectins, Cell-Cell Recognition and Infectious-Disease**. *Febs Letters* 1987, **217**:145-157.
25. Melrose J, Tsurushita N, Liu G, Berg EL: **IFN-gamma inhibits activation-induced expression of E- and P-selectin on endothelial cells**. *Journal of Immunology* 1998, **161**:2457-2464.
26. Watanabe N, Kawashima H, Li YF, Miyasaka M: **Identification and characterization of ligands for L-selectin in the kidney. III. Characterization of L-selectin reactive heparan sulfate proteoglycans**. *Journal of Biochemistry* 1999, **125**:826-831.
27. Ambrosi M, Cameron NR, Davis BG: **Lectins: tools for the molecular understanding of the glycocode**. *Organic & Biomolecular Chemistry* 2005, **3**:1593-1608.
28. Sumner JB: **The globulins of the jack bean, canavalia ensiformis**. *Journal of Biological Chemistry* 1919, **37**:137-U131.
29. Sumner JB, Howell SF: **The role of divalent metals in the reversible inactivation of jack bean hemagglutinin**. *Journal of Biological Chemistry* 1936, **115**:582-588.
30. Cunningham BA, Wang JL, Waxdal MJ, Edelman GM: **Covalent and 3-Dimensional Structure of Concanavalin-a .2. Amino-Acid Sequence of Cyanogen-Bromide Fragment F3**. *Journal of Biological Chemistry* 1975, **250**:1503-1512.
31. Wang JL, Cunningham BA, Waxdal MJ, Edelman GM: **Covalent and 3-Dimensional Structure of Concanavalin-a .1. Amino-Acid Sequence of Cyanogen-Bromide Fragments F1 and F2**. *Journal of Biological Chemistry* 1975, **250**:1490-1502.
32. Edelman GM, Reeke GN, Wang JL, Waxdal MJ, Becker JW, Cunningh.Ba: **Covalent and 3-Dimensional Structure of Concanavalin-A**. *Proceedings of the National Academy of Sciences of the United States of America* 1972, **69**:2580-&.
33. Hardman KD, Ainswort.Cf: **Structure of Concanavalin-a at 2.4-a Resolution**. *Biochemistry* 1972, **11**:4910-4919.
34. Weis WI, Drickamer K: **Structural basis of lectin-carbohydrate recognition**. *Annual Review of Biochemistry* 1996, **65**:441-473.
35. Lis H, Sharon N: **Lectins: Carbohydrate-specific proteins that mediate cellular recognition**. *Chemical Reviews* 1998, **98**:637-674.
36. Naismith JH, Emmerich C, Habash J, Harrop SJ, Helliwell JR, Hunter WN, Raftery J, Kalb AJ, Yariv J: **Refined Structure of Concanavalin-a Complexed with Methyl Alpha-D-Mannopyranoside at 2.0 Angstrom Resolution and Comparison with the Saccharide-Free Structure**. *Acta Crystallographica Section D-Biological Crystallography* 1994, **50**:847-858.
37. Davis BG: **Recent developments in glycoconjugates**. *Journal of the Chemical Society-Perkin Transactions 1* 1999:3215-3237.
38. Rini JM: **Lectin Structure**. *Annual Review of Biophysics and Biomolecular Structure* 1995, **24**:551-577.
39. Vandenbussche S, Diaz D, Fernandez-Alonso MC, Pan WD, Vincent SP, Cuevas G, Canada FJ, Jimenez-Barbero J, Bartik K: **Aromatic-carbohydrate interactions: An NMR and computational study of model systems**. *Chemistry-a European Journal* 2008, **14**:7570-7578.

40. Naismith JH, Field RA: **Structural basis of trimannoside recognition by concanavalin A**. *Journal of Biological Chemistry* 1996, **271**:972-976.
41. Toone EJ: **Structure and Energetics of Protein Carbohydrate Complexes**. *Current Opinion in Structural Biology* 1994, **4**:719-728.
42. Clarke C, Woods RJ, Gluska J, Cooper A, Nutley MA, Boons GJ: **Involvement of water in carbohydrate-protein binding**. *Journal of the American Chemical Society* 2001, **123**:12238-12247.
43. Schwarz FP, Puri KD, Bhat RG, Surolia A: **Thermodynamics of Monosaccharide Binding to Concanavalin-A, Pea (Pisum-Sativum) Lectin, and Lentil (Lens-Culinaris) Lectin**. *Journal of Biological Chemistry* 1993, **268**:7668-7677.
44. Mandal DK, Bhattacharyya L, Koenig SH, Brown RD, Oscarson S, Brewer CF: **Studies of the Binding-Specificity of Concanavalin-A - Nature of the Extended Binding-Site for Asparagine-Linked Carbohydrates**. *Biochemistry* 1994, **33**:1157-1162.
45. Davis BG: **Synthesis of glycoproteins**. *Chemical Reviews* 2002, **102**:579-601.
46. Mammen M, Choi SK, Whitesides GM: **Polyvalent interactions in biological systems: Implications for design and use of multivalent ligands and inhibitors**. *Angewandte Chemie-International Edition* 1998, **37**:2755-2794.
47. Westerlund B, Korhonen TK: **Bacterial Proteins Binding to the Mammalian Extracellular-Matrix**. *Molecular Microbiology* 1993, **9**:687-694.
48. Mammen M, Dahmann G, Whitesides GM: **Effective Inhibitors of Hemagglutination by Influenza-Virus Synthesized from Polymers Having Active Ester Groups - Insight into Mechanism of Inhibition**. *Journal of Medicinal Chemistry* 1995, **38**:4179-4190.
49. Ercolani G: **Assessment of cooperativity in self-assembly**. *Journal of the American Chemical Society* 2003, **125**:16097-16103.
50. Wolfenden ML, Cloninger MJ: **Carbohydrate-functionalized dendrimers to investigate the predictable tunability of multivalent interactions**. *Bioconjugate Chemistry* 2006, **17**:958-966.
51. Corbell JB, Lundquist JJ, Toone EJ: **A comparison of biological and calorimetric analyses of multivalent glycodendrimer ligands for concanavalin A**. *Tetrahedron-Asymmetry* 2000, **11**:95-111.
52. Kitov PI, Bundle DR: **On the Nature of the Multivalency Effect: A Thermodynamic Model**. *Journal of the American Chemical Society* 2003, **125**:16271-16284.
53. Jencks WP: **On the Attribution and Additivity of Binding-Energies**. *Proceedings of the National Academy of Sciences of the United States of America-Biological Sciences* 1981, **78**:4046-4050.
54. Martos V, Castreno P, Valero J, de Mendoza J: **Binding to protein surfaces by supramolecular multivalent scaffolds**. *Current Opinion in Chemical Biology* 2008, **12**:698-706.
55. Lundquist JJ, Toone EJ: **The Cluster Glycoside Effect**. *Chemical Reviews* 2002, **102**:555-578.
56. Lee RT, Lee YC: **Affinity enhancement by multivalent lectin-carbohydrate interaction**. *Glycoconjugate Journal* 2000, **17**:543-551.
57. Van Damme EJM, Peumans WJ, Barre A, Rouge P: **Plant lectins: A composite of several distinct families of structurally and evolutionary related proteins with diverse biological roles**. *Critical Reviews in Plant Sciences* 1998, **17**:575-692.
58. Dimick SM, Powell SC, McMahon SA, Moothoo DN, Naismith JH, Toone EJ: **On the Meaning of Affinity: Cluster Glycoside Effects and Concanavalin A**. *Journal of the American Chemical Society* 1999, **121**:10286-10296.

59. Chaki NK, Vijayamohanan K: **Self-assembled monolayers as a tunable platform for biosensor applications**. *Biosensors & Bioelectronics* 2002, **17**:1-12.
60. Ravoo BJ, Jacquier JC, Wenz G: **Molecular recognition of polymers by cyclodextrin vesicles**. *Angewandte Chemie-International Edition* 2003, **42**:2066-2070.
61. Huskens J, Deij MA, Reinhoudt DN: **Attachment of molecules at a molecular printboard by multiple host-guest interactions**. *Angewandte Chemie-International Edition* 2002, **41**:4467-+.
62. Nijhuis CA, Huskens J, Reinhoudt DN: **Binding control and stoichiometry of ferrocenyl dendrimers at a molecular printboard**. *Journal of the American Chemical Society* 2004, **126**:12266-12267.
63. Rao JH, Yan L, Xu B, Whitesides GM: **Using surface plasmon resonance to study the binding of vancomycin and its dimer to self-assembled monolayers presenting D-Ala-D-Ala**. *Journal of the American Chemical Society* 1999, **121**:2629-2630.
64. Revell DJ, Knight JR, Blyth DJ, Haines AH, Russell DA: **Self-assembled carbohydrate monolayers: Formation and surface selective molecular recognition**. *Langmuir* 1998, **14**:4517-4524.
65. Miura Y, Sasao Y, Dohi H, Nishida Y, Kobayashi K: **Self-assembled monolayers of globotriaosylceramide (Gb3) mimics: surface-specific affinity with shiga toxins**. *Analytical Biochemistry* 2002, **310**:27-35.
66. Zhang Y, Luo SZ, Tang YJ, Yu L, Hou KY, Cheng JP, Zeng XQ, Wang PG: **Carbohydrate-protein interactions by "clicked" carbohydrate self-assembled monolayers**. *Analytical Chemistry* 2006, **78**:2001-2008.
67. Sato Y, Yoshioka K, Tanaka M, Murakami T, Ishida MN, Niwa O: **Recognition of lectin with a high signal to noise ratio: carbohydrate-tri(ethylene glycol)-alkanethiol co-adsorbed monolayer**. *Chemical Communications* 2008:4909-4911.
68. Guo CX, Boullanger P, Jiang L, Liu T: **Highly sensitive gold nanoparticles biosensor chips modified with a self-assembled bilayer for detection of Con A**. *Biosensors & Bioelectronics* 2007, **22**:1830-1834.
69. Bakowsky U, Rettig W, Bendas G, Vogel J, Bakowsky H, Harnagea C, Rothe U: **Characterization of the interactions between various hexadecylmannoside-phospholipid model membranes with the lectin Concanavalin A**. *Physical Chemistry Chemical Physics* 2000, **2**:4609-4614.
70. Liedberg B, Nylander C, Lundstrom I: **Surface-Plasmon Resonance for Gas-Detection and Biosensing**. *Sensors and Actuators* 1983, **4**:299-304.
71. Love JC, Estroff LA, Kriebel JK, Nuzzo RG, Whitesides GM: **Self-assembled monolayers of thiolates on metals as a form of nanotechnology**. *Chemical Reviews* 2005, **105**:1103-1169.
72. Xu J, Li HL: **The Chemistry of Self-Assembled Long-Chain Alkanethiol Monolayers on Gold**. *Journal of Colloid and Interface Science* 1995, **176**:138-149.
73. Vericat C, Vela ME, Benitez GA, Gago JAM, Torrelles X, Salvarezza RC: **Surface characterization of sulfur and alkanethiol self-assembled monolayers on Au(111)**. *Journal of Physics-Condensed Matter* 2006, **18**:R867-R900.
74. Silberzan P, Leger L, Ausserre D, Benattar JJ: **Silanation of Silica Surfaces - a New Method of Constructing Pure or Mixed Monolayers**. *Langmuir* 1991, **7**:1647-1651.
75. Rozlosnik N, Gerstenberg MC, Larsen NB: **Effect of solvents and concentration on the formation of a self-assembled monolayer of octadecylsiloxane on silicon (001)**. *Langmuir* 2003, **19**:1182-1188.
76. Aldrich: **Molecular Self assembly**. *Material Matters* 2006, **1**.
77. Tamm LK, McConnell HM: **Supported Phospholipid-Bilayers**. *Biophysical Journal* 1985, **47**:105-113.

78. Kalb E, Frey S, Tamm LK: **Formation of Supported Planar Bilayers by Fusion of Vesicles to Supported Phospholipid Monolayers**. *Biochimica Et Biophysica Acta* 1992, **1103**:307-316.
79. Plant AL: **Self-Assembled Phospholipid Alkanethiol Biomimetic Bilayers on Gold**. *Langmuir* 1993, **9**:2764-2767.
80. Plant AL, Brigham-Burke M, Petrella EC, Oshannessy DJ: **Phospholipid/alkanethiol bilayers for cell-surface receptor studies by surface plasmon resonance**. *Analytical Biochemistry* 1995, **226**:342-348.
81. Hubbard JB, Silin V, Plant AL: **Self assembly driven by hydrophobic interactions at alkanethiol monolayers: Mechanism of formation of hybrid bilayer membranes**. *Biophysical Journal* 1999, **76**:A431-A431.
82. Zhdanov VP, Kasemo B: **Monte Carlo simulation of denaturation of adsorbed proteins**. *Proteins-Structure Function and Genetics* 1998, **30**:168-176.
83. Su YL, Li C: **Stable multilayer thin films composed of gold nanoparticles and lysozyme**. *Applied Surface Science* 2008, **254**:2003-2008.
84. Wang Y, Angelatos AS, Caruso F: **Template synthesis of nanostructured materials via layer-by-layer assembly**. *Chemistry of Materials* 2008, **20**:848-858.
85. Li LY, Chen SF, Jiang SY: **Protein adsorption on alkanethiolate self-assembled monolayers: Nanoscale surface structural and chemical effects**. *Langmuir* 2003, **19**:2974-2982.
86. Gray JJ: **The interaction of proteins with solid surfaces**. *Current Opinion in Structural Biology* 2004, **14**:110-115.
87. Camarero JA: **Recent developments in the site-specific immobilization of proteins onto solid supports**. *Biopolymers* 2008, **90**:450-458.
88. Scott EA, Nichols MD, Cordova LH, George BJ, Jun YS, Elbert DL: **Protein adsorption and cell adhesion on nanoscale bioactive coatings formed from poly(ethylene glycol) and albumin microgels**. *Biomaterials* 2008, **29**:4481-4493.
89. Ju RF, Syu MJ, Teng HS, Chou SK, Chang YS: **Preparation and identification of beta-cyclodextrin polymer thin film for quartz crystal microbalance sensing of benzene, toluene, and p-xylene**. *Sensors and Actuators B-Chemical* 2008, **132**:319-326.
90. Pei YX, Yu H, Pei ZC, Theurer M, Ammer C, Andre S, Gabius HJ, Yan MD, Ramstrom O: **Photoderivatized polymer thin films at quartz crystal microbalance surfaces: Sensors for carbohydrate-protein interactions**. *Analytical Chemistry* 2007, **79**:6897-6902.
91. Carrigan SD, Scott G, Tabrizian M: **Real-time QCM-D immunoassay through oriented antibody immobilization using cross-linked hydrogel biointerfaces**. *Langmuir* 2005, **21**:5966-5973.
92. Marx KA: **Quartz crystal microbalance: A useful tool for studying thin polymer films and complex biomolecular systems at the solution-surface interface**. *Biomacromolecules* 2003, **4**:1099-1120.
93. Uzawa H, Ito H, Neri P, Mori H, Nishida Y: **Glycochips from polyanionic glycopolymers as tools for detecting Shiga toxins**. *Chembiochem* 2007, **8**:2117-2124.
94. Masson JF, Battaglia TM, Davidson MJ, Kim YC, Prakash AMC, Beaudoin S, Booksh KS: **Biocompatible polymers for antibody support on gold surfaces**. *Talanta* 2005, **67**:918-925.
95. Shankaran DR, Miura N: **Trends in interfacial design for surface plasmon resonance based immunoassays**. *Journal of Physics D-Applied Physics* 2007, **40**:7187-7200.
96. www.fda.gov/consumer/updates/nanotech072507.html. Edited by.

97. Sun YG, Xia YN: **Gold and silver nanoparticles: A class of chromophores with colors tunable in the range from 400 to 750 nm**. *Analyst* 2003, **128**:686-691.
98. Stewart ME, Anderton CR, Thompson LB, Maria J, Gray SK, Rogers JA, Nuzzo RG: **Nanostructured plasmonic sensors**. *Chemical Reviews* 2008, **108**:494-521.
99. Tsai CS, Yu TB, Chen CT: **Gold nanoparticle-based competitive colorimetric assay for detection of protein-protein interactions**. *Chemical Communications* 2005:4273-4275.
100. Jena BK, Raj CR: **Optical sensing of biomedically important polyionic drugs using nano-sized gold particles**. *Biosensors & Bioelectronics* 2008, **23**:1285-1290.
101. Zhao WA, Chiuman W, Lam JCF, Brook MA, Li YF: **Simple and rapid colorimetric enzyme sensing assays using non-crosslinking gold nanoparticle aggregation**. *Chemical Communications* 2007:3729-3731.
102. Gao FX, Yuan R, Chai YQ, Chen SH, Cao SR, Tang MY: **Amperometric hydrogen peroxide biosensor based on the immobilization of HRP on nano-Au/Thi/poly (p-aminobenzene sulfonic acid)-modified glassy carbon electrode**. *Journal of Biochemical and Biophysical Methods* 2007, **70**:407-413.
103. Cui RJ, Huang HP, Yin ZZ, Gao D, Zhu JJ: **Horseradish peroxidase-functionalized gold nanoparticle label for amplified immunoanalysis based on gold nanoparticles/carbon nanotubes hybrids modified biosensor**. *Biosensors & Bioelectronics* 2008, **23**:1666-1673.
104. Pingarron JM, Yanez-Sedeno P, Gonzalez-Cortes A: **Gold nanoparticle-based electrochemical biosensors**. *Electrochimica Acta* 2008, **53**:5848-5866.
105. Cui DX: **Advances and prospects on biomolecules functionalized carbon nanotubes**. *Journal of Nanoscience and Nanotechnology* 2007, **7**:1298-1314.
106. Joshi PP, Merchant SA, Wang YD, Schmidtke DW: **Amperometric biosensors based on redox polymer-carbon nanotube-enzyme composites**. *Analytical Chemistry* 2005, **77**:3183-3188.
107. Balasubramanian K, Burghard M: **Biosensors based on carbon nanotubes**. *Analytical and Bioanalytical Chemistry* 2006, **385**:452-468.
108. Chen RJ, Bangsaruntip S, Drouvalakis KA, Kam NWS, Shim M, Li YM, Kim W, Utz PJ, Dai HJ: **Noncovalent functionalization of carbon nanotubes for highly specific electronic biosensors**. *Proceedings of the National Academy of Sciences of the United States of America* 2003, **100**:4984-4989.
109. Turkevich: *J. Discuss. Faraday Soc.* 1951, **11**:55.
110. Turkevich: *J. Gold Bull.* 1985, **18**:86.
111. Frens G: *Nat. Phys. Sci.* 1973, **20**:241.
112. Brust M, Walker M, Bethell D, Schiffrin DJ, Whyman R: **Synthesis of Thiol-Derivatized Gold Nanoparticles in a 2-Phase Liquid-Liquid System**. *Journal of the Chemical Society-Chemical Communications* 1994:801-802.
113. Varndell JMPaIM: *Immunolabelling for Electron Microscopy*. Amsterdam: Elsevier Science Publishers; 1984.
114. Zhou JF, Ralston J, Sedev R, Beattie DA: **Functionalized gold nanoparticles: Synthesis, structure and colloid stability**. *Journal of Colloid and Interface Science* 2009, **331**:251-262.
115. Kimling J, Maier M, Okenve B, Kotaidis V, Ballot H, Plech A: **Turkevich method for gold nanoparticle synthesis revisited**. *Journal of Physical Chemistry B* 2006, **110**:15700-15707.
116. Pong B-K, Elim HI, Chong J-X, Ji W, Trout BL, Lee J-Y: **New Insights on the Nanoparticle Growth Mechanism in the Citrate Reduction of Gold(III) Salt:**

Formation of the Au Nanowire Intermediate and Its Nonlinear Optical Properties. *The Journal of Physical Chemistry C* 2007, **111**:6281-6287.

117. LaMer VK, Dinegar RH: **Theory, Production and Mechanism of Formation of Monodispersed Hydrosols**. *Journal of the American Chemical Society* 1950, **72**:4847-4854.
118. Brust M, Fink J, Bethell D, Schiffrin DJ, Kiely C: **Synthesis and Reactions of Functionalized Gold Nanoparticles**. *Journal of the Chemical Society-Chemical Communications* 1995:1655-1656.
119. Yee CK, Jordan R, Ulman A, White H, King A, Rafailovich M, Sokolov J: **Novel one-phase synthesis of thiol-fuctionalized gold, palladium, and iridium nanoparticles using superhydride**. *Langmuir* 1999, **15**:3486-3491.
120. Rowe MP, Plass KE, Kim K, Kurdak C, Zellers ET, Matzger AJ: **Single-phase synthesis of functionalized gold nanoparticles**. *Chemistry of Materials* 2004, **16**:3513-3517.
121. de la Fuente JM, Barrientos AG, Rojas TC, Rojo J, Canada J, Fernandez A, Penades S: **Gold glyconanoparticles as water-soluble polyvalent models to study carbohydrate interactions**. *Angewandte Chemie-International Edition* 2001, **40**:2258-+.
122. Ingram RS, Hostetler MJ, Murray RW: **Poly-hetero-omega-functionalized alkanethiolate-stabilized gold cluster compounds**. *Journal of the American Chemical Society* 1997, **119**:9175-9178.
123. Hostetler MJ, Templeton AC, Murray RW: **Dynamics of place-exchange reactions on monolayer-protected gold cluster molecules**. *Langmuir* 1999, **15**:3782-3789.
124. Viudez AJ, Madueno R, Pineda T, Blazquez M: **Stabilization of gold nanoparticles by 6-mercaptopurine monolayers. Effects of the solvent properties**. *Journal of Physical Chemistry B* 2006, **110**:17840-17847.
125. Weisbecker CS, Merritt MV, Whitesides GM: **Molecular self-assembly of aliphatic thiols on gold colloids**. *Langmuir* 1996, **12**:3763-3772.
126. Lin SY, Tsai YT, Chen CC, Lin CM, Chen CH: **Two-step functionalization of neutral and positively charged thiols onto citrate-stabilized Au nanoparticles**. *Journal of Physical Chemistry B* 2004, **108**:2134-2139.
127. Kamat PV: **Photophysical, photochemical and photocatalytic aspects of metal nanoparticles**. *Journal of Physical Chemistry B* 2002, **106**:7729-7744.
128. Schofield CL, Haines AH, Field RA, Russell DA: **Silver and gold glyconanoparticles for colorimetric bioassays**. *Langmuir* 2006, **22**:6707-6711.
129. Hone DC, Haines AH, Russell DA: **Rapid, quantitative colorimetric detection of a lectin using mannose-stabilized gold nanoparticles**. *Langmuir* 2003, **19**:7141-7144.
130. Jana NR, Gearheart L, Murphy CJ: **Evidence for seed-mediated nucleation in the chemical reduction of gold salts to gold nanoparticles**. *Chemistry of Materials* 2001, **13**:2313-2322.
131. Sau TK, Pal A, Jana NR, Wang ZL, Pal T: **Size controlled synthesis of gold nanoparticles using photochemically prepared seed particles**. *Journal of Nanoparticle Research* 2001, **3**:257-261.
132. Meltzer S, Resch R, Koel BE, Thompson ME, Madhukar A, Requicha AAG, Will P: **Fabrication of nanostructures by hydroxylamine seeding of gold nanoparticle templates**. *Langmuir* 2001, **17**:1713-1718.
133. Boal AK, Rotello VM: **Intra- and intermonolayer hydrogen bonding in amide-functionalized alkanethiol self-assembled monolayers on gold nanoparticles**. *Langmuir* 2000, **16**:9527-9532.

134. Boal AK, Rotello VM: **Fabrication and self-optimization of multivalent receptors on nanoparticle scaffolds**. *Journal of the American Chemical Society* 2000, **122**:734-735.
135. Paulini R, Frankamp BL, Rotello VM: **Effects of branched ligands on the structure and stability of monolayers on gold nanoparticles**. *Langmuir* 2002, **18**:2368-2373.
136. Kasper Nørgaard MJW, Kristian Kjaer, Mathias Brust and Thomas Bjørnholm: **Adaptive chemistry of bifunctional gold nanoparticles at the air/water interface. A synchrotron X-ray study of giant amphiphiles**. *Faraday Discussions* 2004, **125**:221-233.
137. Hao E, Bailey RC, Schatz GC, Hupp JT, Li SY: **Synthesis and optical properties of "branched" gold nanocrystals**. *Nano Letters* 2004, **4**:327-330.
138. Mie G: **Articles on the optical characteristics of turbid tubes, especially colloidal metal solutions**. *Annalen Der Physik* 1908, **25**:377-445.
139. Alvarez MM, Khoury JT, Schaaff TG, Shafigullin MN, Vezmar I, Whetten RL: **Optical absorption spectra of nanocrystal gold molecules**. *Journal of Physical Chemistry B* 1997, **101**:3706-3712.
140. Kelly KL, Coronado E, Zhao LL, Schatz GC: **The optical properties of metal nanoparticles: The influence of size, shape, and dielectric environment**. *Journal of Physical Chemistry B* 2003, **107**:668-677.
141. Jain PK, Lee KS, El-Sayed IH, El-Sayed MA: **Calculated absorption and scattering properties of gold nanoparticles of different size, shape, and composition: Applications in biological imaging and biomedicine**. *Journal of Physical Chemistry B* 2006, **110**:7238-7248.
142. Lee KS, El-Sayed MA: **Gold and silver nanoparticles in sensing and imaging: Sensitivity of plasmon response to size, shape, and metal composition**. *Journal of Physical Chemistry B* 2006, **110**:19220-19225.
143. Shimizu T, Teranishi T, Hasegawa S, Miyake M: **Size evolution of alkanethiol-protected gold nanoparticles by heat treatment in the solid state**. *Journal of Physical Chemistry B* 2003, **107**:2719-2724.
144. Elghanian R, Storhoff JJ, Mucic RC, Letsinger RL, Mirkin CA: **Selective colorimetric detection of polynucleotides based on the distance-dependent optical properties of gold nanoparticles**. *Science* 1997, **277**:1078-1081.
145. Huang SH, Minami K, Sakaue H, Shingubara S, Takahagi T: **Optical spectroscopic studies of the dispersibility of gold nanoparticle solutions**. *Journal of Applied Physics* 2002, **92**:7486-7490.
146. Gerardy JM, Ausloos M: **Absorption-Spectrum of Clusters of Spheres from the General-Solution of Maxwells Equations .4. Proximity, Bulk, Surface, and Shadow Effects (in Binary Clusters)**. *Physical Review B* 1983, **27**:6446-6463.
147. Shipway AN, Lahav M, Gabai R, Willner I: **Investigations into the electrostatically induced aggregation of Au nanoparticles**. *Langmuir* 2000, **16**:8789-8795.
148. Ghosh SK, Pal T: **Interparticle coupling effect on the surface plasmon resonance of gold nanoparticles: From theory to applications**. *Chemical Reviews* 2007, **107**:4797-4862.
149. Otsuka H, Akiyama Y, Nagasaki Y, Kataoka K: **Quantitative and reversible lectin-induced association of gold nanoparticles modified with alpha-lactosyl-omega-mercapto-poly(ethylene glycol)**. *Journal of the American Chemical Society* 2001, **123**:8226-8230.
150. Schofield CL, Field RA, Russell DA: **Glyconanoparticles for the colorimetric detection of cholera toxin**. *Analytical Chemistry* 2007, **79**:1356-1361.

151. Zheng M, Davidson F, Huang XY: **Ethylene glycol monolayer protected nanoparticles for eliminating nonspecific binding with biological molecules**. *Journal of the American Chemical Society* 2003, **125**:7790-7791.
152. Giersig M, Mulvaney P: **Preparation of Ordered Colloid Monolayers by Electrophoretic Deposition**. *Langmuir* 1993, **9**:3408-3413.
153. Wang ZL: **Transmission Electron Microscopy of Shape-Controlled Nanocrystals and Their Assemblies**. *The Journal of Physical Chemistry B* 2000, **104**:1153-1175.
154. Labande A, Ruiz J, Astruc D: **Supramolecular gold nanoparticles for the redox recognition of oxoanions: Syntheses, titrations, stereoelectronic effects, and selectivity**. *Journal of the American Chemical Society* 2002, **124**:1782-1789.
155. Templeton AC, Wuelfing MP, Murray RW: **Monolayer protected cluster molecules**. *Accounts of Chemical Research* 2000, **33**:27-36.
156. Badia A, Demers L, Dickinson L, Morin FG, Lennox RB, Reven L: **Gold-sulfur interactions in alkylthiol self-assembled monolayers formed on gold nanoparticles studied by solid-state NMR**. *Journal of the American Chemical Society* 1997, **119**:11104-11105.
157. Badia A, Cuccia L, Demers L, Morin F, Lennox RB: **Structure and dynamics in alkanethiolate monolayers self-assembled on gold nanoparticles: A DSC, FT-IR, and deuterium NMR study**. *Journal of the American Chemical Society* 1997, **119**:2682-2692.
158. Daniel MC, Astruc D: **Gold nanoparticles: Assembly, supramolecular chemistry, quantum-size-related properties, and applications toward biology, catalysis, and nanotechnology**. *Chemical Reviews* 2004, **104**:293-346.
159. Aslan K, Luhrs CC, Perez-Luna VH: **Controlled and reversible aggregation of biotinylated gold nanoparticles with streptavidin**. *Journal of Physical Chemistry B* 2004, **108**:15631-15639.
160. Murphy CJ, Gole AM, Stone JW, Sisco PN, Alkilany AM, Goldsmith EC, Baxter SC: **Gold Nanoparticles in Biology: Beyond Toxicity to Cellular Imaging**. *Accounts of Chemical Research* 2008, **41**:1721-1730.
161. Lee YC, Lee RT: **Carbohydrate-Protein Interactions: Basis of Glycobiology**. *Accounts of Chemical Research* 1995, **28**:321-327.
162. Barrientos AG, de la Fuente JM, Rojas TC, Fernandez A, Penades S: **Gold glyconanoparticles: Synthetic polyvalent ligands mimicking glycocalyx-like surfaces as tools for glycobiological studies**. *Chemistry-a European Journal* 2003, **9**:1909-1921.
163. Schofield CL, Mukhopadhyay B, Hardy SM, McDonnell MB, Field RA, Russell DA: **Colorimetric detection of Ricinus communis Agglutinin 120 using optimally presented carbohydrate-stabilised gold nanoparticles**. *Analyst* 2008, **133**:626-634.
164. Sato Y, Murakami T, Yoshioka K, Niwa O: **12-Mercaptododecyl beta-maltoside-modified gold nanoparticles: specific ligands for concanavalin A having long flexible hydrocarbon chains**. *Analytical and Bioanalytical Chemistry* 2008, **391**:2527-2532.
165. Lin CC, Yeh YC, Yang CY, Chen GF, Chen YC, Wu YC, Chen CC: **Quantitative analysis of multivalent interactions of carbohydrate-encapsulated gold nanoparticles with concanavalin A**. *Chemical Communications* 2003:2920-2921.
166. Hernaiz MJ, de la Fuente JM, Barrientos AG, Penades S: **A model system mimicking glycosphingolipid clusters to quantify carbohydrate self-interactions by surface plasmon resonance**. *Angewandte Chemie-International Edition* 2002, **41**:1554-1557.

167. Reynolds AJ, Haines AH, Russell DA: **Gold glyconanoparticles for mimics and measurement of metal ion-mediated carbohydrate-carbohydrate interactions**. *Langmuir* 2006, **22**:1156-1163.
168. de la Fuente JM, Eaton P, Barrientos AG, Menendez M, Penades S: **Thermodynamic Evidence for Ca2+-Mediated Self-Aggregation of Lewis X Gold Glyconanoparticles. A Model for Cell Adhesion via Carbohydrate-Carbohydrate Interaction**. *Journal of the American Chemical Society* 2005, **127**:6192-6197.
169. Fuss M, Luna M, Alcantara D, de la Fuente JM, Enriquez-Navas PM, Angulo J, Penades S, Briones F: **Carbohydrate-carbohydrate interaction prominence in 3D supramolecular self-assembly**. *Journal of Physical Chemistry B* 2008, **112**:11595-11600.
170. Curie J, Curie P: **An oscillating quartz crystal mass detector**. *Comp Rend* 1880, **91** 294–297.
171. Sauerbrey G: **Verwendung Von Schwingquarzen Zur Wagung Dunner Schichten Und Zur Mikrowagung**. *Zeitschrift Fur Physik* 1959, **155**:206-222.
172. Nomura T, Okuhara M: **Frequency-Shifts of Piezoelectric Quartz Crystals Immersed in Organic Liquids**. *Analytica Chimica Acta* 1982, **142**:281-284.
173. Kanazawa KK, Gordon JG: **Frequency of a quartz microbalance in contact with liquid**. *Analytical Chemistry* 1985, **57**:1770-1771.
174. Voinova MV, Jonson M, Kasemo B: **'Missing mass' effect in biosensor's QCM applications**. *Biosensors & Bioelectronics* 2002, **17**:835-841.
175. Beck R, Pittermann U, Weil KG: **Influence of the Surface Microstructure on the Coupling between a Quartz Oscillator and a Liquid**. *Journal of the Electrochemical Society* 1992, **139**:453-461.
176. Martin SJ, Frye GC, Ricco AJ, Senturia SD: **Effect of Surface-Roughness on the Response of Thickness-Shear Mode Resonators in Liquids**. *Analytical Chemistry* 1993, **65**:2910-2922.
177. Cooper MA, Singleton VT: **A survey of the 2001 to 2005 quartz crystal microbalance biosensor literature: applications of acoustic physics to the analysis of biomolecular interactions**. *Journal of Molecular Recognition* 2007, **20**:154-184.
178. Zhang Y, Telyatnikov V, Sathe M, Zeng XQ, Wang PG: **Studying the interaction of alpha-Gal carbohydrate antigen and proteins by quartz-crystal microbalance**. *Journal of the American Chemical Society* 2003, **125**:9292-9293.
179. Shen ZH, Huang MC, Xiao CD, Zhang Y, Zeng XQ, Wang PG: **Nonlabeled quartz crystal microbalance biosensor for bacterial detection using carbohydrate and lectin recognitions**. *Analytical Chemistry* 2007, **79**:2312-2319.
180. Fawcett NC, Evans JA, Chien LC, Flowers N: **Nucleic-Acid Hybridization Detected by Piezoelectric Resonance**. *Analytical Letters* 1988, **21**:1099-1114.
181. Zhou XC, Huang LQ, Li SFY: **Microgravimetric DNA sensor based on quartz crystal microbalance: comparison of oligonucleotide immobilization methods and the application in genetic diagnosis**. *Biosensors & Bioelectronics* 2001, **16**:85-95.
182. Mannelli F, Minunni A, Tombelli S, Wang RH, Spiriti MM, Mascini M: **Direct immobilisation of DNA probes for the development of affinity biosensors**. *Bioelectrochemistry* 2005, **66**:129-138.
183. Hook F, Ray A, Norden B, Kasemo B: **Characterization of PNA and DNA immobilization and subsequent hybridization with DNA using acoustic-shear-wave attenuation measurements**. *Langmuir* 2001, **17**:8305-8312.
184. Matsuura K, Tsuchida A, Okahata Y, Akaike T, Kobayashi K: **A quartz-crystal microbalance study of adsorption behaviors of artificial glycoconjugate polymers**

onto chemically modified gold surfaces and their interactions with lectins. *Bulletin of the Chemical Society of Japan* 1998, **71**:2973-2977.

185. Huang MC, Shen ZH, Zhang YL, Zeng XQ, Wang PG: **Alkanethiol containing glycopolymers: A tool for the detection of lectin binding**. *Bioorganic & Medicinal Chemistry Letters* 2007, **17**:5379-5383.
186. Stenberg E, Persson B, Roos H, Urbaniczky C: **Quantitative-Determination of Surface Concentration of Protein with Surface-Plasmon Resonance Using Radiolabeled Proteins**. *Journal of Colloid and Interface Science* 1991, **143**:513-526.
187. Su X, Wu Y-J, Knoll W: **Comparison of surface plasmon resonance spectroscopy and quartz crystal microbalance techniques for studying DNA assembly and hybridization**. *Biosensors and Bioelectronics* 2005, **21**:719-726.
188. Boujday S, Méthivier C, Beccard B, Pradier C-M: **Innovative surface characterization techniques applied to immunosensor elaboration and test: Comparing the efficiency of Fourier transform-surface plasmon resonance, quartz crystal microbalance with dissipation measurements, and polarization modulation-reflection absorption infrared spectroscopy**. *Analytical Biochemistry* 2009, **387**:194-201.
189. Shen Z: **Nonlabeled Quartz Crystal Microbalance Biosensor for Bacterial Detection Using Carbohydrate and Lectin Recognitions.** *Analytical Chemistry* 2007, **79**:2312-2319.
190. Hildebrand A, Schaedlich A, Rothe U, Neubert RHH: **Sensing specific adhesion of liposomal and micellar systems with attached carbohydrate recognition structures at lectin surfaces**. *Journal of Colloid and Interface Science* 2002, **249**:274-281.
191. Avila M, Zougagh M, Escarpa A, Rios A: **Molecularly imprinted polymers for selective piezoelectric sensing of small molecules**. *Trac-Trends in Analytical Chemistry* 2008, **27**:54-65.
192. Kim NH, Baek TJ, Park HG, Seong GH: **Highly sensitive biomolecule detection on a quartz crystal microbalance using gold nanoparticles as signal amplification probes**. *Analytical Sciences* 2007, **23**:177-181.
193. Nie LB, Yang Y, Li S, He NY: **Enhanced DNA detection based on the amplification of gold nanoparticles using quartz crystal microbalance**. *Nanotechnology* 2007, **18**:305501/305501-305501/305505.
194. Lyu YK, Lim KR, Lee BY, Kim KS, Lee WY: **Microgravimetric lectin biosensor based on signal amplification using carbohydrate-stabilized gold nanoparticles**. *Chemical Communications* 2008:4771-4773.
195. Immordino ML, Dosio F, Cattel L: **Stealth liposomes: review of the basic science, rationale, and clinical applications, existing and potential**. *International Journal of Nanomedicine* 2006, **1**:297-315.
196. Curatolo W, Yau AO, Small DM, Sears B: **Lectin-Induced Agglutination of Phospholipid-Glycolipid Vesicles**. *Biochemistry* 1978, **17**:5740-5744.
197. Duzgunes N, Hoekstra D: **Agglutination and Fusion of Glycolipid-Phospholipid Vesicles Mediated by Lectins and Calcium-Ions**. *Studia Biophysica* 1986, **111**:5-10.
198. Faivre V, Costa MDL, Boullanger P, Baszkin A, Rosilio V: **Specific interaction of lectins with liposomes and monolayers bearing neoglycolipids**. *Chemistry and Physics of Lipids* 2003, **125**:147-159.
199. Park J, Rader LH, Thomas GB, Danoff EJ, English DS, DeShong P: **Carbohydrate-functionalized catanionic surfactant vesicles: preparation and lectin-binding studies**. *Soft Matter* 2008, **4**:1916-1921.

200. Boullanger P, Lafont D, Bouchu MN, Jiang L, Liu T, Lu W, Guo CX, Li J: **The use of glycolipids inserted in color-changeable polydiacetylene vesicles, as targets for biological recognition**. *Comptes Rendus Chimie* 2008, **11**:43-60.
201. Bendas G, Wilhelm F, Richter W, Nuhn P: **Synthetic glycolipids as membrane-bound cryoprotectants in the freeze-drying process of liposomes**. *European Journal of Pharmaceutical Sciences* 1996, **4**:211-222.
202. Pignataro B, Steinem C, Galla HJ, Fuchs H, Janshoff A: **Specific adhesion of vesicles monitored by scanning force microscopy and quartz crystal microbalance**. *Biophysical Journal* 2000, **78**:487-498.
203. Hopfner M, Rothe U, Bendas G: **Biosensor-based evaluation of liposomal behavior in the target binding process**. *Journal of Liposome Research* 2008, **18**:71-82.
204. Glasmastar K, Larsson C, Hook F, Kasemo B: **Protein adsorption on supported phospholipid bilayers**. *Journal of Colloid and Interface Science* 2002, **246**:40-47.
205. Carion-Taravella B, Chopineau J, Ollivon M, Lesieur S: **Phase behavior of mixed aqueous dispersions of DPPC and dodecyl glycosides: Aggregation states implicated in the micelle-to-vesicle transition**. *Langmuir* 1998, **14**:3767-3777.
206. Spiess M, Hauser H, Rosenbusch JP, Semenza G: **Hydrodynamic Properties of Phospholipid-Vesicles and of Sucrase Isomaltase-Phospholipid Vesicles**. *Journal of Biological Chemistry* 1981, **256**:8977-8982.
207. Anzai J, Kobayashi Y, Nakamura N: **Alternate deposition of concanavalin A and mannose-labelled enzymes on a solid surface to prepare catalytically active enzyme thin films**. *Journal of the Chemical Society-Perkin Transactions 2* 1998:461-462.
208. Mielczarski JA, Dong J, Mielczarski E: **Real time evaluation of composition and structure of concanavalin A adsorbed on a polystyrene surface**. *Journal of Physical Chemistry B* 2008, **112**:5228-5237.
209. Pei Z, Anderson H, Aastrup T, Ramstroem O: **Study of real-time lectin-carbohydrate interactions on the surface of a quartz crystal microbalance**. *Biosensors & Bioelectronics* 2005, **21**:60-66.
210. Haiss W, Thanh NTK, Aveyard J, Fernig DG: **Determination of size and concentration of gold nanoparticles from UV-Vis spectra**. *Analytical Chemistry* 2007, **79**:4215-4221.
211. Leff DV, Ohara PC, Heath JR, Gelbart WM: **Thermodynamic Control of Gold Nanocrystal Size - Experiment and Theory**. *Journal of Physical Chemistry* 1995, **99**:7036-7041.
212. Sweeney EC, Tonevitsky AG, Temiakov DE, Agapov, II, Saward S, Palmer RA: **Preliminary crystallographic characterization of ricin agglutinin**. *Proteins-Structure Function and Genetics* 1997, **28**:586-589.
213. Sharma S, Bharadwaj S, Surolia A, Podder SK: **Evaluation of the stoichiometry and energetics of carbohydrate binding to Ricinus communis agglutinin: a calorimetric study**. *Biochemical Journal* 1998, **333**:539-542.
214. Natchiar SK, Suguna K, Surolia A, Vijayan M: **Peanut agglutinin, a lectin with an unusual quaternary structure and interesting ligand binding properties**. *Crystallography Reviews* 2007, **13**:3 - 28.
215. Masel RI: In *Principles of Adsorption and Reaction on Solid Surfaces*. Edited by: Wiley-Interscience; 1996:239.
216. Katzen HM: **Carbohydrate inhibitors of concanavalin A that inhibit binding of insulin-sepharose to fat cells and antagonize and mimic insulin's bioactivity. A possible role for membrane carbohydrate in insulin's action**. *J. Biol. Chem.* 1979, **254**:2983-2992.

217. Sato K, Kodama D, Anzai J: **Sugar-sensitive thin films composed of concanavalin A and sugar-bearing polymers**. *Analytical Sciences* 2005, **21**:1375-1378.
218. Wen-Chien Lee C-CH, Rouh-Chyu Ruaan **Affinity chromatography of glucose-specific lectin using silica-based support**. *Journal of Chemical Technology & Biotechnology* 1995, **64**:66-72.
219. Oda Y, Kasai K, Ishii S: **Studies on the Specific Interaction of Concanavalin-a and Saccharides by Affinity-Chromatography - Application of Quantitative Affinity-Chromatography to a Multivalent System**. *Journal of Biochemistry* 1981, **89**:285-296.
220. Smith EA, Thomas WD, Kiessling LL, Corn RM: **Surface plasmon resonance imaging studies of protein-carbohydrate interactions**. *Journal of the American Chemical Society* 2003, **125**:6140-6148.
221. Mislovicova D, Masarova J, Svitel J, Mendichi R, Soltes L, Gemeiner P, Danielsson B: **Neoglycoconjugates of mannan with bovine serum albumin and their interaction with lectin concanavalin A**. *Bioconjugate Chemistry* 2002, **13**:136-142.
222. So LL, Goldstei.Ij: **Protein-Carbohydrate Interaction .20. on Number of Combining Sites on Concanavalin a Phytohemagglutinin of Jack Bean**. *Biochimica Et Biophysica Acta* 1968, **165**:398-&.
223. Ooya T, Utsunomiya H, Eguchi M, Yui N: **Rapid binding of concanavalin A and maltose-polyrotaxane conjugates due to mobile motion of alpha-cyclodextrins threaded onto a poly(ethylene glycol)**. *Bioconjugate Chemistry* 2005, **16**:62-69.
224. Borrebaeck C, Mattiasson B: **Lectin-Carbohydrate Interactions Studied by a Competitive Enzyme-Inhibition Assay**. *Analytical Biochemistry* 1980, **107**:446-450.
225. Chervenak MC, Toone EJ: **Calorimetric Analysis of the Binding of Lectins with Overlapping Carbohydrate-Binding Ligand Specificities**. *Biochemistry* 1995, **34**:5685-5695.
226. Derewenda Z, Yariv J, Helliwell JR, Kalb AJ, Dodson EJ, Papiz MZ, Wan T, Campbell J: **The Structure of the Saccharide-Binding Site of Concanavalin-A**. *Embo Journal* 1989, **8**:2189-2193.
227. Bouckaert J, Hamelryck TW, Wyns L, Loris R: **The crystal structures of Man(alpha 1-3)Man(alpha 1-0)Me and Man(alpha 1-6)Man(alpha 1-0)Me in complex with concanavalin A**. *Journal of Biological Chemistry* 1999, **274**:29188-29195.
228. Horan N, Yan L, Isobe H, Whitesides GM, Kahne D: **Nonstatistical binding of a protein to clustered carbohydrates**. *Proceedings of the National Academy of Sciences of the United States of America* 1999, **96**:11782-11786.
229. Baum T, Bethell D, Brust M, Schiffrin DJ: **Electrochemical charge injection into immobilized nanosized gold particle ensembles: Potential modulated transmission and reflectance spectroscopy**. *Langmuir* 1999, **15**:866-871.
230. Musick MD, Pena DJ, Botsko SL, McEvoy TM, Richardson JN, Natan MJ: **Electrochemical properties of colloidal Au-based surfaces: Multilayer assemblies and seeded colloid films**. *Langmuir* 1999, **15**:844-850.
231. Musick MD, Keating CD, Keefe MH, Natan MJ: **Stepwise construction of conductive Au colloid multilayers from solution**. *Chemistry of Materials* 1997, **9**:1499-&.
232. Crespo-Biel O, Dordi B, Reinhoudt DN, Huskens J: **Supramolecular layer-by-layer assembly: Alternating adsorptions of guest- and host-functionalized molecules and particles using multivalent supramolecular interactions**. *Journal of the American Chemical Society* 2005, **127**:7594-7600.
233. Qi ZM, Honma I, Ichihara M, Zhou HS: **Layer-by-layer fabrication and characterization of gold-nanoparticle/myoglobin nanocomposite films**. *Advanced Functional Materials* 2006, **16**:377-386.

234. Zhao J, Zhu XL, Lib T, Li GX: **Self-assembled multilayer of gold nanoparticles for amplified electrochemical detection of cytochrome c**. *Analyst* 2008, **133**:1242-1245.
235. Liu XO, Atwater M, Wang JH, Huo Q: **Extinction coefficient of gold nanoparticles with different sizes and different capping ligands**. *Colloids and Surfaces B-Biointerfaces* 2007, **58**:3-7.
236. Mammen M, Shakhnovich EI, Whitesides GM: **Using a convenient, quantitative model for torsional entropy to establish qualitative trends for molecular processes that restrict conformational freedom**. *Journal of Organic Chemistry* 1998, **63**:3168-3175.
237. Castellana ET, Cremer PS: **Solid supported lipid bilayers: From biophysical studies to sensor design**. *Surface Science Reports* 2006, **61**:429-444.
238. Loeb J: **The recent development of biology**. *Science* 1904, **20**:777-785.
239. Hintzensterna UV, Schwarzb W, Goerigc M, Petermann H: **The history of anesthesia**. Edited by; 2002:609-612. vol 1242.]
240. Fricke H: **The electrical capacity of suspensions with special reference to blood**. *Journal of General Physiology* 1925, **9**:137-152.
241. Gorter E, Grendel F: **On bimolecular layers of lipids on the chromocytes of the blood**. *Journal of Experimental Medicine* 1925, **41**:439-443.
242. SJOSTRAND FS, ANDERSSON-CEDERGREN E, DEWEY MM: **The ultrastructure of the intercalated discs of frog, mouse and guinea pig cardiac muscle**. *Journal of Ultrastructural Research* 1958, **1**:271.
243. Robertson JD: **The ultrastructure of cell membranes and their derivatives**. *Biochemical Society Symposia* 1959 **16**: 3-43.
244. Singer S, Nicholson G: **The fluid mosaic model of the structure of cell membranes**. *Science* 1972, **175**:720-731.
245. Campbell, Reece: *Biology* edn 8th
246. Hille B: *Ion channels of excitable membranes* edn 3rd. Edited by Associates S. Mass.: Sunderland; 2001.
247. **www.virtuallaboratory.net/.../Topic2E_Membranes.htm**.
248. Doyle DA, Cabral JM, Pfuetzner RA, Kuo AL, Gulbis JM, Cohen SL, Chait BT, MacKinnon R: **The structure of the potassium channel: Molecular basis of K+ conduction and selectivity**. *Science* 1998, **280**:69-77.
249. Corry B, Chung SH: **Mechanisms of valence selectivity in biological ion channels**. *Cellular and Molecular Life Sciences* 2006, **63**:301-315.
250. Ketchem RR, Roux B, Cross TA: **High-resolution polypeptide structure in a lamellar phase lipid environment from solid state NMR derived orientational constraints**. *Structure* 1997, **5**:1655-1669.
251. Andersen OS, Koeppe RE, Roux B: **Gramicidin channels**. *Ieee Transactions on Nanobioscience* 2005, **4**:10-20.
252. Dutzler R, Campbell EB, Cadene M, Chait BT, MacKinnon R: **X-ray structure of a CIC chloride channel at 3.0 angstrom reveals the molecular basis of anion selectivity**. *Nature* 2002, **415**:287-294.
253. Corry B, Allen TW, Kuyucak S, Chung SH: **Mechanisms of permeation and selectivity in calcium channels**. *Biophysical Journal* 2001, **80**:195-214.
254. Corry B, Allen TW, Kuyucak S, Chung SH: **A model of calcium channels**. *Biochimica Et Biophysica Acta-Biomembranes* 2000, **1509**:1-6.
255. Corry B, Vora T, Chung SH: **Electrostatic basis of valence selectivity in cationic channels**. *Biochimica Et Biophysica Acta-Biomembranes* 2005, **1711**:72-86.
256. Lipkind GM, Fozzard HA: **Modeling of the outer vestibule and selectivity filter of the L-type Ca2+ channel**. *Biochemistry* 2001, **40**:6786-6794.

257. Barreiro G, Guimaraes CRW, de Alencastro RB: **A molecular dynamics study of an L-type calcium channel model**. *Protein Engineering* 2002, **15**:109-122.
258. Shannon RD: **Revised Effective Ionic-Radii and Systematic Studies of Interatomic Distances in Halides and Chalcogenides**. *Acta Crystallographica Section A* 1976, **32**:751-767.
259. Karplus M, Petsko GA: **Molecular-Dynamics Simulations in Biology**. *Nature* 1990, **347**:631-639.
260. Zaccai G: **Biochemistry - How soft is a protein? A protein dynamics force constant measured by neutron scattering**. *Science* 2000, **288**:1604-1607.
261. Noskov SY, Roux B: **Importance of hydration and dynamics on the selectivity of the KcsA and NaK channels**. *Journal of General Physiology* 2007, **129**:135-143.
262. Zhou YF, Morais-Cabral JH, Kaufman A, MacKinnon R: **Chemistry of ion coordination and hydration revealed by a K+ channel-Fab complex at 2.0 angstrom resolution**. *Nature* 2001, **414**:43-48.
263. Fowler PW, Tai KH, Sansom MSP: **The Selectivity of K+ Ion Channels: Testing the Hypotheses**. *Biophysical Journal* 2008, **95**:5062-5072.
264. Alam A, Jiang YX: **Structural analysis of ion selectivity in the NaK channel**. *Nature Structural & Molecular Biology* 2009, **16**:35-41.
265. Vora T, Bisset D, Chung SH: **Conduction of Na+ and K+ through the NaK channel: Molecular and Brownian dynamics studies**. *Biophysical Journal* 2008, **95**:1600-1611.
266. Cereghetti DM, Carreira EM: **Amphotericin B: 50 years of chemistry and biochemistry**. *Synthesis-Stuttgart* 2006:914-942.
267. Noble CO, Kirpotin DB, Hayes ME, Mamot C, Hong K, Park JW, Benz CC, Marks JD, Drummond DC: **Development of ligand-targeted liposomes for cancer therapy**. *Expert Opinion on Therapeutic Targets* 2004, **8**:335-353.
268. Fyles TM: **Synthetic ion channels in bilayer membranes**. *Chemical Society Reviews* 2007, **36**:335-347.
269. Nakano A, Xie QS, Mallen JV, Echegoyen L, Gokel GW: **Synthesis of a Membrane-Insertable, Sodium-Cation Conducting Channel - Kinetic-Analysis by Dynamic Na-23 Nmr**. *Journal of the American Chemical Society* 1990, **112**:1287-1289.
270. Carmichael VE, Dutton PJ, Fyles TM, James TD, Swan JA, Zojaji M: **Biomimetic Ion-Transport - a Functional-Model of a Unimolecular Ion Channel**. *Journal of the American Chemical Society* 1989, **111**:767-769.
271. Gokel GW, Ferdani R, Liu J, Pajewski R, Shabany H, Uetrecht P: **Hydraphile channels: Models for transmembrane, cation-conducting transporters**. *Chemistry-a European Journal* 2001, **7**:33-39.
272. Shabany H, Gokel GW: **Enhancement of cation transport in synthetic hydraphile channels having covalently-linked headgroups**. *Chemical Communications* 2000:2373-2374.
273. Leevy WM, Gammon ST, Levchenko T, Daranciang DD, Murillo O, Torchilin V, Piwnica-Worms D, Huettner JE, Gokel GW: **Structure-activity relationships, kinetics, selectivity, and mechanistic studies of synthetic hydraphile channels in bacterial and mammalian cells**. *Organic & Biomolecular Chemistry* 2005, **3**:3544-3550.
274. Leevy WM, Weber ME, Schlesinger PH, Gokel GW: **NMR and ion selective electrode studies of hydraphile channels correlate with biological activity in E-coli and B-subtilis**. *Chemical Communications* 2005:89-91.
275. Fyles TM, van Straten-Nijenhuis WF: *Comprehensive Supramolecular Chemistry*, vol 10. Edited by N. RD. Amsterdam/New York: Elsevier Science; 1996.

276. Vandenburg YR, Smith BD, Biron E, Voyer N: **Membrane disruption ability of facially amphiphilic helical peptides**. *Chemical Communications* 2002:1694-1695.
277. Matile S, Som A, Sorde N: **Recent synthetic ion channels and pores**. *Tetrahedron* 2004, **60**:6405-6435.
278. Sakai N, Mareda J, Matile S: **Rigid-rod molecules in biomembrane models: From hydrogen-bonded chains to synthetic multifunctional pores**. *Accounts of Chemical Research* 2005, **38**:79-87.
279. Hartgerink JD, Clark TD, Ghadiri MR: **Peptide nanotubes and beyond**. *Chemistry-a European Journal* 1998, **4**:1367-1372.
280. Sanchez-Quesada J, Kim HS, Ghadiri MR: **A synthetic pore-mediated transmembrane transport of glutamic acid**. *Angewandte Chemie-International Edition* 2001, **40**:2503-+.
281. Fernandez-Lopez S, Kim HS, Choi EC, Delgado M, Granja JR, Khasanov A, Kraehenbuehl K, Long G, Weinberger DA, Wilcoxen KM, et al.: **Antibacterial agents based on the cyclic D,L-alpha-peptide architecture**. *Nature* 2001, **412**:452-455.
282. Fyles TM, Loock D, Zhou X: **A voltage-gated ion channel based on a bis-macrocyclic bolaamphiphile**. *Journal of the American Chemical Society* 1998, **120**:2997-3003.
283. Fyles TM, Loock D, Zhou X: **Ion channels based on bis-macrocyclic bolaamphiphiles: effects of hydrophobic substitutions**. *Canadian Journal of Chemistry-Revue Canadienne De Chimie* 1998, **76**:1015-1026.
284. Goto C, Yamamura M, Satake A, Kobuke Y: **Artificial ion channels showing rectified current behavior**. *Journal of the American Chemical Society* 2001, **123**:12152-12159.
285. Fyles TM, Tong CC: **Long-lived and highly conducting ion channels formed by lipophilic ethylenediamine palladium(II) complexes**. *New Journal of Chemistry* 2007, **31**:655-661.
286. Jung M, Kim H, Baek K, Kim K: **Synthetic ion channel based on metal-organic polyhedra**. *Angewandte Chemie-International Edition* 2008, **47**:5755-5757.
287. Eddaoudi M, Kim J, Wachter JB, Chae HK, O'Keeffe M, Yaghi OM: **Porous metal-organic polyhedra: 25 angstrom cuboctahedron constructed from 12 Cu-2(CO2)(4) paddle-wheel building blocks**. *Journal of the American Chemical Society* 2001, **123**:4368-4369.
288. Furukawa H, Kim J, Plass KE, Yaghi OM: **Crystal structure, dissolution, and deposition of a 5 nm functionalized metal-organic great rhombicuboctahedron**. *Journal of the American Chemical Society* 2006, **128**:8398-8399.
289. Sakai N, Matile S: **Recognition of polarized lipid bilayers by p-oligophenyl ion channels: From push-pull rods to push-pull barrels**. *Journal of the American Chemical Society* 2002, **124**:1184-1185.
290. Carr R, Weinstock IA, Sivaprasadarao A, Muller A, Aksimentiev A: **Synthetic Ion Channels via Self-Assembly: A Route for Embedding Porous Polyoxometalate Nanocapsules in Lipid Bilayer Membranes**. *Nano Letters* 2008, **8**:3916-3921.
291. Muller A, Krickemeyer E, Meyer J, Bogge H, Peters F, Plass W, Diemann E, Dillinger S, Nonnenbruch F, Randerath M, et al.: **[Mo-154(No)(14)O-420(Oh)(28)(H2o)(70)]((25+5)-) - a Water-Soluble Big Wheel with More Than 700 Atoms and a Relative Molecular-Mass of About 24000**. *Angewandte Chemie-International Edition in English* 1995, **34**:2122-2124.
292. Muller A, Krickemeyer E, Bogge H, Schmidtmann M, Peters F: **Organizational forms of matter: An inorganic super fullerene and keplerate based on molybdenum oxide**. *Angewandte Chemie-International Edition* 1998, **37**:3360-3363.

293. Cronin L, Beugholt C, Krickemeyer E, Schmidtmann M, Bogge H, Kogerler P, Luong TKK, Muller A: **"Molecular symmetry breakers" generating metal-oxide-based nanoobject fragments as synthons for complex structures: [{Mo128Eu4O388H10(H2O)(81)}(2)](20-), a giant-cluster dimer**. *Angewandte Chemie-International Edition* 2002, **41**:2805-+.
294. Muller A, Sarkar S, Shah SQN, Bogge H, Schmidtmann M, Sarkar S, Kogerler P, Hauptfleisch B, Trautwein AX, Schunemann V: **Archimedean synthesis and magic numbers: "Sizing" giant molybdenum-oxide-based molecular spheres of the keplerate type**. *Angewandte Chemie-International Edition* 1999, **38**:3238-3241.
295. Muller A, Shah SQN, Bogge H, Schmidtmann M, Kogerler P, Hauptfleisch B, Leiding S, Wittler K: **Thirty electrons "trapped" in a spherical matrix: A molybdenum oxide-based nanostructured Keplerate reduced by 36 electrons**. *Angewandte Chemie-International Edition* 2000, **39**:1614-+.
296. Muller A, Roy S: **En route from the mystery of molybdenum blue via related manipulatable building blocks to aspects of materials science**. *Coordination Chemistry Reviews* 2003, **245**:153-166.
297. Muller A, Das SK, Bogge H, Schmidtmann M, Botar A, Patrut A: **Generation of cluster capsules (I-h) from decomposition products of a smaller cluster (Keggin-T-d) while surviving ones get encapsulated: species with core-shell topology formed by a fundamental symmetry-driven reaction**. *Chemical Communications* 2001:657-658.
298. Muller A, Das SK, Kuhlmann C, Bogge H, Schmidtmann M, Diemann E, Krickemeyer E, Hormes J, Modrow H, Schindler M: **On the option of generating novel type surfaces with multiphilic ligands within the cavity of a giant metal-oxide based wheel type cluster: chemical reactions with well-defined nanoobjects**. *Chemical Communications* 2001:655-656.
299. Liu T: **Supramolecular Structures of Polyoxomolybdate-Based Giant Molecules in Aqueous Solution**. *Journal of the American Chemical Society* 2002, **124**:10942-10943.
300. Muller A, Bogge H, Sousa FL, Schmidtmann M, Kurth DG, Volkmer D, van Slageren J, Dressel M, Kistler ML, Liu TB: **Nanometer-sized molybdenum-iron oxide capsule-surface modifications: External and internal**. *Small* 2007, **3**:986-992.
301. Ross EE, Spratt T, Liu SC, Rozanski LJ, O'Brien DF, Saavedra SS: **Planar supported lipid bilayer polymers formed by vesicle fusion. 2. Adsorption of bovine serum albumin**. *Langmuir* 2003, **19**:1766-1774.
302. Liu G, Cai Y, Liu T: **Automatic and Subsequent Dissolution and Precipitation Process in Inorganic Macroionic Solutions**. *Journal of the American Chemical Society* 2004, **126**:16690-16691.
303. Liu Y, Tang XL, Liu F, Li K: **Selection of ligands for affinity chromatography using quartz crystal biosensor**. *Analytical Chemistry* 2005, **77**:4248-4256.
304. Liu TB, Imber B, Diemann E, Liu G, Cokleski K, Li HL, Chen ZQ, Muller A: **Deprotonations and charges of well-defined {Mo72Fe30} nanoacids simply stepwise tuned by pH allow control/variation of related self-assembly processes**. *Journal of the American Chemical Society* 2006, **128**:15914-15920.
305. Volkmer D, Du Chesne A, Kurth DG, Schnablegger H, Lehmann P, Koop MJ, Muller A: **Toward nanodevices: Synthesis and characterization of the nanoporous surfactant-encapsulated keplerate (DODA)(40)(NH4)(2)[(H2O)(n)subset of Mo132O372(CH3COO)(30)(H2O)(72)]**. *Journal of the American Chemical Society* 2000, **122**:1995-1998.

306. Kurth DG, Lehmann P, Volkmer D, Colfen H, Koop MJ, Muller A, Du Chesne A: **Surfactant-encapsulated clusters (SECs): (DODA)(20)(NH4)[H3Mo57V6(NO)(6)O-183(H2O)(18)], a case study**. *Chemistry-a European Journal* 2000, **6**:385-393.
307. Kurth DG, Lehmann P, Volkmer D, Muller A, Schwahn D: **Biologically inspired polyoxometalate-surfactant composite materials. Investigations on the structures of discrete, surfactant-encapsulated clusters, monolayers, and Langmuir-Blodgett films of (DODA)(40)(NH4)(2)[(H2O)(n)subset of Mo132O372(CH3CO2)(30)(H2O)(72)]**. *Journal of the Chemical Society-Dalton Transactions* 2000:3989-3998.
308. Liu TB: **An Unusually Slow Self-Assembly of Inorganic Ions in Dilute Aqueous Solution**. *Journal ot the American Chemical Society* 2003, **125**:312-313.
309. Muller A, Das SK, Talismanov S, Roy S, Beckmann E, Bogge H, Schmidtmann M, Merca A, Berkle A, Allouche L, et al.: **Trapping cations in specific positions in tuneable "artificial cell" channels: New nanochemistry perspectives**. *Angewandte Chemie-International Edition* 2003, **42**:5039-5044.
310. Merca A HE, Mitra T, Bögge H, Rehder D, Müller A.: **Mimicking biological cation-transport based on sphere-surface supramolecular chemistry: simultaneous interaction of porous capsules with molecular plugs and passing cations.** *Chemistry: A European Journal* 2007, **13**:7650-7658.
311. Rehder D, Haupt ETK, Bogge H, Muller A: **Countereation transport modeled by porous spherical molybdenum oxide based nanocapsules**. *Chemistry-an Asian Journal* 2006, **1**:76-81.
312. Muller A, Rehder D, Haupt ETK, Merca A, Bogge H, Schmidtmann M, Heinze-Bruckner G: **Artificial cells: Temperature-dependent, reversible Li+-ion uptake/release equilibrium at metal oxide nanocontainer pores**. *Angewandte Chemie-International Edition* 2004, **43**:4466-4470.
313. Muller A, Krickemeyer E, Bogge H, Schmidtmann M, Roy S, Berkle A: **Changeable pore sizes allowing effective and specific recognition by a molybdenum-oxide based "nanosponge": En route to sphere-surface and nanoporous-cluster chemistry**. *Angewandte Chemie-International Edition* 2002, **41**:3604-3609.
314. Muller A, Zhou YS, Bogge H, Schmidtmann M, Mitra T, Haupt ETK, Berkle A: **"Gating" the pores of a metal oxide based capsule: After initial cation uptake subsequent cations are found hydrated and supramolecularly fixed above the pores**. *Angewandte Chemie-International Edition* 2006, **45**:460-465.
315. Sakai N, Brennan KC, Weiss LA, Matile S: **Toward Biomimetic Ion Channels Formed by Rigid-Rod Molecules: Length-Dependent Ion-Transport Activity of Substituted Oligo(p-Phenylene)s**. *Journal of the American Chemical Society* 1997, **119**:8726-8727.
316. Weiss LA, Sakai N, Ghebremariam B, Ni C, Matile S: **Rigid Rod-Shaped Polyols: Functional Nonpeptide Models for Transmembrane Proton Channels&#x2020**. *Journal of the American Chemical Society* 1997, **119**:12142-12149.
317. Maureen M. Tedesco BGNSSM: **Modeling the Selectivity of Potassium Channels with Synthetic, Ligand-Assembled pi Slides**. *Angewandte Chemie International Edition* 1999, **38**:540-543.
318. Sidorov V, Kotch FW, Abdrakhmanova G, Mizani R, Fettinger JC, Davis JT: **Ion Channel Formation from a Calix[4]arene Amide That Binds HCl**. *Journal of the American Chemical Society* 2002, **124**:2267-2278.

319. Talukdar P, Bollot G, Mareda J, Sakai N, Matile S: **Ligand-gated synthetic ion channels**. *Chemistry-a European Journal* 2005, **11**:6525-6532.
320. Talukdar P, Bollot G, Mareda J, Sakai N, Matile S: **Synthetic ion channels with rigid-rod pi-stack architecture that open in response to charge-transfer complex formation**. *Journal of the American Chemical Society* 2005, **127**:6528-6529.
321. Sakai N, Houdebert D, Matile S: **Voltage-dependent formation of anion channels by synthetic rigid-rod push-pull beta-barrels**. *Chemistry-a European Journal* 2003, **9**:223-232.
322. Gokel GW, Mukhopadhyay A: **Synthetic models of cation-conducting channels**. *Chemical Society Reviews* 2001, **30**:274-286.
323. Brian AA, McConnell HM: **Allogeneic Stimulation of Cyto-Toxic T-Cells by Supported Planar Membranes**. *Proceedings of the National Academy of Sciences of the United States of America-Biological Sciences* 1984, **81**:6159-6163.
324. McConnell HM, Watts TH, Weis RM, Brian AA: **Supported Planar Membranes in Studies of Cell-Cell Recognition in the Immune-System**. *Biochimica Et Biophysica Acta* 1986, **864**:95-106.
325. Reimhult E: **Intact vesicle adsorption and supported biomembrane formation from vesicles in solution: Influence of surface chemistry, vesicle size, temperature, and osmotic pressure**. *Langmuir* 2003, **19**:1681-1691.
326. Johnson JM: **Early steps of supported bilayer formation probed by single vesicle fluorescence assays**. *Biophysical Journal* 2002, **83**:3371-3379.
327. Cremer PS: **Formation and spreading of lipid bilayers on planar glass supports**. *Journal of Physical Chemistry B* 1999, **103**:2554-2559.
328. Mayer LD: **Vesicles of Variable Sizes Produced by a Rapid Extrusion Procedure**. *Biochimica Et Biophysica Acta* 1986, **858**:161-168.
329. Frisken BJ: **Studies of vesicle extrusion**. *Langmuir* 2000, **16**:928-933.
330. Barenholz Y: **Simple Method for Preparation of Homogeneous Phospholipid Vesicles**. *Biochemistry* 1977, **16**:2806-2810.
331. Keller CA, Kasemo B: **Surface specific kinetics of lipid vesicle adsorption measured with a quartz crystal microbalance**. *Biophysical Journal* 1998, **75**:1397-1402.
332. Keller CA, Glasmastar K, Zhdanov VP, Kasemo B: **Formation of supported membranes from vesicles**. *Physical Review Letters* 2000, **84**:5443-5446.
333. Ha TH: **Adsorption of Lipid Vesicles on Hydrophobic Surface Investigated by Quartz Crystal Microbalance**. *Langmuir* 2001, **17**:1999-2007.
334. Richter R. MAaBA: **Pathways of Lipid Vesicle Deposition on Solid Surfaces:A Combined QCM-D and AFM Study**. *Biophysical Journal* 2003, **85**:3035-3047.
335. Plant AL: **Supported hybrid bilayer membranes as rugged cell membrane mimics**. *Langmuir* 1999, **15**:5128-5135.
336. Anderson NA: **Characterization and control of lipid layer fluidity in hybrid bilayer membranes**. *Journal of the American Chemical Society* 2007, **129**:2094-2100.
337. Richter RP, Berat R, Brisson AR: **Formation of solid-supported lipid bilayers: An integrated view**. *Langmuir* 2006, **22**:3497-3505.
338. Richter R, Mukhopadhyay A, Brisson A: **Pathways of lipid vesicle deposition on solid surfaces: A combined QCM-D and AFM study**. *Biophysical Journal* 2003, **85**:3035-3047.
339. Reviakine I, Simon A, Brisson A: **Effect of Ca2+ on the morphology of mixed DPPC-DOPS supported phospholipid bilayers**. *Langmuir* 2000, **16**:1473-1477.
340. Reviakine I, Brisson A: **Formation of supported phospholipid bilayers from unilamellar vesicles investigated by atomic force microscopy**. *Langmuir* 2000, **16**:1806-1815.

341. Ekeroth J, Konradsson P, Hook F: **Bivalent-ion-mediated vesicle adsorption and controlled supported phospholipid bilayer formation on molecular phosphate and sulfate layers on gold**. *Langmuir* 2002, **18**:7923-7929.
342. Nollert P, Kiefer H, Jahnig F: **Lipid Vesicle Adsorption Versus Formation of Planar Bilayers on Solid-Surfaces**. *Biophysical Journal* 1995, **69**:1447-1455.
343. Mornet S, Lambert O, Duguet E, Brisson A: **The formation of supported lipid bilayers on silica nanoparticles revealed by cryoelectron microscopy**. *Nano Letters* 2005, **5**:281-285.
344. Richter RP, Maury N, Brisson AR: **On the effect of the solid support on the interleaflet distribution of lipids in supported lipid bilayers**. *Langmuir* 2005, **21**:299-304.
345. Wacklin HP, Thomas RK: **Spontaneous formation of asymmetric lipid bilayers by adsorption of vesicles**. *Langmuir* 2007, **23**:7644-7651.
346. Hasenknopf B: **Polyoxometalates: Introduction to a class of inorganic compounds and their biomedical applications**. *Frontiers in Bioscience* 2005, **10**:275-287.
347. Rhule JT, Hill CL, Judd DA, Schinazi RF: **Polyoxometalates in Medicine**. *Chemical Reviews* 1998, **98**:327-358.
348. Judd DA, Nettles JH, Nevins N, Snyder JP, Liotta DC, Tang J, Ermolieff J, Schinazi RF, Hill CL: **Polyoxometalate HIV-1 Protease Inhibitors. A New Mode of Protease Inhibition**. *Journal of the American Chemical Society* 2001, **123**:886-897.
349. Li J, Qi YF, Wang EB, Li JN, Wang HF, Li YG, Lu YN, Hao N, Xu L, Hu CW: **Synthesis, structural characterization and biological activity of polyoxometallate-containing protonated amantadine as a cation**. *Journal of Coordination Chemistry* 2004, **57**:715-721.
350. Shigeta S, Mori S, Yamase T, Yamamoto N, Yamamoto N: **Anti-RNA virus activity of polyoxometalates**. *Biomedicine & Pharmacotherapy* 2006, **60**:211-219.
351. Kim G-S, Judd DA, Hill CL, Schinazi RF: **Synthesis, Characterization, and Biological Activity of a New Potent Class of Anti-HIV Agents, the Peroxoniobium-Substituted Heteropolytungstates**. *Journal of Medicinal Chemistry* 1994, **37**:816-820.
352. Lee IS, Long JR, Prusiner SB, Safar JG: **Selective Precipitation of Prions by Polyoxometalate Complexes**. *Journal of the American Chemical Society* 2005, **127**:13802-13803.
353. Zhang GJ, Keita B, Brochon JC, de Oliveira P, Nadjo L, Craescu CT, Miron S: **Molecular interaction and energy transfer between human serum albumin and polyoxometalates**. *Journal of Physical Chemistry B* 2007, **111**:1809-1814.
354. Zhang G, Keita B, Craescu CT, Miron S, de Oliveira P, Nadjo L: **Polyoxometalate binding to human serum albumin: A thermodynamic and spectroscopic approach**. *Journal of Physical Chemistry B* 2007, **111**:11253-11259.
355. Yamase T: **Polyoxometalates for molecular devices : anti-tumor activity and luminescence**. *Mol Eng* 1993, **3**:241-262.
356. Yamase T: **Medicinal Chemistry of polyoxometalates.Part 1. Potent anti-tumor activity of polyoxomolybdates on animal transplantable tumors and human human cancer zenograft**. *Inoorg. Chim. Acta* 1988, **151**:15-18.
357. Yamase T: **Antitumoral and antiviral polyoxometalates**. *Polymeric Materials Encyclopedia* 1996, **1**:365-373.
358. Ogata A, Mitsui S, Yanagie H, Kasano H, Hisa T, Yamase T, Eriguchi M: **A novel anti-tumor agent, polyoxomolybdate induces apoptotic cell death in AsPC-1 human pancreatic cancer cells**. *Biomedecine & Pharmacotherapy* 2005, **59**:240-244.
359. Yamase T: **Anti-tumor, -viral, and -bacterial activities of polyoxometalates for**

realizing an inorganic drug. *Journal of Materials Chemistry* 2005, **15**:4773-4782.
360. Ogata A, Yanagie H, Ishikawa E, Morishita Y, Mitsui S, Yamashita A, Hasumi K, Takamoto S, Yamase T, Eriguchi M: **Antitumour effect of polyoxomolybdates: induction of apoptotic cell death and autophagy in in vitro and in vivo models**. *Br J Cancer* 2007, **98**:399-409.
361. K. Tomita, T. Yamase, K. Shishido: **Medicinal chemistry of polyoxometalates part 2. Enzymatic study on binding of heptamolybdate to DNA.** *Inoorg. Chim. Acta* 1989, **157**.
362. Hill LMR, George GN, Duhme-Klair A-K, Young CG: **Solution structural studies of molybdate-nucleotide polyanions**. *Journal of Inorganic Biochemistry* 2002, **88**:274-283.
363. Ishikawa E, Yamase T: **31P NMR and isothermal titration calorimetry studies on polyoxomolybdates-catalyzed hydrolysis of ATP**. *Journal of Inorganic Biochemistry* 2006, **100**:344-350.
364. Absillis G, Cartuyvels E, Van Deun R, Parac-Vogt TN: **Hydrolytic Cleavage of an RNA-Model Phosphodiester Catalyzed by a Highly Negatively Charged Polyoxomolybdate [Mo7O24]6− Cluster**. *Journal of the American Chemical Society* 2008, **130**:17400-17408.
365. Aguilar-Perez F, Gomez-Tagle P, Collado-Fregoso E, Yatsimirsky AK: **Phosphate Ester Hydrolysis by Hydroxo Complexes of Trivalent Lanthanides Stabilized by 4-Imidazolecarboxylate**. *Inorganic Chemistry* 2006, **45**:9502-9517.
366. Boudard S, Seantier B, Breffa C, Decher G, Felix O: **Controlling the pathway of formation of supported lipid bilayers of DMPC by varying the sodium chloride concentration**. *Thin Solid Films* 2006, **495**:246-251.
367. Puu G, Gustafson I: **Planar lipid bilayers on solid supports from liposomes - factors of importance for kinetics and stability**. *Biochimica Et Biophysica Acta-Biomembranes* 1997, **1327**:149-161.
368. Jass J, Tjarnhage T, Puu G: **From liposomes to supported, planar bilayer structures on hydrophilic and hydrophobic surfaces: An atomic force microscopy study**. *Biophysical Journal* 2000, **79**:3153-3163.
369. Kistler ML, Bhatt A, Liu G, Casa D, Liu TB: **A complete macroion-"blackberry" assembly-macroion transition with continuously adjustable assembly sizes in {Mo-132} water/acetone systems**. *Journal of the American Chemical Society* 2007, **129**:6453-6460.
370. Liu SQ, Kurth DG, Bredenkotter B, Volkmer D: **The structure of self-assembled multilayers with polyoxometalate nanoclusters**. *Journal of the American Chemical Society* 2002, **124**:12279-12287.
371. Liu SQ, Volkmer D, Kurth DG: **Functional polyoxometalate thin films via electrostatic layer-by-layer self-assembly**. *Journal of Cluster Science* 2003, **14**:405-419.
372. Delajon C, Gutberlet T, Steitz R, Mohwald H, Krastev R: **Formation of poly,electrolyte multilayer architectures with embedded DMPC studied in situ by neutron reflectometry**. *Langmuir* 2005, **21**:8509-8514.
373. Kugler R, Knoll W: **Polyelectrolyte-supported lipid membranes**. *Bioelectrochemistry* 2002, **56**:175-178.
374. Pilbat AM, Szegletes Z, Kota Z, Ball V, Schaaf P, Voegel JC, Szalontai B: **Phospholipid bilayers as biomembrane-like barriers in layer-by-layer polyelectrolyte films**. *Langmuir* 2007, **23**:8236-8242.
375. Muller A, Serain C: **Soluble molybdenum blues - "des pudels kern"**. *Accounts of Chemical Research* 2000, **33**:2-10.

376. Liu TB, Diemann E, Li HL, Dress AWM, Muller A: **Self-assembly in aqueous solution of wheel-shaped Mo-154 oxide clusters into vesicles**. *Nature* 2003, **426**:59-62.
377. Oleinikova A, Weingartner H, Chaplin M, Diemann E, Bogge H, Muller A: **Self-association based on interfacial structured water leads to {Mo-154}approximate to(1165) super clusters: A dielectric study**. *Chemphyschem* 2007, **8**:646-649.
378. Liu G, Liu TB: **Strong attraction among the fully hydrophilic {Mo72Fe30} macroanions**. *Journal of the American Chemical Society* 2005, **127**:6942-6943.
379. Liu G, Liu TB: **Thermodynamic properties of the unique self-assembly of {Mo72Fe30} inorganic macro-ions in salt-free and salt-containing aqueous solutions**. *Langmuir* 2005, **21**:2713-2720.
380. Liu G, Cons M, Liu TB: **The ionic effect on supramolecular associations in polyoxomolybdate solution**. *Journal of Molecular Liquids* 2005, **118**:27-29.
381. Eisenman G, Horn R: **Ionic Selectivity Revisited - the Role of Kinetic and Equilibrium Processes in Ion Permeation through Channels**. *Journal of Membrane Biology* 1983, **76**:197-225.
382. Kiriukhin MY, Collins KD: **Dynamic hydration numbers for biologically important ions**. *Biophysical Chemistry* 2002, **99**:155-168.
383. Neilson GW, Enderby JE: **The Coordination of Metal Aquaions**. *Advances in Inorganic Chemistry* 1989, **34**:195-218.
384. Zschornig O, Arnold K, Binder H: **Interaction of mono and divalent metal ions with phospholipid membranes**. *Biophysical Journal* 2001, **80**:1783.
385. Danielewicz-Ferchmin I, Ferchmin AR: **Mass density in hydration shells of ions**. *Physica B* 1998, **245**:34-44.
386. Muller A, Krickemeyer E, Bogge H, Schmidtmann M, Botar B, Talismanova MO: **Drawing small cations into highly charged porous nanocontainers reveals "Water" assembly and related interaction problems**. *Angewandte Chemie-International Edition* 2003, **42**:2085-2090.
387. Muller A, Toma L, Bogge H, Schaffer C, Stammler A: **Porous capsules allow pore opening and closing that results in cation uptake**. *Angewandte Chemie-International Edition* 2005, **44**:7757-7761.
388. Muller A, Bogge H, Henry M: **Coordination chemistry under confined conditions: a simplified illustrative view**. *Comptes Rendus Chimie* 2005, **8**:47-56.
389. Corbett PT, Leclaire J, Vial L, West KR, Wietor JL, Sanders JKM, Otto S: **Dynamic combinatorial chemistry**. *Chemical Reviews* 2006, **106**:3652-3711.
390. Lehn JM: **From supramolecular chemistry towards constitutional dynamic chemistry and adaptive chemistry**. *Chemical Society Reviews* 2007, **36**:151-160.
391. Valade A, Urban D, Beau JM: **Target-assisted selection of galactosyltransferase binders from dynamic combinatorial libraries. An unexpected solution with restricted amounts of the enzyme**. *Chembiochem* 2006, **7**:1023-1027.
392. Lehn JM: **Dynamers: dynamic molecular and supramolecular polymers**. *Progress in Polymer Science* 2005, **30**:814-831.
393. Severin K: **The advantage of being virtual-target-induced adaptation and selection in dynamic combinatorial libraries**. *Chemistry-a European Journal* 2004, **10**:2565-2580.
394. Ramstrom O, Lehn JM: **In situ generation and screening of a dynamic combinatorial carbohydrate library against concanavalin A**. *Chembiochem* 2000, **1**:41-48.
395. Sando S, Narita A, Aoyama Y: **A facile route to dynamic glycopeptide libraries based on disulfide-linked sugar-peptide coupling**. *Bioorganic & Medicinal Chemistry Letters* 2004, **14**:2835-2838.

396. Bilgicer B, Xing X, Kumar K: **Programmed self-sorting of coiled coils with leucine and hexafluoroleucine cores**. *Journal of the American Chemical Society* 2001, **123**:11815-11816.
397. Krishnan-Ghosh Y, Balasubramanian S: **Dynamic covalent chemistry on self-templating peptides: Formation of a disulfide-linked beta-hairpin mimic**. *Angewandte Chemie-International Edition* 2003, **42**:2171-2173.
398. Whitney AM, Ladame S, Balasubramanian S: **Templated ligand assembly by using G-quadruplex DNA and dynamic covalent chemistry**. *Angewandte Chemie-International Edition* 2004, **43**:1143-1146.
399. Nicolaou KC, Hughes R, Cho SY, Winssinger N, Smethurst C, Labischinski H, Endermann R: **Target-accelerated combinatorial synthesis and discovery of highly potent antibiotics effective against vancomycin-resistant bacteria**. *Angewandte Chemie-International Edition* 2000, **39**:3823-+.
400. Nicolaou KC, Hughes R, Cho SY, Winssinger N, Labischinski H, Endermann R: **Synthesis and biological evaluation of vancomycin dimers with potent activity against vancomycin-resistant bacteria: target-accelerated combinatorial synthesis**. *Chemistry-a European Journal* 2001, **7**:3824-3843.
401. Erlanson DA, Braisted AC, Raphael DR, Randal M, Stroud RM, Gordon EM, Wells JA: **Site-directed ligand discovery**. *Proceedings of the National Academy of Sciences of the United States of America* 2000, **97**:9367-9372.
402. Erlanson DA, Hansen SK: **Making drugs on proteins: site-directed ligand discovery for fragment-based lead assembly**. *Current Opinion in Chemical Biology* 2004, **8**:399-406.
403. Orrillo AG, Escalante AM, Furlan RLE: **Covalent double level dynamic combinatorial libraries: selectively addressable exchange processes**. *Chemical Communications* 2008:5298-5300.
404. Cancilla MT, He MM, Viswanathan N, Simmons RL, Taylor M, Fung AD, Cao K, Erlanson DA: **Discovery of an Aurora kinase inhibitor through site-specific dynamic combinatorial chemistry**. *Bioorganic & Medicinal Chemistry Letters* 2008, **18**:3978-3981.
405. Au-Yeung HY, Pengo P, Pantos GD, Otto S, Sanders JKM: **Templated amplification of a naphthalenediimide-based receptor from a donor-acceptor dynamic combinatorial library in water**. *Chemical Communications* 2009:419-421.
406. Goodwin JT, Lynn DG: **Template-Directed Synthesis - Use of a Reversible-Reaction**. *Journal of the American Chemical Society* 1992, **114**:9197-9198.
407. Huc I, Lehn JM: **Virtual combinatorial libraries: Dynamic generation of molecular and supramolecular diversity by self-assembly**. *Proceedings of the National Academy of Sciences of the United States of America* 1997, **94**:2106-2110.
408. Klekota B, Hammond MH, Miller BL: **Generation of novel DNA-binding compounds by selection and amplification from self-assembled combinatorial libraries**. *Tetrahedron Letters* 1997, **38**:8639-8642.
409. Hochgurtel M, Biesinger R, Kroth H, Piecha D, Hofmann MW, Krause S, Schaaf O, Nicolau C, Eliseev AV: **Ketones as building blocks for dynamic combinatorial libraries: Highly active neuraminidase inhibitors generated via selection pressure of the biological target**. *Journal of Medicinal Chemistry* 2003, **46**:356-358.
410. Hochgurtel M, Kroth H, Piecha D, Hofmann MW, Nicolau C, Krause S, Schaaf O, Sonnenmoser G, Eliseev AV: **Target-induced formation of neuraminidase inhibitors from in vitro virtual combinatorial libraries**. *Proceedings of the National Academy of Sciences of the United States of America* 2002, **99**:3382-3387.

411. Gerber-Lemaire S, Popowycz F, Rodriguez-Garcia E, Asenjo ATC, Robina I, Vogel P: **An efficient combinatorial method for the discovery of glycosidase inhibitors**. *Chembiochem* 2002, **3**:466-470.
412. Bugaut A, Toulme JJ, Rayner B: **Use of dynamic combinatorial chemistry for the identification of covalently appended residues that stabilize oligonucleotide complexes**. *Angewandte Chemie-International Edition* 2004, **43**:3144-3147.
413. Klekota B, Miller BL: **Selection of DNA-binding compounds via multistage molecular evolution**. *Tetrahedron* 1999, **55**:11687-11697.
414. Zameo S, Vauzeilles B, Beau JM: **Dynamic combinatorial chemistry: Lysozyme selects an aromatic motif that mimics a carbohydrate residue**. *Angewandte Chemie-International Edition* 2005, **44**:965-969.
415. Godoy-Alcantar C, Yatsimirsky AK, Lehn JM: **Structure-stability correlations for imine formation in aqueous solution**. *Journal of Physical Organic Chemistry* 2005, **18**:979-985.
416. Larsson R, Pei ZC, Ramstrom O: **Catalytic self-screening of cholinesterase substrates from a dynamic combinatorial thioester library**. *Angewandte Chemie-International Edition* 2004, **43**:3716-3718.
417. Woll MG, Gellman SH: **Backbone thioester exchange: A new approach to evaluating higher order structural stability in polypeptides**. *Journal of the American Chemical Society* 2004, **126**:11172-11174.
418. Lins RJ, Flitsch SL, Turner NJ, Irving E, Brown SA: **Enzymatic generation and in situ screening of a dynamic combinatorial library of sialic acid analogues**. *Angewandte Chemie-International Edition* 2002, **41**:3405-+.
419. Lins RJ, Flitsch SL, Turner NJ, Irving E, Brown SA: **Generation of a dynamic combinatorial library using sialic acid aldolase and in situ screening against wheat germ agglutinin**. *Tetrahedron* 2004, **60**:771-780.
420. Witt D: **Recent developments in disulfide bond formation**. *Synthesis-Stuttgart* 2008:2491-2509.
421. Winterbourn CC, Hampton MB: **Thiol chemistry and specificity in redox signaling**. *Free Radical Biology and Medicine* 2008, **45**:549-561.
422. Ramstrom O, Bunyapaiboonsri T, Lohmann S, Lehn JM: **Chemical biology of dynamic combinatorial libraries**. *Biochimica Et Biophysica Acta-General Subjects* 2002, **1572**:178-186.
423. Ramstrom O, Lohmann S, Bunyapaiboonsri T, Lehn JM: **Dynamic combinatorial carbohydrate libraries: Probing the binding site of the concanavalin A lectin**. *Chemistry-a European Journal* 2004, **10**:1711-1715.
424. Pei ZC, Larsson R, Aastrup T, Anderson H, Lehn JM, Ramstrom O: **Quartz crystal microbalance bioaffinity sensor for rapid identification of glycosyldisulfide lectin inhibitors from a dynamic combinatorial library**. *Biosensors & Bioelectronics* 2006, **22**:42-48.
425. Sakai S, Shigemasa Y, Sasaki T: **A self-adjusting carbohydrate ligand for GalNAc specific lectins**. *Tetrahedron Letters* 1997, **38**:8145-8148.
426. Sakai S, Shigemasa Y, Sasaki T: **Iron(II)-assisted assembly of trivalent GalNAc clusters and their interactions with GalNAc-specific lectins**. *Bulletin of the Chemical Society of Japan* 1999, **72**:1313-1319.
427. Hotchkiss T, Kramer HB, Doores KJ, Gamblin DP, Oldham NJ, Davis BG: **Ligand amplification in a dynamic combinatorial glycopeptide library**. *Chemical Communications* 2005:4264-4266.
428. Pei ZC: **Study of real-time lectin-carbohydrate interactions on the surface of a quartz crystal microbalance**. *Biosensors & Bioelectronics* 2005, **21**:60-66.

429. Pei ZC: **Redox-responsive and calcium-dependent switching of glycosyldisulfide interactions with Concanavalin A**. *Bioorganic & Medicinal Chemistry Letters* 2005, **15**:2707-2710.
430. Corbett PT, Otto S, Sanders JKM: **What are the limits to the size of effective dynamic combinatorial libraries?** *Organic Letters* 2004, **6**:1825-1827.
431. Corbett PT, Otto S, Sanders JKM: **Correlation between host-guest binding and host amplification in simulated dynamic combinatorial libraries**. *Chemistry-a European Journal* 2004, **10**:3139-3143.
432. Saur I, Severin K: **Selection experiments with dynamic combinatorial libraries: the importance of the target concentration**. *Chemical Communications* 2005:1471-1473.
433. Corbett PT, Sanders JKM, Otto S: **Competition between receptors in dynamic combinatorial libraries: Amplification of the fittest?** *Journal of the American Chemical Society* 2005, **127**:9390-9392.
434. Eliseev AV, Nelen MI: **Use of molecular recognition to drive chemical evolution, Part 2. Mechanisms of an automated genetic algorithm implementation**. *Chemistry-a European Journal* 1998, **4**:825-834.
435. Goklen KE, Hatton TA: **Protein Extraction Using Reverse Micelles**. *Biotechnology Progress* 1985, **1**:69-74.
436. Mattoon RW, Mathews MB: **Micelles in Non-Aqueous Media**. *Journal of Chemical Physics* 1949, **17**:496-497.
437. Eicke H, Kvita P: *Reverse micelles and aqueous microphases*. Edited by Luisi PL SB. N.Y., London:: Plenum Press; 1984.
438. Tonova K, Lazarova Z: **Reversed micelle solvents as tools of enzyme purification and enzyme-catalyzed conversion**. *Biotechnology Advances* 2008, **26**:516-532.
439. Luisi PL, Magid LJ: **Solubilization of Enzymes and Nucleic-Acids in Hydrocarbon Micellar Solutions**. *Crc Critical Reviews in Biochemistry* 1986, **20**:409-474.
440. Martinek K, Levashov AV, Khmelnitsky YL, Klyachko NL, Berezin IV: **Colloidal Solution of Water in Organic Solvents - A Microheterogenous Medium for Enzymatic-Reactions**. *Science* 1982, **218**:889-891.
441. De TK, Maitra A: **Solution Behavior of Aerosol Ot in Nonpolar-Solvents**. *Advances in Colloid and Interface Science* 1995, **59**:95-193.
442. Biasutti MA, Abuin EB, Silber JJ, Correa NM, Lissi EA: **Kinetics of reactions catalyzed by enzymes in solutions of surfactants**. *Advances in Colloid and Interface Science* 2008, **136**:1-24.
443. Hilhorst R, Spruijt R, Laane C, Veeger C: **Rules for the Regulation of Enzyme-Activity in Reserved Micelles as Illustrated by the Conversion of Apolar Steroids by 20-Beta-Hydroxysteroid Dehydrogenase**. *European Journal of Biochemistry* 1984, **144**:459-466.
444. Rabie HR, Vera JH: **A simple model for reverse micellar extraction of proteins**. *Separation Science and Technology* 1998, **33**:1181-1193.
445. Cardoso MM, Barradas MJ, Carrondo MT, Kroner KH, Crespo JG: **Mechanisms of amino acid partitioning in cationic reversed micelles**. *Bioseparation* 1998, **7**:65-78.
446. Adachi M, Harada M, Nishita R, Shioi A: **Extraction Kinetics of Small Charged Molecules in Water-in-Oil Microemulsion/Brine System**. *Journal of Physical Chemistry* 1995, **99**:8722-8729.
447. Dungan SR, Bausch T, Hatton TA, Plucinski P, Nitsch W: **Interfacial Transport Processes in the Reversed Micellar Extraction of Proteins**. *Journal of Colloid and Interface Science* 1991, **145**:33-50.

448. Nishiki T, Sato I, Muto A, Kataoka T: **Mass transfer characterization in forward and back extractions of lysozyme by AOT-isooctane reverse micelles across a flat liquid-liquid interface**. *Biochemical Engineering Journal* 1998, **1**:91-97.
449. Hilhorst R, Fijneman P, Heering D, Wolbert RBG, Dekker M, Vantriet K, Bijsterbosch BH: **Protein Extraction Using Reversed Micelles**. *Pure and Applied Chemistry* 1992, **64**:1765-1770.
450. Kawakami K, Harada M, Adachi M, Shioi A: **Mechanism of protein solubilization in sodium bis(2-ethylhexyl) sulfosuccinate water-in-oil microemulsion**. *Colloids and Surfaces a-Physicochemical and Engineering Aspects* 1996, **109**:217-233.
451. Pires MJ, AiresBarros MR, Cabral JMS: **Liquid-liquid extraction of proteins with reversed micelles**. *Biotechnology Progress* 1996, **12**:290-301.
452. Goklen KE, Hatton TA: **Liquid-Liquid-Extraction of Low-Molecular-Weight Proteins by Selective Solubilization in Reversed Micelles**. *Separation Science and Technology* 1987, **22**:831-841.
453. Kinugasa T, Kondo A, Mouri E, Ichikawa S, Nakagawa S, Nishii Y, Watanabe K, Takeuchi H: **Effects of ion species in aqueous phase on protein extraction into reversed micellar solution**. *Separation and Purification Technology* 2003, **31**:251-259.
454. Wolbert RBG, Hilhorst R, Voskuilen G, Nachtegaal H, Dekker M, Vantriet K, Bijsterbosch BH: **Protein Transfer from an Aqueous Phase into Reversed Micelles - the Effect of Protein Size and Charge-Distribution**. *European Journal of Biochemistry* 1989, **184**:627-633.
455. Woll JM: **Bioaffinity Separations Using Reversed Micellar Extraction**. *Biotechnology Progress* 1989, **5**:57-62.
456. Woll JM: **A Simple Phenomenological Thermodynamic Model for Protein Partitioning in Reversed Micellar Systems**. *Bioprocess Engineering* 1989, **4**:193-199.
457. Chen JP: **Extraction of Concanavalin-a with Affinity Reversed Micellar Systems**. *Separation Science and Technology* 1994, **29**:1115-1132.
458. Bhattacharyya L, Brewer CF: **Isoelectric-Focusing Studies of Concanavalin-a and the Lentil Lectin**. *Journal of Chromatography* 1990, **502**:131-142.
459. Matzke SF, Creagh AL, Haynes CA, Prausnitz JM, Blanch HW: **Mechanisms of Protein Solubilization in reverse micelles**. *Biotechnology and Bioengineering* 1992, **40**:91-102.
460. Khmelnitskii YL, Levashov AV, Klyachko NL, Chernyak VY, Martinek K: **Enzymes Incorporated into reversed Micelles of Surface Active Substances in Organic-Solvents-Investigation of the Protein Aerosol OT-H2O-Octane System by the Method of Sedimentation Analysis**. *Biochemistry-Moscow* 1982, **47**:77-89.
461. Wolf R, Luisi PL: **Micellar Solubilization of Enzymes in Hydrocarbon Solvents, Enzymatic-Activity and Spectroscopic Properties of Ribonuclease in N-Octane**. *Biochemical and Biophysical Research Communications* 1979, **89**:209-217.
462. Imai M, Natsume T, Naoe K, Shimizu M, Ichikawa S, Furusaki S: **Hydrophilic surroundings requisite for the solubilization of proteins related with their hydrophobicity in the AOT reversed micellar extraction**. *Bioseparation* 1996, **6**:325-333.
463. Christ S, Schurtenberger P: **Optical Contrast Variation Experiments in Water-in-Oil Microemulsions - Size Distribution and Structure of Protein-Free and Protein-Containing Microemulsions**. *Journal of Physical Chemistry* 1994, **98**:12708-12714.

464. Rahaman RS, Hatton TA: **Structural Characterization of Alpha-Chymotrypsin-Containing Aot Reversed Micelles**. *Journal of Physical Chemistry* 1991, **95**:1799-1811.
465. Hirai M, Kawai-Hirai R, Iwase H, Hayakawa T, Kawabata Y, Takeda T: **Effect of proteins on dynamics of water-in-oil AOT microemulsions**. *Applied Physics A: Materials Science & Processing* 2002, **74**:S1254-S1256.
466. Eicke HF, Shepherd JCW, Steinemann A: **Exchange of Solubilized Water and Aqueous-Electrolyte Solutions between Micelles in Apolar Media** *Journal of Colloid and Interface Science* 1976, **56**:168-176.
467. Robinson BH, Steytler DC, Tack RD: **Ion Reactivity in Reversed-Micellar Systems - Kinetics of Reaction between Micelles Containing Hydrated Nickel(Ii) and Murexide-Containing Micelles in the System Aerosol Ot+Water+Heptane**. *Journal of the Chemical Society-Faraday Transactions I* 1979, **75**:481-496.
468. Luisi PL, Giomini M, Pileni MP, Robinson BH: **Reverse Micelles as Hosts for Proteins and Small Molecules**. *Biochimica Et Biophysica Acta* 1988, **947**:209-246.
469. Jada A, Lang J, Zana R: **Relation between Electrical Percolation and Rate-Constant for Exchange of Material between Droplets in Water in Oil Microemulsions**. *Journal of Physical Chemistry* 1989, **93**:10-12.
470. Steytler DC, Towey TF, Robinson BH, Atay NZ: **Mechanisms of solute interfacial transfer in Winsor-II systems**. *Langmuir* 2001, **17**:417-426.
471. Fletcher PDI, Howe AM, Robinson BH: **The Kinetics of Solubilisate Exchange between Water Droplets of a Water-in-Oil Microemulsion**. *Journal of the Chemical Society-Faraday Transactions I* 1987, **83**:985-1006.
472. Bru R, Sanchezferrer A, Garciacarmona F: **Kinetic-Models in Reverse Micelles**. *Biochemical Journal* 1995, **310**:721-739.
473. Bru R, Garciacarmona F: **Trypsin-Sbti Interaction in Reverse Micelles - a Slow Intermicellar Exchange-Dependent Binding**. *Febs Letters* 1991, **282**:170-174.
474. Nishii Y, Kinugasa T, Nii S, Takahashi K: **Transport behavior of protein in bulk liquid membrane using reversed micelles**. *Journal of Membrane Science* 2002, **195**:11-21.
475. Tsai SW, Wen CL, Chen JL, Wu CS: **Protein Extractions by Supported Liquid Membrane with Reversed Micelles as Carriers**. *Journal of Membrane Science* 1995, **100**:87-97.
476. Ono T, Goto M: **Peroxidative catalytic behavior of cytochrome c solubilized in reverse micelles**. *Biochemical Engineering Journal* 2006, **28**:156-160.
477. Hirai M, Takizawa T, Yabuki S, Kawaihirai R, Oya M, Nakamura K, Kobashi K, Amemiya Y: **Structure and Reactivity of Aerosol-Ot Reversed Micelles Containing Alpha-Chymotrypsin**. *Journal of the Chemical Society-Faraday Transactions* 1995, **91**:1081-1089.
478. Mayer F, Hoppert M: **Functional compartmentalization in bacteria and archaea - A hypothetical interface between cytoplasmic membrane and cytoplasm**. *Naturwissenschaften* 1996, **83**:36-39.
479. Naoe K, Noda K, Kawagoe M, Imai M: **Higher order structure of proteins solubilized in AOT reverse micelles**. *Oct 11-13*; *Yokohama, JAPAN*: Elsevier Science Bv: 2003:179-185.
480. Hagen AJ, Hatton TA, Wang DIC: **Protein refolding in reversed micelles**. *Biotechnology and Bioengineering* 2006, **95**:285-294.
481. Bausch TE, Plucinski PK, Nitsch W: **Kinetics of the Reextraction of Hydrophilic Solutes out of Aot-Reversed Micelles**. *Journal of Colloid and Interface Science* 1992, **150**:226-234.

482. Daliya S. Mathew, Juang R-S: **Role of alcohols in the formation of inverse microemulsions and back extraction of proteins /enzymes in a reverse micellar system**. *Separation and Purification Technology* 2007, **53**:199-215.
483. Douglas G. Hayes CM: **Expulsion of Proteins from water-in-Oil Microemulsions by Treatment with Cosurfactant** *Biotechnology and Bioengineering* 1998, **59**:557-566.
484. Woll JMD, A. S.; Rahman, R. S.; Hatton, T. A: *Protein Purification:micro to macro*. Edited by Burgess R. New York: Alan R. Bliss; 1987.
485. Aires-Barros MRC, J.M.S.: **Selective separation and purification of two lipases from chromobacterium viscosum using AOT reversed micelles**. *Biotechnology and Bioengineering* 1991, **38**:1302.
486. Kocherginsky NM, Yang Q, Seelam L: **Recent advances in supported liquid membrane technology**. *Separation and Purification Technology* 2007, **53**:171-177.
487. Izatt RM, Lamb JD, Bruening RL: **Comparison of Bulk, Emulsion, Thin Sheet Supported, and Hollow Fiber Supported Liquid Membranes in Macrocycle-Mediated Cation Separations**. *Separation Science and Technology* 1988, **23**:1645-1658.
488. Juang RS, Kao HC, Shiau CL: **Kinetic analysis on membrane-based reverse micellar extraction of lysozyme from aqueous solutions**. *Journal of Membrane Science* 2006, **281**:636-645.
489. Miyako E, Maruyama T, Kamiya N, Goto M: **Highly enantioselective separation using a supported liquid membrane encapsulating surfactant-enzyme complex**. *Journal of the American Chemical Society* 2004, **126**:8622-8623.
490. Miyako E, Maruyama T, Kamiya N, Goto M: **A supported liquid membrane encapsulating a surfactant-lipase complex for the selective separation of organic acids**. *Chemistry-a European Journal* 2005, **11**:1163-1170.
491. Miyako E, Maruyama T, Kubota F, Kamiya N, Goto M: **Optical resolution of various amino acids using a supported liquid membrane encapsulating a surfactant-protease complex**. *Langmuir* 2005, **21**:4674-4679.
492. Barboiu M, Guizard C, Luca C, Albu B, Hovnanian N, Palmeri J: **A new alternative to amino acids transport: facilitated transport of L-phenylalanine by hybrid siloxane membranes containing a fixed site macrocyclic complexant**. *Journal of Membrane Science* 1999, **161**:193-206.
493. Brown RD: **Conformation States of Concanavalin a - Kinetics of Transitions Induced by Interaction with Mn2+ and Ca2+ Ions**. *Biochemistry* 1977, **16**:3883-3896.
494. Koenig SH: **Conformation as Determinant of Saccharide Binding in Concanavalin a - Ca2+-Concanavalin-a Complexes**. *Biochemistry* 1978, **17**:4251-4260.
495. Brewer CF: **Metal-Ion Binding and Conformational Transitions in Concanavalin-a - a Structure-Function Study**. *Journal of Biomolecular Structure & Dynamics* 1983, **1**:961-997.
496. Bouckaert J: **The Structural Features of Concanavalin A Governing Non-proline Peptide Isomerization**. *The Journal of Biological Chemistry* 2000, **275**:19778-19787.
497. Schelly ZA: **Dynamics in water-in-oil microemulsions**. *Current Opinion in Colloid & Interface Science* 1997, **2**:37-41.
498. Texter J: **Supramolecular equilibria in microemulsions**. *Colloids and Surfaces a-Physicochemical and Engineering Aspects* 2000, **167**:115-122.
499. Alexandridis P, Holzwarth JF, Hatton TA: **Thermodynamics of Droplet Clustering in Percolating Aot Water-in-Oil Microemulsions**. *Journal of Physical Chemistry* 1995, **99**:8222-8232.

500. Cassin G, Illy S, Pileni MP: **Chemically-Modified Proteins Solubilized in Aot Reverse Micelles - Influence of Proteins Charges on Intermicellar Interactions**. *Chemical Physics Letters* 1994, **221**:205-212.
501. Hong DP, Kuboi R, Komasawa I: **Extraction of proteins and polymers using reverse micelles and percolation process**. *Korean Journal of Chemical Engineering* 1997, **14**:334-340.
502. Eastoe J, Robinson BH, Steytler DC, Thornleeson D: **Structural Studies of Microemulsions Stabilized by Aerosol-Ot**. *Advances in Colloid and Interface Science* 1991, **36**:1-31.
503. Togashi DM, Costa SMB: **Excited state quenching kinetics of zinc meso-tetrakis (N-methylpyridinium-4-yl) porphyrin by methyl viologen in AOT reverse micelles**. *Physical Chemistry Chemical Physics* 2002, **4**:1141-1150.
504. Charlton ID, Doherty AP: **Simultaneous observation of attractive interaction, depletion forces, and "sticky" encounters between AOT reverse micelles in isooctane using microelectrode voltammetry**. *Journal of Physical Chemistry B* 2000, **104**:8061-8067.
505. Vauthier C, Labarre D: **Modular biomimetic drug delivery systems**. *Journal of Drug Delivery Science and Technology* 2008, **18**:59-68.
506. Alaouie AM, Sofou S: **Liposomes with Triggered Content Release for Cancer Therapy**. *Journal of Biomedical Nanotechnology* 2008, **4**:234-244.
507. Kawakami S: **Development and Application of Glycosylated Particulate Carriers for Delivery of Nucleic Acid Medicine**. *Yakugaku Zasshi-Journal of the Pharmaceutical Society of Japan* 2008, **128**:1743-1749.
508. Breunig M, Bauer S, Goefferich A: **Polymers and nanoparticles: Intelligent tools for intracellular targeting?** *European Journal of Pharmaceutics and Biopharmaceutics* 2008, **68**:112-128.
509. Woehrle GH, Warner MG, Hutchison JE: **Molecular-Level Control of Feature Separation in One-Dimensional Nanostructure Assemblies Formed by Biomolecular Nanolithography**. *Langmuir* 2004, **20**:5982-5988.
510. Dahmen J, Frejd T, Magnusson G, Noori G: **Boron-Trifluoride Etherate-Induced Glycosidation - Formation of Alkyl Glycosides and Thioglycosides of "2-Deoxy-2-Phthalimidoglycopyranoses**. *Carbohydrate Research* 1983, **114**:328-330.
511. Toshima K, Tatsuta K: **Recent Progress in O-Glycosylation Methods and Its Application to Natural-Products Synthesis**. *Chemical Reviews* 1993, **93**:1503-1531.
512. Milkereit G, Gerber S, Brandenburg K, Morr M, Vill V: **Synthesis and mesomorphic properties of glycosyl dialkyl- and diacyl-glycerols bearing saturated, unsaturated and methyl branched fatty acid and fatty alcohol chains Part I. Synthesis**. *Chemistry and Physics of Lipids* 2005, **135**:1-14.
513. Kolb HC, Sharpless KB: **The growing impact of click chemistry on drug discovery**. *Drug Discovery Today* 2003, **8**:1128-1137.
514. Binder WH, Kluger C: **Azide/alkyne-"click" reactions: Applications in material science and organic synthesis**. *Current Organic Chemistry* 2006, **10**:1791-1815.
515. Dondoni A: **Triazole: the keystone in glycosylated molecular architectures constructed by a click reaction**. *Chemistry-an Asian Journal* 2007, **2**:700-708.
516. Clement NR, Gould JM: **Pyranine (8-hydroxy-1,3,6-pyrenetrisulfonate) as a probe of internal aqueous hydrogen ion concentration in phospholipid vesicles**. *Biochemistry* 1981, **20**:1534-1538.
517. Sakai N, Matile S: **The determination of the ion selectivity of synthetic ion channels and pores in vesicles**. *Journal of Physical Organic Chemistry* 2006, **19**:452-460.

518. Levashov AV, Klyachko NL: **Micellar enzymology: methodology and technique**. *Russian Chemical Bulletin* 2001, **50**:1718-1732.
519. Adachi M, Harada M, Shioi A, Takahashi H, Katoh S: **Bioaffinity separation of concanavalin A in reverse micellar system composed of AOT/butanol or non-ionic surfactant**. *Journal of Chemical Engineering of Japan* 1996, **29**:982-989.
520. J. Defaye HD, E. Ohleyer, C. Orgeret and C. Viet: **Stereoselective syntheses of 1,2-trans-related 1-thioglycoses** 1984, **130**:317.

RESUME en français

Le but de ce travail était d'explorer l'interaction entre les ensembles supramoléculaires biomimétiques et chimie dynamiques constitutionnels et les motifs biologiques simples. La recherche a été effectuée dans les domaines d'intérêt suivants : l'interaction protéine-saccharides, les vésicules, les bicouches phospholipidiques, les canaux ioniques et le transport à travers une membrane et ont constituer trois axes de projet. Des nanoparticules ont été employées pour l'amplification du signal de fréquence d'une microbalance à cristal de quartz pour la recherche sur l'interaction de lectin-saccharide montrant une haute spécificité et une augmentation d'affinité par multivalence. Les Polyoxomolydates, des nanoarchitectures qui possèdent le potentiel de former des canaux ioniques biomimetiques ont montré qu'ils s'incorporaient spontanément dans les bicouches lipidiques. Cela facilitait les flux des cations. De plus ces nanoclusters anioniques ont démontré une organisation électrostatique sur des bicouches lipidiques qui peuvent être utilisé pour le développement de matériaux hybrides et aussi pour les études des propriétés médicinales des polyoxomolybdates. Pour finir une membrane liquide supporté contenant la lectine Concanavalin A dans une nanoemulsion a été développée pour étudier le transport d'une bibliothèque combinatoire dynamique simple.

TITRE en anglais

Dynamic Constitutional Protein-Carbohydrate and Polyoxometalate Systems–towards Biomimetic Sensors and Membranes.

RESUME en anglais

The aim of this work was to explore the interaction between biomimetic supramolecular and dynamic constitutional chemistry ensembles and simple biological motifs. Research was performed in the following areas of interest: carbohydrate-protein interaction, vesicles, bilayers, ion channels and membrane transport constituting three projects. Quartz crystal microbalance measurement was coupled with nanoparticle mass amplification for investigation of lectin-carbohydrate interaction showing high specificity and affinity enhancement through multivalency. Polyoxomolydates, nanoarchitectures which possess the potential to form biomimetic ion channels were shown to spontaneously partition in lipid bilayers and mediate cation flux, additionally theses anionic nanoclusters demonstrated electrostatic organisation on lipid bilayers which can be applied in hybrid material development and investigation the demonstrated medicinal properties of polyoxomolybdates. Lastly a lectin occluding supported liquid membrane was developed to investigate transport of a simple dynamic combinatorial library.

DISCIPLINE

Chimie et Physicochimie des Materiaux

MOTS-CLES

Chimie supramoléculaire, reconnaissance moléculaire, dynamique, nanoparticules, microbalance à quartz, biomimétique.

INTITULE ET ADRESSE DE L'U.F.R. OU DU LABORATOIRE :

IEM –Institut Européen des Membranes, UMR 5635 CNRS/UM2/ENSCM
Place Eugène Bataillon, CC047, 34095 MONTPELLIER cedex 5